

**AWARD NUMBER:**

W81XWH-14-1-0238

**TITLE:**

Targeting histone abnormality in triple negative breast cancer

**PRINCIPAL INVESTIGATOR:**

Steffi Oesterreich, Ph.D.

**CONTRACTING ORGANIZATION:** University of Pittsburgh

Pittsburgh, PA 15213

**REPORT DATE:** October 2018

**TYPE OF REPORT:**

Final report

**PREPARED FOR:** U.S. Army Medical Research and Materiel Command

Fort Detrick, Maryland 21702-5012

**DISTRIBUTION STATEMENT:** Approved for Public Release;

Distribution Unlimited

The views, opinions and/or findings contained in this report are those of the author(s) and should not be construed as an official Department of the Army position, policy or decision unless so designated by other documentation.

REPORT DOCUMENTATION PAGE			Form Approved OMB No. 0704-0188		
Public reporting burden for this collection of information is estimated to average 1 hour per response, including the time for reviewing instructions, searching existing data sources, gathering and maintaining the data needed, and completing and reviewing this collection of information. Send comments regarding this burden estimate or any other aspect of this collection of information, including suggestions for reducing this burden to Department of Defense, Washington Headquarters Services, Directorate for Information Operations and Reports (0704-0188), 1215 Jefferson Davis Highway, Suite 1204, Arlington, VA 22202-4302. Respondents should be aware that notwithstanding any other provision of law, no person shall be subject to any penalty for failing to comply with a collection of information if it does not display a currently valid OMB control number. PLEASE DO NOT RETURN YOUR FORM TO THE ABOVE ADDRESS.					
1. REPORT DATE October 2018		2. REPORT TYPE Final report		3. DATES COVERED 1 Aug 2014 - 31 Jul 2018	
4. TITLE AND SUBTITLE Targeting histone abnormality in triple negative breast cancer			5a. CONTRACT NUMBER		
			5b. GRANT NUMBER W81XWH-14-1-0238		
			5c. PROGRAM ELEMENT NUMBER N/A		
6. AUTHOR(S) Steffi Oesterreich, PhD  E-Mail: oesterreichs@upmc.edu			5d. PROJECT NUMBER N/A		
			5e. TASK NUMBER N/A		
			5f. WORK UNIT NUMBER N/A		
7. PERFORMING ORGANIZATION NAME(S) AND ADDRESS(ES) University of Pittsburgh Cancer Institute  204 Craft Ave., Pittsburgh, PA 15213			8. PERFORMING ORGANIZATION REPORT NUMBER N/A		
9. SPONSORING / MONITORING AGENCY NAME(S) AND ADDRESS(ES)  U.S. Army Medical Research and Materiel Command Fort Detrick, Maryland 21702-5012			10. SPONSOR/MONITORING ACRONYM(S)  N/A		
			11. SPONSOR/MONITORING REPORT NUMBER(S) N/A		
12. DISTRIBUTION / AVAILABILITY STATEMENT  Approved for Public Release; Distribution Unlimited					
13. SUPPLEMENTARY NOTES N/A					
14. ABSTRACT The main goal of this collaborative project is to combine complementary expertise and strength from two PIs to develop a novel, conceptual, and most importantly, testable plan for a new approach to breast cancer biology and treatment. During the entire grant's period of performance, the PIs worked closely together to decipher the scientific mechanisms underlying the proposed aims of how histone abnormality contributes to development of TNBC and explore how to combine epigenetic agents with other types of therapeutic drugs in the most favorable strategy against TNBC. The joint research team has revealed that enhanced interaction between two important epigenetic modifiers, HDAC5 and LSD1, stabilizes LSD1 protein that could in turn facilitates TNBC tumor growth and progression. The advanced studies have characterized the proteins/complexes associated with key regulatory element at HDAC5 promoter, and identified that sulforaphane (SFN), a natural bioactive HDAC inhibitor, was able to destabilize LSD1 protein through downregulation of HDAC5 transcription. This research also shed novel light on how to combine SFN with LSD1 inhibitor to enhance antineoplastic efficacy against TNBC tumor. Furthermore, our study identifies LSD1 as a potent inhibitor of anti-tumor immunity and demonstrated that inhibition of LSD1 reactivates expression of key cytotoxic T cell attracting chemokines which in turn augments sensitivity of TNBC to immune checkpoint blockade therapy. Adequate progress and accomplishments have been achieved towards the proposed aims, and the research funds has been spent effectively as expected during the entire award period. With this funding support, we have published multiple original research papers in top-tier cancer research journals and presented the research outcomes at national cancer research conferences.					
15. SUBJECT TERMS None listed					
16. SECURITY CLASSIFICATION OF:			17. LIMITATION OF ABSTRACT	18. NUMBER OF PAGES	19a. NAME OF RESPONSIBLE PERSON
a. REPORT	b. ABSTRACT	c. THIS PAGE			USAMRMC
Unclassified	Unclassified	Unclassified	Unclassified	95	19b. TELEPHONE NUMBER (include area code) N/A

## Table of Contents

	<u>Page</u>
1. Introduction	1
2. Keywords	1
3. Accomplishments	.....1
4. Impact	7
5.Changes/Problems...	.7
6. Products	8
7.Participants & Other Collaborating Organizations	.9
8.Special Reporting Requirements	...9
9. Appendices	...attached

## 1. INTRODUCTION

The research proposed in this collaborative project addresses two closely related overarching challenges: (1) eliminate the mortality associated with metastatic breast cancer; (2) identify what drives breast cancer growth and metastasis; identify why some breast cancers become life threatening metastases. This award is focused on triple-negative breast cancer (TNBC) which is a clinically more aggressive subtype of breast cancer. Distant metastases in TNBC patients are more common than their hormone receptor-positive counterparts. Unlike other type of breast cancer, TNBC is not amenable to anti-estrogen therapy or to agents targeting HER2. Therefore, new targeted approaches are urgently needed to improve treatment and prevention for this devastating disease. Emerging data indicate that epigenetic regulation of TNBC proliferation and metastasis may provide novel targets for molecularly directed therapies against this disease. To address the overarching challenges, we proposed three interrelated specific aims based on our early findings that abnormal crosstalk between histone modifiers represents a fundamental mechanism contributing to aberrant epigenetic silencing of tumor suppressor genes that would facilitate TNBC tumorigenesis and metastasis. Our long-term goal is to develop novel therapeutic strategies to improve the efficacy of epi-drugs and reduce the side effects by targeting more specific regions of chromatin and the subset of genes that are associated with most prominent alterations in the breast cancer genome.

We initiated the project through examining the basic mechanisms underlying the potential crosstalk between epigenetic modifiers and its impact on the TNBC progression. We have revealed that enhanced interaction between a key class II histone deacetylase, HDAC5, and a fad-dependent histone demethylase, LSD1, stabilizes LSD1 protein that in turn promotes growth and metastasis of TNBC cells. We advanced the investigation on how to target abnormal crosstalk between HDAC5 and LSD1 as a novel treatment approach for TNBC. We identified that sulforaphane (SFN), a natural HDAC inhibitor, suppresses HDAC5 expression that in turn destabilizes LSD1 protein. By characterizing the proteins/complexes that are associated with key regulatory element at HDAC5 promoter, our studies explored the molecular mechanisms underlying SFN-induced suppression of HDAC5 transcription and evaluated therapeutic effects of combination strategies in animal model. The outcomes from these works have opened a new avenue for the potential utility of crosstalk between histone demethylation and deacetylation as a new therapeutic target for TNBC.

In probing for downstream targets of HDAC5-LSD1 axis, we interestingly found that that inhibition of LSD1 reactivates expression of key cytotoxic T cell attracting chemokines which in turn augments anti-tumor CD8+ cells trafficking and infiltration in breast cancer cells. These findings led us to hypothesize that inhibition of LSD1 augments antitumor immune responses and improves therapeutic efficacy of immune checkpoint blocking antibodies in TNBC. We tested this hypothesis in mouse TNBC xenograft animal model and showed that anti-PD-1 antibody alone failed to elicit obvious therapeutic effect, however, combining LSD1 inhibitors with PD-1 antibody significantly suppressed tumor growth and pulmonary metastasis, which was associated with reduced Ki-67 level and augmented CD8+ T cell infiltration. These findings suggest a new strategy of inhibiting crosstalk between epigenetic modulators and immune compartments as a novel therapeutic strategy for breast cancer patients with poor immune response. Since the development of novel LSD1 inhibitors is progressing rapidly and several clinical trials of LSD1 inhibitors are ongoing in cancer patients, we believe that our new combination strategy would carry high innovation and translational potential.

### KEYWORDS

Triple negative breast cancer, HDAC5, LSD1, sulforaphane, HCI-2509, combination therapy, T-cell chemokine, immunotherapy

## 2. ACCOMPLISHMENTS

### a. What were the major goals of the project?

The major goals for this research award are to understand the molecular mechanisms underlying crosstalk between critical epigenetic modifiers in promoting TNBC progression and seek for novel therapeutic approaches to target aberrant crosstalk between epigenetic modifiers for poorly differentiated and aggressive TNBC. To address these goals, the initiating and patterner PIs have worked closely together to outline and test the following specific aims:

- i. Delineate the molecular basis by which inhibition of LSD1 promotes HDACi-induced apoptosis through reactivation of aberrantly silenced tumor suppressor genes.
- ii. Elucidate the role of LSD1 in HDACi therapy and chemoprevention of TNBC in animal models.
- iii. Evaluate therapeutic effects of combination strategies in patient-derived xenografts (PDXs).

We expect that the results obtained from this project would shed light on which epigenetic changes contribute directly to the aggressive biology of TNBC tumorigenesis and provide a solid foundation for advancing the most promising epigenetic drugs into future clinical application.

### What was accomplished under these goals?

Proposed Aims	Accomplishment
<p><b>Specific Aim 1:</b> Delineate the molecular basis by which inhibition of LSD1 promotes HDACi-induced apoptosis through reactivation of aberrantly silenced tumor suppressor genes.</p>	<p><b>1. Novel insights into the roles of crosstalk of HDAC5 and LSD1 in TNBC progression.</b> Our previous work showed that inhibition of HDAC5 led to a significant increase of H3K4me2, a well-recognized substrate of LSD1, suggesting a potential involvement of HDAC5 in regulating LSD1 activity (Carcinogenesis 2013; 34: 119661207). Building on these studies, TCGA data-mining and IHC studies were carried out and indicated a positive correlation between expression of HDAC5 and LSD1 proteins in breast tumor cell lines and patient tissue specimens. Importantly, increased expression of HDAC5 and LSD1 is correlated with higher stage of breast cancer. We observed for the first time that LSD1 protein stability is promoted through interaction with HDAC5 at its nuclear localization sequence (NLS) domain. Our studies also revealed that HDAC5 regulates LSD1 via enhancement of the protein stability of deubiquitinase USP28. Overexpression of HDAC5 in non-transformed breast epithelial MCF10A cells significantly promoted mutagen-induced malignant transformation. These data indicate that enhanced crosstalk between HDAC5 and LSD1 may represent a critical mechanism contributing to breast tumorigenesis (Summary in Fig. 1; <i>Oncogene</i>, 36:133-145, 2017).</p>

## **2. Sulforaphane as a potent inhibitor of HDAC5-LSD1 axis in**

**TNBC.** Based on the above findings, we tested a panel of HDAC inhibitors for their ability to inhibit HDAC5-LSD1 signaling pathway. Our experiments showed that a natural HDACi, sulforaphane (SFN), suppressed HDAC5 mRNA expression without altering LSD1 mRNA level. Regulatory activity at -356 to -100 bp promoter element was found to play a critical role in governing HDAC5 transcription and a group of factors that bind to this element were identified through DAPA and proteomic assays. Among these factors, Upstream Transcription Factor 1 (USF1) was shown to exert a critical effect in regulating HDAC5 transcription. We also observed that SFN downregulated HDAC5 transcription by blocking USF1 activity. We further determined that SFN significantly inhibited expression of LSD1 protein but had no effect on overexpressed exogenous HDAC5 protein through transfection of pcDNA3.1-HDAC5 plasmids. Moreover, SFN-mediated downregulation of LSD1 protein and USP28 was apparently reversed by HDAC5 overexpression. These results demonstrate that SFN downregulates LSD1 protein stability through modulation of the LSD1-associated ubiquitination system, which is largely dependent on HDAC5 activity (*Int. J. Cancer*, 143: 1388-1401, 2018)

## **3. Comprehensive profiling of genes expression regulated by HDAC5/LSD1 complex: extensive crosstalk at genome level.**

Genome-wide gene expression analysis in MDA-MB-231 cells with stable knockdown of HDAC5 or LSD1 by shRNA showed that more than 30% of genes in each group were overlapping and regulated by HDAC5-KD and LSD1-KD. These results reflect a comprehensive genome wide cooperative effect of HDAC5 and LSD1 on target gene expression. A functional pathway analysis showed that there are multiple important cellular networks whose activities are significantly altered by depletion of HDAC5 or LSD1. These networks are broadly associated with cell death & survival, cell cycle, cellular development, cellular growth/proliferation, carbohydrate metabolism, cell morphology, cell-cell signaling & interaction, cellular assembly & organization, lipid metabolism, molecular transport, small molecule biochemistry and so on. Among the differentially expressed genes (DEGs) potentially regulated by HDAC5/LSD1 complex, we identified a subset of genes whose activities are associated with critical cellular processes in cancer: cell adhesion, metastasis, tumor suppression and cell growth, receptors, therapeutic response and so on. Among these genes, a group of important tumor suppressor genes (TSGs) was shown to be induced by either HDAC5 or LSD1 inhibition. Furthermore, SFN treatment significantly induced expression of most of the TSG genes tested, showing a similar effect on

	<p>activation of TSGs by SFN or HDAC5/LSD1 inhibition (<i>Int. J. Cancer</i>, 143: 1388-1401, 2018).</p>
<p><b>Specific Aim 2:</b> Elucidate the role of LSD1 in HDACi therapy and chemoprevention of TNBC in animal models.</p>	<ol style="list-style-type: none"> <li>1. <b>Role of HDAC5–LSD1 axis in regulation of breast cancer cell sensitivity to sulforaphane.</b> Overexpression of HDAC5 or LSD1 protein in breast cancer cells significantly increased resistance to SFN-mediated growth inhibition. A rescue experiment showed that HDAC5 overexpression attenuated cellular sensitivity to SFN in breast cancer cells but was obviously reversed by LSD1 depletion. We determined the growth inhibitory effect of combined treatment with LSD1 inhibitor HCI-2509 with SFN in multiple breast cancer cell lines and normal breast epithelial MCF10A cells using the combination index (CI) of growth inhibition via the Chou-Talalay model. While an antagonistic effect of SFN and HCI-2509 was obviously seen in MCF10A cells, combination therapy exhibited significant synergy in hindering growth of breast cancer cell lines (<i>Int. J. Cancer</i>, 143: 1388-1401, 2018).</li> <li>2. <b>A novel combinatorial strategy targeting histone abnormality to improve therapeutic efficacy of TNBC.</b> To evaluate whether the above promising in vitro results may translate into in vivo therapeutic efficacy, we investigated the antineoplastic effect of combination therapy in athymic nude mice bearing MDA-MB-231 xenografts. While treatment with either SFN or HCI-2509 alone significantly inhibited the proliferation of MDA-MB-231 xenografts, the combined treatment displayed superior inhibitory effect against tumor growth. Quantitative immunoblotting analysis showed that combination treatment significantly reduced the level of full-length PARP-1 in tumors. The in vivo effect of drug treatment on protein expression of HDAC5 and LSD1 in xenograft tumors was also evaluated. Immunoblots showed that expression of both HDAC5 and LSD1 was attenuated in tumors treated with SFN alone or in combination with HCI-2509. Collectively, these results indicate that SFN monotherapy effectively inhibits growth of MDA-MB-231 xenografts in vivo and exhibits significantly enhanced growth inhibition when used in combination with an LSD1 inhibitor (Summary in Fig. 2; <i>Int. J. Cancer</i>, 143: 1388-1401, 2018). Given that the inherent resistance to HDAC inhibitor develops as a result of combined multifactorial epigenetic abnormalities, our findings provide a rational basis for potential clinical trials combining agents targeting these dysregulated epigenetic targets in breast cancer.</li> </ol>
	<ol style="list-style-type: none"> <li>1. <b>Exploiting therapeutic approach targeting HDAC5-LSD1 axis in TNBC PDXs.</b> One of the most frequently cited causes for the high failure rate of translating bench findings of new agents into clinical setting is the lack of preclinical models that recapitulate the heterogeneity of tumors in patients. The goal of proposed PDX study in this proposal is to establish clinical relevance in preparation for design of clinical trials and</li> </ol>

**Specific Aim 3:** Evaluate therapeutic effects of combination strategies in patient-derived xenografts.

assess the effects of combination treatment on proliferation markers, histone modifications and expression of aberrantly silenced genes a clinically relevant model. PDX lines of TNBC patient tumors were provided by our collaborator Dr. Michael Lewis at Baylor College of Medicine. These PDX lines were selected based on RNA-seq results showing relative high expression levels of LSD1 and/or HDAC5. These tumor lines were re-transplanted into the SCID/Beige mice in our laboratory, and six TNBC PDX lines were observed to successfully grow in mice. Nano-particle formulated siRNA molecules have shown tremendous preclinical therapeutic potential for treating diseases like cancer in which an oncogene is overexpressed. We have successfully formulated nanoliposomal HDAC5 or LSD1 siRNA following the methods outlined in our proposal through collaboration with our colleague at School of Pharmacy at University of Pittsburgh. In the ongoing experiments, we will test the efficacy of Nano-siRNA compounds on proliferation, apoptosis, chromatin alteration and expression of the candidate genes in PDX tumors.

**2. Inhibition of LSD1 as an effective approach to enhance breast tumor immunogenicity and sensitizes refractory TNBC to anti-PD-1 therapy.** Emerging data in clinical trials with immune checkpoint inhibitors suggested that immunotherapy strategies hold great promise as new therapeutic options for TNBC. However, the majority of TNBC patients are still refractory to immunotherapy. Therefore, novel combinatorial approaches are urgently needed to augment response rates of immunotherapy for this devastating disease. Epigenetic silencing has been shown to play a critical role in downregulating the expression of certain immune regulatory molecules that results in the inefficient recognition and elimination of cancer cells by the host immune system. We tested a collection of epigenetic compounds (HDACi, DNMTi, HDMi, etc) and found that multiple LSD1 inhibitors significantly induced expression of CD8+ T-cell chemokines and PD-L1 in TNBC cells. Analysis of TCGA data indicates Negative correlation between expression of LSD1 and immune regulatory genes such as CCL5, CXCL9, CXCL10 and the PD-L1 in TNBC specimens. Concurrent treatment with small interfering RNA or inhibitor of chemokine receptors blocked LSD1 inhibitor-enhanced CD8+ T cell migration, indicating a critical role of key T cell chemokines in LSD1-mediated CD8+ lymphocyte trafficking to the tumor microenvironment. In vivo studies demonstrated that combining LSD1 inhibitors with PD-1 antibody significantly suppressed TNBC tumor growth and metastasis, which was associated with reduced Ki-67 level and augmented CD8+ T cell infiltration in xenograft tumors. These results suggest that therapeutic targeting of LSD1 may enhance the antitumor efficacy of immune checkpoint blockade in TNBC. Our novel strategy of combining LSD1 inhibitor and anti-PD-1 immune checkpoint blockade is innovative and carries



high translational potential. (Summary in Fig. 3; *Oncogene*, Aug 15, 2018. PMID: 30111819).

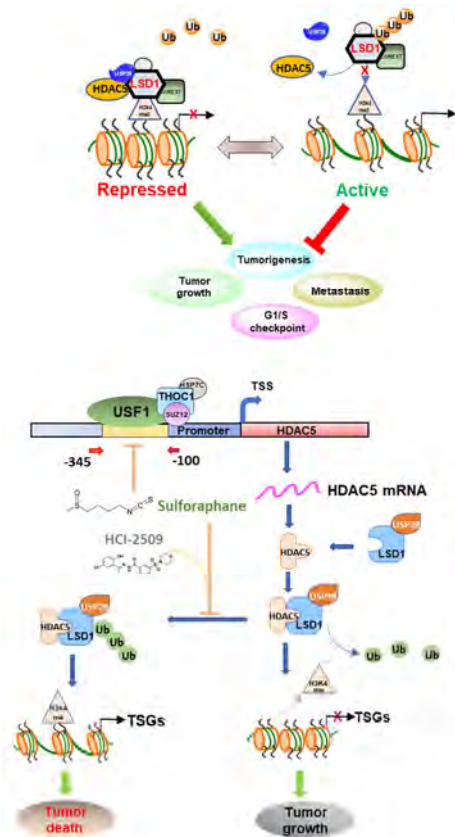


**Figure 1.** Proposed model of the role of HDAC5-LSD1 axis in breast cancer development. *Oncogene*, 36(1):133-145, 2017

**Figure 2.** Proposed model of the role of HDAC5-LSD1 axis in mediating antineoplastic effect of natural HDAC inhibitor SFN in human breast cancer. TSGs, tumor suppressor genes. *Int. J. Cancer*, 143: 1388-1401, 2018.

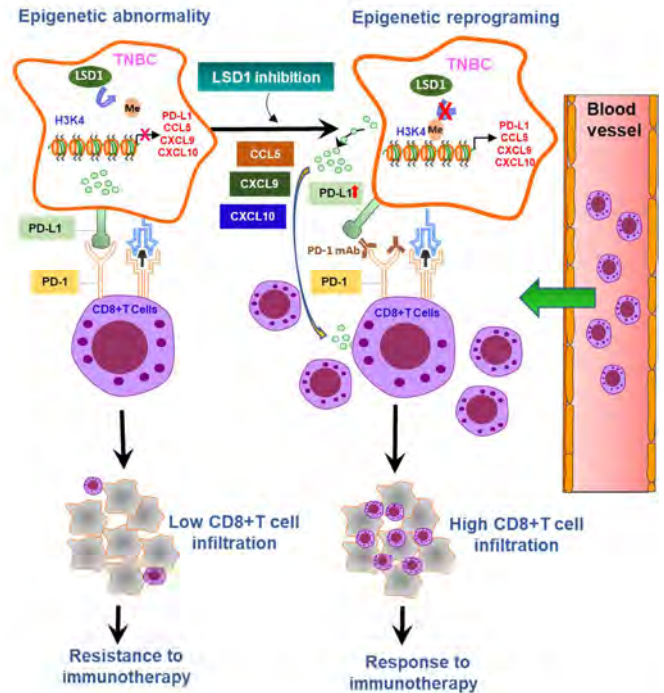


**Figure 3.** A proposed model of the role of LSD1 in regulation of breast tumor immunogenicity, response to immunotherapy and potential clinical outcome. *Oncogene*, Aug 15, 2018.

**b. What opportunities for training and professional development has the project provided?**

This award has provided excellent opportunities of scientific training and professional development for research personnel. Two postdoc fellows and one research specialist are directly supported by this award. This fund also provided generous support to visiting scholars, undergraduate students and Hillman Cancer Center summer academy students for their research activities at Womens Cancer Research Center. The trainees have obtained chances to present their work to their colleagues at campus or national cancer conferences such as AACR annual meeting. Travel costs for postdoc fellows to attend the local or national cancer conferences were in part supported by this award.

**c. How were the results disseminated to communities of interest?**

The research progress and data have been presented in seminal talks, conference poster and publications in cancer research journals. Both PIs promise that the research outcomes and data results generated from this project were shared with other researchers in accordance with the University of Pittsburgh and NIH Grant Policies on sharing of unique research resources. All cell lines, model organisms, plasmids, pharmacological compounds and in vivo samples generated under this project would be disseminated in accordance with policies of University of Pittsburgh and NIH policies. Depending on such policies, materials may be transferred to others under the terms of a material transfer agreement (MTA). Research data that documents, supports and validates research findings will be made available after the main findings have been accepted for publication.

**d. What do you plan to do during the next reporting period to accomplish the goals?**

All the studies for this award have been completed. No extension is requested.

### 3. IMPACT

#### (a) What was the impact on the development of the principal discipline(s) of the project?

This project seeks to address an unmet need to develop novel methods to define which epigenetic changes contribute to TNBC progression and decipher through multiple in vitro and in vivo models how to apply the novel epigenetic reagents in favorable combination strategy against TNBC. The research findings obtained from this project have significant impact on the development of the principal discipline as follows:

1) The information derived from these studies has shown for the first time that HDAC5-LSD1 axis has potential to serve as novel therapeutic biomarkers to predict response to epigenetic therapy in TNBC

2) Targeting HDAC5 with a natural HDACi, sulforaphane, in combination with a newly developed potent LSD1 inhibitor, HCL-2509, has showed superior antineoplastic activity both in vitro and in vivo, which could lead to validation and translation of our new strategy into future trials

3) Our novel strategy of combining LSD1 inhibitor and anti-PD-1 immune checkpoint blockade is innovative and carries high translational potential. Outcomes from this study identify novel therapeutic solutions to reverse effector T cell exclusion in certain breast cancer patients, thus has potential to expand the portion of breast cancer patients showing clinical benefit to immunotherapeutic interventions.

#### (b) What was the impact on other disciplines? Nothing to Report

#### (c) What was the impact on technology transfer? Nothing to Report

### 4. CHANGES/PROBLEMS

#### (a) Changes in approach and reasons for change

No major changes in approach have been made since the initiation of the award.

#### (b) Actual or anticipated problems or delays and actions or plans to resolve them

Nothing to Report

#### (c) Changes that had a significant impact on expenditures

Nothing to Report

#### (d) Significant changes in use or care of human subjects, vertebrate animals, biohazards, and/or select agents

Nothing to Report

### 5. PRODUCTS

#### (a) Publications, conference papers, and presentations supported by this award

**Research Articles:**

1. Cao C, Vasilatos SN, Bhargava R, Fine J, Oesterreich S, Davidson NE, Huang Y. Functional interaction of histone deacetylase 5 (HDAC5) and lysine-specific demethylase 1 (LSD1) promotes breast cancer progression. *Oncogene*, 36(1):133-145, 2017. PMID:27212032
2. Huang Y and Davidson NE. Targeting Tumorigenicity of Breast Cancer Stem-like Cells Using Combination Epigenetic Therapy: Something Old and Something New. *J. Thorac. Dis.*, 8(11):2971-2974, 2016. PMID: 28066560
3. Chen L, Vasilatos SN, Qin Y, Katz T, Cao C, Wu H, Tasdemir N, Levine KM, Oesterreich S, Davidson NE, Huang Y. Functional characterization of lysine-specific demethylase 2 (LSD2/KDM1B) in breast cancer progression. *Oncotarget*, 8(47):81737-81753, 2017. PMID: 29137219
4. Woodcock CS\*, Huang Y\*, Woodcock SR, Salvatore SR, Singh B, Golin-Bisello F, Davidson NE, Neumann CA, Freeman BA, Wendell SG. Nitro-fatty acid inhibition of triple negative breast cancer cell viability, migration, invasion and tumor growth. *J. Biol. Chem.*, 293 (4), 1120-1137, 2018. (\*contributed equally). PMID:29158255 34.
5. Cao C, Wu H, Vasilatos SN, Chandran U, Qin Y, Wan Y, Oesterreich S, Davidson NE, Huang Y. HDAC5-LSD1 axis regulates antineoplastic effect of natural HDAC inhibitor sulforaphane in human breast cancer cells. *Int. J. Cancer*, 143: 1388-1401, 2018. PMID:29633255
6. Qin Y, Vasilatos SN, Chen L, Wu H, Cao Z, Fu Y, Huang M, Vlad AM, Lu B, Oesterreich S, Davidson NE, Huang Y. Inhibition of histone lysine-specific demethylase 1 elicits breast tumor immunity and enhances antitumor efficacy of immune checkpoint blockade. *Oncogene*, Aug 15, 2018, PMID: 30111819

**Conference abstracts/presentation:**

1. Cao C, Vasilatos S, Oesterreich S, Davidson NE, Huang Y. Functional crosstalk between histone deacetylase 5 (HDAC5) and lysine-specific demethylase 1 (LSD1) as a novel therapeutic target in triple-negative breast cancer cells. In: Proceedings of the 106th Annual Meeting of the American Association for Cancer Research; 2015 Apr 18-22; Philadelphia, PA. Philadelphia (PA): AACR; Cancer Res 2015;75(15 Suppl):Abstract nr 3838. doi:10.1158/1538-7445.AM2015-3838.
2. Chen L, Vasilatos SN, Qin Y, Cao C, Wu H, Tasdemir N, Katz TA, Oesterreich S, Davidson NE, Huang Y. New insights into the roles of histone lysine-specific demethylase 2 (LSD2) in breast cancer. In: Proceedings of the American Association for Cancer Research Annual Meeting 2017; 2017 Apr 1-5; Washington, DC. Philadelphia (PA): AACR; Cancer Res 2017;77(13 Suppl):Abstract nr 1385. doi:10.1158/1538-7445.AM2017-1385.

(b) **Website(s) or other Internet site(s)** Nothing to Report

(c) **Technologies or techniques** Nothing to Report

(d) **Inventions, patent applications, and/or licenses** Nothing to Report

(e) **Other Products** Nothing to Report

**6. PARTICIPANTS & OTHER COLLABORATING ORGANIZATIONS**

**a) Individuals have worked on the project**

Name:	Steffi Oesterreich	Yi Huang	Nancy E. Davidson	Ye Qin	Chunyu Cao	Shauna Vasilatos	Hao Wu
Project Role:	Partnering-PI	Initiating-PI	Partnering-PI	Postdoc Fellow	Postdoc Fellow	Technician	Visiting scholar
Researcher Identifier (e.g. ORCID ID):	<a href="https://orcid.org/0000-0002-2537-6923">https://orcid.org/0000-0002-2537-6923</a>	<a href="https://orcid.org/0000-0002-9982-117X">https://orcid.org/0000-0002-9982-117X</a>	N/A	N/A	N/A	N/A	N/A
Nearest person month worked:	1.2	3.6	1.2	9.6	6.0	9.0	12.0
Contribution to Project:	Oversaw epigenetic drug studies and animal experiments, interpreted the results generated from combination and <i>in vivo</i> studies	Designed and oversaw the studies to investigate the molecular mechanisms and biological consequences of the functional interplay between HDAC5 and LSD1 in TNBC	Oversaw IHC studies and animal experiments, and interpreted the results generated from <i>in vivo</i> studies	Postdoc fellow. Performed experiments and prepared manuscript	Studied molecular mechanisms by which LSD1 and HDAC5 interacted, and carried out animal study	Performed microarray studies and data analysis	Carried out the experiments to examine the explore the molecular mechanisms underlying SFN induced suppression of HDAC5 transcription
Funding Support:	CDMRP Breast Cancer Breakthrough Award	CDMRP Breast Cancer Breakthrough Award	CDMRP Breast Cancer Breakthrough Award	CDMRP Breast Cancer Breakthrough Award	CDMRP Breast Cancer Breakthrough Award	CDMRP Breast Cancer Breakthrough Award	CDMRP Breast Cancer Breakthrough Award

**b) Has there been a change in the active other support of the PD/PI(s) or senior/key personnel since the last reporting period?**

N/A

**c) What other organizations were involved as partners?**

N/A

## 7. SPECIAL REPORTING REQUIREMENTS

COLLABORATIVE AWARDS: Initiating PI, Dr. Yi Huang, will submit his annual report separately.

QUAD CHARTS: N/A

**9. APPENDICES:** Copies of publications.

ORIGINAL ARTICLE

# Functional interaction of histone deacetylase 5 (HDAC5) and lysine-specific demethylase 1 (LSD1) promotes breast cancer progression

C Cao<sup>1,2,3</sup>, SN Vasilatos<sup>1,3</sup>, R Bhargava<sup>1,3,4</sup>, JL Fine<sup>1,4</sup>, S Oesterreich<sup>1,2,3</sup>, NE Davidson<sup>1,2,3</sup> and Y Huang<sup>1,2,3</sup>

We have previously demonstrated that crosstalk between lysine-specific demethylase 1 (LSD1) and histone deacetylases (HDACs) facilitates breast cancer proliferation. However, the underlying mechanisms are largely unknown. Here, we report that expression of HDAC5 and LSD1 proteins were positively correlated in human breast cancer cell lines and tissue specimens of primary breast tumors. Protein expression of HDAC5 and LSD1 was significantly increased in primary breast cancer specimens in comparison with matched-normal adjacent tissues. Using HDAC5 deletion mutants and co-immunoprecipitation studies, we showed that HDAC5 physically interacted with the LSD1 complex through its domain containing nuclear localization sequence and phosphorylation sites. Although the *in vitro* acetylation assays revealed that HDAC5 decreased LSD1 protein acetylation, small interfering RNA (siRNA)-mediated HDAC5 knockdown did not alter the acetylation level of LSD1 in MDA-MB-231 cells. Overexpression of HDAC5 stabilized LSD1 protein and decreased the nuclear level of H3K4me1/me2 in MDA-MB-231 cells, whereas loss of HDAC5 by siRNA diminished LSD1 protein stability and demethylation activity. We further demonstrated that HDAC5 promoted the protein stability of USP28, a bona fide deubiquitinase of LSD1. Overexpression of USP28 largely reversed HDAC5-KD-induced LSD1 protein degradation, suggesting a role of HDAC5 as a positive regulator of LSD1 through upregulation of USP28 protein. Depletion of HDAC5 by shRNA hindered cellular proliferation, induced G1 cell cycle arrest, and attenuated migration and colony formation of breast cancer cells. A rescue study showed that increased growth of MDA-MB-231 cells by HDAC5 overexpression was reversed by concurrent LSD1 depletion, indicating that tumor-promoting activity of HDAC5 is an LSD1 dependent function. Moreover, overexpression of HDAC5 accelerated cellular proliferation and promoted acridine mutagen ICR191-induced transformation of MCF10A cells. Taken together, these results suggest that HDAC5 is critical in regulating LSD1 protein stability through post-translational modification, and the HDAC5–LSD1 axis has an important role in promoting breast cancer development and progression.

Oncogene (2017) 36, 133–145; doi:10.1038/onc.2016.186; published online 23 May 2016

## INTRODUCTION

Lysine-specific demethylase 1 (LSD1) is the first identified FAD-dependent histone demethylase that has been typically found in association with a transcriptional repressor complex that includes CoREST, HDAC1/2, BHC80 and others.<sup>1–4</sup> A role for elevated expression of LSD1 has been implicated in tumorigenesis in various cancers including breast cancer.<sup>3,5–9</sup> Studies from our and other laboratories consistently showed that inhibition of LSD1 hindered proliferation of breast cancer cells.<sup>6,8,10</sup> Lim *et al.*<sup>6</sup> reported that LSD1 is highly expressed in estrogen receptor-negative breast cancers. A recent study found that LSD1 is significantly overexpressed in high-grade ductal carcinoma *in situ* or invasive ductal carcinoma versus low/intermediate ductal carcinoma *in situ*.<sup>11</sup> These studies point to a tumor-promoting role for LSD1 in breast cancer. We were among the first to report the use of small-molecule compounds and preclinical treatment strategies that have promise to work through this target in cancer.<sup>8,9,12</sup> The development of novel LSD1 inhibitors is progressing rapidly. For example, a new generation of (bis)urea/(bis)thiourea LSD1 inhibitors displayed improved potency against LSD1 in cancer cells.<sup>13</sup> A newly reported

GSK-LSD1 inhibitor exhibited interesting cell type-specific inhibition against small-cell lung cancer cells in preclinical models.<sup>14</sup>

However, how LSD1 is upregulated in breast cancer and the precise role of LSD1 in breast cancer development are still unclear. Our most recent work showed that small interfering RNA (siRNA)-mediated inhibition of HDAC5 led to a significant increase of H3K4me2, a known substrate of LSD1, suggesting a potential role of HDAC5 in regulating LSD1 activity.<sup>10</sup> However, little is known about the precise role of HDAC5 and mechanisms underlying its regulation on LSD1 activity in breast cancer. HDAC5 is an important member of class IIa histone deacetylase (HDAC) isozymes with important functions in transcriptional regulation, cell proliferation, cell cycle progression and cellular developmental activities.<sup>15,16</sup> HDAC5 has been shown to have important roles in many diseases including cancer.<sup>17,18</sup> In this study, we addressed the following clinically relevant issues that have been understudied: (1) Is elevation of LSD1 expression associated with HDAC5 overexpression during breast cancer development? (2) How is LSD1 regulated by HDAC5 in breast cancer? (3) What is the role of the HDAC5–LSD1 axis in breast cancer initiation, proliferation and metastasis? To answer these questions, we delineated the

<sup>1</sup>University of Pittsburgh Cancer Institute, University of Pittsburgh, Pittsburgh, PA, USA; <sup>2</sup>Department of Pharmacology & Chemical Biology, University of Pittsburgh, Pittsburgh, PA, USA; <sup>3</sup>Women's Cancer Research Center, University of Pittsburgh, Pittsburgh, PA, USA and <sup>4</sup>Department of Pathology, University of Pittsburgh, Pittsburgh, PA, USA. Correspondence: Dr Y Huang, Magee Womens Research Institute, Room 406, 204 Craft Avenue, Pittsburgh, PA 15213, USA. E-mail: yih26@pitt.edu

Received 12 November 2015; revised 21 March 2016; accepted 14 April 2016; published online 23 May 2016

mechanisms underlying the functional link between LSD1 and HDAC5 in chromatin remodeling and demonstrated that these two important chromatin modifiers closely cooperate to mediate proliferation, cell cycle and metastasis of breast cancer cells.

## RESULTS

HDAC5 and LSD1 proteins are coordinately expressed in human breast cancer

To study the potential association of HDAC5 and LSD1 in breast cancer, we first examined mRNA levels of HDAC5 and LSD1 in human immortalized normal mammary epithelial MCF10A cells, fully malignant MCF10A-CA1a cells transformed from MCF10A cells with transfection of *HRAS*,<sup>19</sup> and several human breast cancer cell lines. Quantitative PCR (qPCR) studies showed that there was no clear association of mRNA expression between HDAC5 and LSD1 in breast cancer cell lines (Figure 1a). The Oncomine-TCGA database showed moderate change of the mRNA level of LSD1 and HDAC5 in IBC (Supplementary Figures 1a and b). mRNA levels of both HDAC5 and LSD1 are altered in ~6% of breast cancer patients (www.cbioportal.org) without an apparent association with specific subtypes (Supplementary Figures 1c and d). However, protein expression of both HDAC5 and LSD1 was significantly elevated in malignant breast cell lines compared with MCF10A (Figure 1b), and protein levels of HDAC5 and LSD1 were positively correlated (Figure 1c). The correlation of HDAC5 and LSD1 protein expression was further validated in 50 primary breast cancers using immunohistochemical staining with validated antibodies (Supplementary Figures 2a and b). The  $\chi^2$  analysis showed a statistically significant correlation between HDAC5 and LSD1 protein expression in these tumors (Figure 1d). Furthermore, the immunohistochemistry (IHC) analysis showed that breast cancer tissues ( $n=18$ ) expressed significantly higher level of HDAC5 and LSD1 than matched-normal adjacent tissues ( $n=18$ ) (Figure 1e). The mean H-score for HDAC5 staining in stage 3 breast tumors ( $n=25$ ) was statistically significantly higher than stage 2 counterparts ( $n=25$ ). The mean H-score of LSD1 staining for stage 3 tumors was also higher than that of stage 2 tumors with a  $P$ -value of 0.07 (Figure 1f). These results were further validated with independent manual H-score evaluations by two breast cancer pathologists with moderate interobserver concordance (Supplementary Figures 3a and b). Taken together, these findings suggest that HDAC5 and LSD1 proteins are coordinately overexpressed in breast cancer cell lines and tissue specimens.

Physical interaction of LSD1 and HDAC5 in breast cancer cells

To address whether LSD1 and HDAC5 physically interact, a co-immunoprecipitation study was carried out in MDA-MB-231 and MCF10A-CA1a cells transiently transfected with pcDNA3.1 or pcDNA3.1-FLAG-HDAC5 plasmids. After immunoprecipitation (IP) with LSD1 antibody, we found that both endogenous and exogenous HDAC5 proteins were co-immunoprecipitated with LSD1 protein (Figure 2a). The interaction between native LSD1 and HDAC5 was further validated in additional breast cancer cell lines (Figure 2b). A similar result was obtained in the reciprocal immunoprecipitation using anti-FLAG antibody to confirm that

LSD1 was co-immunoprecipitated with FLAG-HDAC5 (Figure 2c). To precisely map the HDAC5 domain(s) responsible for interaction with LSD1, we expressed a series of HDAC5 deletion mutants engineered in pcDNA3.1-FLAG plasmids in MDA-MB-231 cells (Figure 2d). Immunoprecipitation assays of cells transfected with full-length HDAC5 complementary DNA (cDNA) confirmed the HDAC5–LSD1 interaction and deletion of an N-terminal myocyte enhancer factor-2 (MEF2) binding domain (HDAC5- $\Delta$ 1) alone had no impact on HDAC5–LSD1 interaction. However, removal of both the MEF2 domain and nuclear localization sequence (NLS) (HDAC5- $\Delta$ 2) completely abolished HDAC5–LSD1 interaction. Further deletion of an N-terminal HDAC and nuclear export sequence (HDAC5- $\Delta$ 3) and MEF2 domain (HDAC5- $\Delta$ 4) did not adversely alter LSD1 binding with HDAC5 fragments (Figure 2e). Immunofluorescence studies showed nuclear localization of full-length HDAC5, HDAC5- $\Delta$ 1, HDAC5- $\Delta$ 3 and HDAC5- $\Delta$ 4. Depletion of the NLS-containing domain (HDAC5- $\Delta$ 2) completely blocked HDAC5 nuclear translocation (Figure 2f). *In vitro* pull-down assays by using His-tag recombinant LSD1 protein incubating with HDAC5 full-length or deletion mutants validated that HDAC5 domain containing NLS element is essential for interaction with LSD1 (Supplementary Figure 4).

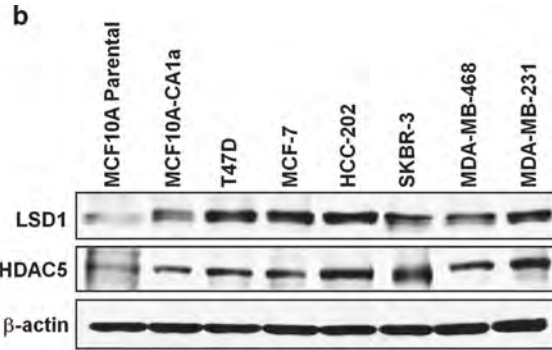
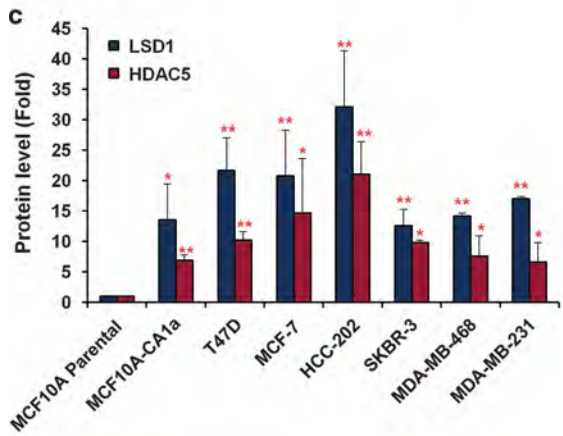
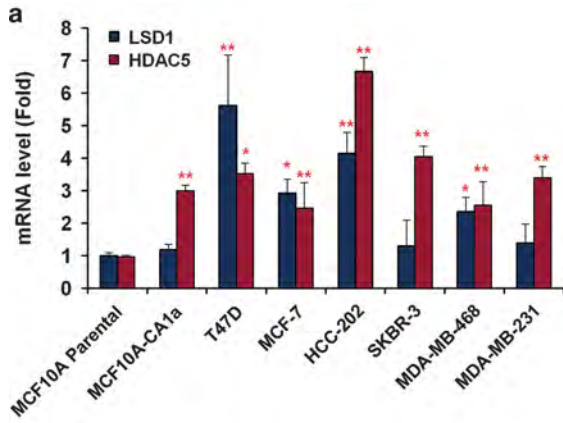
HDAC5 promotes LSD1 protein stability and activity

Next, we examined whether the mRNA or protein levels of HDAC5 and LSD1 were affected by their interaction with each other. Overexpression of HDAC5 in MDA-MB-231 cells failed to alter LSD1 mRNA expression, but led to a significant increase of LSD1 protein expression (Figures 3a and b). HDAC5 knockdown by siRNA attenuated LSD1 protein expression without affecting its mRNA level (Figures 3c and d). The effect of LSD1 on HDAC5 expression was subsequently assessed using our previously established MDA-MB-231-LSD1-KD cells.<sup>10</sup> Depletion of LSD1 exerted no effect on HDAC5 mRNA or protein levels (Figures 3e and f). Simultaneous overexpression of pcDNA3.1-HDAC5 with HDAC5 siRNA significantly reversed the decrease of LSD1 (Supplementary Figure 5a). These results suggest that HDAC5 functions as an upstream regulator that governs LSD1 protein stability via post-translational regulation. Quantitative immunoblots showed that levels of H3K4me1/2 and AcH3K9, the substrates for LSD1 and HDAC5, respectively, were downregulated by HDAC5 overexpression, whereas loss of HDAC5 exerted the opposite effect (Figure 3g; Supplementary Figure 5b), suggesting a critical role of HDAC5 in governing chromatin modifying activity of LSD1. The cycloheximide chase assay showed that overexpression of HDAC5 significantly extended LSD1 protein half-life, whereas depletion of HDAC5 by siRNA decreased LSD1 protein half-life in MDA-MB-231 cells (Figures 3h and i; Supplementary Figure 5c). To determine whether other recognized LSD1 cofactors or HDACs exert similar effects on LSD1 protein stability, MDA-MB-231 cells were treated with siRNA against several LSD1 complex cofactors (CoREST, HDAC1 and HDAC2) or other class II HDAC isozymes (HDAC 4, 6, 7, 9, 10), respectively. Transfection with siRNA probes effectively knocked down mRNA expression of target genes without affecting LSD1 protein level (Figure 3j; Supplementary Figure 6a). To confirm the qPCR results, quantitative immunoblotting (IB) was performed and showed depletion of

**Figure 1.** Correlated overexpression of HDAC5 and LSD1 protein in breast cancer. **(a)** The levels of mRNA expression of HDAC5 and LSD1 in breast cancer cell lines versus MCF10A cells (set as fold 1) using real-time qPCR with  $\beta$ -actin as an internal control. **(b)** Immunoblots with anti-HDAC5 and LSD1 antibodies in indicated cell lines.  $\beta$ -actin protein was blotted as a loading control. **(c)** Histograms represent the mean protein levels of HDAC5 or LSD1 in three determinations relative to  $\beta$ -actin  $\pm$  s.d. as determined by quantitative immunoblots. **(d)** 50 primary human invasive breast tumor samples were immunostained with antibodies against HDAC5 or LSD1. The  $\chi^2$  study was performed by using median H-scores as the cutoff for high- versus low-protein expression. **(e)** Representative HDAC5 and LSD1 staining (200 $\times$ ) in invasive breast carcinoma and adjacent normal tissue specimens from one representative patient. H-scores represent average staining intensity in breast tumors ( $n=18$ ) versus adjacent normal breast tissue ( $n=18$ ). **(f)** Representative HDAC5 and LSD1 staining (200 $\times$ ) in stage 2 and 3 invasive breast carcinoma specimens. H-scores represent average staining intensity in stage 3 breast tumors ( $n=25$ ) versus stage 2 breast tumors ( $n=25$ ). \* $P < 0.05$ , \*\* $P < 0.01$ , \*\*\* $P < 0.001$ , Student's  $t$ -test.

CoREST led to insignificant change of LSD1 protein stability (Supplementary Figure 6b and 6c). Together, these results strengthen the conclusion that HDAC5 functions as a positive regulator of LSD1 protein in breast cancer cells.

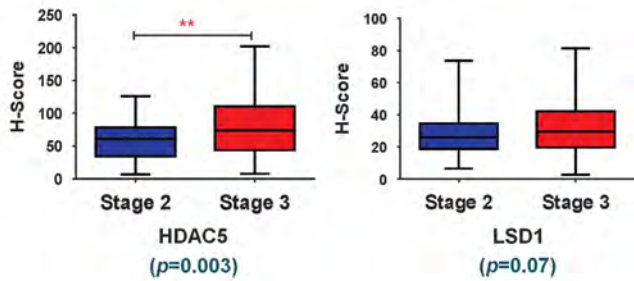
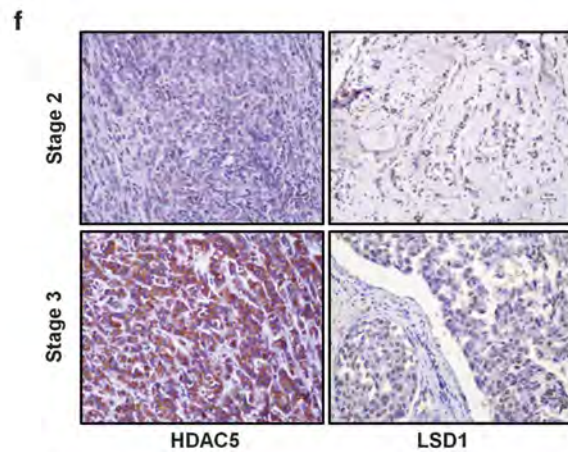
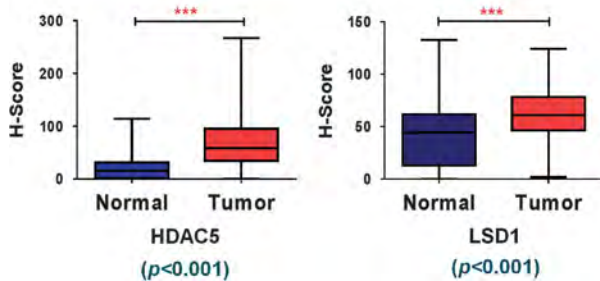
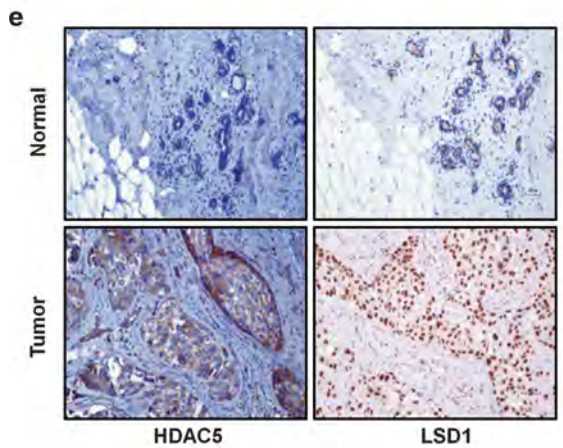
HDAC5 regulates LSD1 protein stability through modulation of the LSD1-associated ubiquitination system  
Protein ubiquitination assays indicated that HDAC5 overexpression significantly attenuated LSD1 polyubiquitination (Figure 4a),



**d** Correlation between HDAC5 and LSD1 expression in invasive breast cancer tissue specimens (n=50)

	HDAC5 High	HDAC5 Low	Total
LSD1 High	15	9	24
LSD1 Low	9	17	26
Total	24	26	50

Chi-square  $p=0.048$





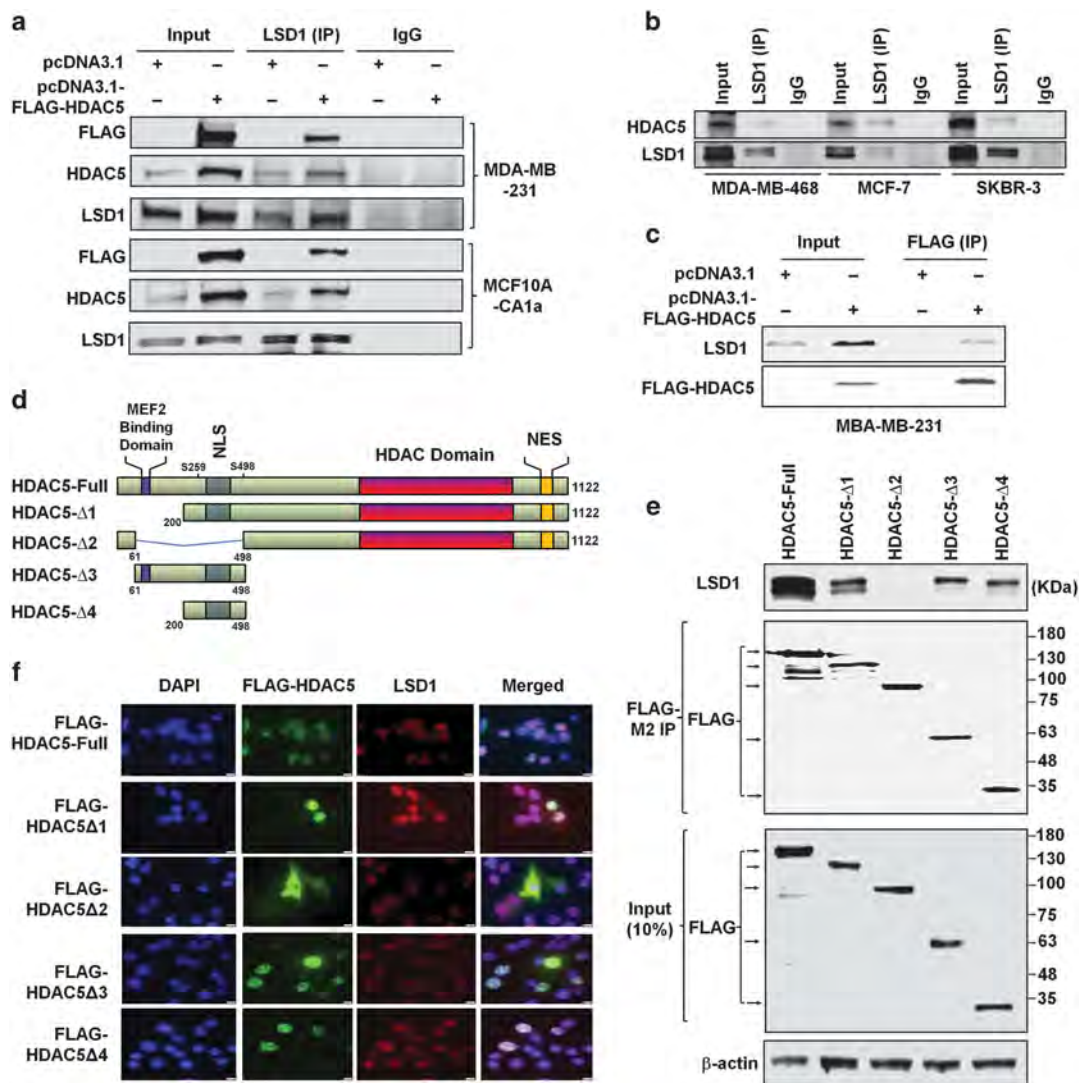


**Figure 2.** HDAC5 and LSD1 physically interact in breast cancer cells. **(a)** MDA-MB-231 or MCF10A-CA1a cells were transfected with control vector pcDNA3.1 or pcDNA3.1-HDAC5 plasmids. IP was performed with anti-LSD1 antibody followed by immunoblotting (IB) with anti-LSD1, anti-FLAG or anti-HDAC5 antibodies, respectively. **(b)** Whole-cell lysates were immunoprecipitated with anti-LSD1 antibody followed by IB with anti-HDAC5 and LSD1 antibodies in indicated breast cancer cell lines. IgG was used as negative control. **(c)** MDA-MB-231 cells were transfected with control vector pcDNA3.1 or pcDNA3.1-HDAC5-FLAG plasmids, and IP was performed with anti-FLAG followed by IB with anti-LSD1 and anti-FLAG antibodies, respectively. **(d)** Schematic representation of full-length and deletion mutants of HDAC5-FLAG constructs. **(e)** FLAG-tagged full-length or deletion mutants of HDAC5 were expressed in MDA-MB-231 cells. Extracts were immunoprecipitated with anti-FLAG antibody, and bound LSD1 was examined by IB using anti-LSD1 antibody. IB with anti-FLAG was used to detect the levels of FLAG-tagged HDAC5 full-length or deletion mutants in IP and input (10%) samples. **(f)** MDA-MB-231 cells were transfected with plasmids expressing FLAG-tagged full-length or deletion mutants of HDAC5 proteins. Immunofluorescence study was performed using anti-FLAG antibody. 4,6-Diamidino-2-phenylindole was used as a control for nuclear staining. All the experiments were performed three times with similar results.

whereas depletion of HDAC5 by siRNA facilitated LSD1 polyubiquitination (Supplementary Figure 7a). Recently, Jade-2 and USP28 were identified as specific E3 ubiquitin ligase and deubiquitinase for LSD1, respectively.<sup>20,21</sup> Our study showing that increase of LSD1 protein expression by Jade-2 siRNA and decrease of LSD1 protein expression by USP28 siRNA in MDA-MB-231 cells confirmed the roles of Jade-2/USP28 as LSD1 ubiquitin ligase/deubiquitinase in breast cancer cells (Figure 4b; Supplementary Figure 7b). qPCR studies demonstrated that mRNA level of either Jade-2 or USP28 was not altered by HDAC5 knockdown or overexpression (Figure 4c). The regulation of HDAC5 on protein expression of Jade-2 or USP28 was subsequently assessed. Due to the lack of highly specific antibody against Jade-2, plasmids expressing Jade-2-FLAG fusion protein were transfected into cells as an alternative approach. MDA-MB-231 and MCF10A-CA1a cells

expressing Jade-2-FLAG protein were simultaneously treated with HDAC5 siRNA to evaluate the effect of HDAC5 on Jade-2 protein expression. Immunoblot showed that depletion of HDAC5 did not change the protein level of Jade-2 (Figure 4d). However, overexpression of HDAC5 led to significant increase of USP28 protein expression in both cell lines (Figure 4e). *In vitro* pull-down assay using His-tag recombinant LSD1 protein incubated with USP28-FLAG protein indicated a direct interaction of LSD1 and USP28 (Supplementary Figure 4), and HDAC5 overexpression significantly attenuated USP28 polyubiquitination (Supplementary Figure 7c). To understand whether HDAC5 may stabilize LSD1 protein through upregulation of USP28 protein stability, a rescue study was carried out in MDA-MB-231 and MCF10A-CA1a cells using concurrent transfection of HDAC5 siRNA and USP28 expression plasmids, and showed that overexpression of USP28

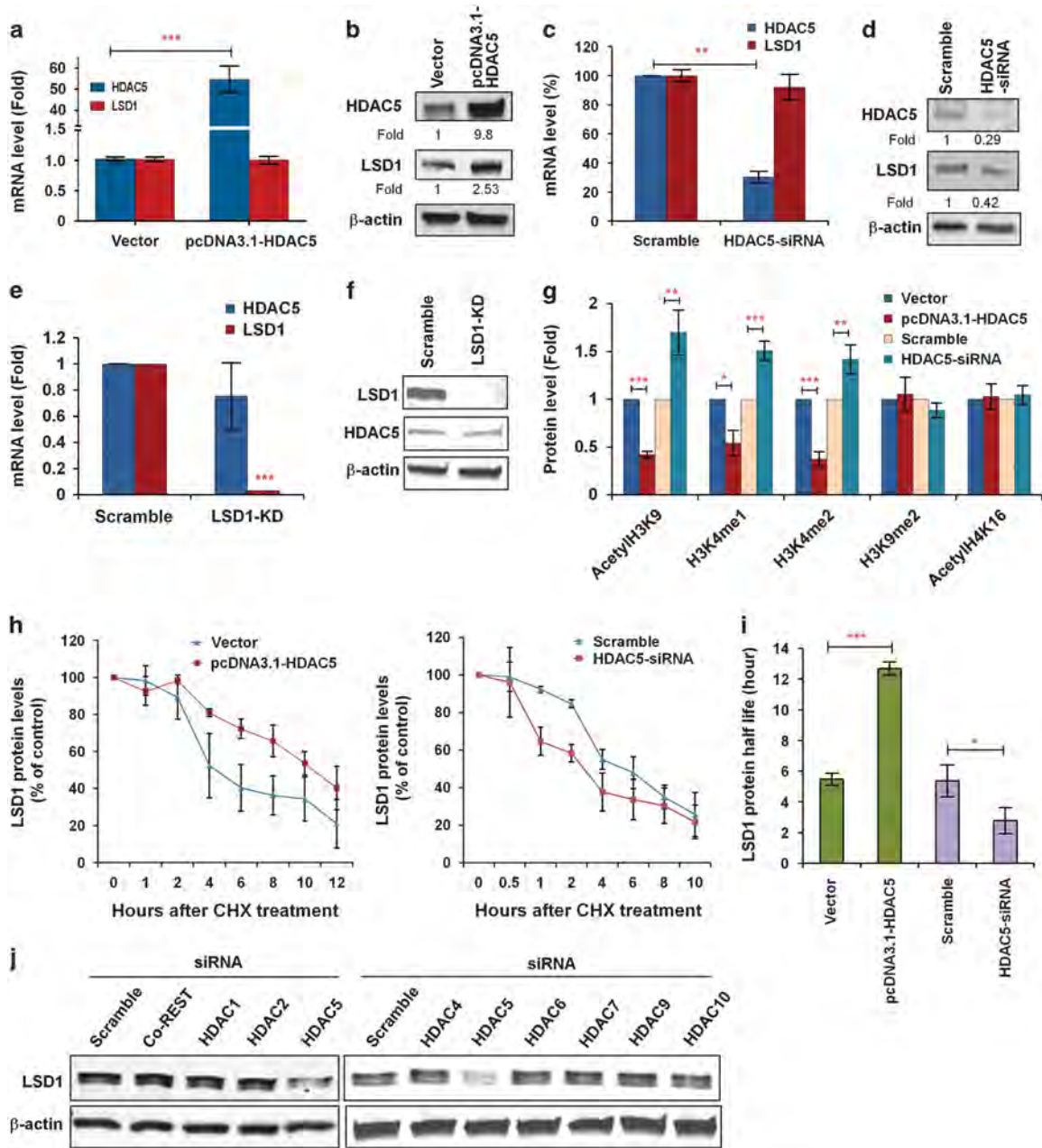


**Figure 3.** HDAC5 stabilizes LSD1 protein in breast cancer cells. **(a)** MDA-MB-231 cells were transfected with control vector pcDNA3.1 or pcDNA3.1-HDAC5 for 48 h. mRNA expression of HDAC5 and LSD1 was measured by quantitative real-time PCR with  $\beta$ -actin as an internal control. **(b)** MDA-MB-231 cells were transfected with control vector pcDNA3.1 or pcDNA3.1-HDAC5 plasmids for 48 h. Effect of HDAC5 overexpression on LSD1 protein expression in MDA-MB-231 cells was evaluated by immunoblots with anti-LSD1 and anti-HDAC5 antibodies. **(c)** MDA-MB-231 cells were transfected with scramble siRNA or HDAC5 siRNA for 48 h. Effect of HDAC5 knockdown on LSD1 mRNA expression was examined by quantitative real-time PCR with  $\beta$ -actin as internal control. **(d)** Effect of HDAC5 siRNA on LSD1 protein expression in MDA-MB-231 cells. **(e)** Effect of depletion of LSD1 on mRNA expression of HDAC5 in MDA-MB-231-Scramble or MDA-MB-231-LSD1-KD cells. **(f)** Effect of LSD1-KD on protein expression of HDAC5 in MDA-MB-231-scramble or MDA-MB-231-LSD1-KD cells. **(g)** MDA-MB-231 cells were transfected with control vector pcDNA3.1, pcDNA3.1-HDAC5, scramble siRNA or HDAC5 siRNA for 48 h and analyzed by immunoblots for nuclear expression of indicated histone marks. Proliferating cell nuclear antigen was used as loading control. **(h)** Effect of HDAC5 overexpression or siRNA on LSD1 protein half-life in cycloheximide chase study. **(i)** Measurement of LSD1 half-life using the CalcuSyn program. **(j)** Effect of siRNA knockdown of LSD1 cofactors or class II HDACs on LSD1 protein level. All the experiments were performed three times. Bars represent the mean of three independent experiments  $\pm$  s.d. \* $P$  < 0.05, \*\* $P$  < 0.01, \*\*\* $P$  < 0.001, Student's *t*-test.

completely blocked the destabilization of LSD1 by HDAC5 depletion (Figure 4f; Supplementary Figure 7d). In an additional rescue experiment, overexpression of HDAC5 failed to promote LSD1 protein expression when cells were simultaneously treated with USP28 by siRNA (Supplementary Figure 7e). All these data

support the notion that HDAC5 stabilizes LSD1 protein by enhancing protein expression of its deubiquitinase.

To examine whether interaction of HDAC5 with the LSD1/USP28 complex deacetylates LSD1 or USP28, *in vitro* protein acetylation assays was first carried out by incubating GST-tagged recombinant

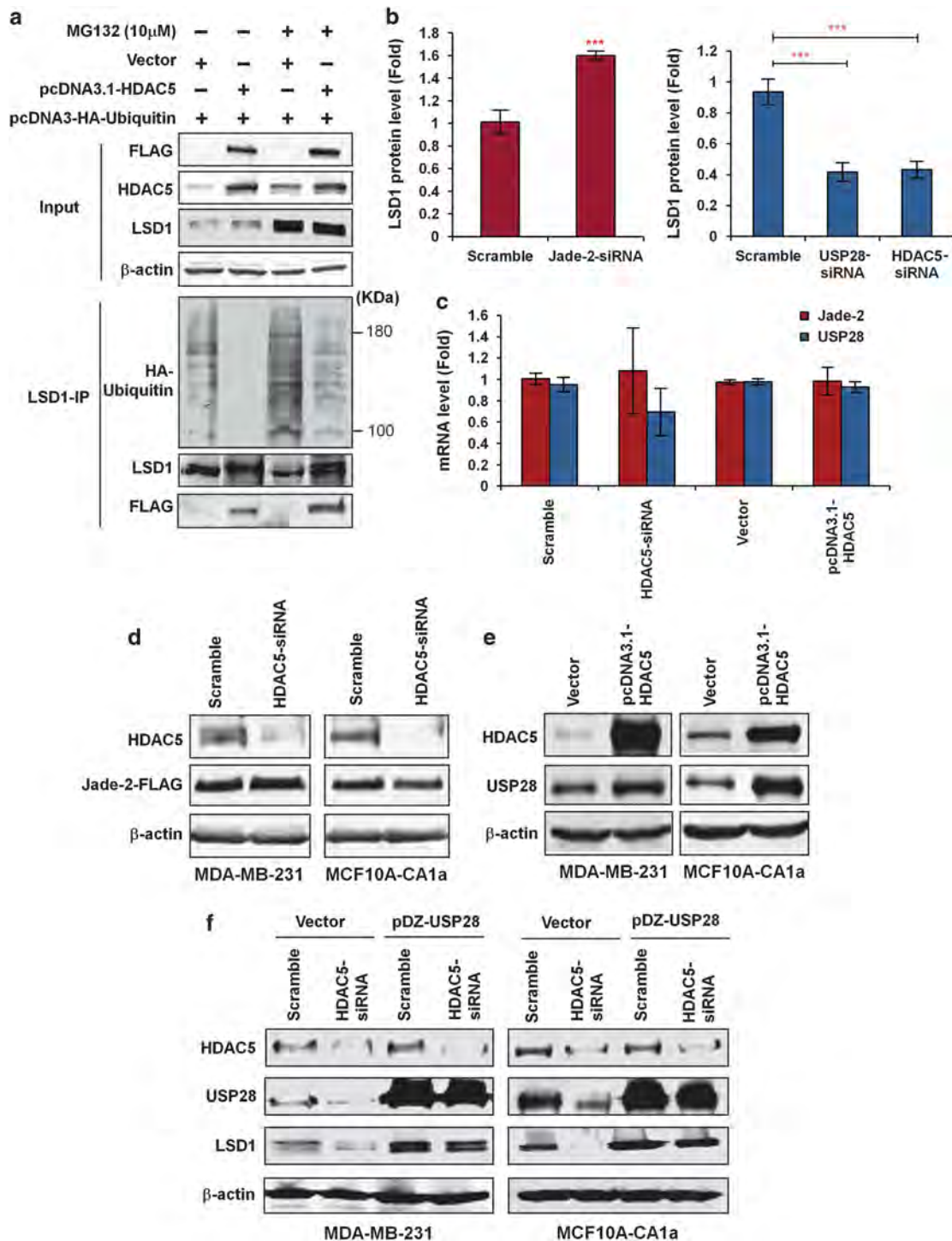


**Figure 4.** HDAC5 regulates LSD1 by altering USP28 stability. **(a)** MDA-MB-231 cells transfected with pcDNA3.1-FLAG, pcDNA3.1-FLAG-HDAC5 or pcDNA3-HA-ubiquitin plasmids were treated with or without proteasome inhibitor 10  $\mu$ M MG132 for 10 h followed by IP using LSD1 antibody and immunoblots with anti-HA, LSD1 or HDAC5 antibodies. **(b)** Effect of siRNA of Jade-2, USP28 and HDAC5 on LSD1 protein expression in MDA-MB-231 cells. Results represent the mean of three independent experiments  $\pm$  s.d.  $***P < 0.001$ , Student's *t*-test. **(c)** MDA-MB-231 cells were transfected with scramble siRNA, HDAC5 siRNA, control vector pcDNA3.1 or pcDNA3.1-HDAC5 plasmids for 48 h. mRNA expression of Jade-2 and USP28 was measured by qPCR.  $\beta$ -actin was used as an internal control. **(d)** MDA-MB-231 or MCF10A-CA1a cells were simultaneously transfected with pcDNA3.1-FLAG-Jade-2 and HDAC5 siRNA for 48 h and subjected to immunoblots with anti-HDAC5 or Jade-2 antibodies.  $\beta$ -actin was used as loading control to normalize target protein levels. **(e)** After MDA-MB-231 or MCF10A-CA1a cells were transfected with control vector pcDNA3.1 or pcDNA3.1-HDAC5 plasmids for 48 h, IB was performed for expression of HDAC5 and USP28. **(f)** MDA-MB-231 or MCF10A-CA1a cells were transfected with scramble or HDAC5 siRNA alone, or in combination with pDZ-USP28 for 48 h. Whole-cell lysates were analyzed for protein levels of HDAC5, USP28 and LSD1.  $\beta$ -actin was used as loading control to normalize target protein levels. The experiments were performed three times with similar results.

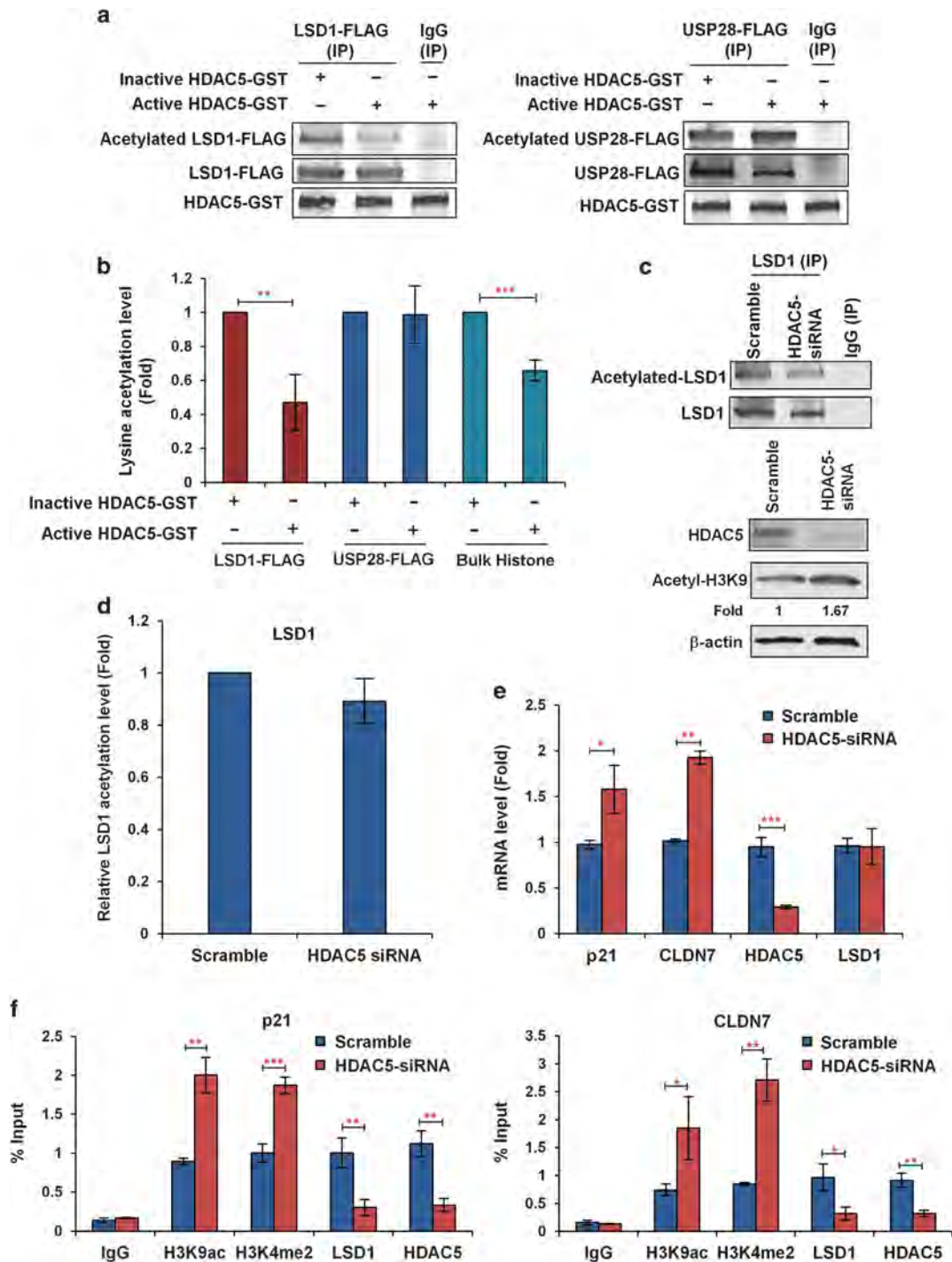
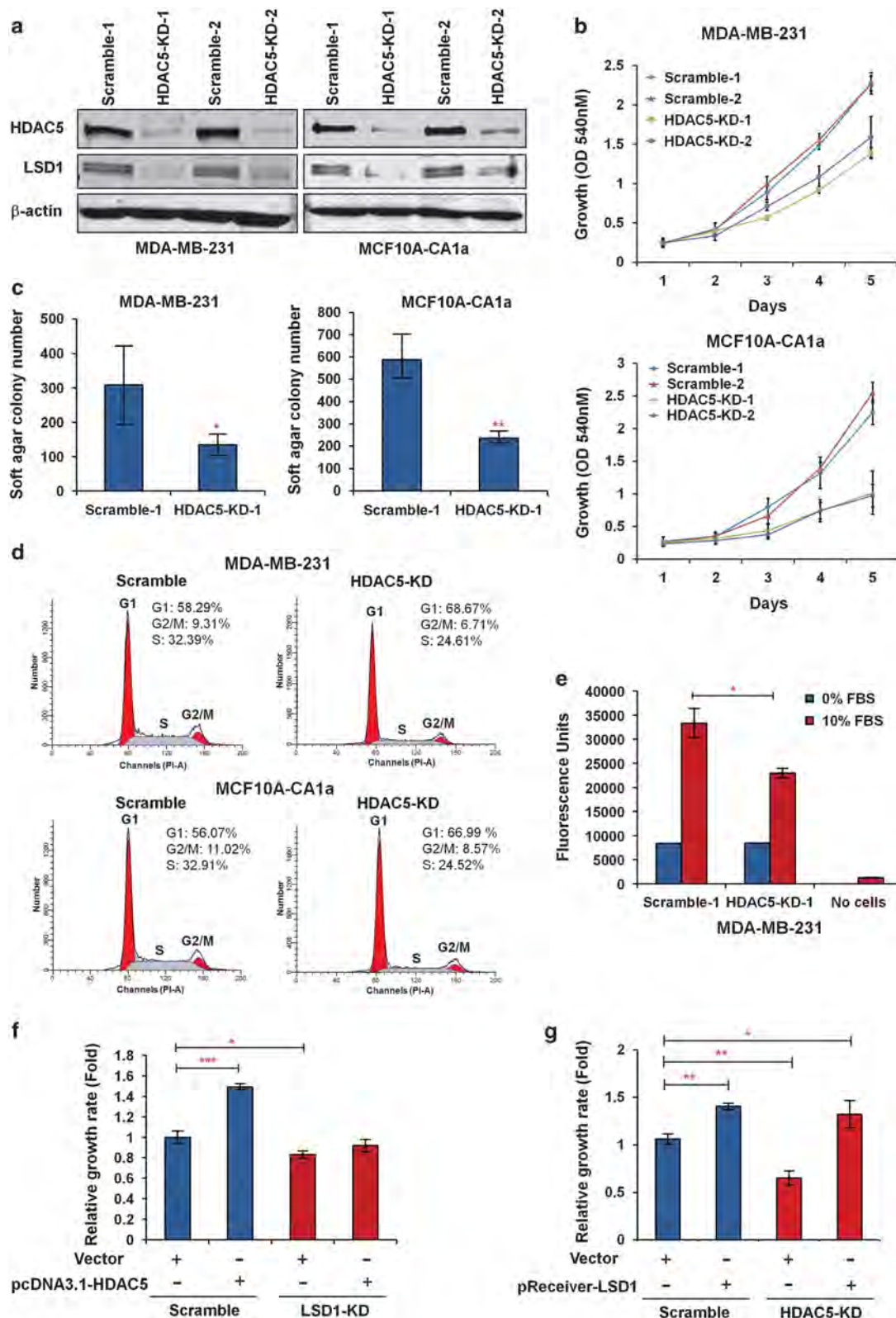


**Figure 5.** Effect of HDAC5 on protein acetylation of LSD1/USP28 and transcription of LSD1 target genes. **(a)** The immunoprecipitates of FLAG using FLAG-M2 agarose from MDA-MB-231 cells overexpressing FLAG-tagged USP28 or FLAG-tagged LSD1 were used as substrates for protein deacetylation assay. IgG was used as negative control. Active or heat inactivated recombinant human GST-tagged HDAC5 protein were mixed with immunoprecipitates and incubated at 37 °C for 6 h as described in ‘Materials and Methods’. The reactions were then subjected to immunoblots with anti-acetyl lysine antibody. FLAG-tagged USP28 or LSD1 proteins were probed with anti-FLAG antibody. HDAC5-GST protein was probed with anti-HDAC5 antibody. **(b)** Histograms represent the means of levels of acetyl-LSD1, acetyl-USP28 and acetyl-histone determined by quantitative IB using infrared IB detection and analysis. **(c)** MDA-MB-231 cell transfected with scramble or HDAC5 siRNAs for 48 h. LSD1 or IgG antibodies were added to cell lysate. IP was performed with anti-LSD1 antibody followed by IB with anti-acetyl lysine and anti-LSD1 antibodies, respectively. Effect of HDAC5 siRNA on AcetylH3K9 protein expression in MDA-MB-231 cells was examined by IB with anti-acetyl-H3K9 antibody. **(d)** Histograms represent the means of relative levels of acetyl-LSD1 determined by quantitative IB using infrared IB detection and analysis. **(e)** mRNA expression of indicated genes in MDA-MB-231 cells transfected with scramble siRNA or HDAC5 siRNA. Data are means  $\pm$  s.d. of three independent experiments. **(f)** Quantitative chromatin immunoprecipitation (ChIP) analysis was used to determine the occupancy by acetyl-H3K9, H3K4me2, LSD1 and HDAC5 at promoters of p21 or CLDN7 in MDA-MB-231 cells transfected with scramble or HDAC5 siRNA. \* $P < 0.05$ , \*\* $P < 0.01$ , \*\*\* $P < 0.001$ , Student’s *t*-test.

HDAC5 protein with cellular pull-down of LSD1-FLAG or USP28-FLAG by IP, and immunoprecipitates of IgG was incubated with recombinant HDAC5 protein as negative control of assays (Figure 5a). Bulk histone was used as control substrate (Supplementary Figure 8). Quantitative immunoblots using antibody against pan-acetylated lysine: showed that HDAC5 reduced

acetylation level of LSD1 without altering the acetylation status of USP28 (Figures 5a and b). Next, the *in vivo* effect of HDAC5 depletion on LSD1 acetylation was investigated in MDA-MB-231 cells transfected with scramble or HDAC5 siRNAs. After immunoprecipitation with LSD1 antibody or IgG (negative control), IB was performed and the results showed that expression levels of both



total LSD1 protein and acetylated LSD1 protein were decreased by HDAC5 depletion (Figure 5c). Quantitative immunoblots indicated that the relative acetylation level of LSD1 was not statistically altered by HDAC5 siRNA in MDA-MB-231 cells (Figure 5d). Acetyl-H3K9 was used as control of substrate and its expression was increased by HDAC5 siRNA (Figure 5c). These results suggest that inhibition of HDAC5 alone is not sufficient enough to increase LSD1 acetylation in breast cancer cells.

Inhibition of HDAC5 reactivates expression of LSD1 target genes. In cancer cells, amplified LSD1 expression is frequently associated with abnormal suppression of key tumor suppressor genes.<sup>3,22</sup> We next examined whether expression of LSD1 target tumor suppressor genes could be reactivated following HDAC5 inhibition. Loss of expression of cyclin-dependent kinase inhibitor p21 and epithelial marker claudin-7 (CLDN7) has been reported to be associated with an aggressive phenotype of breast cancer.<sup>23,24</sup> The transcription activity of p21 and CLDN7 has been found to be suppressed by enhanced activity of LSD1 in breast cancer.<sup>6,25</sup> Transfection of HDAC5 siRNA resulted in significantly increased mRNA expression of p21 and CLDN7 in MDA-MB-231 cells (Figure 5e). Quantitative chromatin immunoprecipitation assays revealed that depletion of HDAC5 decreased occupancy of both HDAC5 and LSD1, and increased enrichment of H3K4me2 and acetyl-H3K9 at the promoters of both genes (Figure 5f). These data suggest that transcriptional de-repression of these genes lies largely in the cooperation between HDAC5 and LSD1 at key active histone marks.

**Inhibition of HDAC5–LSD1 axis hinders breast cancer proliferation and invasion**

To explore the functional role of the HDAC5–LSD1 axis in regulating breast cancer development, stable knockdown of HDAC5 mRNA (HDAC5-KD) was generated in MDA-MB-231 and MCF10A-CA1a cells by infection with short hairpin RNA (shRNA) lentiviral particles. Similar to the effect of transient inhibition of HDAC5 by siRNA, stable knockdown of HDAC5 expression significantly reduced LSD1 protein expression in two independent HDAC5-KD clones (Figure 6a). Loss of HDAC5 in both clones hindered cell proliferation and colony formation in soft agar (Figures 6b and c). The flow cytometry analysis showed that inhibition of HDAC5 resulted in a greater fraction of cells accumulated at G1 phase and reduction of the S-phase cell fraction (Figure 6d; Supplementary Figure 9). Moreover, loss of HDAC5 attenuated motility and invasion of MDA-MB-231 cells in a Boyden chamber assay (Figure 6e). A rescue experiment indicated that HDAC5 overexpression promoted growth of MDA-MB-231-Scramble cells, but failed to alter the growth of MDA-MB-231-LSD1-KD cells (Figure 6f). An additional rescue study revealed that LSD1 overexpression rescued growth inhibition by HDAC5 depletion in MDA-MB-231-HDAC5-KD cells (Figure 6g). Taken together, these results demonstrate that tumor-promoting activity of HDAC5 is dependent on LSD1 activity in breast cancer cells.

Overexpression of HDAC5 promotes mutagen-induced tumorigenic development in MCF10A cells

To address whether enhanced interaction between HDAC5 and LSD1 is a critical epigenetic alteration driving tumorigenic transformation of breast cancer, we generated two MCF10A cell lines overexpressing HDAC5 (MCF10A-HDAC5). Stable overexpression of HDAC5 in MCF10A cells increased LSD1 protein level and promoted cell proliferation of both clones (Figures 7a and b), indicating a growth-promoting role for HDAC5 in MCF10A cells. Inhibition of LSD1 by shRNA significantly hindered MCF10A growth and reversed the growth promotion mediated by HDAC5 overexpression, suggesting that HDAC5 promotes MCF10A growth in an LSD1 dependent manner (Figure 7c; Supplementary Figure 10). To evaluate if MCF10A-HDAC5 cells have altered susceptibility to tumorigenesis, MCF10A-Vector and MCF10A-HDAC5 cells were cultured for 7 months in medium containing 500 ng/ml ICR191. ICR191 generates genomic instability and genetic variability, and has been successfully used to induce epithelial cell transformation in several models including MCF10A.<sup>26,27</sup> MCF10A-HDAC5 cells were subsequently tested for the capacity of anchorage-independent growth in soft agar for 4 weeks. The soft agar colony formation study demonstrated that ICR191 treatment improved the ability of MCF10A cells to form growing colonies, and overexpression of HDAC5 significantly promoted ICR191-induced colony formation in MCF10A cells (Figure 7d). To determine the role of LSD1 in HDAC5 enhanced tumorigenic transformation induced by ICR191, scramble control and LSD1 shRNA lentivirus particles were infected into MCF10A-Vector or MCF10A-HDAC5 cells, which had been treated with ICR191 for 7 months, and the soft agar growth assays showed that loss of LSD1 in MCF10A-HDAC5 cells significantly abolished cellular ability in colony formation (Figure 7e). A model illustrating the role of HDAC5–LSD1 axis in breast cancer development is proposed based on the above findings (Figure 7f).

## DISCUSSION

High levels of HDAC5 have been found to be associated with poor survival in multiple cancer types.<sup>28,29</sup> LSD1 overexpression has been reported to be a poor prognostic factor in basal-like breast cancer, a subtype with aggressive clinical characteristics.<sup>6,30</sup> In this study, the IHC analysis showed that breast cancers expressed higher levels of HDAC5 compared to the matched-normal adjacent breast tissue. Importantly, our study found a positive correlation between HDAC5 and LSD1 proteins in breast tumor cell lines and patient tissue specimens. Increased expression of HDAC5 and LSD1 is correlated with higher stage of breast cancer in our exploratory study. These findings suggest that the coordinated overexpression of HDAC5 and LSD1 may serve as potential novel prognostic markers as well as possible therapeutic targets for breast cancer. More robust studies will be necessary to understand the precise role of elevated protein expression levels of HDAC5 and LSD1 in the risk stratification of breast cancer patients.

**Figure 6.** HDAC5–LSD1 axis is implicated in breast cancer progression. **(a)** Depletion of HDAC5 by shRNA lentivirus infection downregulated LSD1 protein expression in MDA-MB-231 and MCF10A-CA1a cells. **(b)** Scramble shRNA and HDAC5-KD cells were analyzed for growth and viability by crystal violet assays. **(c)** Soft agar colony formation for HDAC5-KD and scramble control of MDA-MB-231 and MCF10A-CA1a cells. **(d)** Scramble shRNA and HDAC5-KD cells were harvested and stained for DNA with propidium iodide for the flow cytometric analysis. The fractions corresponding to G1, S and G2/M phases of the cell cycle are indicated. **(e)** The Boyden Chamber transwell migration assays for cell invasion for MDA-MB-231-Scramble or MDA-MB-231-HDAC5-KD-1 cells. **(f)** MDA-MB-231-Scramble or MDA-MB-231-LSD1-KD cells were transfected with control vector pcDNA3.1 or pcDNA3.1-HDAC5 for 5 days and crystal violet assays for growth were carried out. **(g)** MDA-MB-231-Scramble or MDA-MB-231-HDAC5-KD cells were transfected with empty or pReceiver-LSD1 expression plasmids for 5 days and crystal violet assays for growth were carried out. Bars represent the means of three independent experiments  $\pm$  s.d. \* $P < 0.05$ , \*\* $P < 0.01$ , \*\*\* $P < 0.001$ , Student's *t*-test.

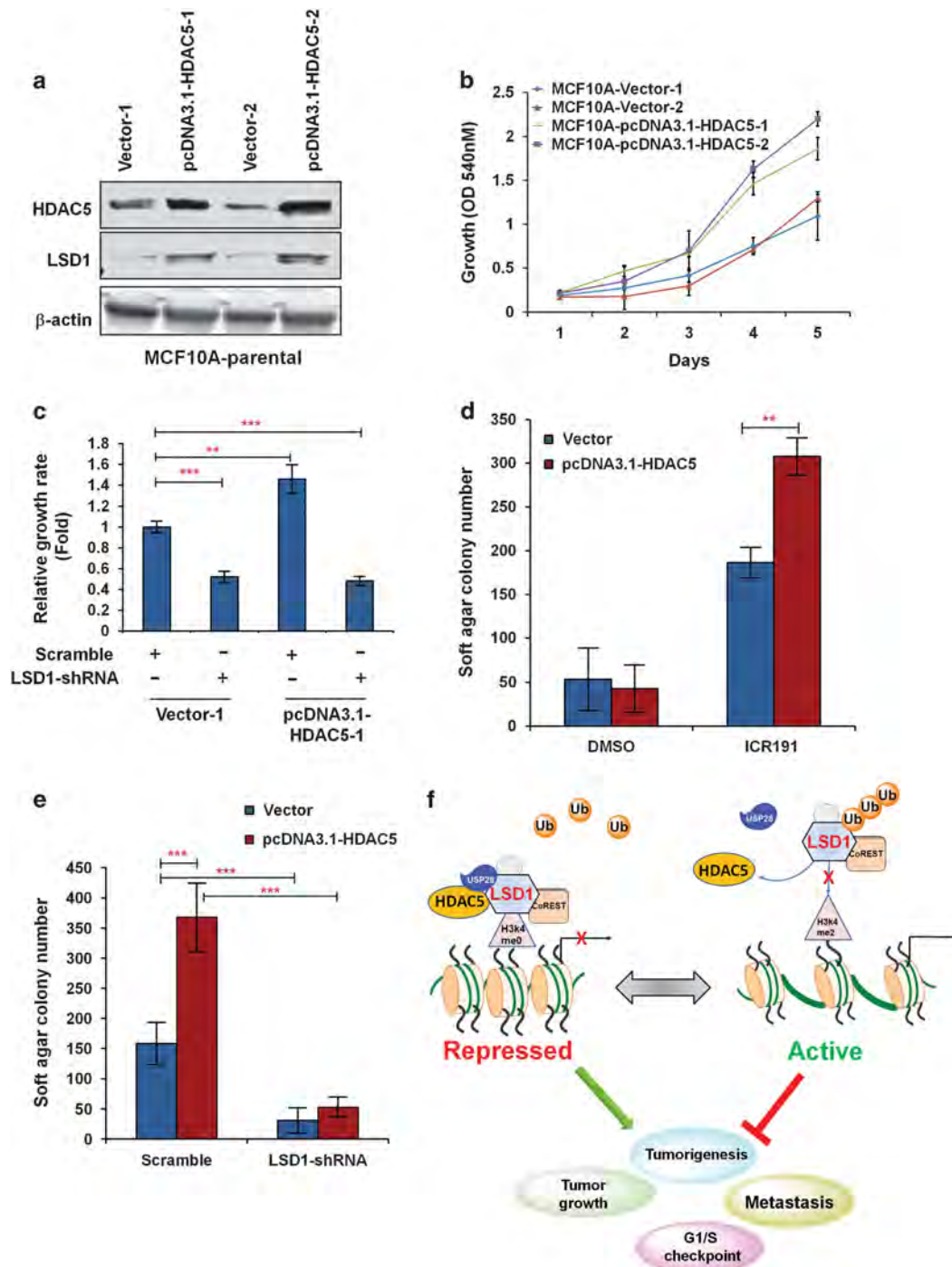


**Figure 7.** Effect of HDAC5 on growth and mutagen-induced tumorigenic transformation in MCF10A cells. **(a)** pcDNA3.1 or pcDNA3.1-HDAC5 transfected MCF10A cells (clone 1 and 2) were analyzed for protein levels of HDAC5 and LSD1 by immunoblots with anti-HDAC5 and anti-LSD1 antibodies. **(b)** The crystal violet assay for growth of MCF10A stably transfected with control vector or pcDNA3.1-HDAC5 plasmids. **(c)** MCF10A-Vector-1 or MCF10A-HDAC5-1 cells were infected with scramble or LSD1 shRNA lentivirus particles for 5 days followed by crystal violet assays for growth. **(d)** MCF10A cells transfected with pcDNA3.1 or pcDNA3.1-HDAC5 plasmids were treated with dimethyl sulfoxide or 500 ng/ml ICR191 for 7 months followed by soft agar colony formation assays. **(e)** After treatment with 500 ng/ml ICR191 for 7 months, MCF10A-HDAC5 cells were infected with scramble control or LSD1 shRNA lentivirus particles and soft agar colony formation assay was carried out. **(f)** Proposed model of the role of HDAC5-LSD1 axis in breast cancer development. Bars represent the means of three independent experiments  $\pm$  s.d.  $**P < 0.01$ ,  $***P < 0.001$ , Student's *t*-test.

LSD1 protein stability is controlled by several post-translational modifications such as ubiquitination and methylation.<sup>20,21,31</sup> However, the precise mechanism of how LSD1 protein stability is regulated is still not understood. A previous study reported that stable depletion of CoREST facilitated LSD1 degradation in HeLa

cells.<sup>32</sup> However, siRNA-mediated knockdown of CoREST alone in breast cancer cells failed to destabilize LSD1 protein, suggesting additional layers of control of LSD1 protein stability are required in breast cancer. In this study, we observed for the first time that LSD1 protein stability is promoted by HDAC5. We further found

that the HDAC5 domain containing NLS is essential for LSD1–HDAC5 interaction. The NLS element provides docking sites for 14-3-3 chaperone binding and has been shown to be critical for HDAC5 import into the nucleus and the regulation of its repressor activity.<sup>17,33</sup> Although an *in vitro* assay demonstrated that HDAC5 reduced LSD1 acetylation, HDAC5 siRNA treatment in breast cancer cells failed to alter acetylation of LSD1 protein. Our *in vivo* results suggest that LSD1 acetylation is likely regulated by a large complex that may involve additional protein deacetylases or cofactors. Further studies are needed to identify the regulatory complex and clarify the precise role of HDAC5 in regulation of LSD1 acetylation in breast cancer cells.

Our studies revealed that HDAC5 regulates LSD1 via enhancement of the protein stability of deubiquitinase USP28. High expression of USP28 has been found to promote the progression of breast and colon cancers.<sup>20,34</sup> Importantly, USP28 has been reported to deubiquitinate important tumor growth regulators such as c-Myc and TP53BP1 that are involved in MYC proto-oncogene stability and DNA damage response checkpoint regulation, respectively.<sup>35,36</sup> Our pilot microarray study revealed that inhibition of the HDAC5–LSD1 axis down-regulates c-Myc expression (data not shown). Sen *et al.*<sup>37</sup> recently reported that HDAC5 is a key component in the temporal regulation of p53-mediated transactivation. All of these findings imply an interaction of HDAC5/LSD1 axis and USP28-associated ubiquitin–proteasome system in regulating downstream targets involved in tumor development. USP28 has been well-characterized for its role in promoting tumorigenesis, and thus is a potential candidate target in cancer therapy. Given the current inability to use drugs to directly target USP28-driven cancer proliferation, our study suggests a novel alternative approach of targeting USP28 stability by development of HDAC5-specific inhibitors in cancer.

Our findings provide supportive evidence showing that HDAC5 control of cell proliferation is largely dependent on LSD1 stabilization. Furthermore, in this study, we showed that non-transformed MCF10A cells overexpressing HDAC5 significantly promoted ICR191-induced transformation of MCF10A cells. The overexpressed HDAC5 is consistently associated with upregulated LSD1 protein expression over the entire course of transformation induction. These data indicate that enhanced crosstalk between HDAC5 and LSD1 may represent a critical mechanism contributing to breast tumorigenesis. HDAC inhibitors hold great promise for cancer therapy. Despite the promising clinical results produced by the HDAC inhibitors in treatment of hematological cancers such as T-cell lymphoma, no apparent clinical evidence indicates that HDAC inhibitors work effectively as a monotherapy against solid tumors including breast tumors.<sup>38–41</sup> From a clinical perspective, our novel findings have significance for design and development of novel combination strategies targeting HDAC5–LSD1 axis as an alternative approach for improvement of therapeutic efficacy of HDAC inhibitors in breast cancer.

As summarized in Figure 7f, we show for the first time that LSD1 protein stability is promoted by HDAC5 through the LSD1 associated ubiquitin–proteasome system, confirming that the regulation of LSD1 by HDAC5 is a post-translational event. Our novel findings also provide supportive evidence that an orchestrated interaction between HDAC5 and LSD1 is a critical epigenetic mechanism to suppress transcriptional activities of important tumor suppressor genes that may contribute to breast cancer development.

## MATERIALS AND METHODS

### Reagents and cell culture conditions

MDA-MB-231, MDA-MB-468, MCF-7, T47D, HCC-202 and SK-BR-3 cell lines were obtained from the ATCC/NCI Breast Cancer SPOR program. MCF10A-parental and MCF10A-CA1a cells were gifts from Dr Saraswati Sukumar

(Johns Hopkins University). Cells were cultured in growth medium as described previously.<sup>10,42</sup>

### Tissue microarrays and immunohistochemistry

Tissue microarrays (US Biomax, Rockville, MD, USA) were stained using LSD1 or HDAC5 antibodies. Standard staining procedure for paraffin sections was used for IHC according to manufacturer's recommendations (Vector Labs Inc., Burlingame, CA, USA). Monoclonal antibodies were used for detection of LSD1 (1:800; Cell Signaling, Danvers, MA, USA) and HDAC5 (1:100; Santa Cruz, CA, USA). The staining was visualized using diaminobenzidine, and quantitated using IHC Profiler, an ImageJ plugin (National Institutes of Health, Bethesda, MD, USA).<sup>43</sup> H-scores were calculated as previously described.<sup>44</sup> The manual scoring of H-scores was also carried out by two breast cancer pathologists.

### Plasmid construction and stable transfection

Plasmids pcDNA3.1(+)-FLAG, pcDNA3.1(+)-FLAG-HDAC5 and pDZ-FLAG-USP28 were purchased from Addgene (Cambridge, MA, USA). pReceiver-FLAG-LSD1 was obtained from Gene Copoeia (Rockville, MD, USA). A FLAG-tagged ORF cDNA clone for Jade-2 was purchased from GenScript (Piscataway, NJ, USA). pcDNA3-HA-ubiquitin was obtained from Dr Yong Wan (University of Pittsburgh). HDAC5 deletion mutants were engineered into pcDNA3.1(+)-FLAG-HDAC5 by PCR with primers shown in Table S1. HDAC5-Δ2 was constructed by digesting full-length plasmids with SacII from amino acid 61 to 489. Stable transfection was carried out using Lipofectamine 3000 transfection reagent (Life Technologies, Grand Island, NY, USA), and colonies were selected with 800 μg/ml G418.

### siRNA and shRNA treatment and stable cell line generation

Pre-designed siRNA and non-targeting scramble siRNA (Santa Cruz) were transfected into cells following the manufacturer's protocol. Cells were collected 48 h post-transfection for further analysis. Scramble control, LSD1-specific or HDAC5-specific shRNA lentiviral particles (Santa Cruz) were infected into cells according to manufacturer's protocol. Cells were treated with 10 μg/ml puromycin 72 h after infection. Single colonies were analyzed for expression of LSD1 or HDAC5 via immunoblots.

### RNA extraction and qPCR

Total RNA extraction and cDNA synthesis used the methods described previously.<sup>10</sup> Quantitative real-time PCR was performed on the StepOne real-time PCR system (Life Technologies). All of the TaqMan gene expression assays were pre-designed and obtained from Life Technologies.

### Western blotting

Western blotting was performed as previously described.<sup>12,45,46</sup> Antibodies used in this study were shown in Supplementary Table S2. Membranes were scanned with Li-Cor BioScience Odyssey Infrared Imaging System (Lincoln, NE, USA).

### Crystal violet and cell invasion assays

The crystal violet proliferation assays were performed as described in our previous study.<sup>47</sup> The invasive capability of breast carcinoma cells was tested with Millipore QCM 24-well invasion assay kit (Merck KGaA, Germany) according to manufacturer's protocol.

### Soft agar colony formation assay

A total of 1.2% Bacto-agar (BD Biosciences, Franklin Lakes, NJ, USA) was autoclaved and mixed with growth medium to produce 0.6% agar. The mixture was quickly plated and solidified for 45 min. Cells were suspended in 0.6 ml 2× growth medium and mixed gently with 0.6 ml 0.8% agar/medium. Overall 1 ml of cells with 0.4% agar/medium mixture was added onto plate for solidification. Colony formation was examined using stereo microscopy and analyzed (CellSens Dimension, Olympus, Shinjuku, Tokyo, Japan).

### Flow cytometry analysis

Cells were collected and fixed with 70% ethanol. The cell pellet was then treated with 1% TritonX-100. Cells were subsequently resuspended in 50 μg/ml propidium iodide (Sigma, St Louis, MO, USA) containing RNaseI (Roche, Indianapolis, IN, USA) followed by analysis on the LSR II XW4400 workstation (BD Biosciences).



### Immunofluorescence

After 48 h of transfection, cells were fixed with 4% paraformaldehyde and incubated with primary antibodies (1:250) overnight at 4 °C. After washing, cells were incubated with fluorescence-labeled secondary antibody (1:100). After washing, coverslips were placed on a glass slide using UltraCruz mounting medium (Santa Cruz) before fluorescence microscope examination.

### Immunoprecipitation, ubiquitination and protein half-life assays

The cell lysate was obtained by using immunoprecipitation lysis buffer as described previously.<sup>48</sup> LSD1 or IgG antibodies were added to cell lysate. Protein G-plus agarose beads (Santa Cruz) or Flag-M2 affinity gel were collected and subjected to IB. HA-Ubiquitin, pcDNA3.1-Flag-HDAC5 or empty vector plasmids were co-transfected into cells for 38 h. Cells were then treated with 10  $\mu$ M MG132 for 10 h and collected for immunoprecipitation assay with protein G-plus agarose beads. For half-life studies 48 h after transfection with pcDNA3.1-HDAC5 or HDAC5 siRNA, cells were treated with 100  $\mu$ g/ml cycloheximide and then collected at indicated times for IB.

### Protein acetylation assay

The immunoprecipitates of FLAG-M2 agarose from MDA-MB-231 cells overexpressing FLAG-tag USP28 or FLAG-tag LSD1 were used as substrates for the protein deacetylation assay. Pull-down of IgG was used as negative control. A total of 0.25  $\mu$ g of recombinant human GST-tagged HDAC5 protein (Creative BioMart, NY, NY) was mixed with 30  $\mu$ l immunoprecipitates or 1.5  $\mu$ g bulk histone at 37 °C for 6 h in a buffer containing 40 mM Tris–HCl (pH 8.0), 2.5 mM MgCl<sub>2</sub>, 50 mM NaCl, 2 mM KCl, 0.5 mM DTT, 1 mM EDTA and protease inhibitor. The reactions were then subjected to immunoblots with anti-acetyl lysine antibody (EMD Millipore, Billerica, MA, USA). FLAG-tagged USP28 or LSD1 and bulk histone were probed with anti-FLAG antibody or H3 antibody as loading control. Inactive HDAC5-GST protein was used as negative control by heating recombinant protein at 95 °C for 5 min. *In vivo* protein acetylation assay was performed using cell lysate of MDA-MB-231 cell transfected with scramble and HDAC5 siRNAs. LSD1 or IgG antibodies were added to cell lysate. Protein G-plus agarose beads (Santa Cruz) were collected and subjected to IB with anti-acetyl lysine or LSD1 antibodies.

### Chromatin immunoprecipitation

Chromatin immunoprecipitation assay was performed as described previously.<sup>12</sup> Primary antibodies against HDAC5, LSD1, H3K4me2 and acetyl-H3K9 were used as indicated for immunoprecipitation of the protein–DNA complexes. PCR primer sets used for amplification of precipitated fragments were shown in Supplementary Table S1. Input DNA was used for normalization.

### Statistical analysis

Data were represented as the mean  $\pm$  s.d of three independent experiments. The quantitative variables were analyzed by the two-tailed Student's *t*-test. The  $\chi^2$  study was used to assess the correlation between HDAC5 and LSD1 protein expression by using median H-scores as the cutoff for high- versus low-protein expression. *P*-value < 0.05 was considered statistically significant for all tests. Statistical analyses were performed using GraphPad Prism 6 (GraphPad Software Inc., La Jolla, CA, USA).

### CONFLICT OF INTEREST

The authors declare no conflict of interest.

### ACKNOWLEDGEMENTS

This work is supported by US Army Breast Cancer Research Program (W81XWH-14-1-0237 to YH; W81XWH-14-1-0238 to NED), Breast Cancer Research Foundation (to NED and SO) and UPCI Genomics Core Facility supported by NCI P30CA047904.

### REFERENCES

- Shi Y, Lan F, Matson C, Mulligan P, Whetstone JR, Cole PA *et al*. Histone demethylation mediated by the nuclear amine oxidase homolog LSD1. *Cell* 2004; **119**: 941–953.
- Lee MG, Wynder C, Cooch N, Shiekhhattar R. An essential role for CoREST in nucleosomal histone 3 lysine 4 demethylation. *Nature* 2005; **437**: 432–435.
- Huang Y, Marton LJ, Woster PM, Casero RA. Polyamine analogues targeting epigenetic gene regulation. *Essays Biochem*. 2009; **46**: 95–110.
- Lee M, Wynder C, Cooch N, Shiekhhattar R. An essential role for CoREST in nucleosomal histone 3 lysine 4 demethylation. *Nature* 2005; **437**: 432–435.
- Garcia-Bassets I, Kwon YS, Telesse F, Prefontaine GG, Hutt KR, Cheng CS *et al*. Histone methylation-dependent mechanisms impose ligand dependency for gene activation by nuclear receptors. *Cell* 2007; **128**: 505–518.
- Lim S, Janzer A, Becker A, Zimmer A, Schule R, Buettner R *et al*. Lysine-specific demethylase 1 (LSD1) is highly expressed in ER-negative breast cancers and a biomarker predicting aggressive biology. *Carcinogenesis* 2010; **31**: 512–520.
- Metzger E, Wissmann M, Yin N, Muller J, Schneider R, Peters A *et al*. LSD1 demethylates repressive histone marks to promote androgen-receptor-dependent transcription. *Nature* 2005; **437**: 436–439.
- Zhu Q, Huang Y, Marton LJ, Woster PM, Davidson NE, Casero RA Jr. Polyamine analogs modulate gene expression by inhibiting lysine-specific demethylase 1 (LSD1) and altering chromatin structure in human breast cancer cells. *Amino Acids* 2012; **42**: 887–898.
- Huang Y, Greene E, Murray Stewart T, Goodwin AC, Baylin SB, Woster PM *et al*. Inhibition of lysine-specific demethylase 1 by polyamine analogues results in reexpression of aberrantly silenced genes. *Proc Natl Acad Sci U S A* 2007; **104**: 8023–8028.
- Vasilatos SN, Katz TA, Oesterreich S, Wan Y, Davidson NE, Huang Y. Crosstalk between lysine-specific demethylase 1 (LSD1) and histone deacetylases mediates antineoplastic efficacy of HDAC inhibitors in human breast cancer cells. *Carcinogenesis* 2013; **34**: 1196–1207.
- Serce N, Gnatzy A, Steiner S, Lorenzen H, Kirfel J, Buettner R. Elevated expression of LSD1 (Lysine-specific demethylase 1) during tumour progression from pre-invasive to invasive ductal carcinoma of the breast. *BMC Clin Pathol* 2012; **12**: 13.
- Huang Y, Stewart TM, Wu Y, Baylin SB, Marton LJ, Perkins B *et al*. Novel oligoamine analogues inhibit lysine-specific demethylase 1 and induce reexpression of epigenetically silenced genes. *Clin Cancer Res* 2009; **15**: 7217–7228.
- Nowotarski SL, Pachaiyappan B, Holshouser SL, Kutz CJ, Li Y, Huang Y *et al*. Structure-activity study for (bis)ureidopropyl- and (bis)thioureidopropylidiamine LSD1 inhibitors with 3-5-3 and 3-6-3 carbon backbone architectures. *Bioorg Med Chem* 2015; **23**: 1601–1612.
- Mohammad HP, Smitheman KN, Kamat CD, Soong D, Federowicz KE, Van Aller GS *et al*. A DNA hypomethylation signature predicts antitumor activity of LSD1 inhibitors in SCLC. *Cancer Cell* 2015; **28**: 57–69.
- Yang XJ, Gregoire S. Class II histone deacetylases: from sequence to function, regulation, and clinical implication. *Mol Cell Biol* 2005; **25**: 2873–2884.
- Martin M, Kettmann R, Dequiedt F. Class IIa histone deacetylases: regulating the regulators. *Oncogene* 2007; **26**: 5450–5467.
- McKinsey TA, Zhang CL, Lu J, Olson EN. Signal-dependent nuclear export of a histone deacetylase regulates muscle differentiation. *Nature* 2000; **408**: 106–111.
- Martin M, Kettmann R, Dequiedt F. Class IIa histone deacetylases: conducting development and differentiation. *Int J Dev Biol* 2009; **53**: 291–301.
- Santner SJ, Dawson PJ, Tait L, Soule HD, Eliason J, Mohamed AN *et al*. Malignant MCF10CA1 cell lines derived from premalignant human breast epithelial MCF10 AT cells. *Breast Cancer Res Treat* 2001; **65**: 101–110.
- Wu Y, Wang Y, Yang XH, Kang T, Zhao Y, Wang C *et al*. The deubiquitinase USP28 stabilizes LSD1 and confers stem-cell-like traits to breast cancer cells. *Cell Rep* 2013; **5**: 224–236.
- Han X, Gui B, Xiong C, Zhao L, Liang J, Sun L *et al*. Destabilizing LSD1 by Jade-2 promotes neurogenesis: an antibraking system in neural development. *Mol Cell* 2014; **55**: 482–494.
- Huang Y, Nayak S, Jankowitz R, Davidson NE, Oesterreich S. Epigenetics in breast cancer: what's new? *Breast Cancer Res* 2011; **13**: 225.
- Abukhdeir AM, Park BH. P21 and p27: roles in carcinogenesis and drug resistance. *Expert Rev Mol Med* 2008; **10**: e19.
- Kominsky SL, Argani P, Korz D, Evron E, Raman V, Garrett E *et al*. Loss of the tight junction protein claudin-7 correlates with histological grade in both ductal carcinoma in situ and invasive ductal carcinoma of the breast. *Oncogene* 2003; **22**: 2021–2033.
- Lin T, Ponn A, Hu X, Law BK, Lu J. Requirement of the histone demethylase LSD1 in Snai1-mediated transcriptional repression during epithelial-mesenchymal transition. *Oncogene* 2010; **29**: 4896–4904.
- Chen WD, Eshleman JR, Aminoshariae MR, Ma AH, Veloso N, Markowitz SD *et al*. Cytotoxicity and mutagenicity of frameshift-inducing agent ICR191 in mismatch repair-deficient colon cancer cells. *J Natl Cancer Inst* 2000; **92**: 480–485.

- 27 Zientek-Targosz H, Kunnev D, Hawthorn L, Venkov M, Matsui S, Cheney RT *et al*. Transformation of MCF-10A cells by random mutagenesis with frameshift mutagen ICR191: a model for identifying candidate breast-tumor suppressors. *Mol Cancer* 2008; **7**: 51.
- 28 Milde T, Oehme I, Korshunov A, Kopp-Schneider A, Remke M, Northcott P *et al*. HDAC5 and HDAC9 in medulloblastoma: novel markers for risk stratification and role in tumor cell growth. *Clin Cancer Res* 2010; **16**: 3240–3252.
- 29 He P, Liang J, Shao T, Guo Y, Hou Y, Li Y. HDAC5 promotes colorectal cancer cell proliferation by up-regulating DLL4 expression. *Int J Clin Exp Med* 2015; **8**: 6510–6516.
- 30 Nagasawa S, Sedukhina AS, Nakagawa Y, Maeda I, Kubota M, Ohnuma S *et al*. LSD1 overexpression is associated with poor prognosis in basal-like breast cancer, and sensitivity to PARP inhibition. *PLoS One* 2015; **10**: e0118002.
- 31 Piao L, Suzuki T, Dohmae N, Nakamura Y, Hamamoto R. SUV39H2 methylates and stabilizes LSD1 by inhibiting polyubiquitination in human cancer cells. *Oncotarget* 2015; **6**: 16939–16950.
- 32 Shi YJ, Matson C, Lan F, Iwase S, Baba T, Shi Y. Regulation of LSD1 histone demethylase activity by its associated factors. *Mol Cell*. 2005; **19**: 857–864.
- 33 Greco TM, Yu F, Guise AJ, Cristea IM. Nuclear import of histone deacetylase 5 by requisite nuclear localization signal phosphorylation. *Mol Cell Proteom* 2011; **10**: M110.004317.
- 34 Diefenbacher ME, Popov N, Blake SM, Schulein-Volk C, Nye E, Spencer-Dene B *et al*. The deubiquitinase USP28 controls intestinal homeostasis and promotes colorectal cancer. *J Clin Invest* 2014; **124**: 3407–3418.
- 35 Popov N, Wanzel M, Madiredjo M, Zhang D, Beijersbergen R, Bernards R *et al*. The ubiquitin-specific protease USP28 is required for MYC stability. *Nat Cell Biol* 2007; **9**: 765–774.
- 36 Zhang D, Zaugg K, Mak TW, Elledge SJ. A role for the deubiquitinating enzyme USP28 in control of the DNA-damage response. *Cell* 2006; **126**: 529–542.
- 37 Sen N, Kumari R, Singh MI, Das S. HDAC5, a key component in temporal regulation of p53-mediated transactivation in response to genotoxic stress. *Mol Cell* 2013; **52**: 406–420.
- 38 Traynor AM, Dubey S, Eickhoff JC, Kolesar JM, Schell K, Huie MS *et al*. Vorinostat (NSC# 701852) in patients with relapsed non-small cell lung cancer: a Wisconsin Oncology Network phase II study. *J Thorac Oncol* 2009; **4**: 522–526.
- 39 Luu TH, Morgan RJ, Leong L, Lim D, McNamara M, Portnow J *et al*. A phase II trial of vorinostat (suberoylanilide hydroxamic acid) in metastatic breast cancer: a California Cancer Consortium study. *Clin Cancer Res* 2008; **14**: 7138–7142.
- 40 Modesitt SC, Sill M, Hoffman JS, Bender DP. A phase II study of vorinostat in the treatment of persistent or recurrent epithelial ovarian or primary peritoneal carcinoma: a Gynecologic Oncology Group study. *Gynecol Oncol* 2008; **109**: 182–186.
- 41 Blumenschein Jr GR, Kies MS, Papadimitrakopoulou VA, Lu C, Kumar AJ, Ricker JL *et al*. Phase II trial of the histone deacetylase inhibitor vorinostat (Zolinza, suberoylanilide hydroxamic acid, SAHA) in patients with recurrent and/or metastatic head and neck cancer. *Invest New Drugs* 2008; **26**: 81–87.
- 42 Shaw PG, Chaerkady R, Wang T, Vasilatos S, Huang Y, Van Houten B *et al*. Integrated proteomic and metabolic analysis of breast cancer progression. *PLoS ONE* 2013; **8**: e76220.
- 43 Varghese F, Bukhari AB, Malhotra R, De A. IHC Profiler: an open source plugin for the quantitative evaluation and automated scoring of immunohistochemistry images of human tissue samples. *PLoS ONE* 2014; **9**: e96801.
- 44 Ishibashi H, Suzuki T, Suzuki S, Moriya T, Kaneko C, Takizawa T *et al*. Sex steroid hormone receptors in human thymoma. *J Clin Endocrinol Metab* 2003; **88**: 2309–2317.
- 45 Huang Y, Hager ER, Phillips DL, Dunn VR, Hacker A, Frydman B *et al*. A novel polyamine analog inhibits growth and induces apoptosis in human breast cancer cells. *Clin Cancer Res* 2003; **9**: 2769–2777.
- 46 Huang Y, Keen J, Pledge A, Marton L, Zhu T, Sukumar S *et al*. Polyamine analogues down-regulate estrogen receptor alpha expression in human breast cancer cells. *J Biol Chem* 2006; **281**: 19055–19063.
- 47 Katz TA, Vasilatos SN, Harrington E, Oesterreich S, Davidson NE, Huang Y. Inhibition of histone demethylase, LSD2 (KDM1B), attenuates DNA methylation and increases sensitivity to DNMT inhibitor-induced apoptosis in breast cancer cells. *Breast Cancer Res Treat* 2014; **146**: 99–108.
- 48 Huang Y, Vasilatos SN, Boric L, Shaw PG, Davidson NE. Inhibitors of histone demethylation and histone deacetylation cooperate in regulating gene expression and inhibiting growth in human breast cancer cells. *Breast Cancer Res Treat* 2012; **131**: 777–789.

Supplementary Information accompanies this paper on the *Oncogene* website (<http://www.nature.com/onc>)

# Targeting tumorigenicity of breast cancer stem-like cells using combination epigenetic therapy: something old and something new

Yi Huang<sup>1,2</sup>, Nancy E. Davidson<sup>1,2,3</sup>

<sup>1</sup>University of Pittsburgh Cancer Institute, Pittsburgh, PA, USA; <sup>2</sup>Department of Pharmacology & Chemical Biology, <sup>3</sup>Department of Medicine, University of Pittsburgh School of Medicine, Pittsburgh, PA, USA

Correspondence to: Yi Huang, MD, PhD. Magee Women Research Institute, Room 406, 204 Craft Ave, Pittsburgh, PA 15213, USA. Email: huangy2@upmc.edu.

Submitted Sep 26, 2016. Accepted for publication Oct 09, 2016.

doi: 10.21037/jtd.2016.11.18

View this article at: <http://dx.doi.org/10.21037/jtd.2016.11.18>

Like most other types of cancers, human breast cancer occurs as a result of a multistep process that generally consists of initiation and progression resulting from uncontrolled cell proliferation and/or aberrant apoptosis as a consequence of cumulative genetic and/or epigenetic alterations in genome. Genetic alterations such as mutations or deletions or rearrangements of specific genes and/or chromosomal instability can inactivate normally expressed genes that would otherwise protect against breast cancer development. Another general mechanism by which expression of growth regulatory genes can be modified is so called “epigenetic alterations” which refer to high level modifications in chromatin structure above the genetic code (1,2). Importantly, epigenetic alterations, unlike mutation, deletion or loss of specific chromosomal regions, are generally reversible. Therefore, it should be theoretically possible to restore normal growth phenotypes by reversing aberrant epigenetic changes through treatment with epigenetic modifying drugs. Multiple primary and interconnected epigenetic mechanisms, such as DNA and histone modifications as well as non-coding RNA expression, have been elucidated (3). The impact of DNA methylation and histone modifications on cancer initiation and progression has been extensively investigated in preclinical models. In addition, many clinical trials using DNA methyltransferase (DNMT) inhibitors have shown clinical benefit in treatment of myelodysplastic syndromes (MDS) and acute myelogenous leukemia (AML) (4,5). The use of drugs that inhibit histone deacetylases (HDAC) also holds great promise for cancer therapy. Several inhibitors of DNMTs or HDACs have already been approved by the US FDA for the clinical treatment of cutaneous

T-cell lymphoma (CTCL) and multiple myeloma (6-8). Unfortunately, the results of initial clinical trials of DNMT inhibitors (DNMTi) and HDAC inhibitors (HDACi) in solid tumors including breast cancer have not been as rewarding. Nonetheless it is critically important to continue to explore the potential effects of epigenetic drugs as a means to improve therapy for epithelial cancers in solid tumor.

In a recent issue of *Cancer Research*, Pathania and colleagues characterized the *in vitro* and *in vivo* antineoplastic effect of a combination of the DNMT inhibitor, 5-azacytidine (5-AzaC), and the HDAC inhibitor, butyrate, on breast cancer stem-like cells (BCSCs) at a genomic level (9). The authors provided interesting evidence to show that Lin<sup>-</sup>CD49<sup>+</sup>CD24<sup>+</sup> cells isolated from tumor tissues of MMTV-Neu-Tg mice possessed tumor-propagating and metastatic potential when these cells were injected into the mammary fat pad of NOD/SCID mice. They further demonstrated that both transformed basal myoepithelial stem cells and luminal progenitor cells developed mammary tumors, and these cells were susceptible to combination treatment with DNMT and HDAC inhibitors (9). RNA-sequencing study identified a subset of genes, whose expression is regulated by DNMT and HDAC inhibitors, are potentially involved in regulation of basal stem cell-driven breast cancer phenotypes. Further analysis through the Ingenuity System Database (IPA) and UCSC cancer genome browser program showed that expression of RAD51AP1 and SPC25 was high in basal breast tumor tissues and cell lines and downregulated by 5-AzaC/butyrate.

DNA methylation and histone post translational modifications (PTMs) are two fundamental epigenetic

regulatory mechanisms that govern chromatin structure, gene transcription and other important biological processes. The functional interaction between DNMTs and HDACs has emerged as a key research issue and a possible novel target for cancer therapy. In breast cancer, dysregulated DNA CpG methylation frequently cooperates with abnormal histone modifications to result collectively in an aberrant chromatin landscape and gene expression profile (2,5,10). Our early work showed that the HDAC inhibitor, Scriptaid, inhibited human breast tumor growth *in vitro* and *in vivo* and acted, in conjunction with the DNMT inhibitor (DNMTi) AZA, to re-express functional Estrogen Receptor Alpha (ER $\alpha$ ) in ER-negative breast cancer cells (11). We also demonstrated that disruption of Hsp90 function by HDACi facilitated DNMT1 degradation through the ubiquitin-proteasome pathway in breast cancer cells (12). Another novel DNMTi, Zebularine, potentiated the inhibitory effect of HDACi on cell proliferation and colony formation in breast cancer cells (13). Studies from our laboratory and others consistently showed that combined treatment of ER negative breast cancer cells with DNMTi and HDACi restored response to endocrine therapy (14,15). The potential translation of these findings into clinical investigation is demonstrated by a “window” clinical trial showing that oral HDACi vorinostat (SAHA) administered to patients with primary breast cancer for 3 days preoperatively was associated with significant reduction in expression of proliferation-related genes such as Ki-67, STK15 and Cyclin B1 (16). Another phase II study assessed the activity of the DNMTi, 5-AzaC, and the HDACi, Entinostat, in patients with advanced breast cancer (17).

Nonetheless, while DNMTi and HDACi have shown promising results in treatment of hematological malignancies, these drugs have proven to be less effective against solid tumors including breast cancer. The likely explanations for the unsatisfactory efficacy of epigenetic agents in solid tumors may include poor pharmacokinetic properties, inadequate incorporation of drugs into tumor cells, lack of specificity in targeting chromatin modifiers and gene expression, and/or toxicity. In addition, insufficient knowledge about the basic mechanisms of epigenetic alterations in a neoplastic disease like breast cancer may impede the progress of future clinical application of the epigenetic agents. To enhance the potential of epigenetic drugs as effective anti-breast tumor agents, it is necessary to better understand how DNMT and HDAC activities are regulated in breast cancer. It is also critical to develop novel combinatorial strategies to improve the efficacy of the

epigenetic drugs.

Since Al-Hajj *et al.* first reported the existence of CSCs in breast cancer (18), increasing lines of evidence have indicated that BCSCs have important implications in breast cancer initiation, progression and therapeutics (19). A recent study used whole genome promoter microarray to compare the DNA methylation portraits of human BCSCs versus non-BCSCs, and showed a distinct DNA methylation landscape in BCSCs as a key epigenetic mediator of their differentiation (20). Epigenetic silencing of the tumor suppressor breast cancer 1 (*BRCA1*) gene due to CpG island hypermethylation in breast cancer which contained expanded luminal progenitor cells was reported in a recent study (21). Another investigation revealed the promise of using the HDACi, Abexinostat, as a differentiation therapy targeting BCSCs (22). In addition, recent evidence showed that Enhancer of Zeste Homolog 2 (EZH2), an important member of the polycomb repressor complex, downregulated the DNA damage repair protein Rad51 which resulted in expansion of the BCSCs population (23). These results suggest that epigenetic alterations in BCSCs play important roles in governing their biological properties.

Compared to non-CSCs, CSCs generally exhibit elevated resistance to conventional chemotherapy and/or radiation therapy. Therapies using purely cytotoxic regimens commonly fail to hinder CSC propagation. There are vigorous research and clinical activities in identifying or developing novel agents and therapeutic approaches that specifically targets the small, phenotypically distinct CSC subpopulations in tumors. Ohm *et al.* proposed a model based on the findings that cancer stem/progenitor cells develop in a stepwise manner as a result of crosstalk between multiple epigenetic mechanisms including DNMT and histone modifications (24). Their findings suggested that targeting aberrant interaction of epigenetic modifiers may represent an effective therapeutic approach in blocking CSC initiation and progression. Pathania and colleagues provided the first evidence that the combined inhibition of DNMTs and HDACs effectively blocks mammary tumorigenesis and attenuates mammosphere-forming capacity of tumor-propagating cells by regulating the expression of key genes that are involved in development of basal stem cell-driven breast cancer (9). Such findings imply that targeting single epigenetic aberration might be insufficient to suppress BCSC expansion. Instead, targeting multiple interactive epigenetic abnormalities may be required to improve the therapeutic efficacy. However, many questions still remain to be answered about the use of DNMT/HDAC inhibitory

strategies in blocking BCSC expansion. For example, the detailed mechanisms underlying the effect of inhibition of DNMT/HDACs on BCSC propagation and other phenotypes are not clear. Alterations in DNA methylation and histone marks in BCSCs due to combination therapy have not been fully elucidated.

Since the impact of inhibition of DNMT and HDAC on global gene expression changes is likely to be very broad, it is critical to map out specific alterations of gene expression that are responsible for the antineoplastic activity of this strategy. Through a comprehensive RNA-seq analysis, Pathania and colleagues identified a subset of genes whose expression was differentially regulated by 5-AzaC/butyrate. These genes are extensively involved in regulation of cell division and cycle, mitosis, chromosome segregation, kinetochore formation, etc. Among the top tier candidate genes, RAD51AP1 and SPC25 were selected for further analysis and found to be highly expressed in basal breast cancer cells. Although these two genes were overexpressed in breast tumor tissues and their expression was downregulated by combination therapy, there was no evidence to indicate that expression of these genes is directly regulated by DNA methylation or histone acetylation. Further studies are needed to clarify the regulatory mechanisms of combination therapy on the transcriptional activity of the key genes involved in BCSC proliferation.

Since DNA methylation and histone acetylation are normal features of the genome, the use of inhibitors targeting DNMT/HDACs may induce changes in the epigenomic landscape that could result in toxicity. Although combination strategies generally use lower doses of epigenetic modulators than those employed when the agents are administered individually, it is possible that cumulative alterations in gene expression or genomic instability could considerably enhance toxicity. Also it remains to be determined whether the combination of DNMTi and HDACi exerts direct cytotoxic actions on BCSC in addition to the effects on the epigenome of tumor cells.

In summary, the recently published research article by Pathania *et al.* demonstrated for the first time that simultaneous blockade of the activity of two important epigenetic modifiers, DNMT and HDAC, significantly reduced BCSC propagation and increased overall survival in tumor-bearing animal models. These findings have significant implications for the hypothesis that dual inhibition of DNMT and HDAC may improve the therapeutic efficacy in refractory or drug resistant breast cancer. Although use of epigenetic therapy with HDAC

and DNMT inhibitors for breast cancer patients has received a lot of attention, numerous technical and clinical obstacles still remain to be overcome. These issues include how to select breast tumor patients that may benefit from epigenetic treatments at the greatest extent, and how to quantitatively measure the therapeutic effect of epigenetic therapy. Pathania *et al.* have completed a valuable study to pave the way for a potential new strategy to eliminate CSCs in breast tumors using epigenetic approaches. The precise role of DNMT/HDAC in regulation of BCSC progression and therapeutic response, however, warrants further investigation.

### Acknowledgements

The authors' work has been supported by US Army Breast Cancer Research Breakthrough Awards (W81XWH-14-1-0237 to Y Huang; W81XWH-14-1-0238 to NE Davidson) and Breast Cancer Research Foundation (to NE Davidson).

### Footnote

*Provenance:* This is an invited Editorial commissioned by the Section Editor Dr. Hongcheng Zhu, MD, PhD (Department of Radiation Oncology, the First Affiliated Hospital of Nanjing Medical University, Nanjing, China).

*Conflicts of Interest:* The authors have no conflicts of interest to declare.

*Comment on:* Pathania R, Ramachandran S, Mariappan G, et al. Combined Inhibition of DNMT and HDAC Blocks the Tumorigenicity of Cancer Stem-like Cells and Attenuates Mammary Tumor Growth. *Cancer Res* 2016;76:3224-35.

### References

1. Dawson MA, Kouzarides T, Huntly BJ. Targeting epigenetic readers in cancer. *N Engl J Med* 2012;367:647-57.
2. Jones PA, Baylin SB. The epigenomics of cancer. *Cell* 2007;128:683-92.
3. Burgess DJ. Epigenetics: Separate paths for epigenomes and genomes in cancer evolution? *Nat Rev Genet* 2016;17:438.
4. Stearns V, Zhou Q, Davidson NE. Epigenetic regulation as a new target for breast cancer therapy. *Cancer Invest* 2007;25:659-65.
5. Katz TA, Huang Y, Davidson NE, et al. Epigenetic

- reprogramming in breast cancer: from new targets to new therapies. *Ann Med* 2014;46:397-408.
6. Falkenberg KJ, Johnstone RW. Histone deacetylases and their inhibitors in cancer, neurological diseases and immune disorders. *Nat Rev Drug Discov* 2014;13:673-91.
  7. Ceccacci E, Minucci S. Inhibition of histone deacetylases in cancer therapy: lessons from leukaemia. *Br J Cancer* 2016;114:605-11.
  8. Heyn H, Esteller M. DNA methylation profiling in the clinic: applications and challenges. *Nat Rev Genet* 2012;13:679-92.
  9. Pathania R, Ramachandran S, Mariappan G, et al. Combined Inhibition of DNMT and HDAC Blocks the Tumorigenicity of Cancer Stem-like Cells and Attenuates Mammary Tumor Growth. *Cancer Res* 2016;76:3224-35.
  10. Huang Y, Nayak S, Jankowitz R, et al. Epigenetics in breast cancer: what's new? *Breast Cancer Res* 2011;13:225.
  11. Keen JC, Yan L, Mack KM, et al. A novel histone deacetylase inhibitor, scriptaid, enhances expression of functional estrogen receptor alpha (ER) in ER negative human breast cancer cells in combination with 5-aza 2'-deoxycytidine. *Breast Cancer Res Treat* 2003;81:177-86.
  12. Zhou Q, Agoston AT, Atadja P, et al. Inhibition of histone deacetylases promotes ubiquitin-dependent proteasomal degradation of DNA methyltransferase 1 in human breast cancer cells. *Mol Cancer Res* 2008;6:873-83.
  13. Billam M, Sobolewski MD, Davidson NE. Effects of a novel DNA methyltransferase inhibitor zebularine on human breast cancer cells. *Breast Cancer Res Treat* 2010;120:581-92.
  14. Fan J, Yin WJ, Lu JS, et al. ER alpha negative breast cancer cells restore response to endocrine therapy by combination treatment with both HDAC inhibitor and DNMT inhibitor. *J Cancer Res Clin Oncol* 2008;134:883-90.
  15. Sharma D, Saxena NK, Davidson NE, et al. Restoration of tamoxifen sensitivity in estrogen receptor-negative breast cancer cells: tamoxifen-bound reactivated ER recruits distinctive corepressor complexes. *Cancer Res* 2006;66:6370-8.
  16. Stearns V, Jacobs LK, Fackler M, et al. Biomarker modulation following short-term vorinostat in women with newly diagnosed primary breast cancer. *Clin Cancer Res* 2013;19:4008-16.
  17. Connolly RM, Jankowitz RC, Andreopoulou E, et al. OT3-01-06: A Phase 2 Study Investigating the Safety, Efficacy and Surrogate Biomarkers of Response of 5-Azacytidine (5-AZA) and Entinostat (MS-275) in Patients with Advanced Breast Cancer. *Cancer Res* 2011;71:Abstract nr OT3-01-06.
  18. Al-Hajj M, Wicha MS, Benito-Hernandez A, et al. Prospective identification of tumorigenic breast cancer cells. *Proc Natl Acad Sci U S A* 2003;100:3983-8.
  19. Keller PJ, Arendt LM, Skibinski A, et al. Defining the cellular precursors to human breast cancer. *Proc Natl Acad Sci U S A* 2012;109:2772-7.
  20. El Helou R, Wicinski J, Guille A, et al. Brief reports: A distinct DNA methylation signature defines breast cancer stem cells and predicts cancer outcome. *Stem Cells* 2014;32:3031-6.
  21. Lim E, Vaillant F, Wu D, et al. Aberrant luminal progenitors as the candidate target population for basal tumor development in BRCA1 mutation carriers. *Nat Med* 2009;15:907-13.
  22. Salvador MA, Wicinski J, Cabaud O, et al. The histone deacetylase inhibitor abexinostat induces cancer stem cells differentiation in breast cancer with low Xist expression. *Clin Cancer Res* 2013;19:6520-31.
  23. Chang CJ, Yang JY, Xia W, et al. EZH2 promotes expansion of breast tumor initiating cells through activation of RAF1- $\beta$ -catenin signaling. *Cancer Cell* 2011;19:86-100.
  24. Ohm JE, Baylin SB. Stem cell chromatin patterns: an instructive mechanism for DNA hypermethylation? *Cell Cycle* 2007;6:1040-3.

**Cite this article as:** Huang Y, Davidson NE. Targeting tumorigenicity of breast cancer stem-like cells using combination epigenetic therapy: something old and something new. *J Thorac Dis* 2016;8(11):2971-2974. doi: 10.21037/jtd.2016.11.18

## Functional characterization of lysine-specific demethylase 2 (LSD2/KDM1B) in breast cancer progression

Lin Chen<sup>1,2</sup>, Shauna N. Vasilatos<sup>1,3</sup>, Ye Qin<sup>1,3</sup>, Tiffany A. Katz<sup>5</sup>, Chunyu Cao<sup>1,3,8</sup>, Hao Wu<sup>1,6</sup>, Nilgun Tasdemir<sup>1,3</sup>, Kevin M. Levine<sup>1,4</sup>, Steffi Oesterreich<sup>1,3</sup>, Nancy E. Davidson<sup>7</sup> and Yi Huang<sup>1,3</sup>

<sup>1</sup> Women's Cancer Research Center, UPMC Hillman Cancer Center, University of Pittsburgh School of Medicine, Pittsburgh, PA, USA

<sup>2</sup> School of Medicine, Tsinghua University, Beijing, P.R. China

<sup>3</sup> Department of Pharmacology & Chemical Biology, University of Pittsburgh School of Medicine, Pittsburgh, PA, USA

<sup>4</sup> Department of Pathology, University of Pittsburgh School of Medicine, Pittsburgh, PA, USA

<sup>5</sup> Center for Precision Environmental Health, Baylor College of Medicine, Houston, TX, USA

<sup>6</sup> Department of Oncology, The First Affiliated Hospital of Nanjing Medical University, Nanjing, Jiangsu, P.R. China

<sup>7</sup> Fred Hutchinson Cancer Research Center and Department of Medicine, University of Washington, Seattle, WA, USA

<sup>8</sup> China Three Gorges University, Yichang, Hubei, P. R. China

Correspondence to: Yi Huang, email: yih26@pitt.edu

Keywords: LSD2/KDM1B, breast cancer, cell growth, migration, invasion

Received: April 19, 2017

Accepted: July 03, 2017

Published: July 19, 2017

Copyright: Chen et al. This is an open-access article distributed under the terms of the Creative Commons Attribution License 3.0 (CC BY 3.0), which permits unrestricted use, distribution, and reproduction in any medium, provided the original author and source are credited.

### ABSTRACT

**Flavin-dependent histone demethylases govern histone H3K4 methylation and act as important chromatin modulators that are extensively involved in regulation of DNA replication, gene transcription, DNA repair, and heterochromatin gene silencing. While the activities of lysine-specific demethylase 1 (LSD1/KDM1A) in facilitating breast cancer progression have been well characterized, the roles of its homolog LSD2 (KDM1B) in breast oncogenesis are relatively less understood. In this study, we showed that LSD2 protein level was significantly elevated in malignant breast cell lines compared with normal breast epithelial cell line. TCGA- Oncomine database showed that LSD2 expression is significantly higher in basal-like breast tumors compared to other breast cancer subtypes or normal breast tissue. Overexpression of LSD2 in MDA-MB-231 cells significantly altered the expression of key important epigenetic modifiers such as LSD1, HDAC1/2, and DNMT3B; promoted cellular proliferation; and augmented colony formation in soft agar; while attenuating motility and invasion. Conversely, siRNA-mediated depletion of endogenous LSD2 hindered growth of multiple breast cancer cell lines while shRNA-mediated LSD2 depletion augmented motility and invasion. Moreover, LSD2 overexpression in MDA-MB-231 cells facilitated mammosphere formation, enriched the subpopulation of CD49f<sup>+</sup>/EpCAM<sup>+</sup> and ALDH<sup>high</sup>, and induced the expression of pluripotent stem cell markers, NANOG and SOX2. In xenograft studies using immune-compromised mice, LSD2-overexpressing MDA-MB-231 cells displayed accelerated tumor growth but significantly fewer lung metastases than controls. Taken together, our findings provide novel insights into the critical and multifaceted roles of LSD2 in the regulation of breast cancer progression and cancer stem cell enrichment.**

## INTRODUCTION

Histone lysine methylation is an important covalent post-translational modification (PTM) of chromatin. Histone lysine methyltransferases (KMTs) and demethylases (KDMs) are groups of enzymes that have pivotal roles in dynamic regulation of numerous chromatin functions such as gene transcription, chromatin stability, DNA replication and repair [1, 2]. To date, two different classes of KDMs have been recognized: the flavin-dependent amine oxidase-containing and the Jumonji C (JmjC)-domain-containing enzymes. The flavin-dependent KDM family includes LSD1 (KDM1A) and LSD2 (KDM1B), which both contain a SWIRM domain and share significant sequence homology in their amine oxidase domains. However, LSD2 possesses an N-terminal zinc finger motif, which is required for binding to methylated histone lysine, while lacking LSD1's co-factor binding tower domain. Both enzymes oxidize Carbon-Nitrogen bonds with subsequent production of a demethylated substrate, lysine 4 of histone 3, in a flavin-dependent manner [3, 4]. Although LSD1 and LSD2 are highly similar in amino acid sequences, catalyzed chemical reactions, and substrates, it is evident that the two enzymes also have distinct functions, and therefore may act differentially in regulating chromatin structure and function. Moreover, while LSD1 is mainly associated with the promoter region of genes, LSD2 tends to bind at transcribed coding regions and does not assemble the same transcription repressor complexes as LSD1 [5, 6]. These findings suggest that LSD1 and LSD2 likely interact with different protein partners in the nucleus and play quite distinct roles in regulating key cellular processes.

In the past decade, the flavin-dependent demethylase family has emerged as a potential therapeutic target for breast cancer. According to the data from The Cancer Genome Atlas (TCGA) database, mRNA expression levels of both LSD1 and LSD2 are greatly increased in breast cancer patient specimens in comparison to normal breast tissues. A role for LSD1 has been consistently implicated in tumorigenesis in various cancers, including breast cancer [7-14]. Importantly, LSD1 expression is highly associated with a more aggressive breast cancer phenotype, and work from our laboratory and others has consistently shown LSD1 depletion hinders proliferation and metastasis of breast cancer cells [8, 11, 15, 16]. Many small molecule inhibitors targeting LSD1 have been developed in the past years, and antineoplastic efficacy of several promising compounds has been tested in clinical trials for treatment of cancers such as acute myeloid leukemia (AML) and lung cancer (<http://clinicaltrials.gov>).

LSD2 has been linked to numerous important biological processes including transcription regulation, chromatin remodeling, genomic imprinting, heterochromatin silencing, growth factor signaling and

somatic cell reprogramming [6, 17-20]. While the roles of LSD2 in breast cancer biology have been emerging, the underlying mechanisms are still largely unknown. Recent studies from our laboratory demonstrated that inhibition of LSD2 attenuates colony formation and downregulates global DNA methylation in breast cancer cells [21]. Combined inhibition of DNA methyltransferase (DNMT) and LSD2 reactivates expression of abnormally silenced genes with important functions in breast cancer and enhances cellular apoptotic responses. These findings suggest that combinatorial therapy targeting LSD2 and DNMTs effectively improves the antitumor efficacy of DNMT inhibitors in breast cancer. In this report, we elucidate the *in vitro* and *in vivo* activities of LSD2 in regulation of breast cancer proliferation, migration, invasion and cancer stem cell propagation. These studies provide novel insight into the multifaceted roles of LSD2 in breast cancer progression.

## RESULTS

### LSD2 expression is elevated in breast cancer cell lines and clinical specimens

We examined LSD2 protein level in several human breast cancer cell lines and the normal immortalized human mammary epithelial cell line, MCF10A. Western blots showed that LSD2 protein expression is elevated in breast cancer cell lines compared with MCF10A cells (Figure 1A and 1B). Next, *in silico* analysis of LSD2 expression in clinical cancer patient samples indicated that compared with corresponding normal tissue counterparts, several cancer types including breast have significantly elevated LSD2 mRNA expression (Figure 1C, Supplementary Table 1) (TCGA PANCAN RSEM TPM data downloaded from <https://toil.xenahubs.net>). Overexpression of LSD2 in several pathological types of breast cancer was also found in METABRIC dataset (Curtis Breast) (Supplementary Table 2) (<https://www.oncomine.org>). Further analysis of LSD2 expression across all molecular subtypes of breast cancer showed that LSD2 mRNA level is significantly higher in basal-like tumors as compared to other breast cancer subtypes or normal tissues (Figure 1D) (TCGA data downloaded from GSE62944). Taken together, these data suggest a consistent increase of LSD2 expression in breast cancer cell lines and clinical tumor samples warranting further investigation into the role of LSD2 in breast cancer progression.



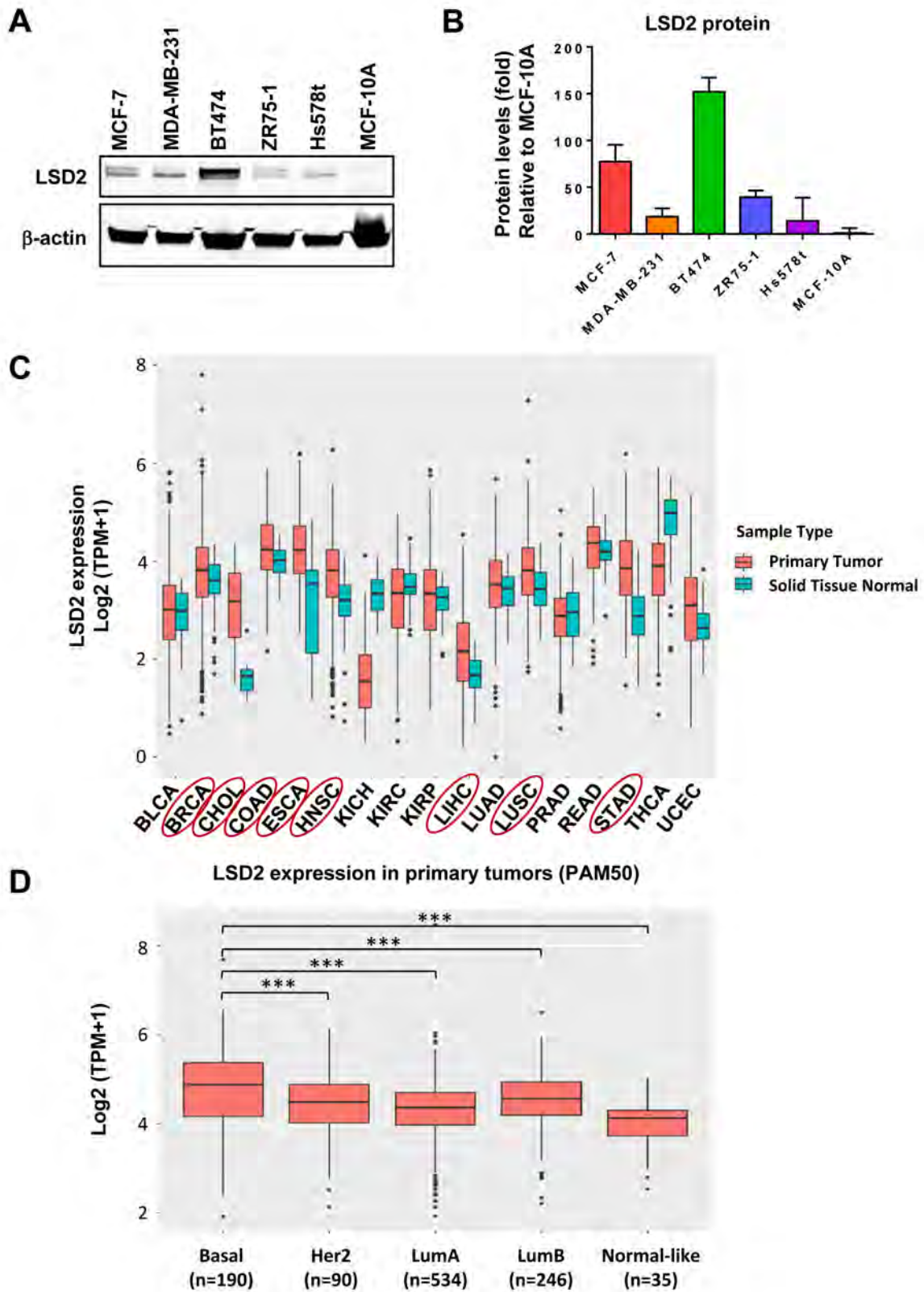


**Figure 1: Expression level of LSD2 in breast cancer cell lines and clinical tumor specimens.** A. Western blot examination of LSD2 protein expression in breast cancer and MCF10A cell lines. B. Quantification of western blot results of LSD2 expression. C. TCGA data analysis of mRNA level of LSD2 in different types of cancer. Cancer types with significantly elevated LSD2 mRNA level were highlighted with Red circle. P-values were calculated using Mann-Whitney U test and corrected for multiple comparisons using Benjamini-Hochberg. D. mRNA levels of LSD2 in different subtypes of breast cancer. Tukey multiple comparisons of means, \*\*\*  $p < 0.001$ .

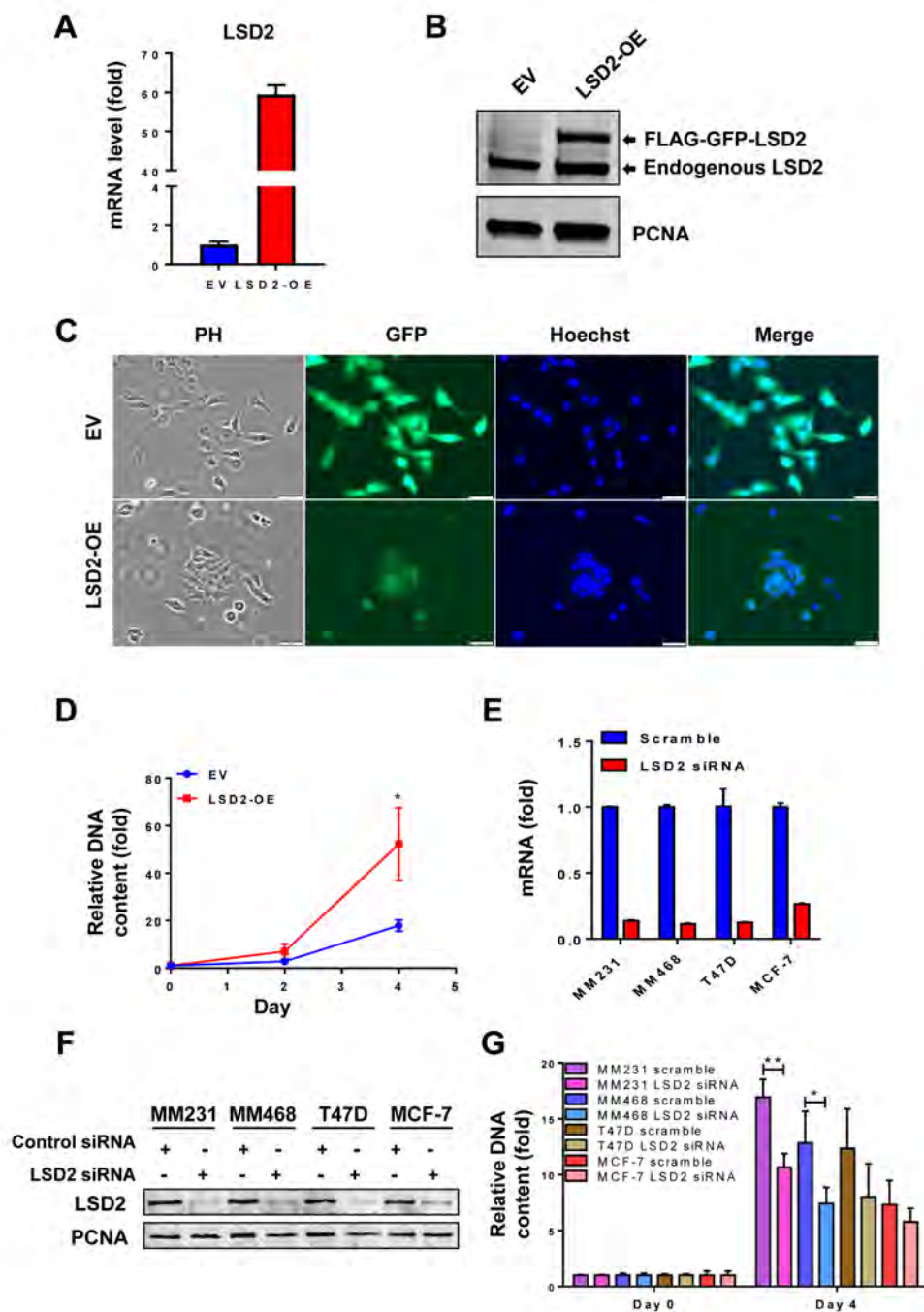


**Figure 2: Effect of LSD2 overexpression or depletion on proliferation of breast cancer cells.** **A.** MDA-MB-231 cells were transfected with control empty vector (EV) or LSD2 overexpression vector (OE) for 48 h followed by selection with G418. mRNA expression of LSD2 was measured by quantitative real-time PCR with GAPDH as an internal control. **B.** Cellular nuclear proteins were extracted, and LSD2 protein expression in MDA-MB-231-EV or LSD2-OE cells was examined by Western blots using anti-LSD2 antibody with proliferating cell nuclear antigen (PCNA) as an internal control. **C.** MDA-MB-231 cells transfected with control empty vector (EV) or LSD2 overexpression vector (LSD2-OE) were fixed with 4% PFA followed by Hoechst 33258 staining. Bright field and fluorescent images were taken to observe cellular morphology and LSD2-GFP protein expression. PH, Phase Contrast. **D.** MDA-MB-231 cells transfected with control empty vector (EV) or LSD2 overexpression vector (LSD2-OE) were analyzed for growth using fluorometric dsDNA quantitation method. **E.** Human breast cancer MDA-MB-231, MDA-MB-468, MCF-7 and T47D cells were transfected with scramble or LSD2 siRNA for 96 h followed by qPCR examination of LSD2 mRNA expression level.  $\beta$ -actin was used as an internal control. **F.** Cells transfected with scramble or LSD2 siRNA were examined for LSD2 protein expression by western blots with PCNA as an internal control. **G.** Fluorometric dsDNA quantitation assays were performed to evaluate growth of breast cancer cells which were transfected with scramble or LSD2 siRNA for 96 h. All experiments were performed at least three times and bars represent the means of three independent experiments  $\pm$  s.d. \*  $p < 0.05$ , \*\*  $p < 0.01$ , Student's t-test.

## LSD2 promotes breast cancer cell growth and colony formation

To explore the functional role of LSD2 in regulating breast cancer development, we stably overexpressed eGFP and Flag-dually tagged LSD2 in MDA-MB-231 (LSD2-OE) and validated the overexpression at the mRNA and protein levels (Figure 2A and 2B). Tracking of the GFP tag through fluorescent microscopy showed that the LSD2-eGFP-Flag localizes exclusively to the nucleus in MDA-MB-231 cells (Figure 2C). While cells transfected with control empty vector (EV) display the spindle shaped morphology of parental MDA-MB-231 cells, LSD2 overexpression induces a cobblestone-like morphology with apparent cell-cell adhesion (Figure 2C).

Next, we investigated the potential impact of increased LSD2 expression on breast cancer cell proliferation. Cellular proliferation assays showed that stable overexpression of LSD2 in MDA-MB-231 cells

significantly promoted cellular growth rate (Figure 2D). To further validate this phenotypic change, two basal-like/triple-negative breast cancer (TNBC) cell lines, MDA-MB-231 and MDA-MB-468, and two luminal/Estrogen Receptor positive (ER+) cell lines, T47D and MCF-7, were transfected with non-targeting scramble or LSD2-specific siRNA. LSD2-targeting siRNA effectively suppressed endogenous LSD2 mRNA and protein expression in all lines (Figure 2E and 2F). Although depletion of LSD2 hindered the cell proliferation in all lines, this effect was more pronounced and statistically significant in TNBC cell lines as compared to ER+ cell lines (Figure 2G).

Our previous study demonstrated that shRNA-mediated inhibition of LSD2 leads to a significant reduction in 2D colony formation in MDA-MB-231 cells, indicating a survival-promoting role for LSD2 in breast cancer cells [21]. In this study, we investigated the effect of LSD2 overexpression on 2D colony formation of MDA-MB-231 cells. In agreement with the effect of LSD2 knockdown, ectopic expression of LSD2 in MDA-

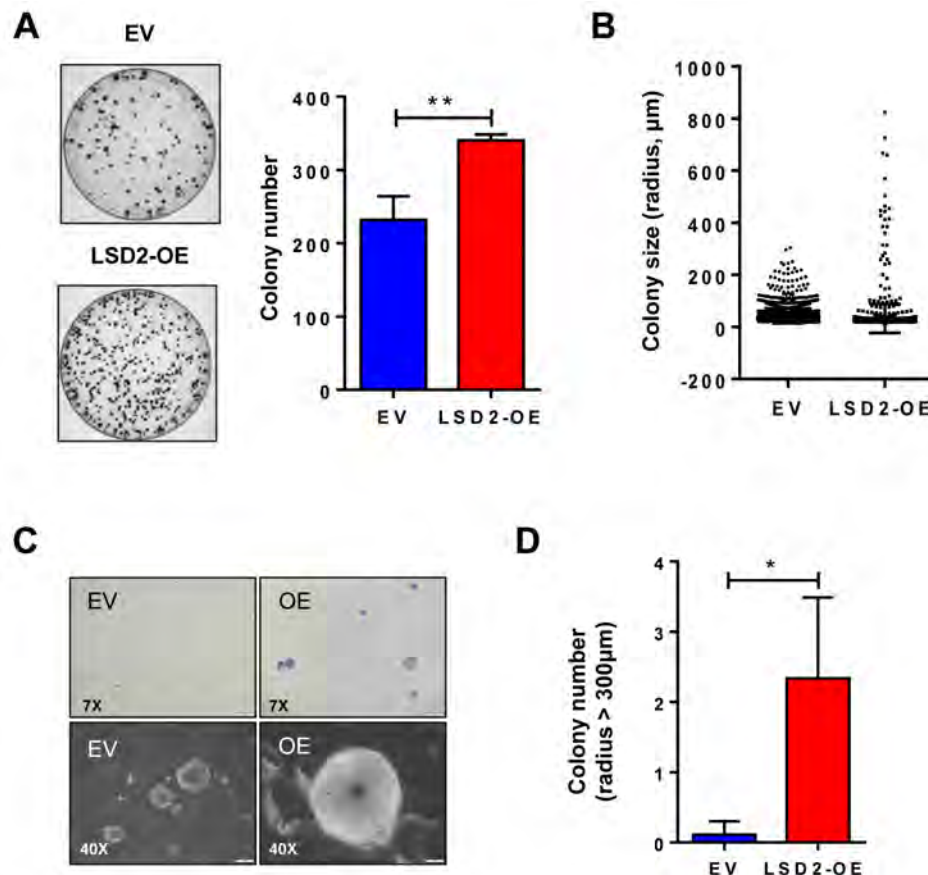


**Figure 3: LSD2 enhances the colony formation capacity of MDA-MB-231 cells.** A. 500 cells stably transfected with empty vector or LSD2 expression plasmids were plated in 10cm dish. After 14 days, colonies formed were stained with 0.5% crystal violet and counted. B. 10,000 cells per dish were seeded in 0.4% soft agar in 35mm dish. After 3 weeks, colonies were stained with 0.005% crystal violet and counted using CellSens software. Individual colonies formed by empty vector control or LSD2 overexpressing MDA-MB-231 cells were plotted based to colony size ( $\mu\text{m}$ ). C. Representative microscopy images (7x and 40x) of cellular colonies after 3 weeks of seeding the cells on soft agar coated wells. D. Average numbers of colony whose radius is over 300 mm. Error bar represents  $\pm$  s.d. from three independent experiments. \*  $p < 0.05$ , \*\*  $p < 0.01$ , Student's t-test.

MB-231 cells significantly increases the number of 2D colonies (Figure 3A). We then extended our investigation to an anchorage-independent soft-agar colony formation assay to further dissect the role of LSD2 in breast tumorigenicity. The soft agar results showed that, although there was no significant difference in average colony size (Figure 3B), LSD2-OE cells developed an increased number of larger colonies (> 300  $\mu$ m) than empty vector cells (Figures 3B, 3C and 3D). Collectively, these results suggest that LSD2 enhances *in vitro* colony formation capacity of breast tumor cells.

### **LSD2 attenuates motility and invasion of breast cancer cells**

Enhanced motility and invasion are positively associated with the aggressive behavior and poor prognosis of breast cancer. We anticipated that accelerated growth rate by LSD2 overexpression would lead to corresponding augmentation of cellular motility and invasion and tested this hypothesis through transwell Boyden chamber assays. Unexpectedly, we found that LSD2 overexpression significantly reduced migration and invasion of MDA-MB-231 cells (Figure 4A and 4B). To validate this result, we performed the same experiments using a pool of MDA-MB-231 cells stably expressing shRNA against LSD2, which decreased LSD2 mRNA expression by about 75% as compared with scramble control cells (Supplementary Figure 1). Boyden chamber assays demonstrated that loss of LSD2 facilitated cell migration and invasion of MDA-MB-231 cells (Figure 4C and 4D). To further verify these results, we performed *in vitro* wound-healing assay and found that MDA-MB-231 cells transfected with control empty vector closed the wound much more efficiently than LSD2-overexpressing cells (Figure 4E and 4F). On the contrary, inhibition of LSD2 in MDA-MB-231 cells significantly augmented the wound-healing rate (Figure 4G and 4H). Collectively, these results point to an inhibitory role of LSD2 in mediating breast cancer cell migration and invasion.

### **LSD2 overexpression promotes breast cancer stem cell-like characteristics**

Breast cancer stem-like cells (BCSCs) possess features of multipotent, oncogenic, and self-renewal capacity, which are responsible for breast tumor heterogeneity [22, 23]. Recent studies have shown that LSD1 plays a critical role in promoting the differentiation and self-renewal of cancer stem cells (CSCs) in human breast cancer and in other cancer types [24, 25]. To elucidate the potential implication of LSD2 in breast cancer stem cell phenotypes, mammosphere formation assay was carried out, which showed that LSD2 overexpression significantly increases the size and

number of both primary and tertiary spheres (Figure 5A and 5B), suggesting the enrichment of a subpopulation of CSCs with self-renewal capacity in LSD2-OE cells. Flow cytometry analysis of LSD2-OE cells indicated a significantly increased CD49<sup>+</sup>/EpCAM<sup>-</sup> subpopulation, which is considered to be enriched for stem/basal progenitor cells (Figure 5C and 5D). We also examined the nuclear protein expression of four embryonic stem cell (ESC) markers, KLF4, NANOG, OCT4 and SOX2 and observed that LSD2 overexpression increases expression of NANOG and SOX2 (Figure 5E and 5F). Finally, we investigated the level and activity of Aldehyde Dehydrogenase (ALDH) in LSD2-OE cells. Recent studies indicate that enhanced ALDH activity is a hallmark of cancer stem cells [26, 27]. In line with previous report that MDA-MB-231 cells express very low level of ALDH (0%-1% positive) [28], no obvious ALDH<sup>high</sup> cells were detected in MDA-MB-231 EV cells (around 0%) whereas LSD2 overexpression increased ALDH<sup>high</sup> cell population to about 1.5% (Supplementary Figure 2). In addition, mRNA expression of many ALDH family members was increased by LSD2-OE based on our recently microarray study (Supplementary Table 3). Collectively, all these data point to the critical function of LSD2 in promoting BCSC-like properties.

### **Overexpression of LSD2 alters expression of key**

Our recent studies have revealed that dysregulated regulatory networks formed by aberrant crosstalk between histone methylation and histone acetylation or DNA methylation profoundly impact breast cancer progression [13, 15, 21, 29]. To explore the involvement of LSD2 in these regulatory processes, we assessed the impact of LSD2 overexpression or deficiency on mRNA and protein expression of key members of DNMT, HDAC and KDM families. Quantitative RT-PCR results showed that LSD2 overexpression significantly increased the mRNA levels of LSD1, HDAC1, 2, 3, 5, 6, 8, DNMT3B and 3L, KDM4B and KDM5B (Figure 6A). On the other hand, expression of only a few genes was affected by LSD2 stable knockdown, including HDAC9 and DNMT3L (Figure 6B). In LSD2 siRNA-transfected MDA-MB-231 cells, mRNA levels of LSD1, HDAC4, and DNMT3B were decreased while HDAC1 mRNA level was increased (Supplementary Figure 3). The protein expression of several genes was further tested to determine if there is correlated alteration between mRNA and protein expression. Quantitative western blots showed that LSD2 overexpression significantly increased the protein expression of LSD1, HDAC1, 2, 6, 8 and DNMT3B, and inhibited the expression of HDAC5 and DNMT3L (Figure 6C), whereas DNMT3B was the only factor altered by LSD2-KD (Figure 6D).

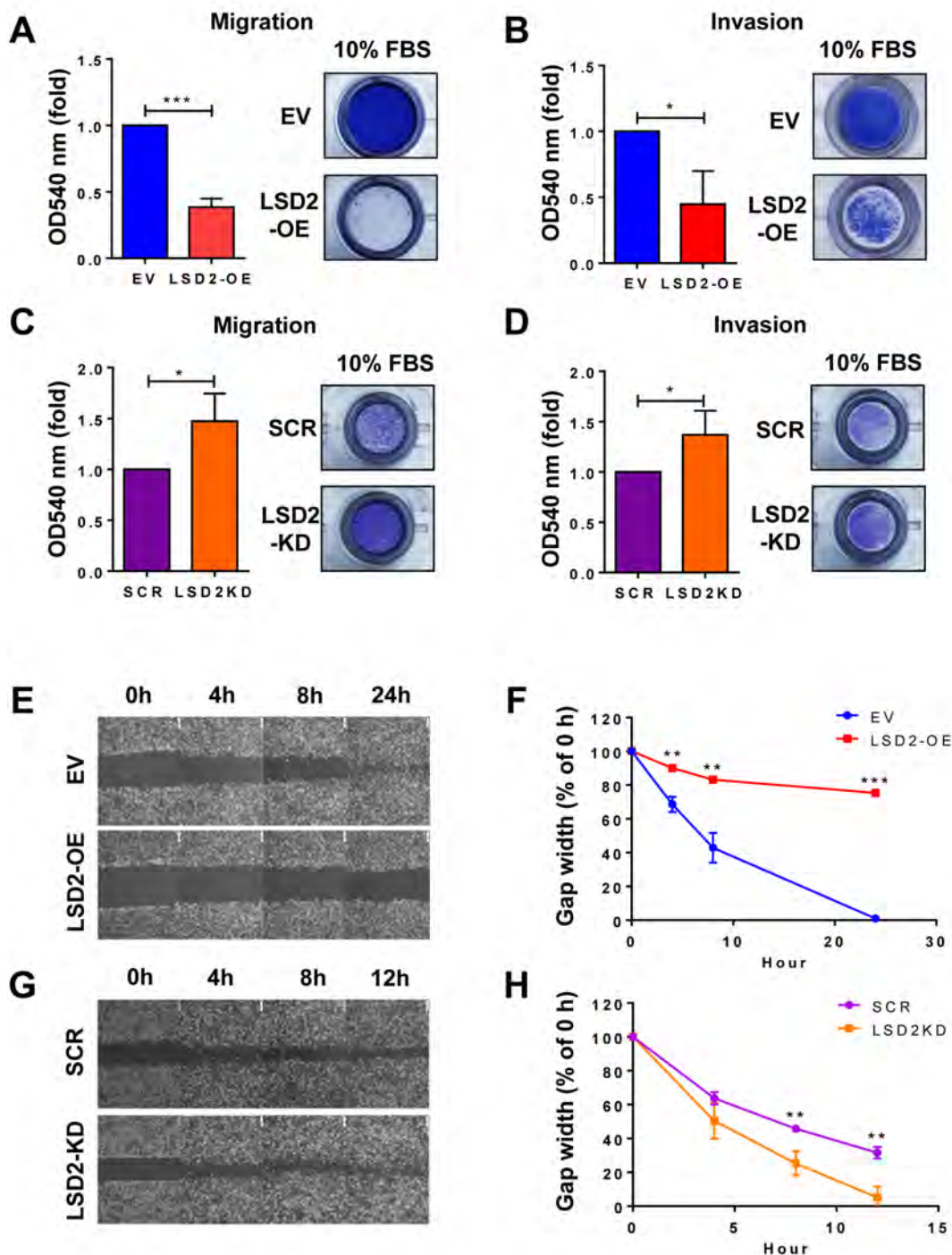


**Figure 4: LSD2 regulates migration and invasion in MDA-MB-231 cells.** **A.** Transwell migration assay was performed to detect the migratory capacity of MDA-MB-231 EV and LSD2-OE cells. Quantification of the migrated cells was done by solubilization of crystal violet and spectrophotometric reading at OD 540. **B.** Quantification of the invasive MDA-MB-231 EV and LSD2-OE cells. Transwell invasion assay was performed and the invasive cells were quantified by solubilization of crystal violet and spectrophotometric reading at OD 540. **C.** Quantification of the migratory MDA-MB-231 cells transfected with scramble and LSD2 shRNA plasmids. **D.** Quantification of the invasive MDA-MB-231 cells transfected with scramble and LSD2 shRNA plasmids. **E.** Confluent monolayers of EV and LSD2-OE MDA-MB-231 cells were wounded by scratch with a pipette tip. Cells were then incubated for 24 h. Images were taken at the end points to be compared to 0 h to measure wound healing. **F.** The average of wound closure rate during the first 24 h of wound healing was calculated. **G.** Confluent monolayers of scramble shRNA and LSD2-KD MDA-MB-231 cells were wounded by scratch. Cells were then incubated for 12h. Images were taken at the end points to be compared to 0h to measure wound healing. **H.** The average of wound closure rate during the first 12 h of wound healing was measured and quantified. All experiments were independently performed at least three times and values represent the mean  $\pm$  s.d. \*  $p < 0.05$ , \*\*  $p < 0.01$ , \*\*\*  $p < 0.001$ , Student's t-test.

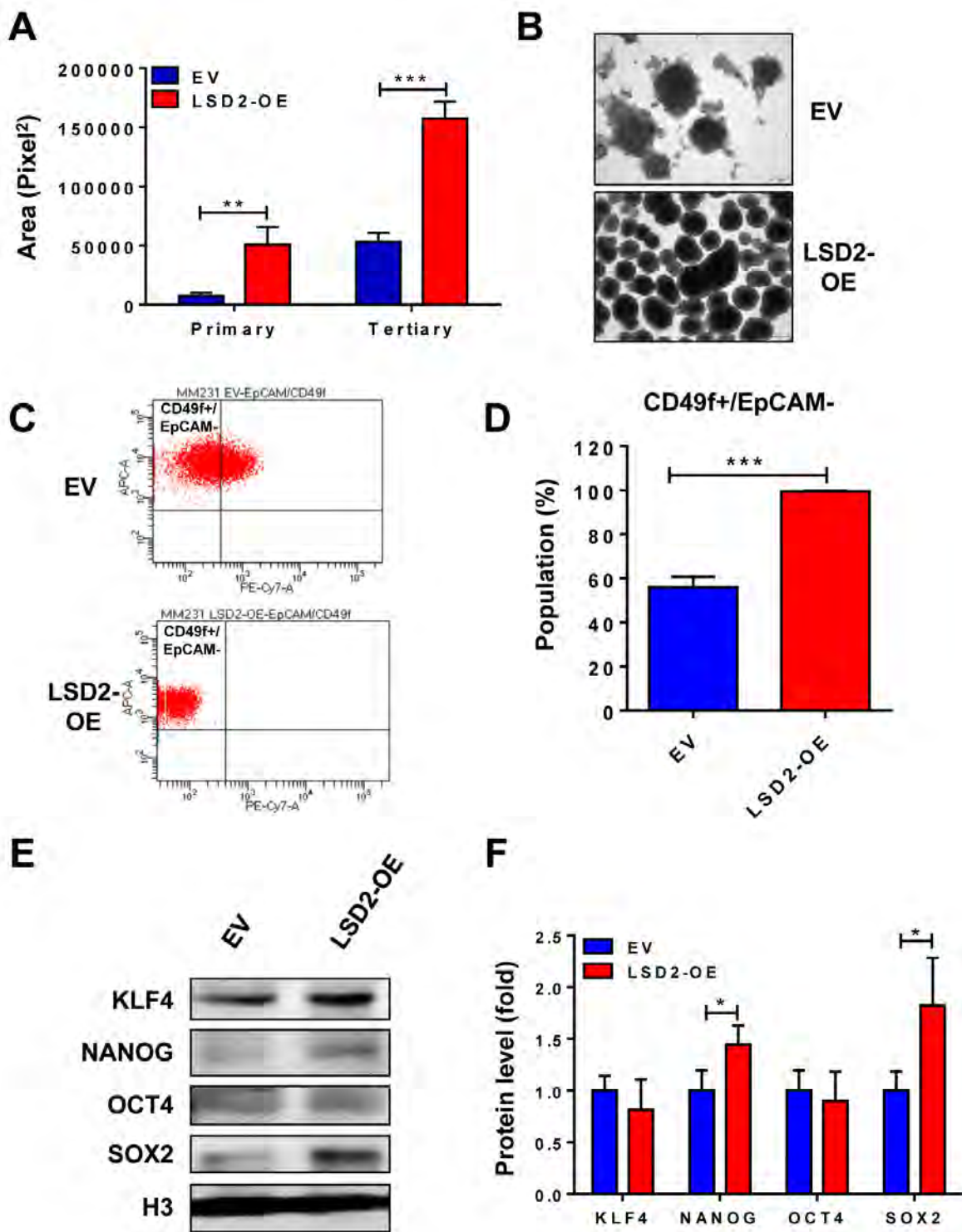


**Figure 5: Overexpression of LSD2 facilitates breast cancer stem cell characteristics.** A. MDA-MB-231 EV or LSD2-OE cells were suspended in tumor sphere medium and seeded in 6-well plate with ultra-low attachment surface. After 7-day incubation, spheres were collected and digested into single cells. Same density of digested cells was seeded for secondary mammosphere and tertiary mammosphere formation. Quantification of primary and tertiary mammospheres was performed using CellSens software. B. Representative pictures of tertiary mammospheres formed by EV and LSD2-OE cells. C. Flow cytometry analysis of cell surface marker CD49f and EpCAM in EV and LSD2-OE cells. D. The percentage of CD49f<sup>+</sup>/EpCAM<sup>-</sup> cells was quantified from three independent experiments. E. Western blot examinations on nuclear protein levels of KLF4, NANOG, OCT4 and SOX2 in EV and LSD2-OE cells. Histone 3 (H3) was used as internal control. F. The experiments were performed three times with similar results. Values represent means  $\pm$  s.d. \*  $p < 0.05$ , \*\*\*  $p < 0.001$ , Student's t-test.

Increased LSD1 expression in LSD2-OE cells raises an important question as to whether the tumor growth promoting activities of LSD1 and LSD2 are interdependent. To address this question, a rescue experiment was carried out to knock down LSD1 expression by siRNA in EV and LSD2-OE cells. Treatment with siRNA effectively depleted the mRNA expression of LSD1 without altering LSD2 expression

levels (Supplementary Figure 4). Rescue with LSD1 siRNA hindered the growth of both MDA-MB-231 EV and LSD2-OE cells, but exhibited a similar extent of rescue efficiency (decreases of about 35% vs 39%) (Figure 6E). This result clearly indicates that LSD2 promotes breast cancer cell proliferation in an LSD1-independent manner.

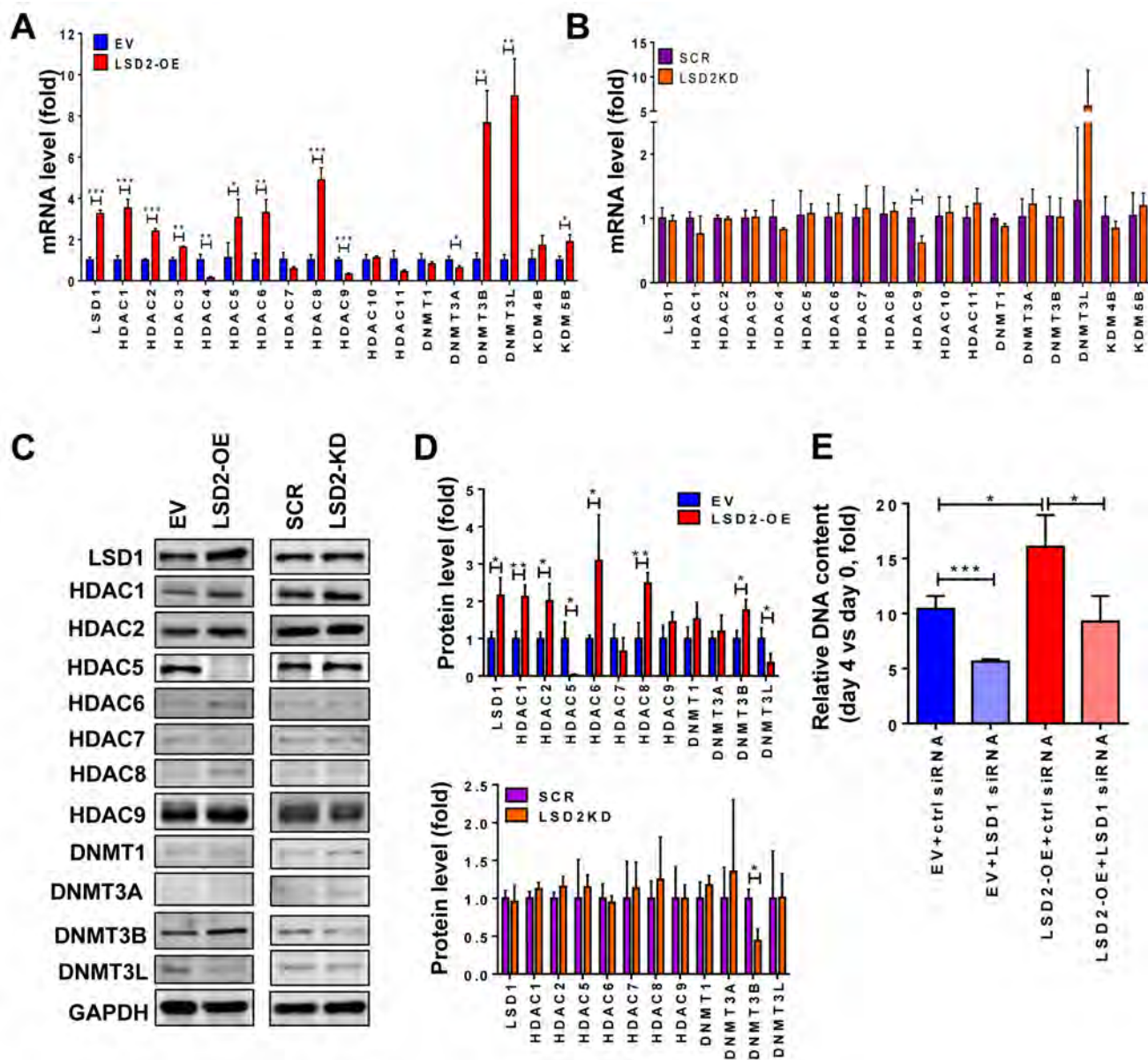


**Figure 6: Effect of LSD2 on expression of key epigenetic**

A. RNA was extracted from MDA-MB-231 EV and LSD2-OE cells and cDNA was synthesized and subjected to quantitative real-time PCR for the indicated genes using TaqMan probes. GAPDH expression was used as an internal standard. B. mRNA expression of chromatin modifying factors in MDA-MB-231 cells stably transfected with scramble (SCR) or LSD2 shRNA (LSD2-KD). GAPDH expression was used as an internal standard. C. Indicated chromatin modifying factors were analyzed for their protein levels by western blots in MDA-MB-231 EV, LSD2-OE, scramble shRNA and LSD2-KD cells. GAPDH was used as a loading control. D. Histograms represent the average protein levels of indicated chromatin modifiers in three independent experiments relative to GAPDH protein  $\pm$  s.d. as determined by quantitative immunoblots. E. MDA-MB-231 EV and LSD2-OE cells were transfected with scramble or LSD1 targeting siRNA for 96 h followed by growth assay using fluorometric dsDNA quantitation. Column with error bar represents mean  $\pm$  s.d. from three independent experiments. \*  $p < 0.05$ , \*\*  $p < 0.01$ , \*\*\*  $p < 0.001$ , Student's t-test.

## Overexpression of LSD2 promotes growth and inhibits lung metastasis of MDA-MB-231 xenograft tumors in nude mice

To confirm our *in vitro* results, we implanted MDA-MB-231 EV and LSD2-OE cells into the mammary fat pads of athymic nude mice. LSD2 overexpression led to accelerated tumor growth, with approximately three-fold increase in average tumor size over empty vector cells

(Figure 7A and 7B). Statistical analysis of *in vivo* tumor growth is summarized in Supplementary Table 4. Average weight of LSD2-OE tumors was statistically higher than control group at the end of the experiment (Figure 7C). Both groups of animals had normal body weight gains (Figure 7D). To evaluate *in vivo* effect of LSD2 on tumor metastasis, we quantified mRNA expression of human housekeeping gene HPRT1 in mouse lung tissue samples by real-time RT-PCR using a probe that does not cross-react with its mouse counterpart. Our results showed that

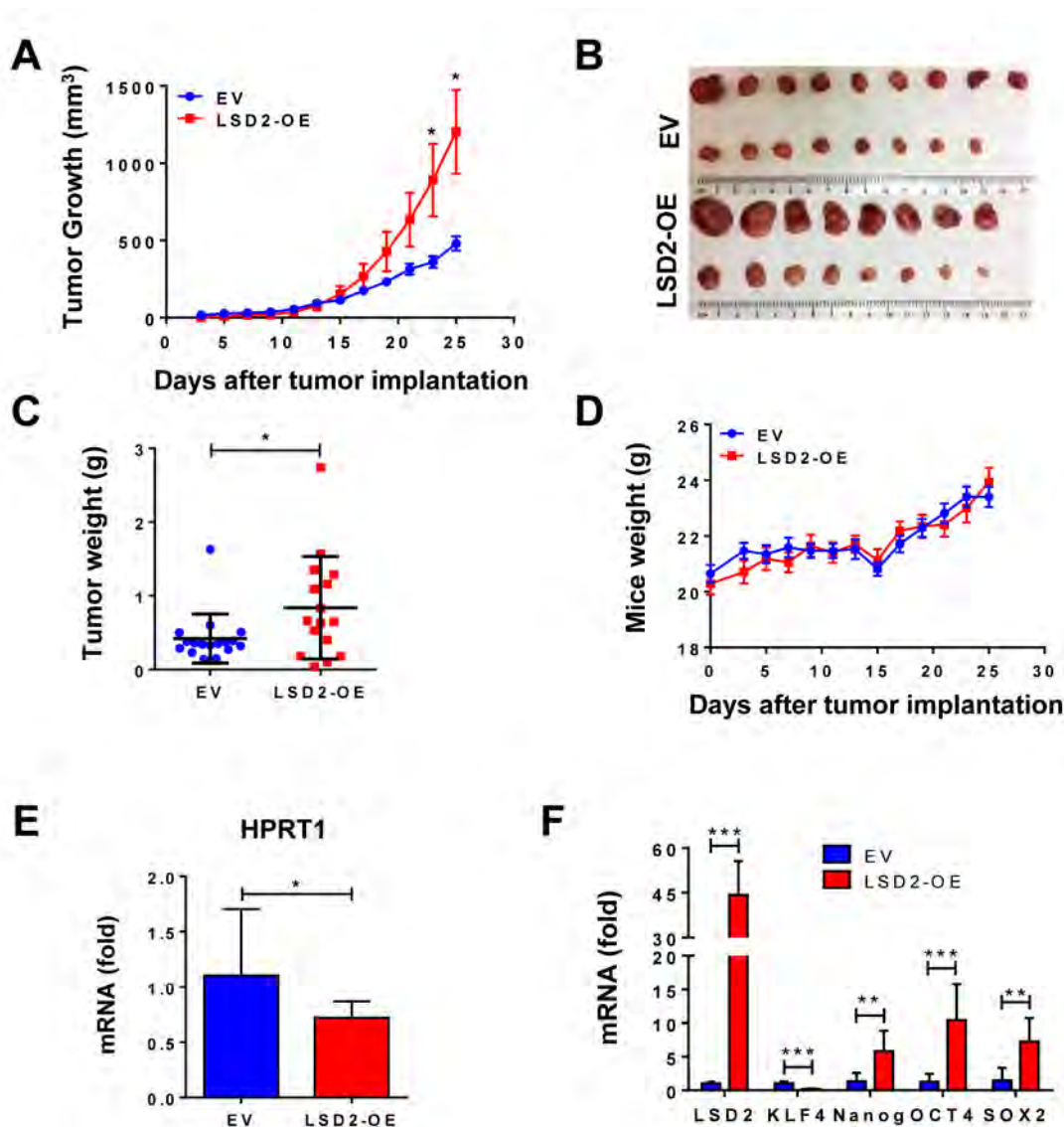


**Figure 7: *In vivo* effect of LSD2 on proliferation and metastasis in mice bearing MDA-MB-231 xenograft.** A. MDA-MB-231 cells transfected with empty vectors ( $n = 17$ ) or LSD2 expression vectors ( $n = 16$ ) were transplanted into the mammary fat pad of nude mice. Tumor volumes were regularly assessed every two days. Shown are average tumor volumes  $\pm$  s.e. B. Orthotopically implanted tumors were removed after terminating the experiments. Shown are pictures of implanted tumors. C. Weight of individual animal tumor was measured at the end of experiment. D. Weights of mice were measured on the indicated days. Points, mean mouse weight (g); bars, mean  $\pm$  s.d. E. Tumor cells metastasized to mice lung were assessed by quantification of mRNA expression of human HPRT1 gene (EV,  $n = 10$ ; LSD2-OE,  $n = 16$ ). Mouse b-actin was used as internal control. Graph was plotted as fold change with normalization to EV. F. Total RNA was extracted from 7 randomly selected tumors from each group and mRNA levels of the four embryonic stem cell markers were evaluated by qPCR. \* $p < 0.05$ , \*\* $p < 0.01$ , \*\*\* $p < 0.001$ , Student's t-test.



mRNA level of hHPRT1 gene was significantly reduced in lung tissues of mice bearing LSD2-OE tumors (Figure 7E). Normal mouse lung tissue was used as a negative control, and no expression of hHPRT1 was detected, thus validating the specificity of the hHPRT1 probe (Data not shown). To determine the *in vivo* impact of LSD2 overexpression on cancer stem cell markers, qPCR analysis was performed on RNA from tumors, which showed that the mRNA expression of NANOG, OCT4 and SOX2 were significantly induced in LSD2-OE xenograft tumor cells (Figure 7F). In agreement with *in vitro* results, the findings from this mouse study suggest that LSD2 promotes breast tumor growth and BCSC characteristics, while simultaneously attenuating cell invasion and dissemination *in vivo*.

## DISCUSSION

Histone demethylases have emerged as a novel class of epigenetic regulators controlling cancer initiation and progression [30]. Dysregulated expression and functions of histone lysine demethylases are found in many types of cancers, and thus represent novel promising therapeutic targets for cancer. In the past decade, rapid progress has been made in understanding the molecular basis of histone demethylase-dependent functions in breast cancer biology [16, 20]. Among these enzymes, LSD1 is the first recognized histone lysine demethylase and perhaps one of the best-characterized histone-targeted enzymes in breast cancer. However, the involvement of LSD2, the only identified homolog of LSD1, in breast cancer is still very elusive. *In silico* data indicate a significant elevation of LSD2 expression in aggressive basal-like breast tumors as compared with other breast cancer subtypes and normal tissues, suggesting a potential link between LSD2 overexpression and aggressiveness of breast cancer. However, the molecular mechanism of LSD2 upregulation in breast cancer and the long-term clinical impact of elevated LSD2 expression in the risk stratification of breast cancer patients are still unclear. Therefore, more robust studies are needed to clarify these questions.

While LSD1 is typically associated with oncogenic phenotypes in almost all types of cancer, little is known about the function of LSD2 in mediating tumor progression. A recent study by Yang *et al* reported that LSD2 acts as an E3 ubiquitin ligase and inhibits A549 lung cancer cell growth through proteasomal degradation of O-GlcNAc transferase (OGT) [31], suggesting that LSD2 may inhibit the growth of certain types of cancer in a ubiquitination-dependent manner. The *in vivo* effect of LSD2 on A549 cell growth warrants further examination. In our study, we utilized both *in vitro* and *in vivo* models to investigate the potential implication of LSD2 in regulating breast cancer proliferation and metastasis. We found that overexpression of LSD2 in breast cancer cells consistently enhances MDA-MB-231

cell growth *in vitro* as well as in tumor xenografts in mice, whereas depletion of LSD2 by siRNA hinders the growth of multiple breast cancer cell lines. We also showed that LSD2 overexpression increases the number of colonies in 2D monolayer culture and large colonies in anchorage-independent 3D culture, indicating that LSD2 may potentiate the malignant transformative capacity of breast cancer cells. Interestingly, overexpression of LSD2 results in an increase of mRNA and protein expression of LSD1. A rescue study demonstrated that simultaneous treatment with LSD1 siRNA in control and LSD2-OE cells exerts similar effect on LSD2-mediated tumor cell growth. This result suggests that LSD1 and LSD2 may have non-redundant roles in promoting breast cancer proliferation.

The concept of breast cancer stem cells (BCSCs) was first introduced by Al-Hajj *et al* [32]. BCSCs are a rare subpopulation that originates from a small fraction of tumor initiating cells with the abilities of self-renewal, unlimited propagation and multipotent differentiation. Importantly, BCSCs are associated with poorer clinical outcome and are intrinsically resistant to therapy. Wu *et al* recently reported that the deubiquitinase USP28 promotes breast cancer stem cell (BCSC)-like characteristics *in vitro* and *in vivo* through stabilizing LSD1 protein [24]. We explored the potential regulation of LSD2 on BCSC features and showed that LSD2 overexpression facilitates the formation of several generations of mammospheres, enriches the CD49<sup>+</sup>/EpCAM<sup>+</sup> stem/basal progenitor subpopulation and promotes the expression of several pluripotent stem cell markers *in vitro* and in MDA-MB-231 xenograft tumors. Our findings indicate that, like LSD1, LSD2 has an important role in conferring CSC-like traits to breast cancer cells. In ESCs, the histone modification landscape profoundly influences the crosstalk of transcriptional regulators [33, 34]. Increasing lines of evidence suggest that the two key histone marks, H3K4 methylation and H3K27 methylation, serve as critical histone bivalent marks controlling developmental regulatory genes in embryos and ESCs [33, 35, 36]. LSD1 has been shown to act as a key histone modifier in the maintenance of pluripotency by occupying the promoter of a subset of developmental genes containing bivalent domains (H3K4 di/trimethylation and H3K27 trimethylation marks) and regulating the balance between self-renewal and differentiation in human ESCs [37]. It is probable that LSD2, in collaboration with LSD1, provides an additional layer of epigenetic modification in governing breast cancer stem cell features through modulation of the level of H3K4 methylation at pluripotent regulatory genes. Future study using genome-wide mapping approaches would aid in probing the subset of LSD2 target genes and histone mark alterations that are associated with biological processes in BCSC development.

Our studies point to potentially opposite roles of LSD2 in regulating breast cancer cell growth and invasion. Our *in vivo* study validated *in vitro* results showing that

lung metastasis is attenuated in mice bearing LSD2-overexpressing tumors. This opposite effect may reflect a broad and complex involvement of LSD2 in regulating histone function and gene transcriptional activities that could ultimately up-regulate growth-associated gene expression, while suppressing motility and invasion genes. Indeed, several other studies have reported that a number of genes possess opposite effects on cancer proliferation and metastasis [38, 39]. Morphologically, MDA-MB-231 LSD2-OE cells acquire tightly cohesive, cobblestone-like epithelial cell morphology as compared to the elongated fibroblast-like control cells. This finding suggests that increased LSD2 expression may induce a mesenchymal-epithelial transition (MET) through acquisition of epithelial markers with concurrent loss of mesenchymal features, which in turn leads to loss of migratory and invasive ability of tumor cells. Indeed, a number of genes involved in tight junction or apical-basal polarity such as OCLN, DSP, SCRIB, etc., were upregulated by LSD2-OE while VIM and FN1 were downregulated according to results of our recent microarray analysis (Supplementary Table 5). Some early studies have revealed that activated EMT program in non-transformed epithelial cells could confer properties of stem cells which may facilitate the development of tumor initiating cells [40]. However, a number of groups have recently reported that EMT may not be necessarily associated with cancer stemness features. For example, Schmidt *et al.*, have shown that activities of EMT and stemness are somehow antagonistic and attenuation of the EMT process is required for the full acquisition of stem cell properties [41]. The Weinberg lab demonstrated that the EMT program may not be sufficient to induce changes of stemness in differentiated luminal cells, and additional genetic programs are needed to interact with EMT environment to induce phenotypic alteration of cancer stemness [42]. Future studies using appropriate *in vitro* and *in vivo* models are required to completely understand the precise role of LSD2 in regulating cross-talk between EMT/MET and stemness and its relevance in breast cancer progression and metastasis.

Our study also revealed that the expression levels of many key chromatin modifiers are altered by LSD2 overexpression, indicating a significant role of LSD2 in the epigenetic regulatory network in breast cancer cells. For example, stable LSD2 overexpression significantly increases the expression of LSD1, HDAC1, and HDAC2, which are important components of the NuRD (nucleosome remodeling and histone deacetylase) complex that has important implications in cancer biology [43, 44]. LSD2 overexpression also promotes the expression of DNMT3B, which is a critical epigenetic player in inducing aberrant DNA methylation and gene silencing in cancer [45]. The molecular mechanisms linking LSD2 to transcriptional regulation remain elusive. A study by Fang *et al* used CHIP-chip tiling array to map

LSD2 binding loci on a genome-wide scale and found that, in addition to H3K4 demethylase activity, LSD2 may act as a positive regulator of gene transcription through binding to highly transcribed coding regions enriched in active histone marks such as H3K36me3 [6]. They also reported that LSD2 forms a complex with euchromatic histone methyltransferases EHMT1/2 and NSD3 as well as active transcription elongation factors such as Pol II and cyclin T1 [6]. We also noted that stable and transient knockdown of LSD2 exerted distinct impact on expression of epigenetic modifiers. It is possible that long-term suppression of LSD2 may intrinsically alter the genomic expression of other proteins and leads cells to compensate by increasing or reducing the expression of other signaling proteins. Further investigation is required to define the exact mechanisms by which LSD2 alters transcription of key epigenetic modifiers through mediating histone disassembly/reassembly and transcription elongation at gene coding regions.

In summary, our studies provide novel insight into the previously unrecognized roles of LSD2 in human breast cancer cells. We have shown for the first time that LSD2 augments proliferative and cancer stem cell traits, and attenuates motility and invasiveness of breast cancer cells. All of these findings suggest that LSD2 has complex and multifaceted roles in breast oncogenesis. In the future, better understanding of epigenetic downstream target genes and pathways controlled by LSD2 would aid in developing novel small molecule inhibitors and combination strategies which might confer selective effects against breast cancer.

## MATERIALS AND METHODS

### Cell lines and culture conditions

Human breast cancer cell lines MDA-MB-231, MDA-MB-468, MCF-7, T47D and normal immortalized breast epithelial cell line, MCF10A, were obtained from the ATCC/NCI Breast Cancer SPORE program. Cells were cultured in growth medium as described previously [15, 46]. Stable transfectant lines were maintained with 800 µg/mL G418 (Geneticin).

### Plasmid construction and stable transfection

Full length human LSD2 cDNA from MCF-7 cells was originally cloned by PCR into pcDNA3.1/V5-His TOPO. PCR primers engineered with KpnI sites were used to amplify LSD2 and then cloned into eGFP-Flag vector (using KpnI site in MC1) purchased from Gene Copoeia (Rockville, MD). Empty eGFP-flag vector (EV) or LSD2-eGFP-Flag (LSD2-OE) was transfected into MDA-MB-231 cells using Lipofectamine 3000 (Thermo Fisher

Scientific, Waltham, MA) according to manufacturer's instructions. After 48-hour transfection, cells were selected with 800 µg/mL G418 for several weeks. Then eGFP-positive cells were further sorted three times by flow cytometry to enrich LSD2-eGFP-Flag overexpressing cells.

### Small interfering RNA treatment

Pre-designed LSD2 or LSD1 siRNA and non-targeting scramble siRNA (Santa Cruz Biotechnology, Dallas, TX) were transfected into cells following manufacturer's protocol. Briefly, cells were seeded in 96-well plates the day before transfection. siRNA was prepared in transfection medium (sc-36868) with transfection reagent (sc-29528). Cells were washed using transfection medium before 100 µL of siRNA complexes were added. After 5-hour incubation at 37°C, 100 µL normal growth medium containing 2x fetal bovine serum was added to each well. After 96-hour incubation, relative cell number was evaluated using FluoReporter Blue Fluorometric dsDNA Quantitation Kit (Thermo Fisher Scientific) according to manufacturer's protocol.

### shRNA treatment and stable cell line generation

Scramble and 4 different LSD2 shRNAs were purchased from SABiosciences (Germantown, MD) and reverse transfected with Attractene transfection reagent (using GFP expression plasmids first, followed by Gentamycin expression plasmids) into MDA-MB-231 cells. At 48 h post-transfection, cells were first selected with 800 µg/ml G418 for several weeks, and then sorted by flow cytometry to enrich for GFP+ cells. All transfections were assayed by qPCR and western blot analysis for the best knockdown efficiency.

### RNA extraction and qPCR

Total RNA was extracted using RNeasy kit (Qiagen, Valencia, CA) following manufacturer's instructions. Tissues were directly homogenized in RNA lysis buffer which in this kit is RLT buffer. cDNA was synthesized using M-MLV Reverse Transcriptase (Thermo Fisher Scientific). Quantitative real-time PCR was performed on the StepOne real-time PCR system using TaqMan Gene Expression Assays (ThermoFisher Scientific).

### Immunoblotting

Whole cell lysate and nuclear proteins were extracted as described previously [15, 21, 29]. Briefly, 60 µg whole cellular protein or 30 µg nuclear protein was separated on Mini-PROTEAN® TGX™ 4-20% acrylamide

gels and transferred onto NC membranes. Antibodies used in this study are shown in Supplementary Table 6. CD49f-APC and EpCAM-PE-Cy7 antibodies (BD Biosciences, Franklin Lakes, NJ) were provided by Dr. Mei Zhang (University of Pittsburgh Cancer Institute). Membranes were scanned with Odyssey Infrared Imaging System (Li-Cor Biosciences, Lincoln, NE).

### Cell proliferation assay

Cells were seeded at 1000 to 5000 cells per well in 96-well plates. At each time point, medium was discarded by inverting the plates. Then the plates were frozen in -80°C freezer until ready to be measured. 100 µl distilled water was added into each well after the plates were thawed to room temperature. Then the plates with water were incubated at 37°C for 1h. Plates were frozen and thawed again to lyse the cells in order to release DNA completely. The DNA content was measured using FluoReporter Blue Fluorometric dsDNA Quantitation Kit (Thermo Fisher Scientific) by adding 100 µL of aqueous Hoechst 33258 in TNE buffer into each well and then measured using VICTOR X4 plate reader (PerkinElmer, Waltham, MA).

### Monolayer culture colony formation assay

Empty vector and LSD2-OE MM231 cells were seeded at 500 cells per 10cm dish. After 14 days, cells were stained with 0.5% crystal violet, dried overnight and colonies were counted. Colonies that contained >50 cells were scored. All experiments were carried out independently at least three times. The results were expressed as means ± s.d.

### Soft agar colony formation assay

1.2% Bacto-agar (BD Biosciences) was autoclaved and then warmed to 42°C. By mixing 1.2% agar with growth medium 1:1, 0.6% agar/medium was generated and then 1.5 ml of the mixture was quickly plated into 35mm dishes as base layer. Solidification was completed at room temperature for 45 min. Then 4.5x10<sup>4</sup> cells were suspended in 3 ml growth medium supplemented with 3x serum and non-essential amino acids (NEAA, Thermo Fisher), then mixed with 1.5 ml 1.2% agar. The resulting mixture, 1 ml of cells/0.4% agar/medium (10,000 cells/ml) was quickly and gently added onto each plate for solidification. Formed colonies were examined using SZX-16 microscope and analyzed by CellSens Dimension software (Olympus, Shinjuku, Tokyo, Japan).

## Transwell cell migration and invasion assays

Cells were starved in serum-free DMEM for 24h before the experiment. Then cells were harvested, washed and counted. Appropriate amounts of pre-warmed medium (no serum or 10% FBS) was added to the wells, then the inserts were carefully put into these wells using sterile forceps (for migration assays, we used Corning 8.0um PET track-etched membrane, 24 or 12 well format; for invasion assays, we used Corning Biocoat Matrigel Invasion Chamber, 24 well format). Then  $1 \times 10^5$  cells (for 24 well plates) or  $5 \times 10^5$  cells (for 12 well plates) in serum-free DMEM were added to the inserts. After 48h incubation, cells migrated through the membrane were stained with 0.5% crystal violet and cells not migrated through were removed using cotton swab. The stain was dissolved in 0.1M Sodium Citrate and the absorbance was read at 540nm on a plate reader.

## Scratch wound healing assay

$1 \times 10^6$  cells per well were placed in a 6-well plate. The “wound” was made by scratching the confluent monolayer across the well using a 200  $\mu$ l pipette tip. At each time point, closure of the gap was recorded by taking pictures. Then the width of the gap was measured and normalized with 0 h.

## Mammosphere formation assay

The mammosphere assay was developed as an approach to propagate mammary epithelial stem cells [47]. This assay was performed according to an online protocol (<http://www.bio-protocol.org/e325>). Briefly, tumorsphere medium was made by adding 20ng/ml epidermal growth factor (EGF), 10ng/ml basic fibroblast growth factor (bFGF), 5ug/ml Insulin and 0.4% Bovine Serum Albumin in DMEM/F12 (50/50) medium, and B27 supplement (Thermo Fisher) was freshly added to tumorsphere medium. Cells were collected, washed and counted followed by resuspending in tumorsphere medium with B27 supplement at a final concentration of 10,000 cells/ml. Then 2 ml cells were added to each well of an ultra-low attachment 6-well plate (Corning). After 7-day incubation, pictures of each well were taken and colonies were quantified using CellSens Dimension software. Secondary or tertiary mammospheres were generated by digesting primary mammospheres or secondary mammospheres and were seeded at the same density as primary mammospheres. All experiments were performed three times and bars represent the means of three independent experiments  $\pm$  s.d.

## Flow cytometry analysis

$1 \times 10^6$  cells were collected and stained with antibodies or isotypes for 30 min on ice. Stained cells were washed with FACS buffer (PBS with 2% FBS) followed by fixing in 4% Paraformaldehyde (PFA) for 20 min. Fixed cells were then suspended in FACS buffer and analyzed on the LSR II XW4400 workstation (BD Biosciences).

## Animal studies

4-5-week-old female BALB/c nu/nu athymic nude mice (Envigo, Madison, WI) were implanted with  $3 \times 10^6$  MDA-MB-231 cells transfected with empty vector ( $n = 17$ ) or LSD2 expression vector ( $n = 16$ ) into the mammary fat pad. Tumor volumes were regularly assessed every two days by measuring  $0.5 \times \text{length (mm)} \times \text{width (mm)} \times \text{width (mm)}$ . Mice were also weighed every two days. At the end of study, tumor or lung tissues of animals were collected and fixed with 4% paraformaldehyde. Tissues were processed into paraffin sections, and then subjected to hematoxylin-eosin (H&E) staining at the histological core facility at Magee Womens Research Institute.

## Statistical analysis

Data were represented as the mean  $\pm$ SD or  $\pm$ SEM of three independent experiments. Two-tailed Student's t-test was used to determine the quantitative variables. Statistical analyses were performed using GraphPad Prism 6 (GraphPad Software Inc., La Jolla, CA). *P*-values  $< 0.05$  were considered statistically significant for all tests.

## Abbreviations

KMT, histone lysine methyltransferase; KDM, histone lysine demethylases; LSD1/KDM1A, histone lysine-specific demethylase 1/1A; LSD2/KDM1B, histone lysine-specific demethylase 2/1B; TCGA, The Cancer Genome Atlas; AML, acute myeloid leukemia; DNMT, DNA methyltransferase; TNBC, triple-negative breast cancer; BCSC, breast cancer stem cell; ALDH, Aldehyde Dehydrogenase; MET, mesenchymal-epithelial transition; HDAC histone deacetylase; NuRD, nucleosome remodeling and histone deacetylase; PCNA, proliferating cell nuclear antigen; ESC, embryonic stem cell; CSC, cancer stem cell

## Author contributions

LC, SNV and YH conceptualized and designed the experiments. YH, NED and OS provided funding support. LC, SNV, TPK, YQ and HW performed all experimental

procedures related to the study. NT and CC provided technical support. LC, SNV, KL and YH analyzed the data. LC and YH wrote the manuscript. SNV, SO and NED edited it. All authors contributed to the data analysis during discussions at joint meetings.

## ACKNOWLEDGMENTS

The authors gratefully acknowledge MWRI animal, histological and flow cytometry facilities. LC was supported by a China Scholarship Council award through Tsinghua Medical School, Beijing, China. This project used the UPCI Cancer Genomics Facility and UPCI Cancer Bioinformatics Services that are supported in part by NCI award P30CA047904.

## CONFLICTS OF INTEREST

The authors declare no conflict of interest.

## FUNDING

This work is supported by US Army Breast Cancer Research Programs (W81XWH-14-1-0237 to YH; W81XWH-14-1-0238 to NED/SO), University of Pittsburgh Cancer Institute CCSG P30 CA047904, and Breast Cancer Research Foundation (to NED and SO).

## REFERENCES


1. Shi Y. Histone lysine demethylases: emerging roles in development, physiology and disease. *Nat Rev Genet.* 2007; 8:829–33.
2. Højfeldt JW, Agger K, Helin K. Histone lysine demethylases as targets for anticancer therapy. *Nat Rev Drug Discov.* 2013; 12:917–30.
3. Karytinis A, Forneris F, Profumo A, Ciossani G, Battaglioli E, Binda C, Mattevi A. A novel mammalian flavin-dependent histone demethylase. *J Biol Chem.* 2009; 284:17775–82.
4. Shi Y, Lan F, Matson C, Mulligan P, Whetstine JR, Cole PA, Casero RA, Shi Y. Histone demethylation mediated by the nuclear amine oxidase homolog LSD1. *Cell.* 2004; 119:941–53.
5. Garcia RN, D'Avila MF, Robe LJ, Loreto EL, Panzera Y, de Heredia FO, Valente VL. First evidence of methylation in the genome of *Drosophila willistoni*. *Genetica.* 2007; 131:91–105.
6. Fang R, Barbera AJ, Xu Y, Rutenberg M, Leonor T, Bi Q, Lan F, Mei P, Yuan GC, Lian C, Peng J, Cheng D, Sui G, et al. Human LSD2/KDM1b/AOF1 regulates gene transcription by modulating intragenic H3K4me2 methylation. *Mol Cell.* 2010; 39:222–33.
7. Garcia-Bassets I, Kwon YS, Telese F, Prefontaine GG,

- Hutt KR, Cheng CS, Ju BG, Ohgi KA, Wang J, Escoubet-Lozach L, Rose DW, Glass CK, Fu XD, Rosenfeld MG. Histone methylation-dependent mechanisms impose ligand dependency for gene activation by nuclear receptors. *Cell.* 2007; 128:505–18.
8. Lim S, Janzer A, Becker A, Zimmer A, Schüle R, Buettner R, Kirfel J. Lysine-specific demethylase 1 (LSD1) is highly expressed in ER-negative breast cancers and a biomarker predicting aggressive biology. *Carcinogenesis.* 2010; 31:512–20.
9. Metzger E, Wissmann M, Yin N, Müller JM, Schneider R, Peters AH, Günther T, Buettner R, Schüle R. LSD1 demethylates repressive histone marks to promote androgen-receptor-dependent transcription. *Nature.* 2005; 437:436–39.
10. Huang Y, Marton LJ, Woster PM, Casero RA Jr. Polyamine analogues targeting epigenetic gene regulation. *Essays Biochem.* 2009; 46:95–110.
11. Zhu Q, Huang Y, Marton LJ, Woster PM, Davidson NE, Casero RA Jr. Polyamine analogs modulate gene expression by inhibiting lysine-specific demethylase 1 (LSD1) and altering chromatin structure in human breast cancer cells. *Amino Acids.* 2012; 42:887–98.
12. Huang Y, Greene E, Murray Stewart T, Goodwin AC, Baylin SB, Woster PM, Casero RA Jr. Inhibition of lysine-specific demethylase 1 by polyamine analogues results in reexpression of aberrantly silenced genes. *Proc Natl Acad Sci USA.* 2007; 104:8023–28.
13. Cao C, Vasilatos SN, Bhargava R, Fine JL, Oesterreich S, Davidson NE, Huang Y. Functional interaction of histone deacetylase 5 (HDAC5) and lysine-specific demethylase 1 (LSD1) promotes breast cancer progression. *Oncogene.* 2017; 36:133–45.
14. Huang Y, Stewart TM, Wu Y, Baylin SB, Marton LJ, Perkins B, Jones RJ, Woster PM, Casero RA Jr. Novel oligoamine analogues inhibit lysine-specific demethylase 1 and induce reexpression of epigenetically silenced genes. *Clin Cancer Res.* 2009; 15:7217–28.
15. Vasilatos SN, Katz TA, Oesterreich S, Wan Y, Davidson NE, Huang Y. Crosstalk between lysine-specific demethylase 1 (LSD1) and histone deacetylases mediates antineoplastic efficacy of HDAC inhibitors in human breast cancer cells. *Carcinogenesis.* 2013; 34:1196–207.
16. Huang Y, Nayak S, Jankowitz R, Davidson NE, Oesterreich S. Epigenetics in breast cancer: what's new? *Breast Cancer Res.* 2011; 13:225.
17. Ciccone DN, Su H, Hevi S, Gay F, Lei H, Bajko J, Xu G, Li E, Chen T. KDM1B is a histone H3K4 demethylase required to establish maternal genomic imprints. *Nature.* 2009; 461:415–18.
18. van Essen D, Zhu Y, Sacconi S. A feed-forward circuit controlling inducible NF-κB target gene activation by promoter histone demethylation. *Mol Cell.* 2010; 39:750–60.

19. Lin SL, Chang DC, Lin CH, Ying SY, Leu D, Wu DT. Regulation of somatic cell reprogramming through inducible mir-302 expression. *Nucleic Acids Res.* 2011; 39:1054–65.
20. Katz TA, Huang Y, Davidson NE, Jankowitz RC. Epigenetic reprogramming in breast cancer: from new targets to new therapies. *Ann Med.* 2014; 46:397–408.
21. Katz TA, Vasilatos SN, Harrington E, Oesterreich S, Davidson NE, Huang Y. Inhibition of histone demethylase, LSD2 (KDM1B), attenuates DNA methylation and increases sensitivity to DNMT inhibitor-induced apoptosis in breast cancer cells. *Breast Cancer Res Treat.* 2014; 146:99–108.
22. Campbell LL, Polyak K. Breast tumor heterogeneity: cancer stem cells or clonal evolution? *Cell Cycle.* 2007; 6:2332–38.
23. Liu S, Wicha MS. Targeting breast cancer stem cells. *J Clin Oncol.* 2010; 28:4006–12.
24. Wu Y, Wang Y, Yang XH, Kang T, Zhao Y, Wang C, Evers BM, Zhou BP. The deubiquitinase USP28 stabilizes LSD1 and confers stem-cell-like traits to breast cancer cells. *Cell Reports.* 2013; 5:224–36.
25. Zhang X, Lu F, Wang J, Yin F, Xu Z, Qi D, Wu X, Cao Y, Liang W, Liu Y, Sun H, Ye T, Zhang H. Pluripotent stem cell protein Sox2 confers sensitivity to LSD1 inhibition in cancer cells. *Cell Reports.* 2013; 5:445–57.
26. Marcato P, Dean CA, Giacomantonio CA, Lee PW. Aldehyde dehydrogenase: its role as a cancer stem cell marker comes down to the specific isoform. *Cell Cycle.* 2011; 10:1378–84.
27. Moreb JS. Aldehyde dehydrogenase as a marker for stem cells. *Curr Stem Cell Res Ther.* 2008; 3:237–46.
28. Charafe-Jauffret E, Ginestier C, Iovino F, Wicinski J, Cervera N, Finetti P, Hur MH, Diebel ME, Monville F, Dutcher J, Brown M, Viens P, Xerri L, et al. Breast cancer cell lines contain functional cancer stem cells with metastatic capacity and a distinct molecular signature. *Cancer Res.* 2009; 69:1302–13.
29. Huang Y, Vasilatos SN, Boric L, Shaw PG, Davidson NE. Inhibitors of histone demethylation and histone deacetylation cooperate in regulating gene expression and inhibiting growth in human breast cancer cells. *Breast Cancer Res Treat.* 2012; 131:777–89.
30. Jambhekar A, Anastas JN, Shi Y. Histone Lysine Demethylase Inhibitors. *Cold Spring Harb Perspect Med.* 2017; 7:7.
31. Yang Y, Yin X, Yang H, Xu Y. Histone demethylase LSD2 acts as an E3 ubiquitin ligase and inhibits cancer cell growth through promoting proteasomal degradation of OGT. *Mol Cell.* 2015; 58:47–59.
32. Al-Hajj M, Wicha MS, Benito-Hernandez A, Morrison SJ, Clarke MF. Prospective identification of tumorigenic breast cancer cells. *Proc Natl Acad Sci USA.* 2003; 100:3983–88.
33. Bernstein BE, Mikkelsen TS, Xie X, Kamal M, Huebert DJ, Cuff J, Fry B, Meissner A, Wernig M, Plath K, Jaenisch R, Wagschal A, Feil R, et al. A bivalent chromatin structure marks key developmental genes in embryonic stem cells. *Cell.* 2006; 125:315–26.
34. Azuara V, Perry P, Sauer S, Spivakov M, Jørgensen HF, John RM, Gouti M, Casanova M, Warnes G, Merkenschlager M, Fisher AG. Chromatin signatures of pluripotent cell lines. *Nat Cell Biol.* 2006; 8:532–38.
35. Vastenhouw NL, Schier AF. Bivalent histone modifications in early embryogenesis. *Curr Opin Cell Biol.* 2012; 24:374–86.
36. Pan G, Tian S, Nie J, Yang C, Ruotti V, Wei H, Jonsdottir GA, Stewart R, Thomson JA. Whole-genome analysis of histone H3 lysine 4 and lysine 27 methylation in human embryonic stem cells. *Cell Stem Cell.* 2007; 1:299–312.
37. Adamo A, Sesé B, Boue S, Castaño J, Paramonov I, Barrero MJ, Izpisua Belmonte JC. LSD1 regulates the balance between self-renewal and differentiation in human embryonic stem cells. *Nat Cell Biol.* 2011; 13:652–59.
38. Gil-Henn H, Patsialou A, Wang Y, Warren MS, Condeelis JS, Koleske AJ. Arg/Abl2 promotes invasion and attenuates proliferation of breast cancer in vivo. *Oncogene.* 2013; 32:2622–30.
39. Liu Z, Hu Y, Liang H, Sun Z, Feng S, Deng H. Silencing PRDX3 Inhibits Growth and Promotes Invasion and Extracellular Matrix Degradation in Hepatocellular Carcinoma Cells. *J Proteome Res.* 2016; 15:1506–14.
40. Mani SA, Guo W, Liao MJ, Eaton EN, Ayyanan A, Zhou AY, Brooks M, Reinhard F, Zhang CC, Shipitsin M, Campbell LL, Polyak K, Brisken C, et al. The epithelial-mesenchymal transition generates cells with properties of stem cells. *Cell.* 2008; 133:704–15.
41. Schmidt JM, Panzilius E, Bartsch HS, Irmeler M, Beckers J, Kari V, Linnemann JR, Dragoi D, Hirschi B, Kloos UJ, Sass S, Theis F, Kahlert S, et al. Stem-cell-like properties and epithelial plasticity arise as stable traits after transient Twist1 activation. *Cell Reports.* 2015; 10:131–39.
42. Guo W, Keckesova Z, Donaher JL, Shibue T, Tischler V, Reinhardt F, Itzkovitz S, Noske A, Zürcher-Härdi U, Bell G, Tam WL, Mani SA, van Oudenaarden A, Weinberg RA. Slug and Sox9 cooperatively determine the mammary stem cell state. *Cell.* 2012; 148:1015–28.
43. Whyte WA, Bilodeau S, Orlando DA, Hoke HA, Frampton GM, Foster CT, Cowley SM, Young RA. Enhancer decommissioning by LSD1 during embryonic stem cell differentiation. *Nature.* 2012; 482:221–25.
44. Lai AY, Wade PA. Cancer biology and NuRD: a multifaceted chromatin remodelling complex. *Nat Rev Cancer.* 2011; 11:588–96.
45. Beaulieu N, Morin S, Chute IC, Robert MF, Nguyen H, MacLeod AR. An essential role for DNA methyltransferase DNMT3B in cancer cell survival. *J Biol Chem.* 2002; 277:28176–81.

46. Shaw PG, Chaerkady R, Wang T, Vasilatos S, Huang Y, Van Houten B, Pandey A, Davidson NE. Integrated proteomic and metabolic analysis of breast cancer progression. *PLoS One*. 2013; 8:e76220.
47. Dontu G, Abdallah WM, Foley JM, Jackson KW, Clarke MF, Kawamura MJ, Wicha MS. In vitro propagation and transcriptional profiling of human mammary stem/progenitor cells. *Genes Dev*. 2003; 17:1253–70.

# HDAC5–LSD1 axis regulates antineoplastic effect of natural HDAC inhibitor sulforaphane in human breast cancer cells

Chunyu Cao<sup>1,2§</sup>, Hao Wu<sup>1,2,3§</sup>, Shauna N. Vasilatos<sup>1,2</sup>, Uma Chandran<sup>4</sup>, Ye Qin<sup>1,2</sup>, Yong Wan<sup>1</sup>, Steffi Oesterreich<sup>1,2</sup>, Nancy E. Davidson<sup>5</sup> and Yi Huang<sup>1,2</sup> 

<sup>1</sup> Women's Cancer Research Center, UPMC Hillman Cancer Center, University of Pittsburgh School of Medicine, Pittsburgh, PA

<sup>2</sup> Department of Pharmacology & Chemical Biology, University of Pittsburgh School of Medicine, Pittsburgh, PA

<sup>3</sup> Department of Oncology, The First Affiliated Hospital of Nanjing Medical University, Nanjing, People's Republic of China

<sup>4</sup> Department of Biomedical Informatics, University of Pittsburgh School of Medicine, Pittsburgh, PA

<sup>5</sup> Fred Hutchinson Cancer Research Center, Seattle Cancer Care Alliance, and University of Washington, Seattle, WA

Our recent studies have shown that cross-talk between histone deacetylase 5 (HDAC5) and lysine-specific demethylase 1 (LSD1) facilitates breast cancer progression. In this work, we demonstrated that regulatory activity at –356 to –100 bp promoter element plays a critical role in governing HDAC5 transcription. By using DNA affinity precipitation and mass spectrometry, we identified a group of factors that bind to this element. Among these factors, Upstream Transcription Factor 1 (USF1) was shown to play a critical role in controlling HDAC5 transcription. Through screening a panel of epigenetic modifying drugs, we showed that a natural bioactive HDAC inhibitor, sulforaphane, downregulated HDAC5 transcription by blocking USF1 activity. Sulforaphane facilitated LSD1 ubiquitination and degradation in an HDAC5-dependent manner. A comparative microarray analysis demonstrated a genome wide cooperative effect of HDAC5 and LSD1 on cancer-related gene expression. shRNA knockdown and sulforaphane inhibition of HDAC5/LSD1 exhibited similar effects on expression of HDAC5/LSD1 target genes. We also showed that coordinated cross-talk of HDAC5 and LSD1 is essential for the antitumor efficacy of sulforaphane. Combination treatment with sulforaphane and a potent LSD1 inhibitor resulted in synergistic growth inhibition in breast cancer cells, but not in normal breast epithelial cells. Furthermore, combined therapy with sulforaphane and LSD1 inhibitor exhibited superior inhibitory effect on MDA-MB-231 xenograft tumor growth. Taken together, our work demonstrates that HDAC5–LSD1 axis is an effective drug target for breast cancer. Inhibition of HDAC5–LSD1 axis with sulforaphane blocks breast cancer growth and combined treatment with LSD1 inhibitor improves the therapeutic efficacy of sulforaphane.

Epigenetic alterations include post-translational histone modifications such as acetylation or methylation and abnormal DNA methylation in important genes.<sup>1,2</sup> Histone acetylation is typically associated with transcriptionally active chromatin and

is a result of a dynamic balance between activities of histone acetyltransferases (HATs) and histone deacetylases (HDACs). Abnormally high expression of HDACs in breast cancer cells may lead to the anomalous loss of expression of genes that are important in curbing tumor growth.<sup>3,4</sup> Our recent work has provided novel insights into molecular mechanisms by which histone deacetylase and demethylase interact in breast cancer cells. We identified a unique feature of HDAC5 in facilitating protein stabilization of FAD-dependent histone demethylase 1 (LSD1), leading to a dysregulated chromatin landscape which functions as an antibraking system in breast cancer development.<sup>5</sup> Coordinated overexpression of HDAC5 and LSD1 proteins was observed in breast cancer cell lines and clinical patient samples. By gain- and loss-of-function studies using a breast tumor progression model, we have observed that HDAC5 possesses a critical oncogenic function in driving MCF10A transformation via blocking LSD1 protein degradation and reshaping epigenetic landscape.<sup>5</sup> Our findings have revealed an important mechanism about the epigenetic regulation of LSD1 activity by HDAC5 that may lead to an alternative treatment approach against breast cancer.

HDAC5 is a key member of class II HDAC family. The class II HDAC isozymes, HDAC4, 5, 7 and 9, are unique due

**Key words:** breast cancer, HDAC5, LSD1, USF1, sulforaphane, HCI-2509, combination therapy

Additional Supporting Information may be found in the online version of this article.

<sup>§</sup>C.C. and H.W. contributed equally to this work

**Conflicts of interest:** The authors declare no conflict of interest.

**Grant sponsor:** US Army Breast Cancer Research Programs; **Grant**

**numbers:** W81XWH-14-1-0237, W81XWH-14-1-0238; **Grant**

**sponsor:** Breast Cancer Research Foundation; **Grant sponsor:** NIH;

**Grant number:** P30CA047904; **Grant sponsor:** China Scholarship

Council and Project of Science and Technology Department of

Qinghai Province of China; **Grant number:** 2015-ZJ-751

**DOI:** 10.1002/ijc.31419

**History:** Received 21 Dec 2017; Accepted 28 Mar 2018; Online 6 Apr 2018

**Correspondence to:** Yi Huang, M.D., Ph.D., Magee Womens Research Institute, Room 406, 204 Craft Ave, Pittsburgh, PA 15213, USA, Tel.: +1-412-641-3589; E-mail: yih26@pitt.edu



**What's new?**

The post-translational modification of histones through acetylation serves an important role in the regulation of gene expression. Histone deacetylases (HDACs) are a critical component of this system. This study sheds light on regulatory mechanisms of HDAC5 transcription and shows that sulforaphane, an HDAC inhibitor, suppresses HDAC5 expression through downregulation of upstream transcription factor 1 (USF1). USF1 downregulation in turn destabilizes lysine-specific demethylase 1 (LSD1) protein in breast cancer cells. The findings suggest that targeting the HDAC5–LSD1 axis through combined sulforaphane and LSD1 inhibitor treatment could be an effective approach to enhancing antineoplastic efficacy of epigenetic agents against breast cancer.

to their ability to shuttle between the nucleus and cytoplasm.<sup>6,7</sup> HDAC5 has been found to play critical roles in development of many pathogenic conditions including cancer.<sup>8,9</sup> Ozdag *et al.* reported that overexpression of HDAC1, 5 and 7 may serve as a molecular biomarker of malignant *versus* normal tissues.<sup>10</sup> Both HDAC5 and HDAC9 are overexpressed in tumors from high-risk medulloblastoma patients, suggesting a close linkage between their expression and poor survival of patients.<sup>11</sup> These findings also imply that HDAC5 overexpression may act as an effective prognostic marker as well as a potential therapeutic target for cancer. However, little is known about the specific roles of HDAC5 in cancer initiation and progression. Therefore, it is important to fully elucidate the changes of molecular events leading to HDAC5 overexpression in cancer.

As the first identified histone demethylase, LSD1 has shown great potential as an effective target in cancer therapy.<sup>12–17</sup> The activity of the LSD1 complex has been implicated in tumorigenesis of various cancers.<sup>18–20</sup> Thus, there has been increasing interest in testing known compounds or designing new chemical entities that can inhibit LSD1 activity and function as novel therapeutic agents for cancer. Our previous studies have reported that LSD1 activity can be successfully inhibited by specific inhibitors in colorectal and breast cancer cells.<sup>12,13,21,22</sup> The rapid development of LSD1 inhibitors has led to the evaluation of several novel LSD1 inhibitors in early phase clinical trials.<sup>23–25</sup>

In this study, we have investigated the potential effect of targeting cross-talk between HDAC5 and LSD1 as a novel strategy for breast cancer treatment. The data presented here suggest that a natural HDAC inhibitor sulforaphane (SFN) suppresses HDAC5 expression, which in turn destabilizes LSD1 protein. SFN in combination with a novel LSD1 inhibitor has shown improved antineoplastic activity both *in vitro* and *in vivo*.

**Experimental Procedures****Reagents and cell culture**

Sulforaphane was purchased from LKT Laboratories (Minneapolis, MN), Vorinostat (SAHA) was obtained from Cayman Chemical (Ann Arbor, MI). Trichostatin A (TSA) and MG-132 were obtained from Sigma-Aldrich (St. Louis, MO). MC-1568, LBH-589, Belinostat (PXD-101), MS-275 and Romidepsin were from Selleckchem (Houston, TX). HCI-2509 was purchased from Xcess Biosciences Inc (San Diego, CA). MDA-MB-231,

MDA-MB-468, BT-474 and MCF-7 cell lines were obtained from ATCC. MCF10A and MCF10A-CA1a lines were provided by Dr Saraswati Sukumar (Johns Hopkins University). Cells were cultured under the conditions as previously described.<sup>26</sup>

**Plasmid construction**

HDAC5 promoter elements were amplified by PCR with primers indicated in Supporting Information Table 1. The PCR products were engineered into the pGL2-Enhancer plasmid. Plasmids pcDNA3.1(+)-FLAG and pcDNA3.1(+)-FLAG-HDAC5 were purchased from Addgene (Cambridge, MA). pReceiver-FLAG-LSD1 was from Gene Copoeia (Rockville, MD). pcDNA3.1(+)-FLAG-Jade-2 was purchased from GenScript (Piscataway, NJ).

**RNAi transfection**

Pre-designed hUSF1 siRNA (ThermoFisher, Boston, MA), THOC1 siRNA (Santa Cruz) or scramble control siRNA were transfected into cells according to the manufacturer's protocol. Cells were harvested 48 hr post-transfection for further analysis.

**Real-time qPCR**

Quantitative real-time PCR was carried out using the StepOne real-time PCR system as previously described.<sup>5</sup> All the probes for TaqMan<sup>®</sup> Gene Expression Assays were pre-designed and provided by Life Technologies.

**Immunoblotting**

Whole-cell lysate and nuclear proteins were extracted using methods described previously.<sup>26–29</sup> Antibodies sources: H3K4me2, H3K4me1, and acetyl-H3K9 (Millipore, Billerica, MA); USP28 (Abcam, Cambridge, MA); LSD1 and HA (Cell Signaling Technology, Beverly, MA); Flag antibody (Sigma Aldrich); PARP1 (Active Motif, Carlsbad, CA); HDAC5, USF1, THOC1, PCNA and  $\beta$ -actin (Santa Cruz Biotechnology). Membranes were scanned using Li-Cor BioScience Odyssey Infrared Imager (Lincoln, NE).

**Luciferase assays**

$2 \times 10^5$  cells per well were seeded into 24 well plates and 250 ng plasmid DNA were transiently co-transfected with 2.5 ng pRL-TK, a Renilla Luciferase Control Reporter Vector, (Promega, Madison, WI) using Lipofectamine 3000 (ThermoFisher).

Cells were harvested 48 hr post-transfection and luciferase activity was measured on a GLOMAX<sup>®</sup> 20/20 luminometer (Promega). Luciferase values (relative light units, RLUs) were normalized to Renilla luciferase activity and expressed as the fold change relative to pGL2-Enhancer transfected wells.

#### Cellular growth inhibition and drug combination index (CI) analysis

Crystal violet assays were performed as previously described.<sup>5,30</sup> The median effects (IC<sub>50</sub>) were determined using CalcuSyn software from Biosoft (Cambridge, UK). Effects of synergy, additivity or antagonism of combination treatment were determined using the Chou–Talalay median effect/combination index (CI) model.

#### Chromatin immunoprecipitation (ChIP)

ChIP assays were performed as described previously.<sup>21</sup> Primary antibodies against USF1 protein were used for immunoprecipitation of protein–DNA complexes. Forward primer 5'-CATGCTAGCCTCGGCCGAACCCTGTGC-3' and reverse primer 5'-CATAAGCTTACCCCTCCCCTGCCTCT-3' were used for PCR amplification. Sheared genomic DNA was used as a positive control (Input).

#### Ubiquitination assays

The assay was performed as previously described.<sup>5</sup> Whole cell lysate was obtained using RIPA lysis buffer. After preclearing with Protein G-Plus Agarose beads (Santa Cruz Biotechnology), LSD1 or IgG antibody (Abcam) was added to whole cell lysate and rotated overnight at 4°C. Then, 40 µl of Protein G-Plus Agarose beads was added for another 2 hr. The agarose beads were washed and then subjected to immunoblotting.

#### *In vitro* DNA affinity precipitation assays (DAPA) and mass spectrometry analysis

Biotinylated primers (Integrated DNA Technologies, Coralville, IA) were used to generate double-stranded biotinylated HDAC5 promoter probes. For HDAC5 promoter –356 to –100 probe, forward primer 5'-biotin-CATGCTAGCAGAT TGCACCATCCACGTTTTG-3' and reverse primer 5'-biotin-CATAAGCTTACCCCTCCCCTGCCTCT-3' were used for PCR amplification. The nonrelevant biotinylated probes—sense: 5'-biotin-AGAGTGGTCACTACCCCTCTG-3', antisense: 5'-biotin-CAGAGGGGGTAGTGACCACTCT-3'—were also synthesized as a negative control. Streptavidin-agarose bead suspension was added to a mixture of nuclear proteins with double-strand biotinylated oligonucleotides. Mixture was placed on a gently rocking platform for 2 hr and was centrifuged. DNA–protein complexes were washed and 2× protein sample buffer (Invitrogen) was added to the avidin-precipitated DNA–protein complex, which was then boiled for 5 min to dissociate the complexes. The proteins were fractionated on SDS acrylamide gels and silver stained. The silver-stained bands were excised from the gel and digested in gel with sequence-grade trypsin. The mass spectrometry analysis was performed at Biomedical Mass Spectrometry Center of University of Pittsburgh.

#### Microarray analysis of gene expression

Total RNA from three independent biological replicates was extracted using QIAgen RNeasy kit (Valencia, CA). cRNA was hybridized to HG U133A 2.0 arrays (Affymetrix, Inc., Santa Clara, CA). The data were processed as RMA files (Affymetrix Robust Multi-Array Average). The raw intensity data were background corrected, log<sub>2</sub> transformed and quantile normalized according to Affymetrix recommendations. Differential gene expression was performed using BRB array tools (NCI). Refer to the Supporting Information material more detailed methods for microarray processing and analysis.

#### Animal studies

Four- to five-week-old female BALB/c nu/nu athymic nude mice (Harlan Labs, Indianapolis, IN) were implanted with 4 × 10<sup>6</sup> human breast cancer MDA-MB-231 cells into the mammary fat pad. Five days after implantation, mice were randomly assigned into groups of vehicle control (10% DMSO), SFN (50 mg/kg), HCI-2509 (30 mg/kg) or combination treatment. Mice were treated by intraperitoneal injection once a day for 27 days. Tissues were processed into paraffin sections, and then subjected to hematoxylin–eosin staining at the Histology and Micro-Imaging Core at Magee Womens Research Institute. After staining, samples were examined and photographed by microscope (Nikon, Eclipse 90i).

#### Statistical analysis

Data were shown as the mean ± s.d. of three independent experiments. The quantitative variables were analyzed by Student's *t* test or one-way ANOVA. *p* values <0.05 was considered statistically significant for all tests. GraphPad Prism 6 program (GraphPad Software Inc., La Jolla, CA) was used for statistical analyses.

## Results

#### Characterization of transcriptional regulatory activity at HDAC5 promoter

To better understand how changes of HDAC5 transcriptional regulation lead to HDAC5 overexpression in breast tumors, we engineered a series of deletion constructs of the HDAC5 5' flanking promoter elements into luciferase reporter pGL2-Enhancer vector (Fig. 1a). The plasmids were transfected into MDA-MB-231 cells followed by quantitative luciferase activity assays. While deletion of downstream element +24 to +656 bp (P2) or additional truncation of upstream elements from –1262 to –356 bp (P2, P3, P4, P5) exerted no obvious effect on luciferase reporter activity, extra truncation of –356 to –200 bp (P6) significantly attenuated and depletion of –356 to –100 bp (P7) nearly abolished luciferase reporter activity (Fig. 1b). To characterize the role of the –356 to –100 bp element in regulation of HDAC5 transcription, we engineered –356 to –100 bp element (P8) into the pGL2-Enhancer vector and showed that transfection of P8 element

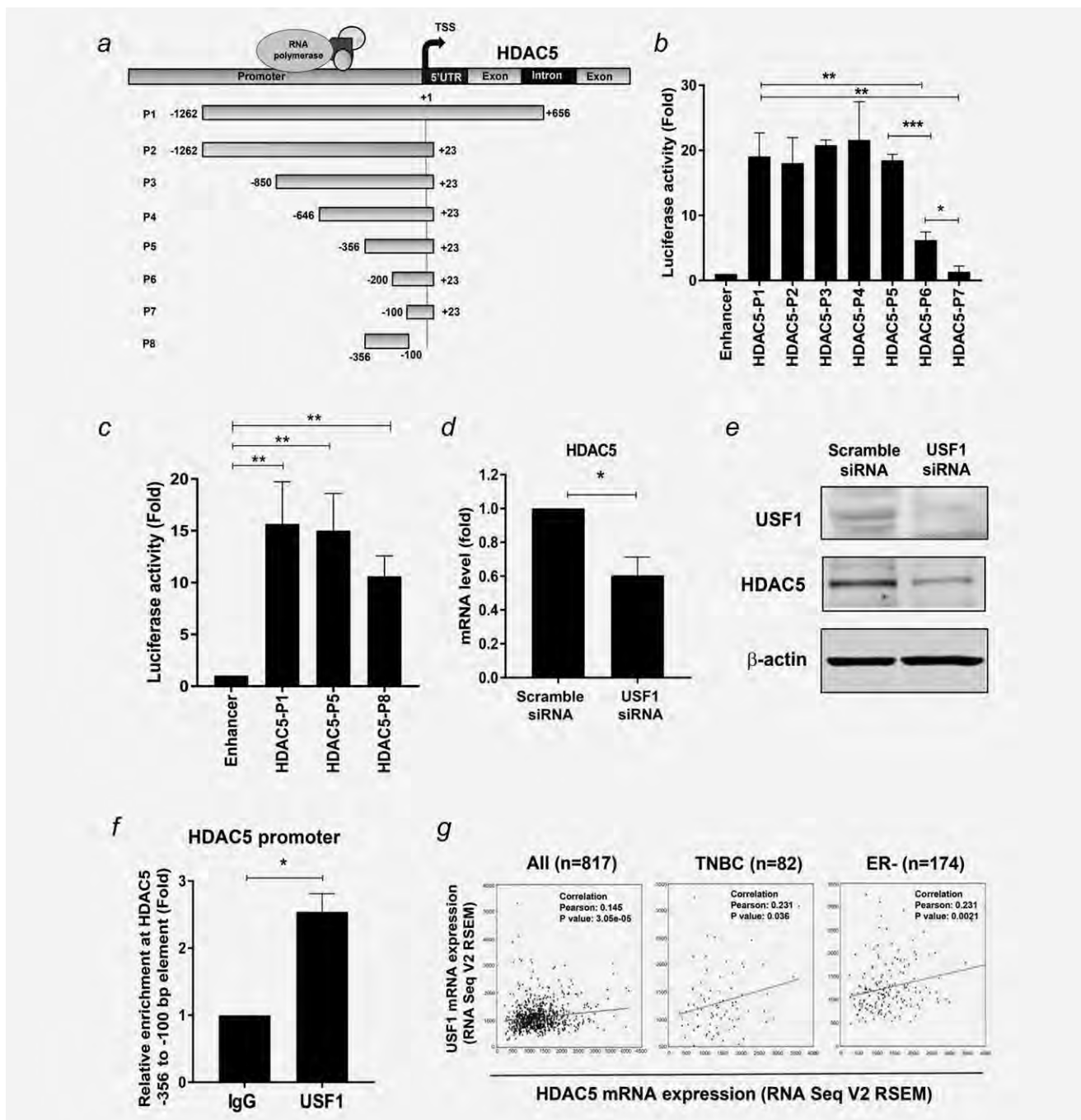


**Figure 1.** Analysis of transcriptional activity at HDAC5 promoter. (a) Map of deletion constructs of HDAC5 promoter and coding region. TSS, transcription start site. (b) MDA-MB-231 cells were co-transfected with pGL2-Enhancer or pGL2-Enhancer-HDAC5 promoter elements and pRL-TK. Reporter gene activities were measured 48 hr post-transfection. The relative luciferase activity of fragments P2–P7 was compared with that of full-length P1. Transfection of pGL2-Enhancer plasmids was used as negative control. (c) MDA-MB-231 cells were co-transfected with pGL2-Enhancer or constructs of pGL2-Enhancer-HDAC5 promoter elements P1, P5 or P8 and pRL-TK. Reporter gene activities were measured 48 hr post-transfection. Transfection of pGL2-enhancer was used as negative control. (d) MDA-MB-231 cells were transiently transfected with scramble or USF1 siRNA for 48 hr. Effect of USF1 knockdown on HDAC5 mRNA expression was measured by quantitative PCR with  $\beta$ -actin as an internal control. (e) MDA-MB-231 cells were transfected with scramble or USF1 siRNA for 48 hr. Effect of USF1 knockdown on HDAC5 protein expression was examined by immunoblots with  $\beta$ -actin as loading control. (f) Quantitative ChIP analysis was used to determine the occupancy of USF1 protein at –356 to –100 bp element of HDAC5 promoter. (g) The Pearson correlation between mRNA expression of USF1 (y-axis) and HDAC5 (x-axis) in clinical TNBC- or ER-negative breast cancer specimens. Bars represent the mean of three independent experiments  $\pm$  s.d. \* $p$  < 0.05, \*\* $p$  < 0.01, \*\*\* $p$  < 0.001, Student's  $t$  test.

could generate significant luciferase activity when compared with the full-length P1 or P5 elements (Fig. 1c). The results indicate that regulatory activity from –356 to –100 bp at HDAC5 promoter is essential for transcription regulation of HDAC5.

To identify coregulatory proteins that are associated with the –356 to –100 bp element (P8), *in vitro* DNA affinity precipitation assays (DAPA) and mass spectrometry analysis were performed. Biotin end-labeled sense and antisense oligonucleotides corresponding to P8 promoter element were custom synthesized. Nondenatured nuclear proteins from MDA-MB-231 cells were extracted and incubated with P8 oligonucleotides, and SDS-PAGE was performed, followed by silver staining. This experiment showed multiple protein complexes bound to P8 element, but absent from the negative scramble probe (Supporting Information Fig. 1a). Mass spectrometry analysis identified a group of potential binding proteins from recovered samples (Supporting Information Fig. 1b). Through functional analysis, several factors that play a role in chromatin remodeling and transcriptional regulation were selected to validate their physical association with the P8 element, such as polycomb protein SUZ12 (SUZ12), THO complex subunit 1 (THOC1) and upstream stimulatory factor 1 (USF1). Western blot results indicated that these factors exhibited stronger binding ability to P8 probe (Supporting Information Fig. 1c). To determine if activity of these factors is involved in regulation of HDAC5 transcription, MDA-MB-231 cells were transiently transfected with siRNA against these factors. Among these factors, we found that depletion of USF1 exhibits most significant inhibitory effect on HDAC5 mRNA expression (Fig. 1d). Depletion of SUZ12 or THOC1 in MDA-MB-231 cells exerted only marginal effect on the HDAC5 transcription activity (Supporting Information, Figs. 2a and 2b). Western blots indicated that USF1 siRNA significantly decreased HDAC5 protein expression (Fig. 1e). To further confirm the binding ability of these factors in living cells, ChIP study was carried out and showed that USF1 is capable of physically binding to the P8 promoter region (Fig. 1f). Taken together, these studies identified USF1 as an important regulatory factor of HDAC5 transcription.

#### **USF1 is overexpressed and positively associated with HDAC5 expression in TNBC/ER– breast tumors**

*In silico* analysis using TCGA data (downloaded from GSE62944) indicates a significantly elevated mRNA level of USF1 in breast tumor specimens ( $n = 1095$ ) compared with normal tissue samples ( $n = 113$ ). Among these breast cancer tumors, estrogen receptor (ER)-negative tumors ( $n = 237$ ) express significantly higher USF1 than ER-positive counterparts ( $n = 808$ ) (Supporting Information, Figs. 3a and 3b). Study of USF1 expression across all molecular subtypes of breast cancer showed that USF1 mRNA level is higher in basal-like tumors as compared to other breast cancer subtypes, such as Her2+, Luminal A, Luminal B or normal-like (Supporting Information, Figs. 3c and 3d). Analysis of TCGA

database also showed that clinical TNBC specimens express significantly higher level of USF1 mRNA when compared with non-TNBC tissues ( $p = 0.0013$ ) (Supporting Information, Fig. 3e). By assessing Pearson correlation coefficient, positively correlated mRNA expressions between USF1 and HDAC5 were observed. Triple negative breast cancer (TNBC) or ER negative tumors exhibit a stronger positive correlation than ER or Her2 positive subtypes (Fig. 1g and Supporting Information, Fig. 3f). These data suggest that USF1 is positively correlated with HDAC5 expression in more aggressive subtypes of breast cancer which may warrant further investigation into its role in aggressive phenotypes of breast cancer.

#### **Sulforaphane suppresses transcriptional activity of HDAC5 in breast cancer cells**

Next, we tested the effect of clinically relevant HDAC inhibitors (HDACi) on HDAC5 expression. The selected HDACi compounds include hydroxamic acid derivatives SAHA (Vorinostat), TSA (Trichostatin A), LBH-589 (Panobinostat) and PXD-101 (Belinostat); a benzamide analog MS-275 (Entinostat); a selective class II HDAC inhibitor MC-1568; a natural product from the bacterium *Chromobacterium violaceum* Romidepsin and a natural bioactive HDACi sulforaphane (SFN). In MDA-MB-231 cells, treatment with most of the HDACis led to a significant increase of HDAC5 mRNA expression in a dose-dependent style. However, exposure of cells to SFN significantly inhibited mRNA expression of HDAC5 (Fig. 2a). While protein expression of HDAC5 was induced by TSA, SAHA, MS-275 LBH-589, PXD-101 and Romidepsin, SFN suppressed HDAC5 protein expression in MDA-MB-231 cells (Fig. 2b). A similar effect of SAHA and SFN on HDAC5 protein expression was also found in additional breast cancer cell lines including TNBC MDA-MB-468 and MCF10A-CA1a, ER+ MCF-7 and HER2+ BT474 cells (Fig. 2c and Supporting Information, Fig. 4a). These results suggest that SFN, which is different from most other classes of HDACi, exhibited potent inhibitory effect against HDAC5 expression in breast cancer cells.

#### **Sulforaphane suppresses transcriptional activity of –356 to –100 bp element at HDAC5 promoter**

SFN failed to suppress exogenous HDAC5 mRNA expression driven by CMV promoter in MDA-MB-231 cells transfected with pcDNA3.1-HDAC5 plasmid (Fig. 2d), suggesting that SFN inhibited HDAC5 mRNA expression through repression of the transcriptional activity at its natural promoter. While SFN significantly inhibited the luciferase reporter activity in MDA-MB-231 cells or MDA-MB-468 cells, exposure of both cell lines to SAHA promoted reporter gene activity of the full-length construct (P1) (Fig. 2e and Supporting Information, Fig. 4b). An opposite effect of SFN and SAHA on luciferase activity of P8 element was also detected in MDA-MB-231 cells (Fig. 2f). Treatment with SFN inhibited mRNA and protein expression of USF1 in a dose-dependent manner (Supporting Information, Figs. 4c and 4d). ChIP study showed that binding of USF1 to P8

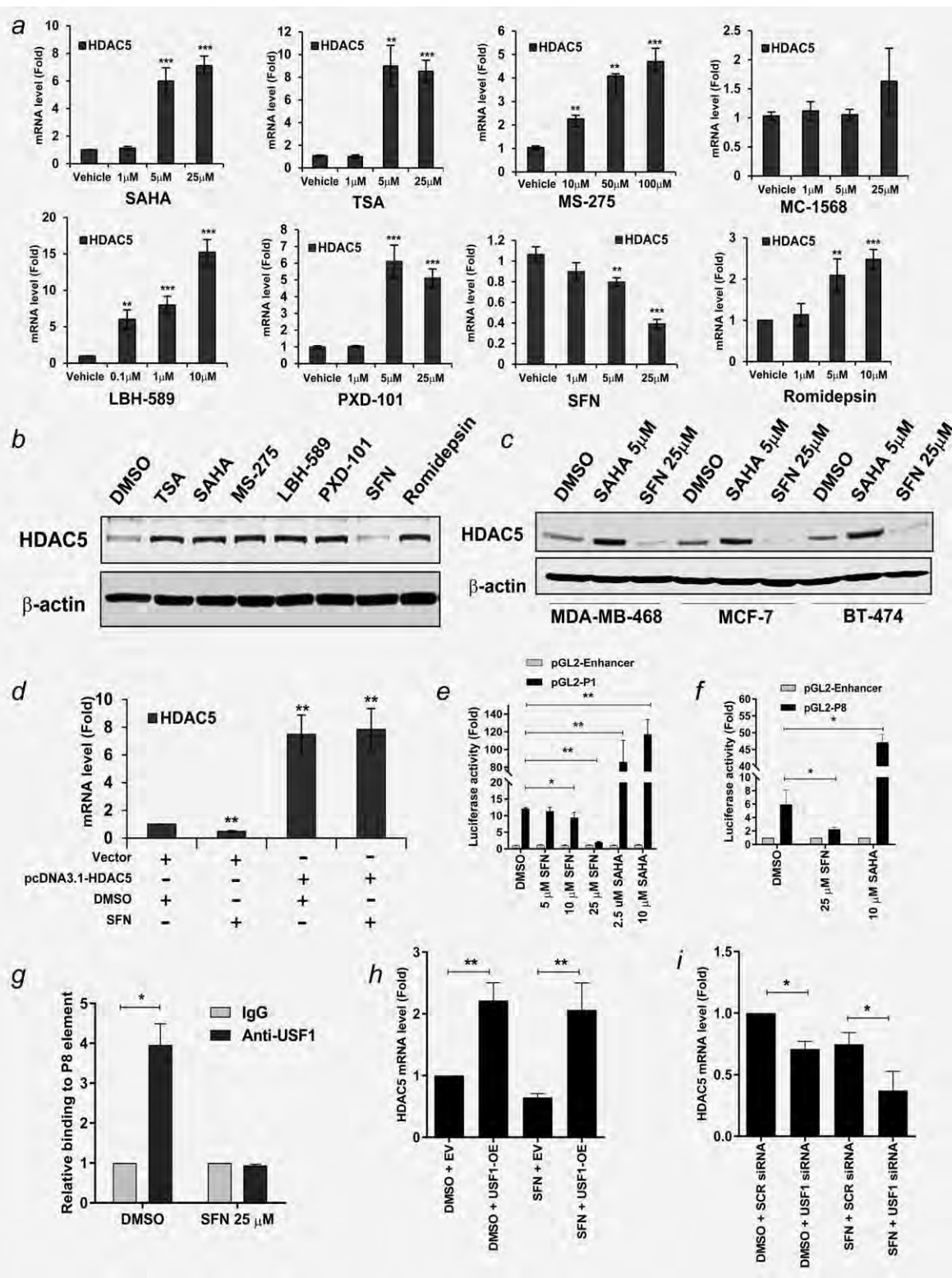


**Figure 2.** Effect of HDAC inhibitors on expression of HDAC5 in human breast cancer cells. (a) After MDA-MB-231 cells were exposed to a variety of HDAC inhibitors for 24 hr, mRNA expression of HDAC5 was quantitatively measured by real-time PCR. β-actin gene was used as an internal control. (b) MDA-MB-231 cells were treated with TSA (5 μM), SAHA (5 μM), MS-275 (50 μM), LBH-589 (1 μM), PXD-101 (5 μM), SFN (25 μM) and Romidepsin (5 μM) for 24 hr. Whole cell lysates were extracted and analyzed for protein expression of HDAC5 through Western blotting. β-actin was used as a loading control. (c) MDA-MB-468, MCF-7 or BT-474 cells were treated with 5 μM SAHA or 25 μM SFN for 24 hr. Whole cell lysates were analyzed for protein expression of HDAC5 by Western blotting. β-actin was used as a loading control. (d) MDA-MB-231 cells transfected with pcDNA3.1 or pcDNA3.1-HDAC5 plasmids were treated with 25 μM SFN for 24 hr. mRNA expression of HDAC5 was analyzed by quantitative RT-PCR with β-actin as an internal control. (e) pGL2-Enhancer plasmids or pGL2-P1 construct (-1262 to +656 bp) were transfected into MDA-MB-231 cells followed by treatment with indicated concentrations of SFN or SAHA for 24 hr. Reporter gene activities were then measured. (f) pGL2-Enhancer or pGL2-P8 construct (-356 to -100 bp) were transfected into MDA-MB-231 cells followed by treatment with 25 μM SFN or 10 μM SAHA for 24 hr. Reporter gene activities were then measured. (g) MDA-MB-231 cells were treated with DMSO or 25 μM SFN for 24 hr. Quantitative ChIP analysis was used to determine the occupancy of USF1 at P8 element of HDAC5 promoter. (h) MDA-MB-231 cells were transiently transfected with USF1 expression plasmid followed by treatment with 25 μM SFN for 48 hr. mRNA expression of HDAC5 was measured by qPCR. (i) MDA-MB-231 cells were transiently transfected with USF1 siRNA followed by treatment with 25 μM SFN for 48 hr. mRNA expression of HDAC5 was measured by qPCR. β-actin was used as an internal control. All experiments were performed three times and showed similar results. Bars represent the mean of three independent experiments ± s.d. \**p* < 0.05, \*\**p* < 0.01, \*\*\**p* < 0.001, Student's *t* test.

element was abolished by SFN (Fig. 2g). A rescue study indicated that USF1 overexpression prevented downregulation of HDAC5 mRNA expression by SFN in MDA-MB-231 cells (Fig. 2h). Moreover, knockdown of USF1 by siRNA significantly enhanced SFN-induced suppression of HDAC5 transcription (Fig. 2i). These results suggest that USF1 plays an important role in regulating SFN-mediated HDAC5 transcription activity.

#### **Sulforaphane destabilizes LSD1 protein in an HDAC5-dependent manner**

We further addressed whether SFN could disrupt activity of the HDAC5–LSD1 axis. Immunoblotting studies showed that unlike other HDAC inhibitors, SFN significantly inhibited expression of LSD1 protein (Fig. 3a). Exposure of MDA-MB-231 to SFN resulted in similar inhibition of HDAC5 and LSD1 protein in a dose-dependent manner (Supporting Information, Fig. 5). qPCR studies demonstrated that LSD1 mRNA level was not affected by SFN treatment in MDA-MB-231 cells (Fig. 3b). SFN treatment increased nuclear levels of H3K4me1/2 and AcH3K9 without altering methylation of H3K36 and H3K27 in MDA-MB-231 or MCF10A-CA1a cells which is a transformed malignant line of MCF10A (Fig. 3c). We recently demonstrated that HDAC5 stabilizes LSD1 protein through downregulation of LSD1 ubiquitination and degradation.<sup>5</sup> To decipher whether SFN destabilizes LSD1 protein by regulating its ubiquitination modification, protein ubiquitination assays were conducted and showed that exposure to SFN led to a profound increase of LSD1 polyubiquitination in MDA-MB-231 cells (Fig. 3d). Next, we assessed the potential effect of SFN on protein expression of LSD1 E3 ubiquitin ligase and deubiquitinase, Jade-2 or USP28. As the absence of specific antibody against Jade-2, plasmids expressing Jade-2-FLAG fusion protein were used as an alternative approach. Whereas depletion of HDAC5 did not alter Jade-2 protein expression, treatment with SFN significantly decreased USP28 protein levels (Fig. 3e). We performed a rescue expression of HDAC5 in MDA-MB-231 cells through transfection of pcDNA3.1-HDAC5 vector and observed that SFN had no effect on exogenous HDAC5 protein. SFN-mediated downregulation of LSD1 protein and USP28 was apparently reversed (Fig. 3f). These results demonstrate that SFN downregulates LSD1 protein stability through affecting LSD1-associated ubiquitination activity, which is largely dependent on HDAC5 activity.

#### **Effect of sulforaphane on genome-wide transcription targets of the HDAC5/LSD1 complex**

To define a comprehensive profile of genes whose expression is regulated by HDAC5/LSD1 complex, we performed genome-wide gene expression analysis in MDA-MB-231 cells with stable knockdown of HDAC5 or LSD1 by shRNA. We identified 3370 and 2963 genes whose expression was significantly changed by inhibition of HDAC5 and LSD1, respectively (Fig. 4a). Data has been deposited into Gene Expression Omnibus as GSE72687. Strikingly, >30% of genes in each group were overlapping and regulated by HDAC5-KD and LSD1-KD, reflecting

a comprehensive genome wide cooperative effect of HDAC5 and LSD1 on target gene expression. A functional pathway analysis using the Ingenuity Pathway Analysis application showed that there are multiple important cellular networks whose activities are significantly altered by depletion of HDAC5 or LSD1 (Fig. 4b). These networks are associated with cell death & survival, cell cycle, cellular development, cellular growth/proliferation, carbohydrate metabolism, cell morphology, cell–cell signaling & interaction, cellular assembly & organization, lipid metabolism, molecular transport, small molecule biochemistry and so on. Figure 4c lists the top canonical pathways that are regulated by HDAC5–LSD1 complex. Depletion of HDAC5 or LSD1 activates several key tumor suppressive signaling pathways such as ATM, PTEN, p53 and so on, and downregulates multiple tumor promoting signaling pathways including PI3K/AKT, JAK/Stat, PDGF and so on. Among the differentially expressed genes (DEGs) potentially regulated by HDAC5/LSD1 complex, we identified a subset of genes whose activities are associated with critical cellular processes in cancer: cell adhesion, metastasis, tumor suppression and cell growth, receptors, therapeutic response and so on (Fig. 4d). Among these genes, a group of important tumor suppressor genes (TSGs) was shown to be induced by either HDAC5 or LSD1 inhibition. These TSGs include FAS, CTDSPL, ISG15, GLIPR1, CYLD, EGLN1, TFPI2, PPP2R1B, EGLN3 and so on. Induction of most of these TSGs was validated by qPCR (Fig. 4e). Furthermore, the effect of SFN on expression of these TSGs was examined in MDA-MB-231 cells. SFN treatment significantly induced expression of most of the TSG genes tested (Fig. 4f), showing a similar effect on activation of TSGs by SFN or HDAC5/LSD1 inhibition.

#### **The HDAC5–LSD1 axis is essential for breast cancer cell sensitivity to sulforaphane**

To determine whether HDAC5–LSD1 axis plays a role in regulating breast cancer sensitivity to SFN, MDA-MB-231 and MDA-MB-468 cells were transfected with pcDNA3.1-HDAC5 or pReceiver-LSD1 plasmids. In both cell lines, overexpression of HDAC5 or LSD1 protein increased resistance to SFN-mediated growth inhibition which was indicated by significantly increased IC<sub>50</sub> values (Figs. 5a and 5b). shRNA-mediated depletion of LSD1 sensitized MDA-MB-231 cells to SFN which was evidenced by significantly reduced IC<sub>50</sub> value (Fig. 5c). A rescue experiment showed that HDAC5 overexpression attenuated cellular sensitivity to SFN in MDA-MB-231-Scramble cells but was obviously reversed by LSD1 depletion in MDA-MB-231-LSD1-KD cells (Fig. 5d). Taken together, these results demonstrate that LSD1 acts as an important downstream effector of HDAC5 signaling in regulating cellular sensitivity to SFN in breast cancer.

HCI-2509 is a highly potent, specific, non-MAOA and MAOB inhibitor of LSD1 which binds the FAD pocket of the enzyme.<sup>31</sup> Proliferation assay showed that MDA-MB-231 cells were susceptible to HCI-2509 induced growth inhibition with a low IC<sub>50</sub> value of 0.5 μM (Fig. 5e). Combined treatment with low dose of SFN (5 μM) and HCI-2509 (0.1 μM) generated

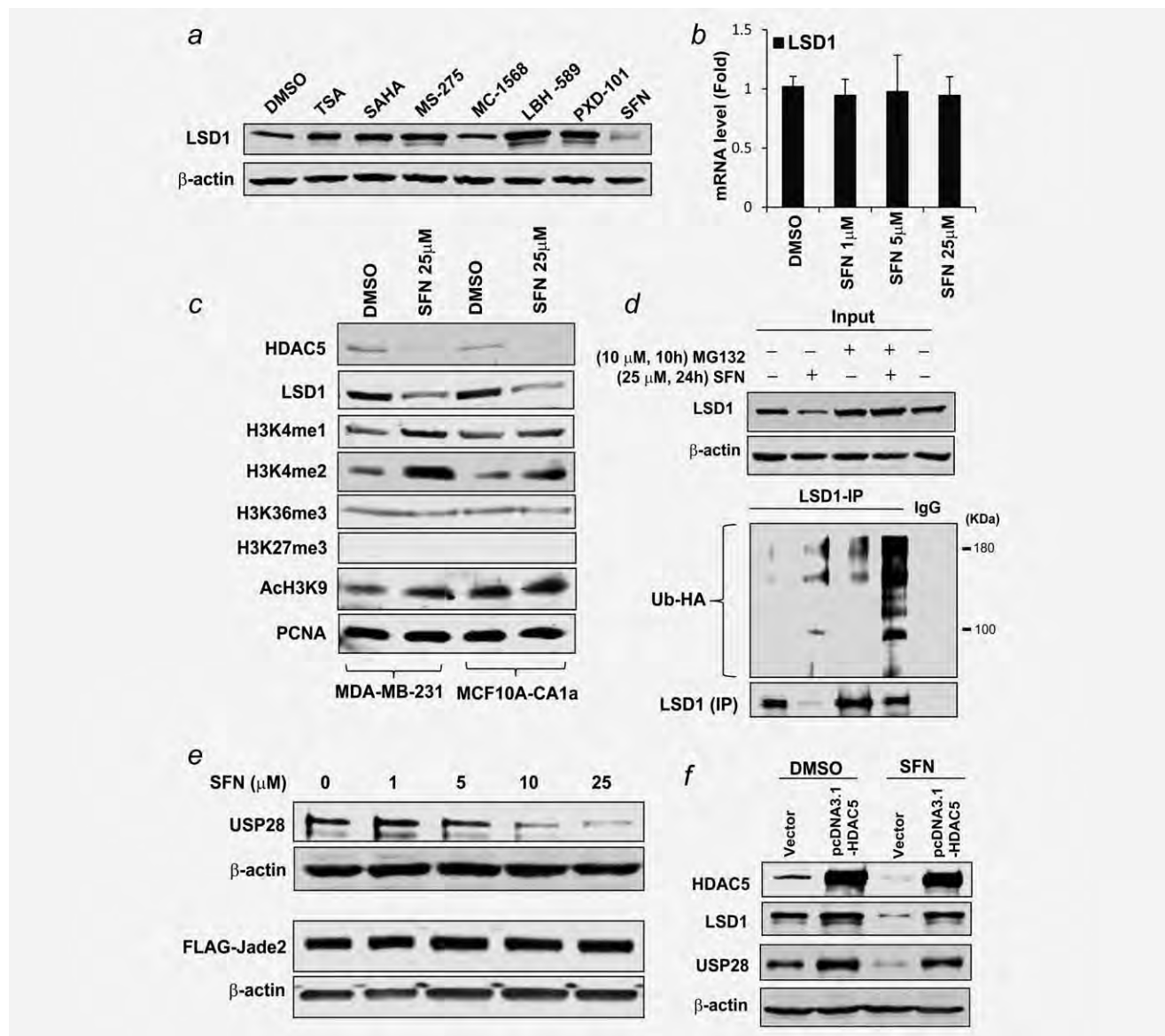


**Figure 3.** SFN downregulates LSD1 protein stability through HDAC5 modulated LSD1 ubiquitination system. (a) MDA-MB-231 cells were treated with TSA (5  $\mu$ M), SAHA (5  $\mu$ M), MS-275 (50  $\mu$ M), MC-1568 (25  $\mu$ M), LBH-589 (1  $\mu$ M), PXD-101 (5  $\mu$ M) and SFN (25  $\mu$ M) for 24 hr. Whole cell lysates were extracted and Western blotting was performed to analyze the expression of LSD1 protein.  $\beta$ -actin was used as a loading control. (b) MDA-MB-231 cells was treated with 25  $\mu$ M SFN for 24 hr. mRNA expression of LSD1 was measured by qPCR.  $\beta$ -actin was used as an internal control. (c) MDA-MB-231 and MCF10A-CA1a cells were exposed to 25  $\mu$ M SFN for 24 hr and analyzed for expression of indicated chromatin marks by immunoblots. PCNA was used as a loading control. (d) MDA-MB-231 cells were treated with 25  $\mu$ M SFN for 24 hr followed by treatment with proteasome inhibitor 10  $\mu$ M MG132 for 10 hr. IP was carried out using LSD1 antibody and immunoblots with anti-HA or LSD1 antibodies. (e) MDA-MB-231 cells were treated with increasing concentrations of SFN for 24 hr. Whole cell lysates were analyzed for protein levels of USP28 and FLAG-Jade2.  $\beta$ -actin was used as loading control to normalize target protein levels. (f) MDA-MB-231 cells were transfected with empty or HDAC5 expression vectors for 48 hr followed by treatment with 25  $\mu$ M SFN for 24 hr. Immunoblotting was performed for expression of HDAC5, LSD1 and USP28. All experiments were performed three times. Bars represent the mean of three independent experiments  $\pm$  s.d. \* $p$  < 0.05, \*\* $p$  < 0.01, \*\*\* $p$  < 0.001, Student's  $t$  test.

great synergistic effect on growth inhibition in MDA-MB-231 cells (Fig. 5f and Supporting Information, Fig. 6a). We determined the growth inhibitory effect of combined treatment with HCI-2509 with SFN in multiple breast cancer cell lines and normal breast epithelial MCF10A cells using the combination index (CI) of growth inhibition via the Chou-Talalay

model.<sup>32,33</sup> While an antagonistic effect of SFN and HCI-2509 was obviously seen in MCF10A cells (CI > 1 indicates antagonism), combination therapy exhibited significant synergy in hindering growth of breast cancer cell lines MCF10A-CA1a, MDA-MB-231 or MDA-MB-468 (CI < 1 indicates synergy) (Fig. 5g). In addition, combination therapy resulted in a robust

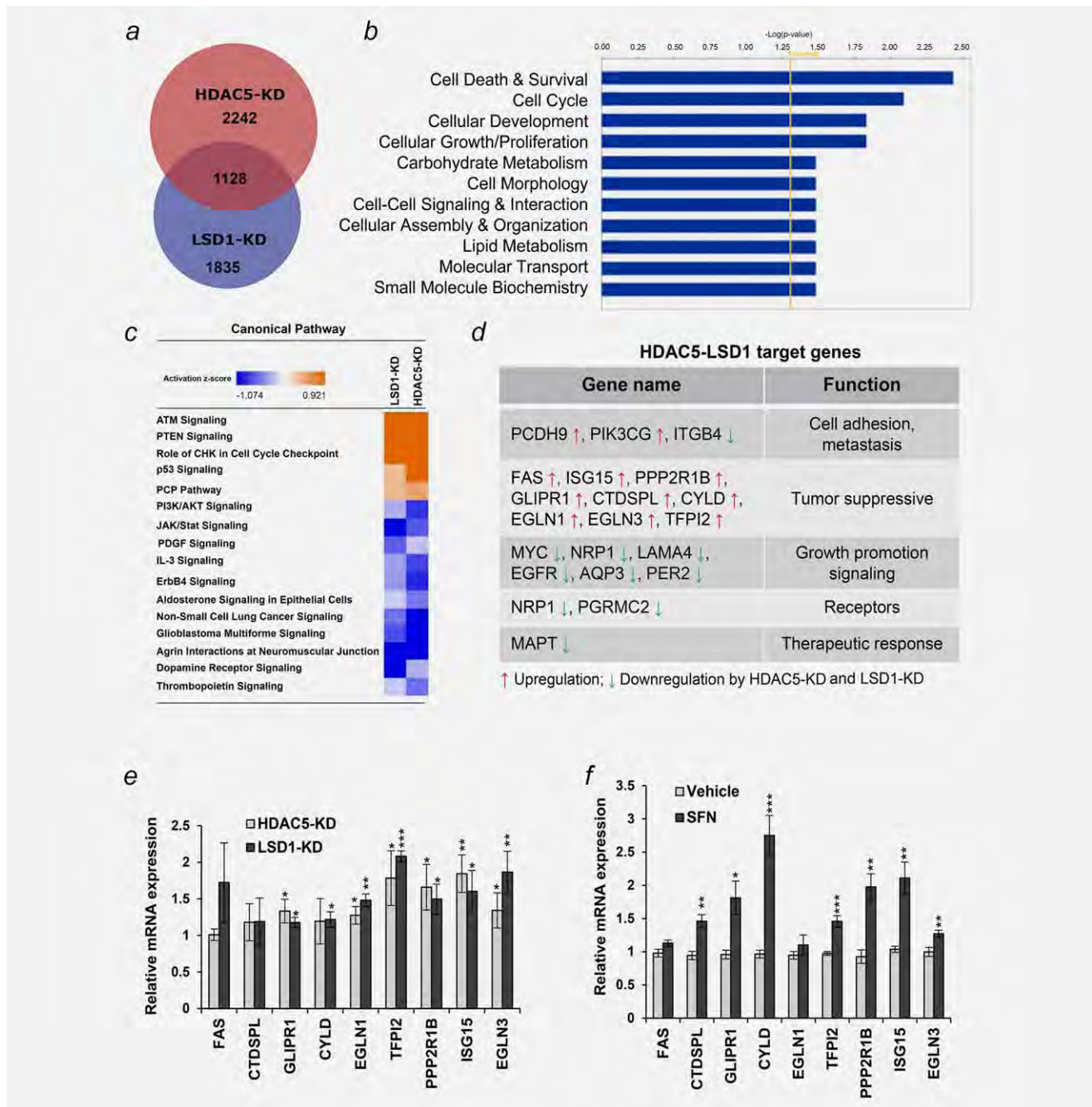


**Figure 4.** Genome-wide microarray analysis. (a) Venn diagram illustration of gene expression similarity between HDAC5-KD and LSD1-KD microarray data. Numbers shown depict genes whose expression was significantly altered in the knockdown cell line compared to scramble cell line and the union of both datasets shows the number of genes significantly altered in both knockdown cell lines. (b) Functional analysis of genes whose expression is modulated by stable knockdown of both HDAC5 and LSD1 in MDA-MB-231 cells. The bar graphs were identified by Ingenuity Pathway Analysis (IPA). The statistically significant biological functions changed by knockdown of both genes are shown. Fisher’s exact test was used to calculate the significance ( $p < 0.05$ ). The threshold line shows the cutoff for significance. (c) Top canonical pathways affected by stable knockdown of HDAC5 in MDA-MB-231 cells. Ingenuity Pathway Analysis “Core analysis” enriched top canonical pathways are shown here. Straight orange vertical line running through the bars is threshold for  $p$  values for the particular pathway’s enrichment. Bars represent overlap of genes from dataset with genes from that canonical pathway. (d) List of representative target genes of HDAC5-LSD1 complex which have critical roles in cellular processes of breast cancer. (e) Relative expression levels of HDAC5 target genes identified by HDAC5-KD microarray were validated in MDA-MB-231 cells depleted of HDAC5 or LSD1 using qPCR. (f) MDA-MB-231 cells were treated with 25  $\mu$ M SFN or vehicle DMSO for 24 hr. mRNA expression was measured by qPCR for a group of tumor suppressor genes (TSGs) regulated by HDAC5-KD/LSD1-KD.  $\beta$ -actin was used as an internal control. Bars depict mRNA level as a fold change compared to that in vehicle treated cells. All experiments were performed three times. Student’s  $t$  test was performed to assess significance. \* $p < 0.05$ , \*\* $p < 0.01$ , \*\*\* $p < 0.001$ .



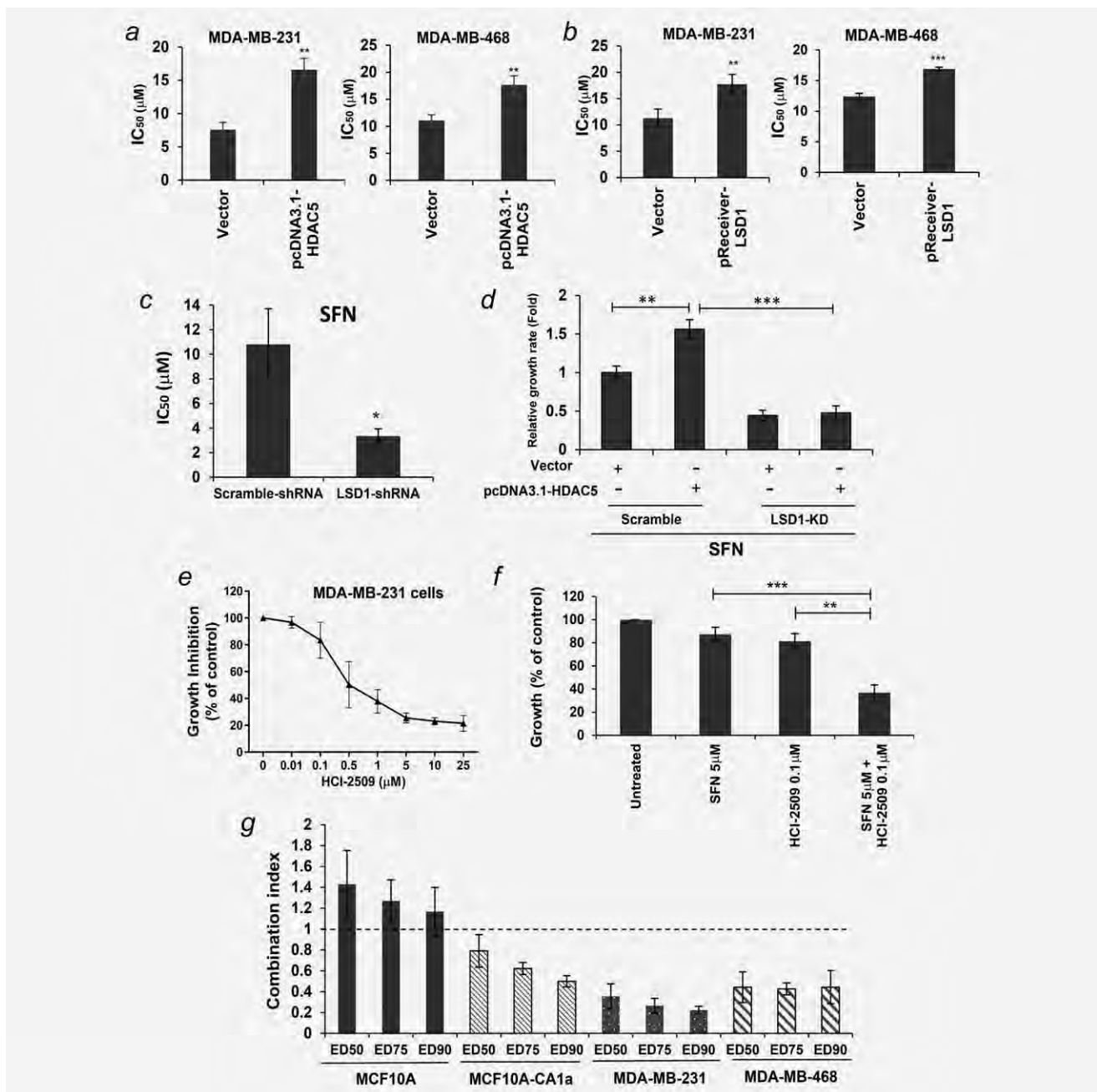


**Figure 5.** LSD1 inhibitor sensitizes breast cancer cells to SFN-induced growth inhibition. (a) MDA-MB-231 and MDA-MB-468 cells were transiently transfected with pcDNA3.1-HDAC5 flag plasmid followed by treatment with a series of concentrations of SFN for 48 hr. Cell proliferation was analyzed by crystal violet assays. The median effects (IC<sub>50</sub>) were determined by CalcuSyn software. (b) MDA-MB-231 and MDA-MB-468 cells were transiently transfected with pReceiver-LSD1-flag plasmid followed by treatment with a series of concentrations of SFN for 48 hr. Cell proliferation was analyzed by crystal violet assays. The median effects (IC<sub>50</sub>) were determined by CalcuSyn software. (c) Scramble or LSD1-shRNA transfected MDA-MB-231 cells were treated with 25 μM SFN for 72 hr. Cell proliferation was analyzed by crystal violet assays. (d) MDA-MB-231-Scramble or MDA-MB-231-LSD1-KD cells were transfected with control vector pcDNA3.1 or pcDNA3.1-HDAC5 followed by treatment with 25 μM SFN for 72 hr. Crystal violet assays for cell proliferation were carried out. (e) MDA-MB-231 cells were treated with increasing concentrations of HCl-2509 for 72 hr followed by crystal violet growth assays. (f) MDA-MB-231 cells were treated with 5 μM SFN, 0.1 μM HCl-2509 or both drugs for 72 hr. Cell proliferation was analyzed by crystal violet assays. (g) Effect of combination therapy on growth of breast cancer cells. Synergy was defined as any CI < 1, additivity as CI = 1 and antagonism as any CI > 1. Shown are means ± s.d. of three independent experiments. Student's *t* test was performed to assess significance. \**p* < 0.05, \*\**p* < 0.01, \*\*\**p* < 0.001.

increase of nuclear H3K4me2 level (Supporting Information Fig. 6b), indicating an apparent synergy between SFN and HCI-2509 against LSD1 activity.

### Sulforaphane in combination with LSD1 inhibitor profoundly inhibits growth of breast tumor xenografts in mice

To evaluate whether the above promising *in vitro* results may translate into *in vivo* therapeutic efficacy, we investigated the antineoplastic effect of combination therapy in athymic nude mice bearing MDA-MB-231 xenografts. While treatment with either SFN or HCI-2509 alone significantly inhibited the proliferation of MDA-MB-231 xenografts, the combined treatment displayed superior inhibitory effect against tumor growth (Fig. 6a). Average tumor weights were significantly lower in mice receiving combination treatment compared to those treated with either SFN or HCI-2509 alone (Fig. 6b). Statistical analysis between each group is shown in Supporting Information, Table 2. At the end of experiments, xenograft tumors were extracted for further analysis of expression of key markers (Fig. 6c). To determine whether combination therapy promotes tumor cell apoptosis, PARP-1 cleavage was analyzed. Quantitative analysis showed that only the combination treatment significantly reduced the level of full-length PARP-1, which is cleaved in smaller fragments during apoptosis (Fig. 6d). The *in vivo* effect of drug treatment on protein expression of HDAC5 and LSD1 in xenograft tumors was also evaluated. Immunoblots showed that expression of both HDAC5 and LSD1 was attenuated in tumors treated with SFN alone or in combination with HCI-2509 (Fig. 6e). During the entire course of experiment, drug toxicity was acceptable as demonstrated by modest weight loss observed in animals with combination treatment, and no animal lethality occurring in any treatment group (Supporting Information, Fig. 7a). Statistical analysis of animal weight between groups is shown in Supporting Information, Table 3. To further evaluate *in vivo* toxicity, we performed hematoxylin-eosin (H&E) staining of animal liver and kidneys, and found no apparent changes in these tissues treated with SFN or HCI-2509 alone, or in combination (Supporting Information Fig. 7b). Collectively, these results indicate that SFN monotherapy effectively inhibits growth of MDA-MB-231 xenografts *in vivo* and exhibits significantly enhanced growth inhibition when used in combination with an LSD1 inhibitor. Based on these findings, we proposed a model to summarize the role of HDAC5–LSD1 axis in mediating antineoplastic effect of natural HDAC inhibitor sulforaphane in human breast cancer (Fig. 6f).

### Discussion

Class II HDACs have been intensively investigated for their ability to regulate gene transcription and shape the epigenetic landscape. This class of HDAC enzymes has been recognized as important regulators of numerous cellular processes in human diseases. The increasing knowledge on regulatory

signaling pathways of class II HDACs has provided novel targets and approaches for potential clinical intervention in cancer. HDAC5 is a key class II HDAC isozyme that has been shown to possess critical roles in many diseases including cancers.<sup>8,9,34,35</sup> Our recent tissue microarray study found that breast tumors express overall higher levels of HDAC5 protein compared to the matched adjacent normal tissues.<sup>5</sup> Importantly, our analysis showed that elevated HDAC5 protein expression is positively correlated with higher stages of clinical breast cancer.<sup>5</sup> These findings suggest that elevated expression of HDAC5 may serve as a potential novel prognostic marker as well as a possible therapeutic target for aggressive breast cancer. However, little is known about the regulatory roles of HDAC5 or other class II HDACs in human breast cancer. In this study, we explored the molecular mechanisms by which HDAC5 mRNA expression is upregulated during breast cancer progression. Through engineering a series of HDAC5 5' flanking promoter deletion elements in luciferase reporter plasmids, we showed that activity of an element at –356 to –100 bp of the HDAC5 promoter is essential in mediating its transcriptional activity. Further use of *in vitro* DAPA and mass spectrometry analysis identified USF1 as an important regulatory factor that binds to –356 to –100 bp element at HDAC5 promoter. USF1 is a member of the basic helix–loop–helix leucine zipper family and functions as a cellular transcription factor to activate transcription through pyrimidine-rich initiator elements and E-box motifs.<sup>36,37</sup> The dysfunction of USF1 has been reported to be linked with multiple human diseases and disorders, such as lipid metabolism, atherosclerosis and acute cardiovascular events.<sup>38</sup> The precise roles of USF1 activity in breast initiation and progression are still unclear. *In silico* data analysis indicates a significant elevation of USF1 expression in aggressive basal-like or ER-negative breast tumors versus other breast cancer subtypes or normal adjacent tissues, suggesting a positive correlation between USF1 overexpression and aggressive phenotypes of breast cancer. Continuous exploration of the underlying mechanisms would aid in understanding how USF1 upregulates HDAC5 expression and the clinical impact of elevated USF1 expression on the risk stratification of breast cancer patients.

In our recent study, we have showed for the first time that HDAC5 stabilizes LSD1 protein through regulation of LSD1 associated ubiquitin-proteasome enzyme.<sup>5</sup> To further explore whether the HDAC5–LSD1 axis has potential to be a novel therapeutic target for breast cancer, we surveyed a panel of clinically relevant HDAC inhibitors for their ability to alter the activity of the HDAC5–LSD1 axis. While most of the clinically relevant HDAC inhibitors significantly upregulated transcriptional level of HDAC5 which in turn led to increased expression of LSD1 protein, we found that SFN potently inhibited HDAC5 transcription in multiple breast cancer cell lines. SFN is generated by the hydrolytic conversion of glucoraphanin after ingestion of cruciferous vegetables, particularly broccoli and broccoli sprouts. As Myzak *et al.* first reported that SFN inhibited *in vitro* HDAC activity

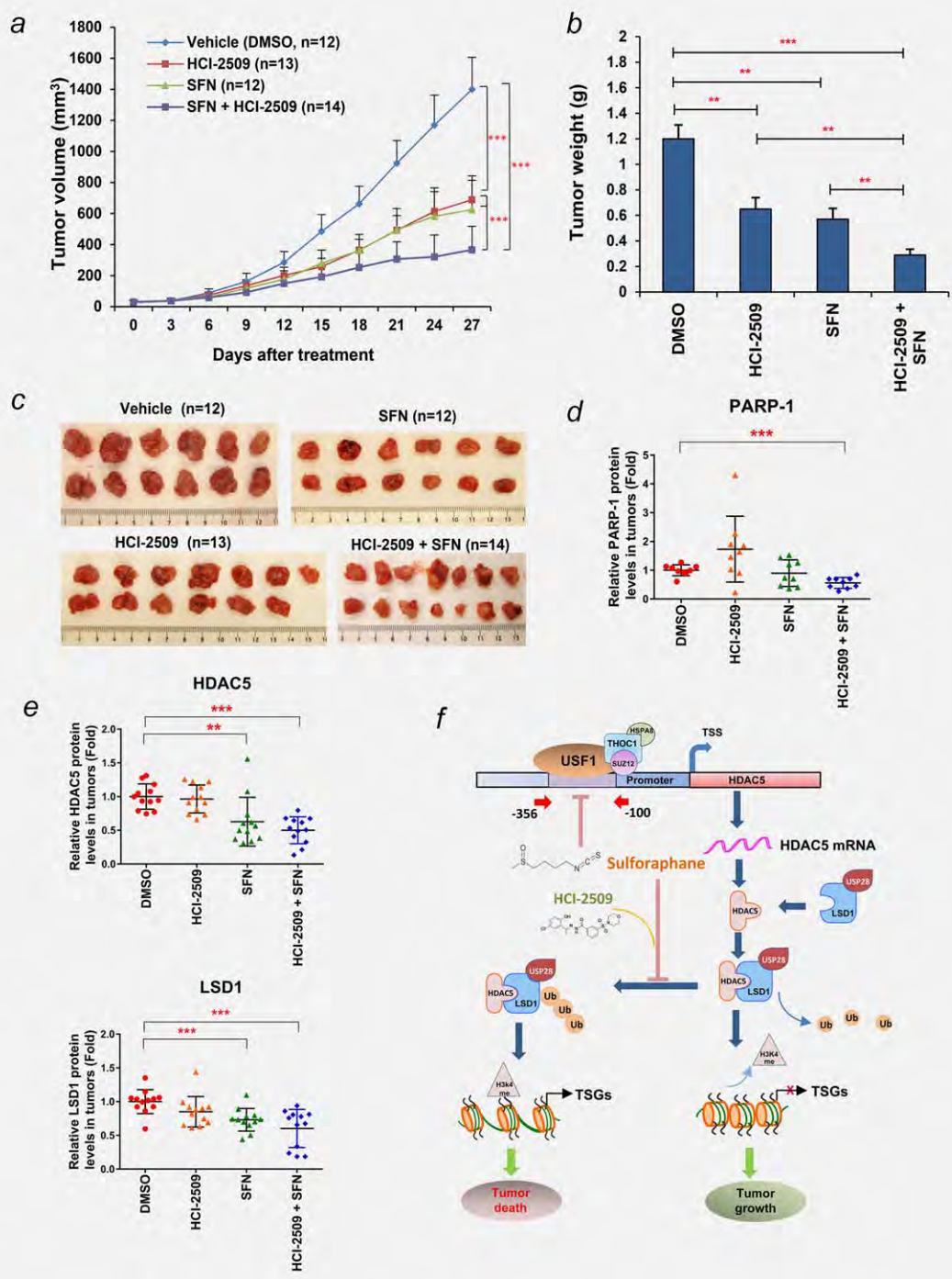


**Figure 6.** LSD1 inhibitor sensitizes MDA-MB-231 xenografts to sulforaphane induced growth inhibition in nude mice. (a) MDA-MB-231 cells were transplanted into the mammary gland fat pads of athymic nude mice. Seven days after implantation, Sulforaphane (50 mg/kg,  $n = 12$ ), HCl-2509 (30 mg/kg,  $n = 13$ ), combination (SFN 50 mg/kg + HCl-2509 30 mg/kg,  $n = 14$ ) or vehicle (DMSO,  $n = 12$ ) were delivered via i.p. injection once a day for 5 days/week  $\times$  4 weeks. The vertical bars indicate mean tumor size (mm<sup>3</sup>)  $\pm$  s.d. One-way ANOVA was performed to determine statistical significance between groups, with  $p < 0.05$  considered significant. (b) Weight of animal tumors was measured at the end of experiment. (c) Images of xenograft tumors from each treatment group were taken at the end of experiment. (d) Protein was extracted from tumor samples of MDA-MB-231 xenografts treated with vehicle, HCl-2509, SFN or combination ( $n = 12$  for each group). Quantitative immunoblotting was used to determine the expression of full-length PARP-1 protein.  $\beta$ -actin was used as loading control. (e) Protein was extracted from tumor samples of MDA-MB-231 xenografts treated with vehicle, HCl-2509, SFN or combination ( $n = 12$  for each group). Quantitative immunoblotting was used to determine the expression of LSD1 and HDAC5 proteins.  $\beta$ -actin was used as loading control. (f) Proposed model of the role of HDAC5–LSD1 axis in mediating antineoplastic effect of SFN in human breast cancer. A complex of multiple factors (USF1, SUZ12, THOC1, HSPA8, etc.) was identified to be associated with  $-356$  to  $-100$  bp element at HDAC5 promoter. Among these factors, USF1 was shown to play an important role in governing HDAC5 transcription. A natural bioactive HDACi, sulforaphane (SFN), downregulates HDAC5 transcription by blocking USF1 activity. SFN facilitates LSD1 degradation through enhancing protein stability of LSD1 deubiquitinase USP28 in an HDAC5-dependent manner. SFN increases H3K4me2 level at promoter of tumor suppressor genes (TSGs) and promotes expression of TSGs. Combination treatment with SFN and a potent LSD1 inhibitor HCl-2509 results in synergistic growth inhibition of breast cancer proliferation in cell culture and xenograft models. TSGs, tumor suppressor genes; Ub, ubiquitination; HSPA8, heat shock cognate 71 kDa protein.

by its two major metabolites, SFN-cysteine and SFN-N-acetylcysteine, numerous studies have demonstrated that SFN exhibits inhibitory effect against HDAC activity in many types of cancers including breast cancer.<sup>39–43</sup> We have reported that SFN blocked growth, activated apoptosis, inhibited HDAC activity, and decreased the expression of key proteins involved in breast cancer proliferation.<sup>41</sup> But the mechanisms of the inhibitory effect of SFN on HDAC activity in breast cancer has not been fully elucidated. In this study, we obtained new evidence to show that SFN downregulated HDAC5 mRNA expression, largely through inhibiting the transcriptional activities at the –356 to –100 bp element of gene promoter, therefore, identifying this element and its associated factors as important targets for SFN. Future clarification of the function of key coregulatory proteins/complexes associated with this element would aid in elucidating the precise mechanism of SFN-induced downregulation of HDAC5 transcription in breast cancer. Our recent study showed that suppression of active histone marks H3K4 methylation and H3K9 acetylation mediated by enhanced activity of HDAC5–LSD1 signaling at promotes of tumor suppressor genes (TSGs) are important chromatin signature contributing to silencing of key TSGs in breast cancer cells.<sup>5</sup> SFN significantly increases levels of both H3K4me and Acetyl H3K9, suggesting that SFN may act as an important epigenetic modulator to reactivate expression of TSGs through inhibiting cross-talk between LSD1 and HDAC5 in breast cancer cells.

We found that the suppressive effect of SFN on transcriptional activity was unique among the tested panel of HDAC inhibitors (HDACi), including clinically approved SAHA and Romidepsin. Several studies indicated that inherent resistance to HDACi was commonly observed in clinical trials of breast cancer patients.<sup>44–48</sup> However, the mechanism of HDACi resistance in breast cancer is still unclear. Based on the findings from our work, we speculate that enhanced HDAC5 expression in response to treatment with conventional HDACi could contribute to refractoriness to HDACi therapy. Additional evidence supporting this hypothesis includes the findings that overexpression of HDAC5 or LSD1 in breast cancer cells significantly reduced sensitivity to growth inhibition mediated by several HDAC inhibitors. Future work is needed to explore the potential strategy of combining

reagents targeting the HDAC5–LSD1 axis with clinically approved HDAC inhibitors to improve their therapeutic efficacy in breast cancer.

We recently demonstrated that HDAC5 promotes LSD1 protein stability through inhibition of the LSD1 associated ubiquitin-proteasome system, suggesting that the modulation of LSD1 protein stability by HDAC5 is a post-translational activity.<sup>5</sup> In this study, we showed that SFN suppresses HDAC5 expression, subsequently leading to degradation of LSD1 protein. SFN destabilizes LSD1 protein through inhibition of the LSD1 deubiquitinase, USP28, without affecting LSD1 mRNA expression. These results were further validated by a rescue strategy with overexpression of exogenous HDAC5 cDNA lacking a native promoter, showing that SFN treatment indeed leads to degradation of LSD1 protein in an HDAC5-dependent manner. Treatment with SFN or LSD1 inhibitor alone significantly inhibited the growth of MDA-MB-231 xenograft tumors in nude mice, but the greatest inhibition of tumor growth was observed when these two drugs were used in combination. These data clearly suggest that inhibition of HDAC5–LSD1 pathway by SFN in combination with a potent LSD1 inhibitor may serve as an effective approach to reduce nonspecific side effects of SFN in breast cancer. Given that the inherent resistance to HDACi develops as a result of combined multifactorial epigenetic abnormalities, our findings provide a rational basis for clinical trials combining agents targeting these dysregulated epigenetic targets in breast cancer.

As summarized in Figure 6f, we have demonstrated that HDAC5–LSD1 axis is an effective drug target in breast cancer. Inhibition of HDAC5–LSD1 axis with sulforaphane suppresses breast cancer growth *in vitro* and *in vivo*. Notably, combined treatment with a novel and potent LSD1 inhibitor improves the anticancer efficacy of sulforaphane in breast cancer cells.

### Acknowledgements

This project used the University of Pittsburgh Hillman Cancer Center Bioinformatics, Cancer Proteomics and Cancer Genomics Services. The authors also gratefully acknowledge the animal and histological core facilities of Magee Womens Research Institute. They thank Lin Chen for technical support.


### References

1. Baylin SB, Ohm JE. Epigenetic gene silencing in cancer - a mechanism for early oncogenic pathway addiction? *Nat Rev Cancer* 2006;6:107–16.
2. Jenuwein T, Allis CD. Translating the histone code. *Science* 2001;293:1074–80.
3. Stearns V, Zhou Q, Davidson NE. Epigenetic regulation as a new target for breast cancer therapy. *Cancer Invest* 2007;25:659–65.
4. Connolly R, Stearns V. Epigenetics as a therapeutic target in breast cancer. *J Mammary Gland Biol Neoplasia* 2012;17:191–204.
5. Cao C, Vasilatos SN, Bhargava R, et al. Functional interaction of histone deacetylase 5 (HDAC5) and lysine-specific demethylase 1 (LSD1) promotes breast cancer progression. *Oncogene* 2017;36:133–45.
6. Yang XJ, Gregoire S. Class II histone deacetylases: from sequence to function, regulation, and clinical implication. *Mol Cell Biol* 2005;25:2873–84.
7. Martin M, Kettmann R, Dequiedt F. Class IIa histone deacetylases: regulating the regulators. *Oncogene* 2007;26:5450–67.
8. McKinsey TA, Zhang CL, Lu J, et al. Signal-dependent nuclear export of a histone deacetylase regulates muscle differentiation. *Nature* 2000;408:106–11.
9. Martin M, Kettmann R, Dequiedt F. Class IIa histone deacetylases: conducting development and differentiation. *Int J Dev Biol* 2009;53:291–301.
10. Özdağ H, Teschendorff AE, Ahmed A, et al. Differential expression of selected histone modifier genes in human solid cancers. *BMC Genomics* 2006;7:90.
11. Milde T, Oehme I, Korshunov A, et al. HDAC5 and HDAC9 in medulloblastoma: novel markers for risk stratification and role in tumor cell growth. *Clin Cancer Res* 2010;16:3240–52.
12. Huang Y, Marton LJ, Woster PM, et al. Polyamine analogues targeting epigenetic gene regulation. *Essays Biochem* 2009;46:95–110.

13. Huang Y, Greene E, Murray Stewart T, et al. Inhibition of lysine-specific demethylase 1 by polyamine analogues results in reexpression of aberrantly silenced genes. *Proc Natl Acad Sci USA* 2007;104:8023–8.
14. Shi Y, Lan F, Matson C, et al. Histone demethylation mediated by the nuclear amine oxidase homolog LSD1. *Cell* 2004;119:941–53.
15. Huang Y, Nayak S, Jankowitz R, et al. Epigenetics in breast cancer: what's new? *Breast Cancer Res* 2011;13:225.
16. Huang Y, Marton LJ, Woster PM. The design and development of polyamine-based analogues with epigenetic targets. *Royal Society of Chemistry Drug Discovery Series No 17, Thomas Graham House* 2012; 238–56.
17. Katz TA, Huang Y, Davidson NE, et al. Epigenetic reprogramming in breast cancer: from new targets to new therapies. *Ann Med* 2014;46:397–408.
18. Garcia-Bassets I, Kwon YS, Telese F, et al. Histone methylation-dependent mechanisms impose ligand dependency for gene activation by nuclear receptors. *Cell* 2007;128:505–18.
19. Lim S, Janzer A, Becker A, et al. Lysine-specific demethylase 1 (LSD1) is highly expressed in ER-negative breast cancers and a biomarker predicting aggressive biology. *Carcinogenesis* 2010;31:512–20.
20. Metzger E, Wissmann M, Yin N, et al. LSD1 demethylates repressive histone marks to promote androgen-receptor-dependent transcription. *Nature* 2005;437:436–9.
21. Huang Y, Stewart TM, Wu Y, et al. Novel oligoamine analogues inhibit lysine-specific demethylase 1 and induce reexpression of epigenetically silenced genes. *Clin Cancer Res* 2009;15:7217–28.
22. Zhu Q, Huang Y, Marton LJ, et al. Polyamine analogues modulate gene expression by inhibiting Lysine-Specific Demethylase 1 (LSD1) and altering chromatin structure in human breast cancer cells. *Amino Acids* 2011;42:887–98.
23. Maiques-Diaz A, Somervaille TC. LSD1: biologic roles and therapeutic targeting. *Epigenomics* 2016.
24. Mohammad HP, Smitheman KN, Kamat CD, et al. A DNA hypomethylation signature predicts antitumor activity of LSD1 inhibitors in SCLC. *Cancer Cell* 2015;28:57–69.
25. Cui S, Lim KC, Shi L, et al. The LSD1 inhibitor RN-1 induces fetal hemoglobin synthesis and reduces disease pathology in sickle cell mice. *Blood* 2015;126:386–96.
26. Vasilatos SN, Katz TA, Oesterreich S, et al. Crosstalk between lysine-specific demethylase 1 (LSD1) and histone deacetylases mediates antineoplastic efficacy of HDAC inhibitors in human breast cancer cells. *Carcinogenesis* 2013;34:1196–207.
27. Huang Y, Vasilatos SN, Boric L, et al. Inhibitors of histone demethylation and histone deacetylation cooperate in regulating gene expression and inhibiting growth in human breast cancer cells. *Breast Cancer Res Treat* 2012;131:777–89.
28. Katz TA, Vasilatos SN, Harrington E, et al. Inhibition of histone demethylase, LSD2 (KDM1B), attenuates DNA methylation and increases sensitivity to DNMT inhibitor-induced apoptosis in breast cancer cells. *Breast Cancer Res Treat* 2014; 146:99–108.
29. Chen L, Vasilatos SN, Qin Y, et al. Functional characterization of lysine-specific demethylase 2 (LSD2/KDM1B) in breast cancer progression. *Oncotarget* 2017;8:81737–53.
30. Huang Y, Hager ER, Phillips DL, et al. A novel polyamine analog inhibits growth and induces apoptosis in human breast cancer cells. *Clin Cancer Res* 2003;9:2769–77.
31. Sankar S, Bell R, Stephens B, et al. Mechanism and relevance of EWS/FLI-mediated transcriptional repression in Ewing sarcoma. *Oncogene* 2013;32:5089–100.
32. Chou TC, Talalay P. A simple generalized equation for the analysis of multiple inhibitions of Michaelis-Menten kinetic systems. *J Biol Chem* 1977;252:6438–42.
33. Chou TC. Drug combination studies and their synergy quantification using the Chou-Talalay method. *Cancer Res*. 2010;70:440–6.
34. He P, Liang J, Shao T, et al. HDAC5 promotes colorectal cancer cell proliferation by up-regulating DLL4 expression. *Int J Clin Exp Med* 2015;8:6510–6.
35. Hsieh TH, Hsu CY, Tsai CF, et al. HDAC inhibitors target HDAC5, upregulate microRNA-125a-5p, and induce apoptosis in breast cancer cells. *Mol Ther* 2015;23:656–66.
36. Shieh BH, Sparkes RS, Gaynor RB, et al. Localization of the gene-encoding upstream stimulatory factor (USF) to human chromosome 1q22-q23. *Genomics* 1993;16:266–8.
37. Gregor PD, Sawadogo M, Roeder RG. The adenovirus major late transcription factor USF is a member of the helix-loop-helix group of regulatory proteins and binds to DNA as a dimer. *Genes Dev* 1990;4:1730–40.
38. Kristiansson K, Ilveskoski E, Lehtimäki T, et al. Association analysis of allelic variants of USF1 in coronary atherosclerosis. *Arterioscler Thromb Vasc Biol* 2008;28:983–9.
39. Tortorella SM, Royce SG, Licciardi PV, et al. Dietary sulforaphane in cancer chemoprevention: the role of epigenetic regulation and hdac inhibition. *Antioxid Redox Signal* 2015;22:1382–424.
40. Ho E, Clarke JD, Dashwood RH. Dietary sulforaphane, a histone deacetylase inhibitor for cancer prevention. *J Nutr* 2009;139:2393–6.
41. Pledger-Tracy A, Sobolewski MD, Davidson NE. Sulforaphane induces cell type-specific apoptosis in human breast cancer cell lines. *Mol Cancer Ther* 2007;6:1013–21.
42. Atwell LL, Zhang Z, Mori M, et al. Sulforaphane bioavailability and chemopreventive activity in women scheduled for breast biopsy. *Cancer Prev Res (Phila)*. 2015;8:1184–91.
43. Myzak MC, Karplus PA, Chung FL, et al. A novel mechanism of chemoprotection by sulforaphane: inhibition of histone deacetylase. *Cancer Res* 2004;64:5767–74.
44. Traynor AM, Dubey S, Eickhoff JC, et al. Vorinostat (NSC# 701852) in patients with relapsed non-small cell lung cancer: a Wisconsin Oncology Network phase II study. *J Thorac Oncol* 2009;4:522–6.
45. Luu TH, Morgan RJ, Leong L, et al. A phase II trial of vorinostat (suberoylanilide hydroxamic acid) in metastatic breast cancer: a California Cancer Consortium study. *Clin Cancer Res* 2008; 14:7138–42.
46. Modesitt SC, Sill M, Hoffman JS, et al. A phase II study of vorinostat in the treatment of persistent or recurrent epithelial ovarian or primary peritoneal carcinoma: a Gynecologic Oncology Group study. *Gynecol Oncol* 2008;109:182–6.
47. Blumenschein GR, Jr., Kies MS, Papadimitrakopoulou VA, et al. Phase II trial of the histone deacetylase inhibitor vorinostat (Zolinza, suberoylanilide hydroxamic acid, SAHA) in patients with recurrent and/or metastatic head and neck cancer. *Invest New Drugs* 2008;26:81–7.
48. Mithraprabhu S, Khong T, Spencer A. Overcoming inherent resistance to histone deacetylase inhibitors in multiple myeloma cells by targeting pathways integral to the actin cytoskeleton. *Cell Death Dis*. 2017;5:e1134.



# Inhibition of histone lysine-specific demethylase 1 elicits breast tumor immunity and enhances antitumor efficacy of immune checkpoint blockade

Ye Qin<sup>1,2</sup> · Shauna N. Vasilatos<sup>1</sup> · Lin Chen<sup>1</sup> · Hao Wu<sup>1</sup> · Zhishen Cao<sup>3</sup> · Yumei Fu<sup>4</sup> · Min Huang<sup>2</sup> · Anda M. Vlad<sup>3,5</sup> · Binfang Lu<sup>5</sup> · Steffi Oesterreich<sup>1,2</sup>  · Nancy E. Davidson<sup>6</sup> · Yi Huang<sup>1,2</sup>

Received: 25 January 2018 / Revised: 18 June 2018 / Accepted: 21 July 2018  
© Springer Nature Limited 2018

## Abstract

Immunotherapy strategies have been emerging as powerful weapons against cancer. Early clinical trials reveal that overall response to immunotherapy is low in breast cancer patients, suggesting that effective strategies to overcome resistance to immunotherapy are urgently needed. In this study, we investigated whether epigenetic reprogramming by modulating histone methylation could enhance effector T lymphocyte trafficking and improve therapeutic efficacy of immune checkpoint blockade in breast cancer with focus on triple-negative breast cancer (TNBC) subtype. In silico analysis of The Cancer Genome Atlas (TCGA) data shows that expression of histone lysine-specific demethylase 1 (LSD1) is inversely associated with the levels of cytotoxic T cell-attracting chemokines (C–C motif chemokine ligand 5 (CCL5), C–X–C motif chemokine ligand 9 and 10 (CXCL9, CXCL10)) and programmed death-ligand 1 (PD-L1) in clinical TNBC specimens. Tiling chromatin immunoprecipitation study showed that re-expression of chemokines by LSD1 inhibition is associated with increased H3K4me2 levels at proximal promoter regions. Rescue experiments using concurrent treatment with small interfering RNA or inhibitor of chemokine receptors blocked LSD1 inhibitor-enhanced CD8+ T cell migration, indicating a critical role of key T cell chemokines in LSD1-mediated CD8+ lymphocyte trafficking to the tumor microenvironment. In mice bearing TNBC xenograft tumors, anti-PD-1 antibody alone failed to elicit obvious therapeutic effect. However, combining LSD1 inhibitors with PD-1 antibody significantly suppressed tumor growth and pulmonary metastasis, which was associated with reduced Ki-67 level and augmented CD8+ T cell infiltration in xenograft tumors. Overall, these results suggest that LSD1 inhibition may be an effective adjuvant treatment with immunotherapy as a novel management strategy for poorly immunogenic breast tumors.

**Electronic supplementary material** The online version of this article (<https://doi.org/10.1038/s41388-018-0451-5>) contains supplementary material, which is available to authorized users.

✉ Yi Huang  
yih26@pitt.edu

- <sup>1</sup> Women's Cancer Research Center, UPMC Hillman Cancer Center, University of Pittsburgh, Pittsburgh, PA, USA
- <sup>2</sup> Department of Pharmacology and Chemical Biology, University of Pittsburgh School of Medicine, Pittsburgh, PA, USA
- <sup>3</sup> Department of Obstetrics, Gynecology and Reproductive Sciences, University of Pittsburgh, Pittsburgh, PA, USA
- <sup>4</sup> Allegheny General Hospital Pathology, Pittsburgh, PA, USA
- <sup>5</sup> Department of Immunology, University of Pittsburgh School of Medicine, Pittsburgh, PA, USA
- <sup>6</sup> Fred Hutchinson Cancer Research Center, Seattle Cancer Care Alliance, and University of Washington, Seattle, WA, USA

## Introduction

Unlike some other types of tumors, breast cancer was thought to be non-immunogenic and the relevance of the host immune response to breast tumors has long been debated. A growing body of evidence has shown that some breast tumors, particularly the more aggressive triple-negative breast cancer (TNBC), do elicit host antitumor immune responses, and the robustness of the response correlates with prognosis [1–3]. Recent data from phase I trials with immune checkpoint inhibitors (ICIs) in TNBC patients reported an encouraging overall response (OR), up to 20%, with durable clinical responses [4–7]. However, the majority of TNBC patients are still refractory to immunotherapy. This raises the question of whether combining immunotherapy with other approaches could augment clinical response rate for this devastating disease.

One of the best predictors of response to immunotherapy is the number and phenotype of tumor-infiltrating CD8<sup>+</sup> cytotoxic T lymphocytes that are recruited at the tumor site by the locally secreted chemokines [8]. Chemokines are a family of small heparin-binding proteins, which mediates immune cell trafficking and lymphoid tissue development [9]. Among these chemokines, elevated levels of the C–C motif chemokine ligand 5 (CCL5) and T helper 1 (Th1)-type chemokines, C–X–C motif chemokine ligand 9 and 10 (CXCL9 and CXCL10), are frequently associated with increased recruitment of CD8<sup>+</sup> T lymphocytes to tumor sites [10–12]. A large body of evidence exists to show that increased expression of cytotoxic T cell-attracting chemokines correlates with decreased levels of cancer metastasis and improved clinical outcome in cancer patients [13, 14]. However, it is not well understood about the molecular mechanisms controlling down-regulation of cytotoxic T cell chemokine expression in cancer and how reduced expression of these chemokines subsequently deters effector T cell trafficking to the tumor microenvironment.

Epigenetic alterations are associated with all stages of breast tumor formation and progression [15, 16]. The best characterized chromatin dysregulation is epigenetically mediated transcriptional silencing which is typically associated with increased DNA methylation and histone function abnormalities [17, 18]. Recent studies indicate that epigenetic dysregulation plays a critical role in silencing expression of certain effector T cell chemokines, which may lead to inefficient recognition and elimination of cancer cells by the host immune system [11, 12]. The results from these studies also suggest that aberrant suppression of effector T cell chemokines could be reversed by epigenetic reprogramming, which may, in turn, improve T cell infiltration and expand the efficacy of immunotherapy. However, the nature of epigenetic silencing in governing cancer immunopathology and immunotherapy remains very elusive.

In this study, we explored the mechanisms of how epigenetic dysregulation of expression and activity of cytotoxic T cell chemokines impedes trafficking of antitumor immune cells and facilitates TNBC progression. We also investigated whether epigenetic agents could augment antitumor immune responses and improve therapeutic efficacy of immune checkpoint blocking antibodies. Our findings indicate that a key epigenetic modifier, lysine-specific demethylase 1 (LSD1), plays an important role in mediating epigenetic reprogramming that alters the T cell landscape in TNBC. We have also put forth preclinical evidence that combined use of LSD1 inhibitor effectively enhances the therapeutic efficacy of anti-PD-1 immunotherapy.

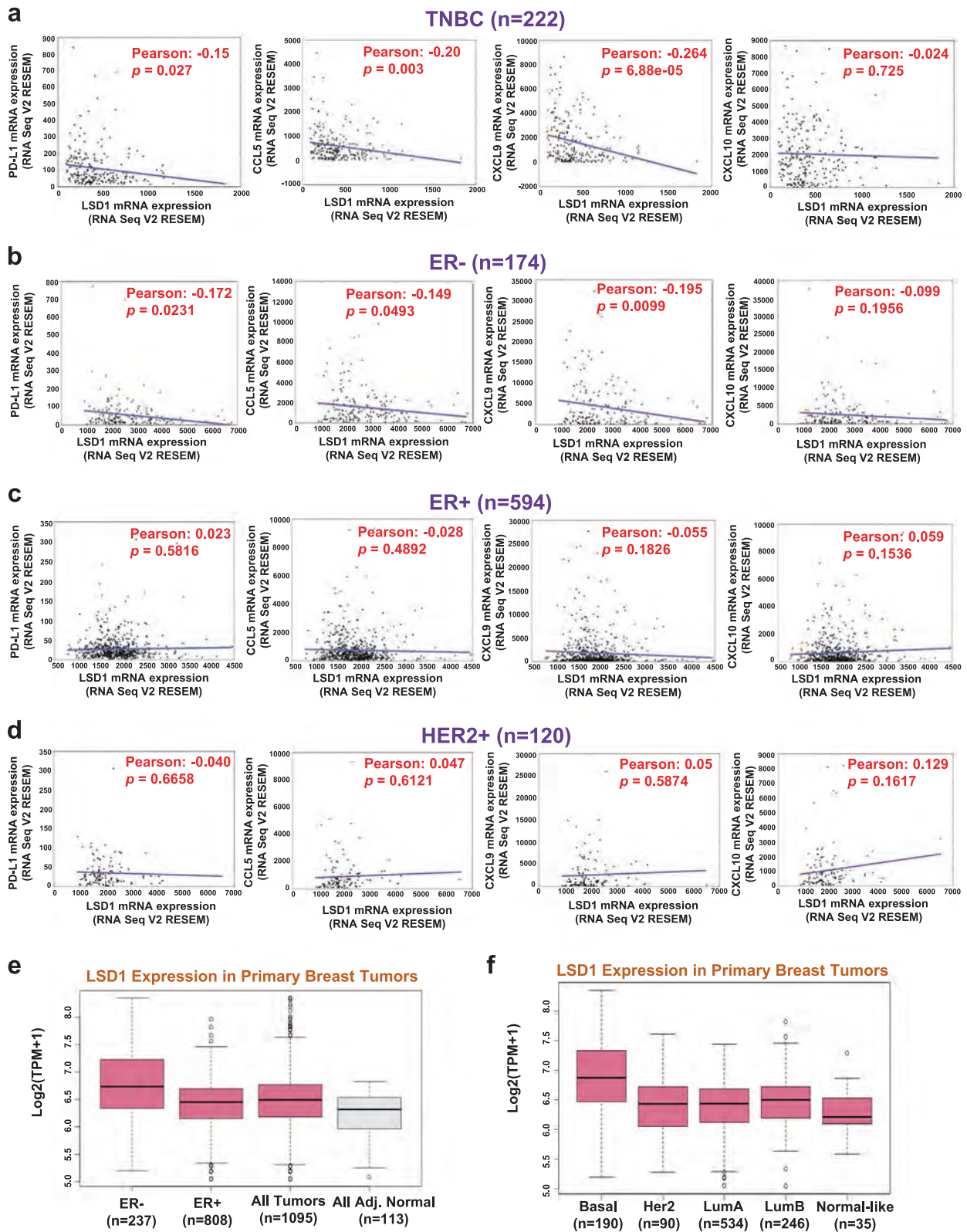
## Results

### Negative correlation between expression of LSD1 and immune regulatory genes in TNBC specimens

The correlation of expression between key epigenetic modifiers (histone deacetylases, histone lysine demethylases, DNA methyltransferases, etc.) and immune signature genes such as CD8<sup>+</sup> T cell-attracting chemokines (CCL5, CXCL9, CXCL10) and the immune checkpoint molecule programmed death-ligand 1 (PD-L1) was first evaluated in a cohort of 222 TNBC clinical specimens [19]. We observed a negative correlation between multiple epigenetic regulators and immune-related genes (Supplementary Table 1). Among these epigenetic modifiers, the flavin adenine dinucleotide-dependent histone demethylase, LSD1, appears to be negatively correlated with the chemokines and PD-L1 with most overall significant *p* values (Supplementary Table 1; Fig. 1a). Further analysis showed that LSD1 gene expression was inversely associated with these immune factors in estrogen receptor-negative (ER<sup>−</sup>), but not in ER<sup>+</sup> or HER2<sup>+</sup> tumors (Fig. 1b–d). Overall, these *in silico* data revealed a negative correlation between expression of LSD1 and cytotoxic T cell-attracting chemokines and PD-L1 in aggressive TNBC or ER<sup>−</sup> breast tumors. Analysis of the TCGA data indicates that LSD1 expression is greatly increased in breast tumor specimens compared with adjacent normal tissues (Fig. 1e; Supplementary Figure 1a). The analysis also indicated a significantly elevated level of LSD1 messenger RNA (mRNA) expression in ER negative or basal-like breast cancer in comparison to other subtypes (Fig. 1e, f; Supplementary Figure 1b).

### Inhibition of LSD1 induces expression of effector T cell-attracting chemokines and PD-L1

The dysregulation of LSD1 activity has been implicated in tumorigenesis for various cancers including breast cancer [20–22]. To determine whether overexpression of LSD1 aberrantly suppresses expression of immune-protective factors, we tested several LSD1 inhibitors for their impact on expression of CD8<sup>+</sup> T cell-attracting chemokines and PD-L1. Among these LSD1 inhibitors, HCI-2509 and tranylcypromine (TCP) significantly increased the expression of PD-L1, CCL5, CXCL9, and CXCL10 in human TNBC MDA-MB-231 cells (Fig. 2a). TCP is an irreversible LSD1 inhibitor that has been used as a chemical scaffold to design new generations of LSD1 inhibitors [21] (Supplementary Figure 2a). HCI-2509 is a non-competitive and highly potent reversible LSD1 inhibitor that effectively inhibits LSD1 activity at micromolar levels in MDA-MB-231 cells (Supplementary Figure 2b). HCI-2509 induced mRNA



expression of PD-L1 and T cell chemokines in a dose-dependent manner in MDA-MB-231 cells, and mouse TNBC cell line models, 4T1 and EMT6 (Fig. 2b). In

agreement with the effects of the LSD1 inhibitors, depletion of LSD1 by small interfering RNA (siRNA) in MDA-MB-231 or MDA-MB-468 cells significantly increased the



◀ **Fig. 1** LSD1 expression and its correlation with immune-related factors in breast cancer TCGA database. **a–d** The Pearson's correlation between immune regulatory factors and LSD1 across breast cancer subtypes: TNBC (**a**), ER-negative (**b**), ER-positive (**c**) or HER2-amplified (**d**) breast cancer. **e** LSD1 mRNA level in ER-positive vs. ER-negative breast cancer specimens and all tumors vs. adjacent normal tissues (downloaded from the TCGA database: <https://www.ncbi.nlm.nih.gov/pubmed/26209429>). **f** LSD1 mRNA level in PAM50 intrinsic breast cancer subtypes in the TCGA data

expression of CCL5, CXCL9, and CXCL10 (Fig. 2c; Supplementary Figure 3a), whereas overexpression of LSD1 via transfection of pReceiver-LSD1 plasmids attenuated expression of these genes in both cell lines (Fig. 2d; Supplementary Figure 3b). It is noted that either depletion or overexpression of LSD1 exerted negligible effects on expression of other types of chemokines such as CCL2, CCL3, or CCL4 whose activities are known to have pro-tumor roles [23], suggesting that targeting LSD1 may have a favorable impact on promoting antitumor immunity. Similarly, transfection of a second LSD1 siRNA also significantly induced mRNA expression of CCL5, CXCL9, and CXCL10 in both MDA-MB-231 and MDA-MB-468 cells (Supplementary Figures 3c, d). Moreover, stable LSD1 knockdown in 4T1 cells was established through infection with shRNA lentiviral particles. In two LSD1-KD clones showing best knockdown efficacy (Supplementary Figure 4a), stable loss of LSD1 consistently induced mRNA expression of CCL5, CXCL9, and CXCL10 (Supplementary Figure 4b).

Next, we investigated whether LSD1 inhibitor-induced expression of chemokines was accompanied by changes in H3K4me2 levels at specific gene promoters. Primers spanning the proximal promoter region for chemokines and PD-L1, from approximately  $-1200$  to  $+400$  bp relative to the transcriptional start site (TSS), were designed for quantitative tiling chromatin immunoprecipitation (ChIP) assays (Fig. 3a). Treatment with HCI-2509 led to increased enrichment of H3K4me2 at proximal elements or core regions of transcription start site (P4, P5, or P6) at promoters of chemokines and PD-L1. HCI-2509 also enhanced H3K4me2 occupancy at distant region upstream of the TSS site of CCL5 and PD-L1 promoters (Fig. 3b). These studies illustrate the effect of LSD1 inhibitor on the enrichment of the active histone mark, H3K4me2, in important promoter regions that are likely responsible for LSD1 inhibitor-induced re-expression of immune regulatory genes.

Next, we used a mouse chemokine array to determine whether upregulation of T cell chemokine expression by LSD1 inhibition would increase chemokine protein synthesis and secretion. Supernatants from 4T1 cells were collected and incubated with the detection antibody, and then added onto the blocked membrane that contains various chemokine capture antibodies (Supplementary Figure 4c).

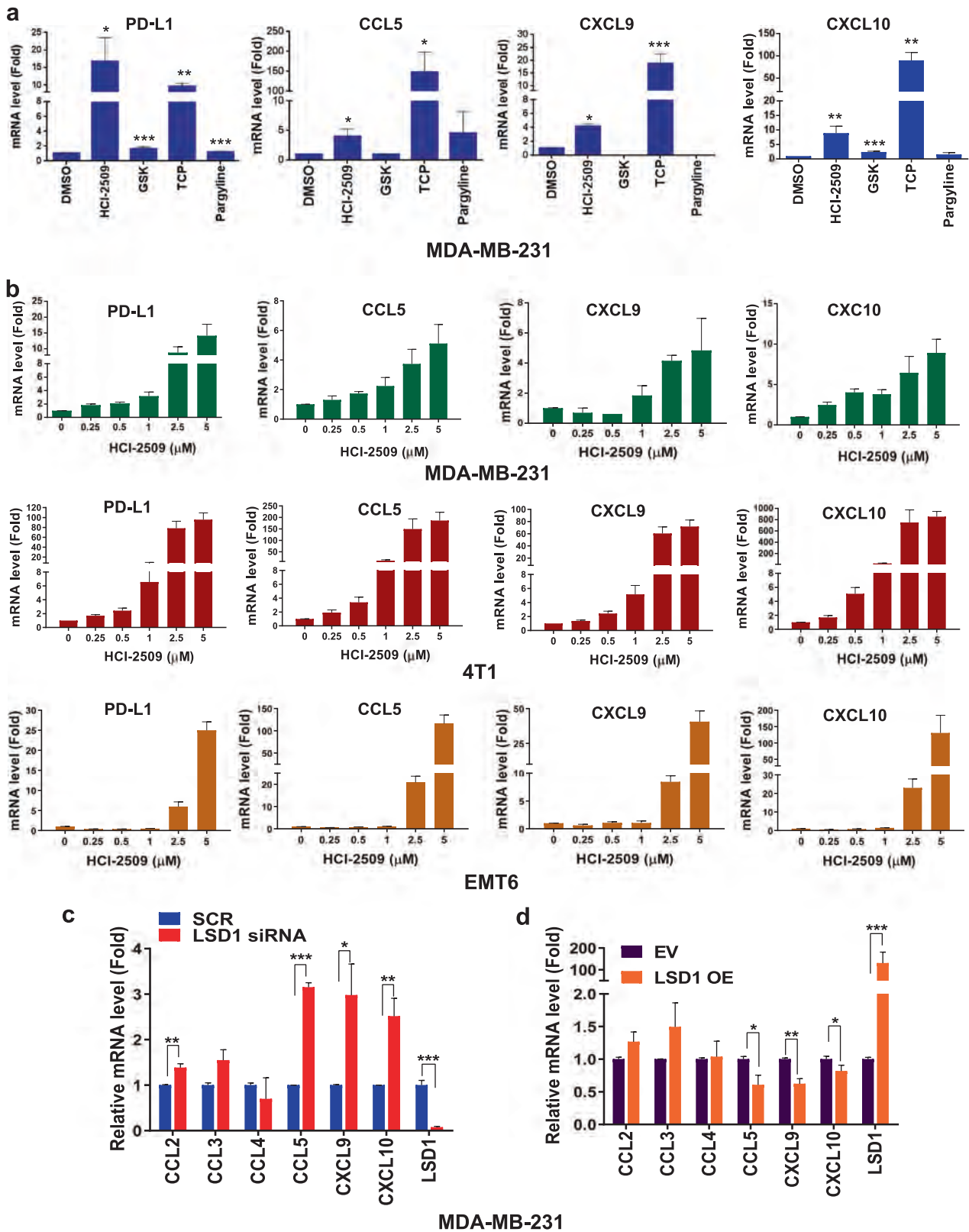
Immunoblotting results indicated that LSD1 RNA interference (RNAi) or treatment with HCI-2509 stimulated the protein secretion of CCL5 and CXCL10 in 4T1 culture medium. CXCL9 protein level was elevated by HCI-2509 but was basically not affected by LSD1 RNAi (Fig. 3c, d; Supplementary Figures 4d, e).

PD-L1 is a transmembrane glycoprotein that binds to its receptor, PD-1, on T cells, which leads to suppression of immune function [24]. PD-L1 expression has been speculated as a critical predictive parameter of sensitivity to therapeutic agents targeting the PD-L1/PD-1 immune checkpoints [25]. To test whether LSD1 inhibitor-induced PD-L1 expression results in increased cell surface expression, fluorescence-activated cell sorting (FACS) analysis was used to measure the PD-L1 level on the cell surface of several TNBC cell lines, with IgG as a negative control. We found that the basal membranous PD-L1 expression is very low in TNBC cells and treatment with HCI-2509 significantly up-regulated surface expression of PD-L1 (Fig. 3e, f; Supplementary Table 2).

### LSD1 inhibits CD8<sup>+</sup> T lymphocyte trafficking in TNBC microenvironment

To examine whether LSD1 inhibition-induced chemokine products could enhance CD8<sup>+</sup> T cell trafficking and tumor infiltration, we carried out an ex vivo chemotaxis assay. Briefly, naïve CD8<sup>+</sup> T cells were purified from mouse spleen and activated with Dynabeads containing mouse T-activator CD3/CD28 and recombinant mouse interleukin-2 (IL-2) (Fig. 4a). A pool of activated CD8<sup>+</sup> T cells was subsequently collected (Supplementary Figure 5a) and then placed onto top chambers of plates and allowed to migrate for 24 h towards cellular supernates of 4T1 cells that were treated with dimethyl sulfoxide (DMSO) or HCI-2509. The flow cytometry (FCM) result showed that HCI-2509 significantly increased the migration of CD8<sup>+</sup> T cells (Fig. 4b).

To characterize the role of CD8<sup>+</sup> T cell chemokines in LSD1 inhibition-induced T cell recruitment, a rescue study was carried out. 4T1 or EMT6 cellular supernatants were added with TAK-779, a potent antagonist for CCR5 and CXCR3, which are the receptors for CCL5 and CXCL9/10/11, respectively [26]. Chemotaxis assays showed that concurrent treatment with TAK-779 hindered HCI-2509-enhanced CD8<sup>+</sup> T cell migration in both cell lines (Fig. 4c). We validated this result by concurrent transfection of CCL5 or CXCL10 siRNA into EMT6 cells. Transfection with siRNAs effectively knocked down more than 70% of mRNA expression of CCL5 or CXCL10 (Supplementary Figure 5b). Chemotaxis assay demonstrated that simultaneous depletion of either CCL5 or CXCL10 effectively blocked HCI-2509-induced T cell migration (Fig. 4d).



Collectively, these results point to an important role of T cell chemokines in regulation of CD8+ T cell recruitment to tumor microenvironment.

To evaluate the potential effect of LSD1 inhibitor on normal activities of immune tissues, splenocytes were extracted from BALB/c mice and treated with various

◀ **Fig. 2** LSD1 inhibition induces expression of CD8<sup>+</sup> T cell-attracting chemokines and PD-L1. Real-time RT-PCR analysis was performed to analyze relative mRNA expression level of indicated genes.  $\beta$ -Actin was included as an internal control. **a** MDA-MB-231 cells were treated with LSD1 inhibitors (2.5  $\mu$ M HCI-2509, 100  $\mu$ M GSK-LSD1, 2.5 mM tranlycypromine or 2.5 mM pargyline) for 24 h. Relative mRNA expression of indicated immune regulatory factors is shown. **b** MDA-MB-231, 4T1, and EMT6 cells were exposed to increasing concentrations of HCI-2509 for 24 h. Relative mRNA expression of PD-L1, CCL5, CXCL9, and CXCL10 compared to vehicle control (set to fold change = 1) is shown. **c** MDA-MB-231 cells were transiently transfected with scramble or LSD1 siRNA for 48 h. Effect of LSD1 knockdown on mRNA expression of indicated chemokines was examined by real-time RT-PCR. **d** MDA-MB-231 cells were transiently transfected with control or pReceiver-FLAG-LSD1 plasmids for 48 h and analyzed by real-time RT-PCR for expression of indicated chemokines. Histograms represent the mean fold change in mRNA expression compared to control group (set to fold change = 1) for three independent determinations  $\pm$  s.d. Bars marked with asterisks indicate a statistical difference by Student's *t* test. \* $p$  < 0.05, \*\* $p$  < 0.01, and \*\*\* $p$  < 0.001. EV empty vector, OE overexpression

concentrations of HCI-2509 for 24 h. Quantitative PCR (qPCR) results indicated that HCI-2509 had no noticeable impact on the mRNA expression of examined immune factors (Supplementary Figure 5c). Next, we examined the potential influence of LSD1 inhibition on expression of key T cell exhaustion regulators, PD-1, tumor necrosis factor- $\alpha$  (TNF $\alpha$ ) and interferon- $\gamma$  (IFN $\gamma$ ), and chemokine receptors CCR5 and CXCR3 in activated CD8<sup>+</sup> cells. Naïve CD8<sup>+</sup> T cells were purified from mouse spleen and stimulated with Dynabeads with mouse T-activator CD3/CD28 and recombinant mouse IL-2. Activated CD8<sup>+</sup> cells were then treated with 2.5  $\mu$ M HCI-2509 for 24 h. Results of quantitative RT-PCR indicated that HCI-2509 significantly decreased mRNA expression of PD-1 and increased level of CCR5 in activated CD8<sup>+</sup> cells (Fig. 4e). Treatment with LSD1 inhibitor resulted in a small reduction of TNF $\alpha$  expression and the impact on IFN $\gamma$  failed to attain statistical significance (Fig. 4e). FACS results showed that decreased PD-1 mRNA expression by HCI-2509 led to reduced cell surface expression of PD-1 (Supplementary Figure 5d).

### LSD1 inhibition potentiates in vivo response of TNBC tumor xenografts to anti-PD-1 immunotherapy

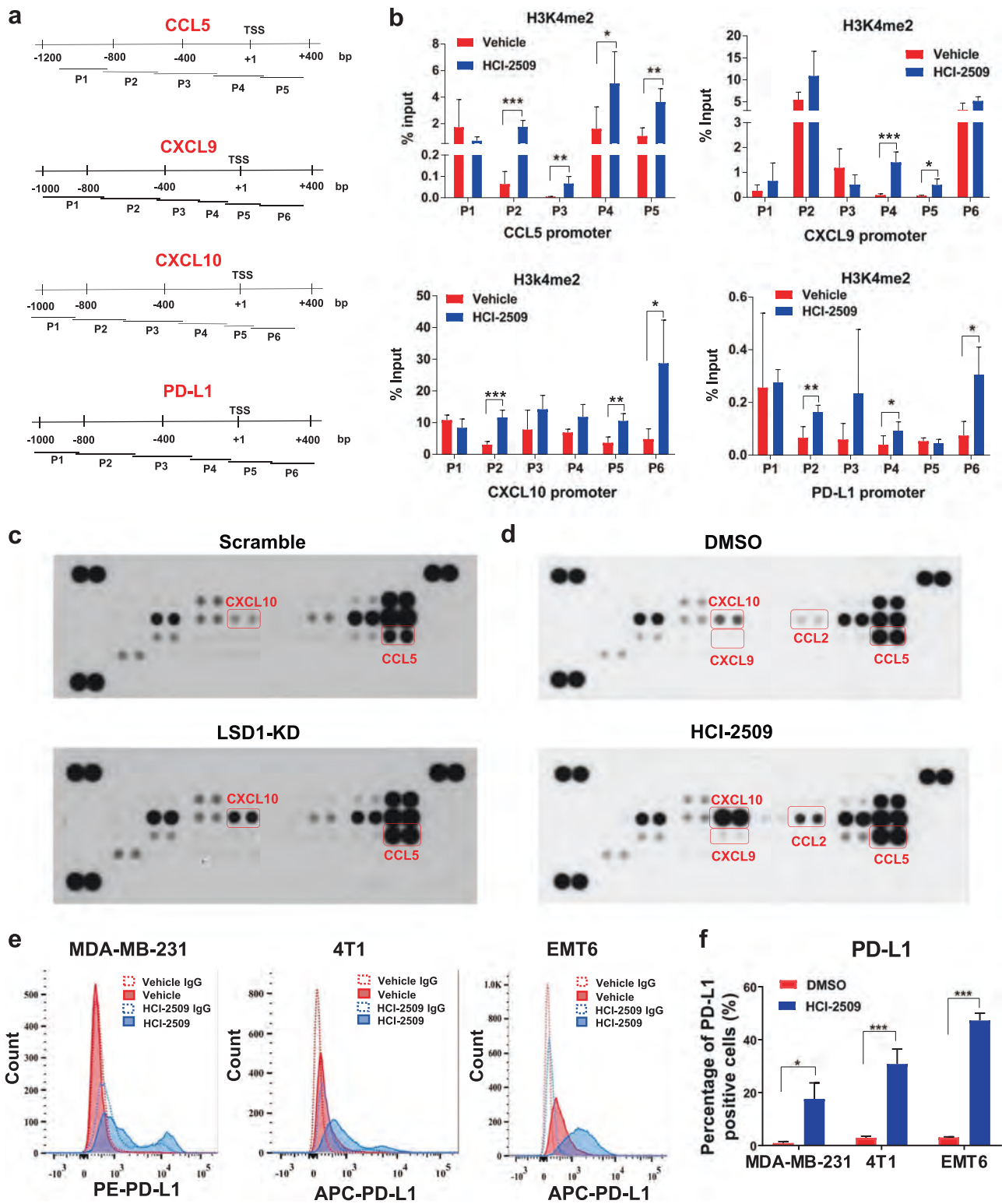
Next, we investigated the in vivo effect of LSD1 inhibitors on efficacy of anti-PD-1 therapy in BALB/c mice bearing orthotopic EMT6 tumors. Treatment with PD-1 antibody alone failed to elicit obvious therapeutic effects on EMT6 tumor growth. However, combination therapy with HCI-2509 and PD-1 monoclonal antibody (mAb) displayed superior inhibitory effect against tumor progression and resulted in 70% reduction in tumor burden as compared to vehicle control group (Fig. 5a, b). At the termination of the

experiment, the tumor weight in each mouse was measured. Average tumor weight in the combination group was significantly lower than that of control group (Fig. 5c). Statistical analysis of average tumor volumes between each group was shown in Supplementary Table 3. Immunohistochemical analysis showed that HCI-2509 decreased Ki-67 expression, and combination therapy led to a more significant reduction of Ki-67 expression in EMT6 tumors (Fig. 5d, e).

Mouse 4T1 cell line is highly metastatic and a widely used breast cancer metastasis model. The effect of combination therapy of LSD1 inhibitors and anti-PD-1 antibody on 4T1 tumor growth and metastasis was evaluated in BALB/c mice bearing 4T1 tumors in the mammary fat pads. Mice were treated with HCI-2509 every 2 days or TCP 5 days a week. Mice were injected intraperitoneally (i.p.) with anti-PD-1 antibodies once every 6 days. While PD-1 mAb by itself had no obvious impact on 4T1 tumor growth, combining either HCI-2509 or TCP with PD-1 mAb resulted in nearly 40% reduction in primary tumor volumes as compared with the control or single-agent treatment group (Supplementary Figures 6a, b). At the end of experiments, histological assessment was performed to visualize the microscopic tumor lesions in the lungs. 4T1 tumors spontaneously produced highly metastatic lesions in lung tissues. Treatment with HCI-2509 or PD-1 alone had no significant impact on 4T1 metastasis. However, combination therapy significantly reduced the areas of pulmonary metastatic lesions as compared with the control or single-agent treatment group (Fig. 5f, g). Similar results were observed in combination therapy of TCP and PD-1 mAb (Supplementary Figures 7a, b). These results indicate that combining LSD1 inhibitors with PD-1 antibody is more effective than either treatment alone in preventing 4T1 tumor metastasis. Overall toxicity of combination therapy against animals in all these studies was insignificant as demonstrated by no animal weight loss (Supplementary Figure 8).

### LSD1 inhibitor synergizes with PD-1 mAb to enhance in vivo breast tumor immunogenicity

LSD1 inhibitor in combination with PD-1 mAb significantly increased the mRNA expression of PD-L1, CCL5, CXCL9, CXCL10, and CCR5 (receptor of CCL-5) in EMT6 tumors (Fig. 6a). The immunohistochemistry (IHC) assay indicated that recruitment of CD8<sup>+</sup> T lymphocyte to EMT6 tumors was increased by HCI-2509 treatment, which was further induced in tumors receiving combination therapy (Fig. 6b, c). Many clinical studies suggest that lymphatic network facilitates systemic breast tumor metastasis via providing a portal for tumor cell spreading [27, 28]. Subtypes of T lymphocytes were sorted and quantified by



flow cytometry to determine the effect of combination therapy on status of T cell infiltration in peripheral lymph nodes adjacent to mammary glands with tumor implantation. The combination therapy significantly increased the population of CD3+CD8+ T cells in lymph nodes adjacent

to EMT6 tumors (Fig. 6d). The ratio of CD4+ to CD8+ T cells in lymph nodes was significantly reduced by combination therapy (Fig. 6e). An attenuated CD4+/CD8+ ratio of tumor-infiltrating lymphocytes clearly indicates an enhanced capacity of antitumor immunogenicity [29]. The

◀ **Fig. 3** Inhibition of LSD1 promotes protein production and secretion of chemokines and PD-L1. **a** Tiling ChIP primers were designed spanning from -1200 to +400 bp around the transcription start sites (TSS) of indicated genes. **b** MDA-MB-231 cells were treated with 2.5  $\mu$ M HCI-2509 for 24 h. Quantitative ChIP studies were conducted to characterize the enrichment of H3K4me2 at promoters of indicated genes. **c, d** Mouse chemokine antibody array was performed following the manufacturer's protocol to detect secreted chemokines from 4T1 cells that were **c** infected with scramble or LSD1 shRNA lentivirus, or **d** exposed to DMSO or 2.5  $\mu$ M HCI-2509 for 24 h. Red boxes designate the chemokines whose expression was altered by LSD1 RNAi or inhibitor. **e** Flow cytometry analysis was carried out to detect the percentage of PD-L1-positive MDA-MB-231, 4T1, or EMT6 cells after treatment with DMSO or 2.5  $\mu$ M HCI-2509 for 24 h. IgG was used as a negative control to normalize the expression levels of PD-L1 on the surface of the tumor cells. Shown are representative FACS images. **f** Histogram shows the quantified percentage of PD-L1-positive cells after treatment with vehicle or HCI-2509. All the experiments were performed three times. Student's *t* test was performed to assess significance. \* $p < 0.05$ , \*\* $p < 0.01$ , and \*\*\* $p < 0.001$

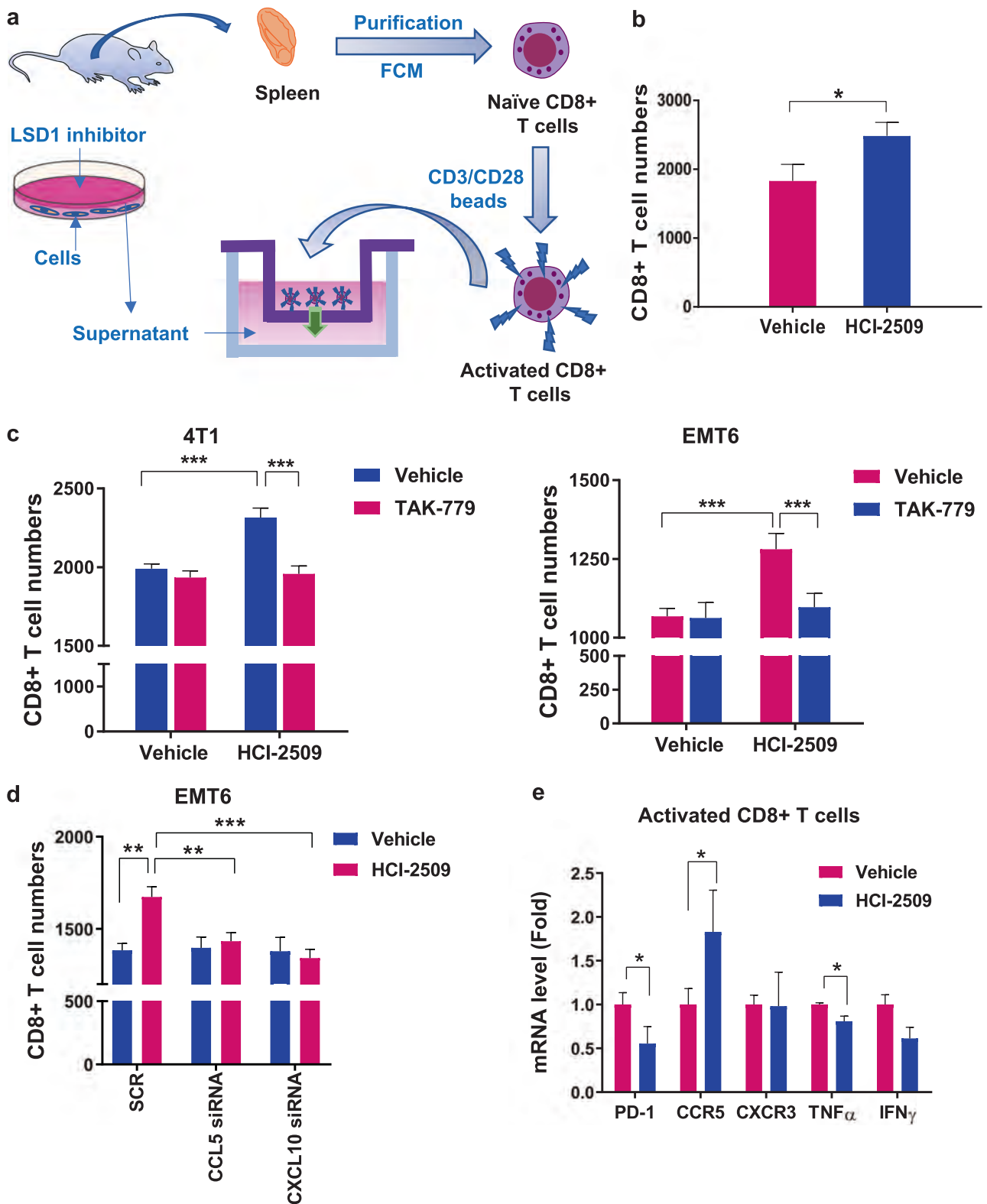
similar results were observed in lymph nodes adjacent to 4T1 xenograft tumors (Supplementary Figure 9). Taken together, our novel findings demonstrate that LSD1 inhibition triggers cytotoxic CD8<sup>+</sup> T cell infiltration that in turn enhances the *in vivo* antitumor efficacy of immune checkpoint blockade antibody. A model is proposed to summarize the role of LSD1 regulation on chemokine silencing, effector T cell trafficking, breast tumor immunity, and response to immunotherapy (Fig. 7).

## Discussion

Accumulating evidence indicates that abnormal epigenetic modifications play important roles in silencing expression of effector T cell chemokines in cancer [11, 12]. Analysis of a cohort of TCGA invasive breast cancer datasets revealed that LSD1 expression is negatively correlated with the expression of certain CD8<sup>+</sup> T cell-attracting chemokines and PD-L1. LSD1 is the first identified histone demethylase that has shown great potential as a target in cancer therapy in preclinical models [17, 18, 30–33]. In line with *in silico* results, we demonstrated that suppression of LSD1 expression by RNAi or small-molecule inhibitors induced expression and activity of antitumor chemokines, but exerted marginal effect on the expression of those chemokines with pro-tumor activity. The molecular details underlying LSD1 regulation on chemokine transcription are not completely understood. LSD1 has been typically found to be associated with multiple transcription repressors, such as HDAC1, HDAC2, and CoREST, to assemble a transcriptional repressor complex [32, 34, 35]. Recent studies showed that knockdown of LSD1 cofactors HDAC1 and HDAC2 failed to affect expression of chemokines and PD-L1 [12, 36]. We recently reported that HDAC5, which is a

key member of class II histone deacetylase, physically interacts and stabilizes LSD1 protein through up-regulating the expression of LSD1 deubiquitinase in breast cancer cells [37]. Similar to data from TCGA TNBC patients for LSD1 mRNA expression, HDAC5 mRNA expression is also negatively associated with CD8<sup>+</sup> T cell chemokines and PD-L1 in TNBC patients (Supplementary Table 1). Additional studies would be necessary to address the potential role of HDAC5 in LSD1-mediated repression of T cell chemokine expression. Moreover, the regulation of expression of chemokines by other H3K4me-targeting histone demethylases has been recently reported. For example, the H3K4me3 histone demethylase, Fbx110, has been found to be associated with promoter of chemokine, CCL7, and mediate its transcription activity [38]. Li et al. [39] has demonstrated that CCL14, an epithelial derived chemokine, is an important regulator of the JARID1B/LSD1/NuRD complex in regulation of angiogenesis and metastasis in breast cancer. These findings indicate that multiple histone modifications are involved in regulation of chemokine expression. Continuous studies are needed to clarify the mechanism of how coordinated interaction between LSD1 and other epigenetic modifiers governs chemokines expression.

ICIs have been hailed as a major breakthrough for treatment of malignant diseases, including a subset of breast cancers [40, 41]. However, clinical benefit of ICIs remains limited to a fraction of breast cancer patients. The intrinsic mechanisms of resistance to ICI therapy are multifaceted, dynamic, and interdependent, which may be due to the lack of effective antigen presentation, impaired formation of T cell memory, modified immune checkpoint pathways, changed cellular signaling pathways, and tumor micro-environment, etc. However, the precise mechanisms of innate and acquired resistance to ICI therapy in breast cancer patients are still unclear. Our studies have linked the resistance to anti-PD-1 immunotherapy to LSD1-mediated epigenetic silencing of effector T cell chemokines. This notion is supported by the following experimental evidence obtained from our studies: (1) siRNA depletion of specific T cell chemokines, CCL5 or CXCL10, is sufficient to reverse LSD1 inhibitor-induced CD8<sup>+</sup> T cell trafficking; (2) PD-1 mAb alone exerts no obvious effect on CD8<sup>+</sup> T lymphocyte infiltration and combination therapy leads to significantly increased presence of CD8<sup>+</sup> lymphocytes in tumors. Based on these novel findings, we tested a conceptually new strategy to target LSD1 and defective immune system combinatorially to correct the aberrant T cell landscape in low immunogenic TNBC, which is an important research area that has been understudied. Our *in vivo* results show that combination therapy significantly enhanced the response to PD-1 immunotherapy in TNBC. Importantly, in addition to enhancing chemokine expression



and infiltration of effector CD8<sup>+</sup> T cells in tumors, our combination approach also increased the ratio of CD8<sup>+</sup>/CD4<sup>+</sup> T cells in lymph tissues adjacent to mouse

mammary glands, which is considered as an important marker of immunological defense against tumor spreading.

Although PD-L1 is generally regarded as an immunosuppressive molecule, several clinical trials have shown the

◀ **Fig. 4** LSD1 inhibition induces effector T cell migration and tumor infiltration. **a** Schematic diagram of ex vivo chemotaxis assay of CD8+ T cell activation and migration. **b** Treatment with HCI-2509 induces CD8+ T cell migration. Bar graph shows mean total number of CD8+ T cells  $\pm$  s.d. **c** 4T1 cells were treated with DMSO or 2.5  $\mu$ M HCI-2509 for 1 h. Cellular supernatants were then added with vehicle or 5 nM TAK-779. Chemotaxis assay was subsequently performed to determine the effect of TAK-779 on HCI-2509-induced CD8+ T cell migration. **d** EMT6 cells were transiently transfected with CCL5 or CXCL10 siRNA followed by treatment with DMSO or 2.5  $\mu$ M HCI-2509 for 24 h. Chemotaxis assay was performed to assess the impact of chemokine siRNA on HCI-2509-induced CD8+ T cell migration and tumor infiltration. **e** Activated CD8+ cells were treated with 2.5  $\mu$ M HCI-2509 for 24 h. mRNA expression of indicated genes was examined by real-time RT-PCR. Histograms represent mean fold change  $\pm$  s.d. for three independent experiments. Student's *t* test was performed to assess significance. \**p* < 0.05, \*\**p* < 0.01, and \*\*\**p* < 0.001

positive association of PD-L1 expression with higher OR rates to anti-PD-1/PD-L1 therapy [40, 42]. Thus, PD-L1 has been considered as a predictive parameter of sensitivity to therapeutic agents targeting the PD-L1/PD-1 pathway in cancer patients [43, 44]. Elevated PD-L1 expression has been reported to correlate with increased infiltrating lymphocytes, which in turn leads to stronger cytotoxic immune response and improved survival in breast tumors [45, 46]. By using large-scale genomic data sets of solid tissue tumor biopsies, Rooney et al. reported that amplification of PD-L1 was positively associated with high local immune cytolytic activity [47]. Our recent bisulfite sequencing study depicted that CpG islands at PD-L1 promoter are mostly unmethylated in MDA-MB-231 cells and treatment with DNMT inhibitor exerted insignificant effect on PD-L1 expression (data not shown). We speculate that dysregulated histone functions such as LSD1-mediated H3K4 demethylation at key elements of PD-L1 promoter could be a critical epigenetic mechanism contributing to PD-L1 silencing.

It is still unclear about the mechanism of how LSD1 inhibition potentiates anti-PD-1 therapy in breast cancer. One major function of CD8+ T cell destruction of targeted cancer cells is via Fas/FasL interaction. Anti-PD-1/PD-L1 therapy renders tumor cells sensitive to CD8+ T cell and FasL-mediated lysis [48, 49]. Moreover, multiple lines of evidence showed that adaptive resistance to anti-PD-1 therapy is mediated by the phosphatidylinositol-3-kinase (PI3K)/Akt pathway in cancer [50, 51]. Our recent microarray has shown that inhibition of LSD1 increases the expression of Fas and down-regulates PI3K/Akt signaling [52]. Future work is needed to determine whether inhibition of LSD1 enhances therapeutic efficacy of immune checkpoint blockade through regulation of activities of Fas and PI3K/Akt signaling in TNBC.

In conclusion, we have demonstrated that inhibition of LSD1 reactivates key immune checkpoint regulator and cytotoxic T cell-attracting chemokines, which in turn

augments sensitivity of TNBC to immune checkpoint blocking antibodies (Fig. 7). Our studies identify a new strategy to target crosstalk between epigenetic modulators and immune compartments as a novel therapeutic strategy for breast cancer patients with poor immune response. The development of novel LSD1 inhibitors is progressing rapidly and several clinical trials of LSD1 inhibitors are ongoing in cancer patients. We strongly believe that our new combination strategy, using these potent LSD1 inhibitors with immune modulators, would carry high innovation and translational potential.

## Materials and methods

### Cells and reagents

MDA-MB-231, MDA-MB-468, and EMT6 cell lines were from ATCC. 4T1 cell line was provided by Dr. Adrian Lee (University of Pittsburgh). HCI-2509 was purchased from Xcessbio Biosciences Inc. (San Diego, CA, USA). GSK-LSD1 and TAK-779 were obtained from Sigma (St. Louis, MO, USA).

### LSD1 siRNA transfection and shRNA infection

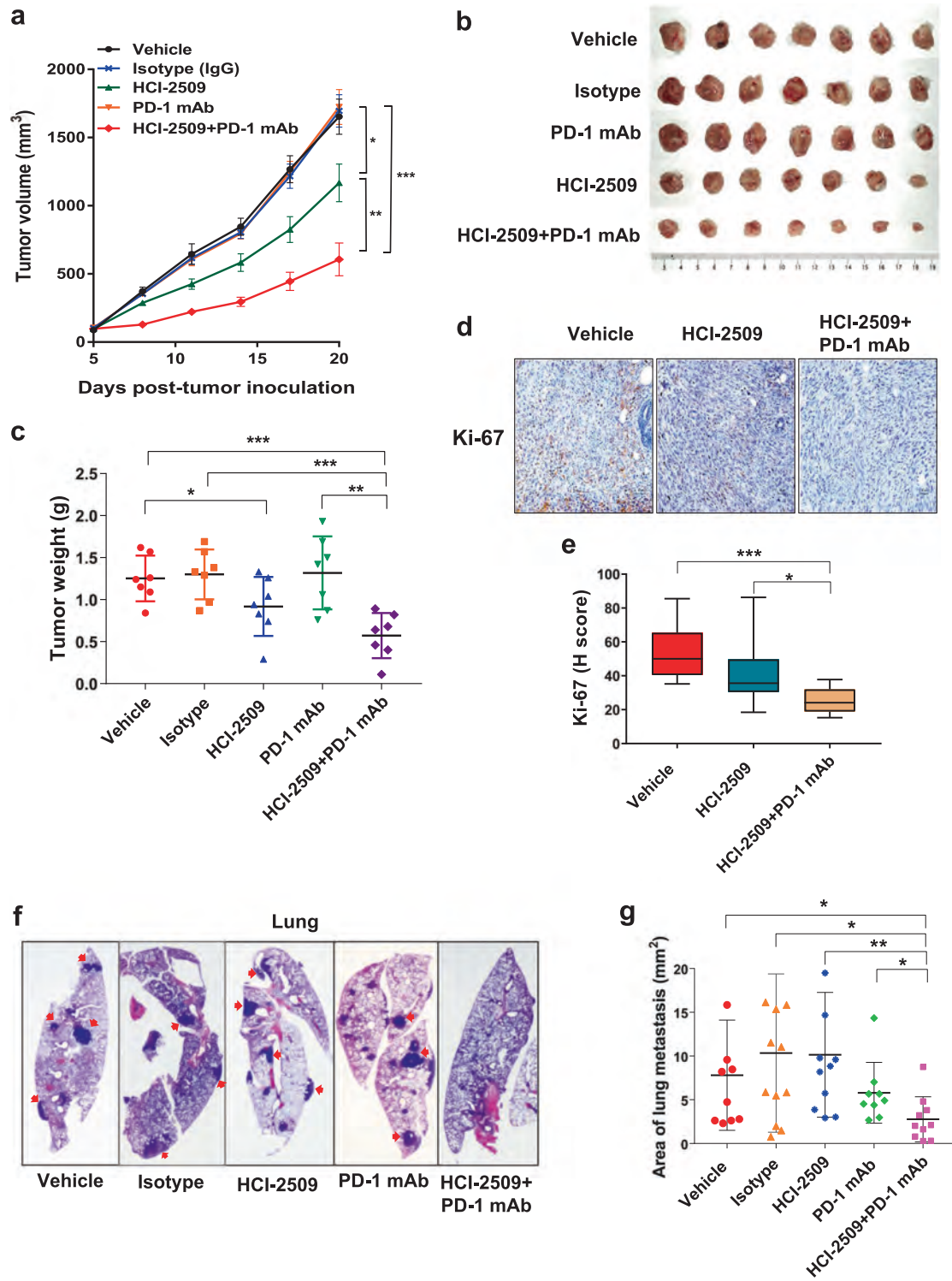
Pre-designed LSD1 siRNA #1 (Santa Cruz Biotechnology, Dallas, TX, USA) and siRNA #2 (Thermo Fisher Scientific, Waltham, MA, USA) were transfected into cells following the manufacturer's protocol. Scramble control and LSD1-specific shRNA lentiviral particles (Santa Cruz Biotechnology) were infected into 4T1 cells, according to the manufacturer's protocol. Cells were harvested 72 h post infection and seeded into dishes with 2  $\mu$ g/ml puromycin. Individual colonies were picked and analyzed for LSD1 expression.

### Quantitative PCR

Total RNA was extracted using RNeasy kit (Qiagen, Valencia, CA, USA) as described previously [53, 54]. Quantitative real-time PCR was performed on the StepOne Real-Time PCR System (Life Technologies). TaqMan<sup>®</sup> Gene Expression Assays were pre-designed and obtained from Life Technologies.

### Immunoblotting

Western blotting was performed as previously described [55, 56]. Antibodies used in this study are shown in Supplementary Table 4. Nitrocellulose membranes were scanned using the Odyssey Infrared Imaging System (Li-Cor Biosciences, Lincoln, NE, USA).



### Proteome antibody arrays

Mouse chemokine array kit ARY020 (R&D Systems, Minneapolis, MN, USA) was used to detect 25 mouse chemokines. Briefly, cell culture supernatant was collected and incubated with the detection antibody cocktail. The

sample/antibody mixture was then added onto the blocked membrane, containing 25 different capture antibodies. After washing, membrane was incubated with diluted streptavidin-horse radish peroxidase and Chemi Reagent Mix was added, and the membrane was then exposed to X-ray film.



**Fig. 5** LSD1 inhibitor potentiates antitumor efficacy of PD-1 antibody in mice bearing TNBC tumors. **a** Mouse EMT6 cells were engrafted into the mammary fat pad of BALB/c mice. When established tumors were palpable, mice were treated with vehicle (DMSO,  $n = 7$ ), isotype (IgG,  $n = 7$ ), HCI-2509 (50 mg/kg, 7 days per week,  $n = 7$ ), PD-1 mAb (10 mg/kg, once every 3 days,  $n = 7$ ), or combination ( $n = 7$ ) via i.p. injection. Tumors were measured with calipers, and values were plotted. The vertical bars indicate mean tumor size ( $\text{mm}^3$ )  $\pm$  s.e. **b** EMT6 tumors in each group were harvested and photographed at the end of the experiment. Shown are photographs of the xenograft tumors. **c** Tumor weights were measured for each treatment group at autopsy. Values are mean  $\pm$  s.d. **d** Representative immunohistochemistry staining of Ki-67 in EMT6 xenograft tumors treated with vehicle, HCI-2509, or HCI-2509 + PD-1 mAb. **e** H-scores represent average staining intensity of Ki-67 in EMT6 xenograft tumors, which were treated with vehicle, HCI-2509, or HCI-2509 + PD-1 mAb ( $n = 9$ ). **f** 4T1 cells were implanted into the mammary gland of BALB/c mice. Vehicle (DMSO,  $n = 10$ ), isotype (IgG,  $n = 12$ ), HCI-2509 (30 mg/kg, every 2 days,  $n = 11$ ), PD-1 mAb (10 mg/kg, once every 6 days,  $n = 11$ ), and combination (HCI-2509 30 mg/kg + PD-1 mAb 10 mg/kg,  $n = 10$ ) were delivered via i.p. injection. Lung specimens were stained with hematoxylin and eosin. Arrows indicate large metastatic lesions. **g** Areas of 4T1 metastasis in each histological section were calculated by microscope and the CellSens Dimension software. Vehicle,  $n = 10$ ; isotype,  $n = 12$ ; HCI-2509,  $n = 11$ ; PD-1 mAb,  $n = 11$ ; combination,  $n = 10$ . \* $p < 0.05$ , \*\* $p < 0.01$ , and \*\*\* $p < 0.001$ , Student's  $t$  test was used to analyze the significance of the results

## Flow cytometry analysis

One million cells were collected and stained with a variety of antibodies (Supplementary Table 4) or isotype control antibody. Stained cells and fixed cells were suspended in FACS buffer and analyzed on the LSR-II flow cytometer (BD Biosciences, San Jose, CA). Data were processed with FACSDIVA™ software (BD Biosciences).

## Chromatin immunoprecipitation

ChIP was performed using methods as reported previously [37]. Cells treated with vehicle or LSD1 inhibitor were exposed to 1% formaldehyde to cross-link proteins, and two million cells were used for each ChIP assay and performed as previously described [31, 56]. Quantitative ChIP confirmed changes in H3K4me2 at the promoters of examined genes using qPCR with primer sets indicated in Supplementary Table 5.

## Activation of effector CD8<sup>+</sup> T cells

Naïve CD8<sup>+</sup> T cells were purified from mouse spleen using EasySep mouse CD8<sup>+</sup> T cell isolation kit (StemCell Technologies, Cambridge, MA, USA). Isolated naïve CD8<sup>+</sup> T cells were stimulated with Dynabeads, mouse T-activator CD3/CD28 (Thermo Fisher Scientific) and recombinant mouse IL-2 (R&D Systems) for 10 days. After activation,

effector CD8<sup>+</sup> T cells were harvested using magnetic plate and counted for further analysis.

## Chemotaxis assay

After treatment, cell culture medium was replaced with drug-free medium for 24 h. Cell-free supernatant was then transferred to 24-well plates with membranes of 5  $\mu\text{m}$  pore size (Corning, Corning, NY, USA). Effector CD8<sup>+</sup> T cells ( $2 \times 10^5$ ) were loaded onto the top chambers and allowed to migrate for 24 h towards cell supernatants. The migrated cells were harvested and re-suspended in 4% paraformaldehyde solution to fix. The number of CD8<sup>+</sup> T cells was quantified by fixed 30 s runs on LSR-II flow cytometer.

## Immunohistochemistry

Tumors were fixed in Bouin's solution (Sigma) and processed for paraffin embedding. Antigen retrieval was performed using citrate buffer and stained with primary antibodies overnight at 4 °C. Secondary antibody (1:200, eBioscience) was used followed by 3,3'-diaminobenzidine (Thermo Fisher Scientific) and then counterstained with hematoxylin (Sigma). The percentage of CD8<sup>+</sup> cells was analyzed using the Image-pro Plus software (Media Cybernetics, Rockville, MD, USA) and the staining of Ki-67 was quantitated by ImageJ as previously described [37] through blinded evaluation.

## Animal studies

All animal studies were conducted in accordance with protocol approved by IACUC of the University of Pittsburgh. In EMT6 xenografts,  $0.5 \times 10^6$  cells were injected into mammary fat pad of 6–8-week-old female BALB/c mice (The Jackson Laboratory, Bar Harbor, ME, USA). When tumor volume reached 50–100  $\text{mm}^3$ , mice were randomized into experimental groups. HCI-2509 was injected i.p. (50 mg/kg) every day and anti-PD-1 antibodies (10 mg/kg, i.p.) were injected every 3 days. Vehicle and isotype control antibodies were injected in the control mice. Tumor volumes were assessed every 4 days. In 4T1 xenograft model, HCI-2509 was injected (30 mg/kg, i.p.) every 2 days. TCP was injected (10 mg/kg, i.p.) 5 days a week. Anti-PD-1 antibodies were injected (10 mg/kg, i.p.) every 6 days. At the end of the study, animal lung tissues were processed into paraffin sections, and then subjected to hematoxylin–eosin staining at the histology and microimaging core facility at MWRI. The blinded evaluation of metastasis was conducted by a pathologist (Y.F.) and the areas were calculated by SZX-16 microscope and CellSens Dimension software (Olympus, Shinjuku, Tokyo, Japan).

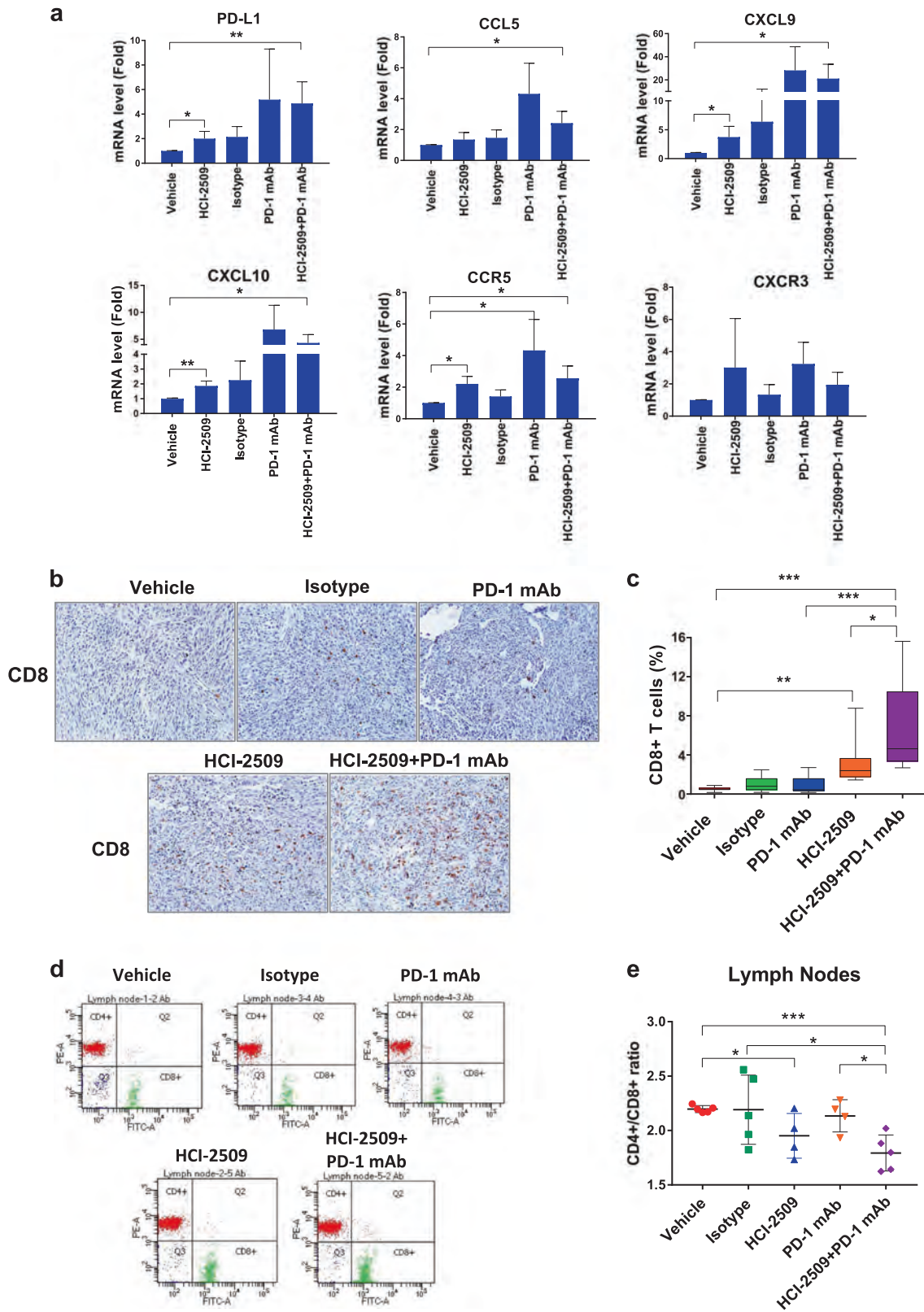
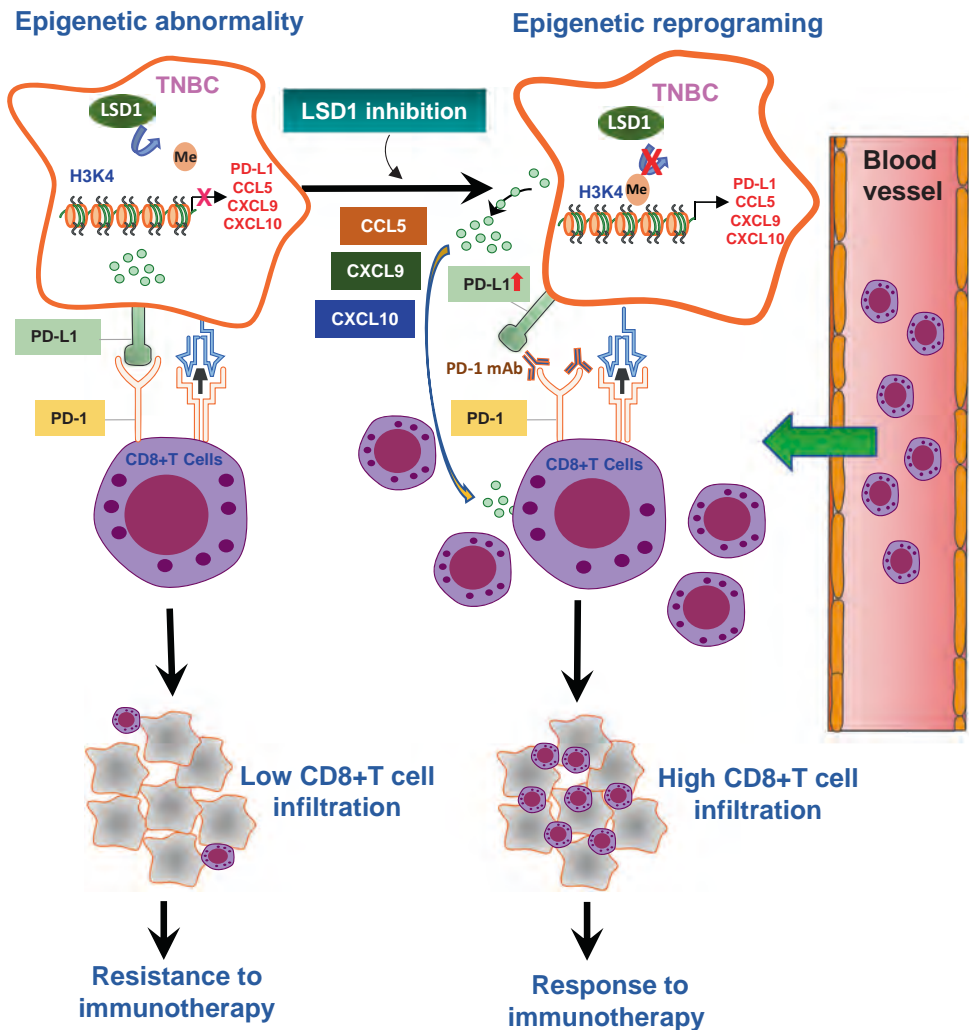


**Fig. 6** LSD1 inhibitor promotes tumor immunogenicity in vivo. **a** Real-time RT-PCR was performed to detect mRNA expression of indicated immune factors in EMT6 xenograft tumors. **b** Histological analysis of immune infiltration of CD8+ T cells after therapy. Shown are representative immunohistochemistry staining of CD8+ T lymphocytes in EMT6 tumors treated with vehicle, isotype, PD-1 mAb, HCl-2509, or combination. **c** The percentages of CD8+ T lymphocytes in EMT6 tumors were measured and analyzed by software Image-pro Plus. **d** The lymph node tissue adjacent to the fourth (inguinal) mammary glands were collected, and subtypes of T lymphocytes were quantified by flow cytometry assay. **e** The ratios of CD4+ to CD8+ T cells in lymph nodes of each group were quantified by FCM. Student's *t* test was performed to assess significance. \**p* < 0.05, \*\**p* < 0.01, and \*\*\**p* < 0.001

statistical programming language. The data files were combined and then background corrected, log<sub>2</sub> transformed, normalized, and summarized using Robust Multi-chip Average algorithm to generate the expression data. For those genes containing multiple corresponding probe sets in a microarray, the expression measure of the probe set with the maximum interquartile expression range value was used.

**Fig. 7** A proposed model of the role of LSD1 in regulation of breast tumor immunogenicity, response to immunotherapy, and potential clinical outcome. Our work demonstrated that inhibition of histone lysine-specific demethylase 1 (LSD1) increases the expression of key immune checkpoint regulators and effector T cell-attracting chemokines, which in turn increases CD8+ T cell tumor infiltration and improves the efficacy of immunotherapy. These findings provide supportive evidence to suggest that modulation of breast tumor immunogenicity by drugs that target epigenetic abnormalities may represent a promising area for translational research and clinical intervention for breast cancer therapy



## Statistical analysis

Two-tailed Student's *t* test was used to determine the quantitative variables. Gene expression profiles in 222 TNBC patient specimens were analyzed using Affymetrix Human Genome U133A Plus 2.0 microarray data files from 21 breast cancer data sets [19]. Data files were then processed using the affy and bioconductor packages in the R

**Acknowledgements** This work is supported by US Army Breast Cancer Research Program (W81XWH-14-1-0237 to YH; W81XWH-14-1-0238 to NED/SO), Breast Cancer Research Foundation (to NED and SO), NIH/NCI P30CA047904 and Natural Science Foundation of China (81502366 to YQ).

## Compliance with ethical standards

**Conflict of interest** The authors declare that they have no conflict of interest.

## References

- Adams S, Gray RJ, Demaria S, Goldstein L, Perez EA, Shulman LN, et al. Prognostic value of tumor-infiltrating lymphocytes in triple-negative breast cancers from two phase III randomized adjuvant breast cancer trials: ECOG 2197 and ECOG 1199. *J Clin Oncol.* 2014;32:2959–66.
- Loi S, Michiels S, Salgado R, Sirtaine N, Jose V, Fumagalli D, et al. Tumor infiltrating lymphocytes are prognostic in triple negative breast cancer and predictive for trastuzumab benefit in early breast cancer: results from the FinHER trial. *Ann Oncol.* 2014;25:1544–50.
- Ali HR, Provenzano E, Dawson SJ, Blows FM, Liu B, Shah M, et al. Association between CD8+ T-cell infiltration and breast cancer survival in 12,439 patients. *Ann Oncol.* 2014;25:1536–43.
- Nanda R, Chow LQ, Dees EC, Berger R, Gupta S, Geva R, et al. Pembrolizumab in patients with advanced triple-negative breast cancer: Phase Ib KEYNOTE-012 Study. *J Clin Oncol.* 2016;34:2460–7.
- Rugo H, Delord J-P, Im S-A, Ott P, Piha-Paul S, Bedard P, et al. Abstract S5-07: Preliminary efficacy and safety of pembrolizumab (MK-3475) in patients with PD-L1-positive, estrogen receptor-positive (ER+)/HER2-negative advanced breast cancer enrolled in KEYNOTE-028. *Cancer Res.* 2016;76 Suppl:S5-07-S5-07.
- Bhatti S, Heldstab J, Lehn C, Tawfik O, Ash RM, Hout DR, et al. Clinical activity of pembrolizumab in a patient with metastatic triple-negative breast cancer without tumor programmed death-ligand 1 expression: a case report and correlative biomarker analysis. *JCO Precis Oncol.* 2017;1:1–6.
- Dirix L, Takacs I, Nikolinakos P, Jerusalem G, Arkenau H-T, Hamilton E, et al. Abstract S1-04: Avelumab (MSB0010718C), an anti-PD-L1 antibody, in patients with locally advanced or metastatic breast cancer: a Phase Ib JAVELIN Solid Tumor Trial. *Cancer Res.* 2016;76 Suppl:S1-04-S1-04.
- Balkwill F. Cancer and the chemokine network. *Nat Rev Cancer.* 2004;4:540–50.
- Griffith JW, Sokol CL, Luster AD. Chemokines and chemokine receptors: positioning cells for host defense and immunity. *Annu Rev Immunol.* 2014;32:659–702.
- Muthuswamy R, Berk E, Junecko BF, Zeh HJ, Zureikat AH, Normolle D, et al. NF-kappaB hyperactivation in tumor tissues allows tumor-selective reprogramming of the chemokine microenvironment to enhance the recruitment of cytolytic T effector cells. *Cancer Res.* 2012;72:3735–43.
- Peng D, Kryczek I, Nagarsheth N, Zhao L, Wei S, Wang W, et al. Epigenetic silencing of TH1-type chemokines shapes tumour immunity and immunotherapy. *Nature.* 2015;527:249–53.
- Zheng H, Zhao W, Yan C, Watson CC, Massengill M, Xie M, et al. HDAC inhibitors enhance T-cell chemokine expression and augment response to PD-1 immunotherapy in lung adenocarcinoma. *Clin Cancer Res.* 2016;22:4119–32.
- Hopewell EL, Zhao W, Fulp WJ, Bronk CC, Lopez AS, Massengill M, et al. Lung tumor NF-kappaB signaling promotes T cell-mediated immune surveillance. *J Clin Invest.* 2013;123:2509–22.
- Nagarsheth N, Wicha MS, Zou W. Chemokines in the cancer microenvironment and their relevance in cancer immunotherapy. *Nat Rev Immunol.* 2017;17:559–72.
- Sandhu R, Roll JD, Rivenbark AG, Coleman WB. Dysregulation of the epigenome in human breast cancer: contributions of gene-specific DNA hypermethylation to breast cancer pathobiology and targeting the breast cancer methylome for improved therapy. *Am J Pathol.* 2015;185:282–92.
- Pasculli B, Barbano R, Parrella P. Epigenetics of breast cancer: biology and clinical implication in the era of precision medicine. *Semin Cancer Biol.* 2018;51:22–35.
- Katz TA, Huang Y, Davidson NE, Jankowitz RC. Epigenetic reprogramming in breast cancer: from new targets to new therapies. *Ann Med.* 2014;46:397–408.
- Huang Y, Nayak S, Jankowitz R, Davidson NE, Oesterreich S. Epigenetics in breast cancer: what's new? *Breast Cancer Res.* 2011;13:225.
- Lehmann BD, Bauer JA, Chen X, Sanders ME, Chakravarthy AB, Shyr Y, et al. Identification of human triple-negative breast cancer subtypes and preclinical models for selection of targeted therapies. *J Clin Invest.* 2011;121:2750–67.
- Garcia-Bassets I, Kwon YS, Telese F, Prefontaine GG, Hutt KR, Cheng CS, et al. Histone methylation-dependent mechanisms impose ligand dependency for gene activation by nuclear receptors. *Cell.* 2007;128:505–18.
- Lim S, Janzer A, Becker A, Zimmer A, Schule R, Buettner R, et al. Lysine-specific demethylase 1 (LSD1) is highly expressed in ER-negative breast cancers and a biomarker predicting aggressive biology. *Carcinogenesis.* 2010;31:512–20.
- Metzger E, Wissmann M, Yin N, Muller J, Schneider R, Peters A, et al. LSD1 demethylates repressive histone marks to promote androgen-receptor-dependent transcription. *Nature.* 2005;437:436–9.
- Nagarsheth N, Wicha MS, Zou W. Chemokines in the cancer microenvironment and their relevance in cancer immunotherapy. *Nat Rev Immunol.* 2017;17:559–72.
- Dong H, Zhu G, Tamada K, Chen L. B7-H1, a third member of the B7 family, co-stimulates T-cell proliferation and interleukin-10 secretion. *Nat Med.* 1999;5:1365–9.
- Solinas C, Gombos A, Latifyan S, Piccart-Gebhart M, Kok M, Buisseret L. Targeting immune checkpoints in breast cancer: an update of early results. *ESMO Open.* 2017;2:e000255.
- Akahori T, Sho M, Kashizuka H, Nomi T, Kanehiro H, Nakajima Y. A novel CCR5/CXCR3 antagonist protects intestinal ischemia/reperfusion injury. *Transplant Proc.* 2006;38:3366–8.
- Ran S, Volk L, Hall K, Flister MJ. Lymphangiogenesis and lymphatic metastasis in breast cancer. *Pathophysiology.* 2010;17:229–51.
- Cunnick GH, Jiang WG, Gomez KF, Mansel RE. Lymphangiogenesis and breast cancer metastasis. *Histol Histopathol.* 2002;17:863–70.
- Wang K, Shen T, Siegal GP, Wei S. The CD4/CD8 ratio of tumor-infiltrating lymphocytes at the tumor–host interface has prognostic value in triple-negative breast cancer. *Hum Pathol.* 2017;69:110–7.
- Huang Y, Marton LJ, Woster PM, Casero RA. Polyamine analogues targeting epigenetic gene regulation. *Essays Biochem.* 2009;46:95–110.
- Huang Y, Greene E, Murray Stewart T, Goodwin AC, Baylin SB, Woster PM, et al. Inhibition of lysine-specific demethylase 1 by polyamine analogues results in reexpression of aberrantly silenced genes. *Proc Natl Acad Sci USA.* 2007;104:8023–8.
- Shi Y, Lan F, Matson C, Mulligan P, Whetstone JR, Cole PA, et al. Histone demethylation mediated by the nuclear amine oxidase homolog LSD1. *Cell.* 2004;119:941–53.
- Huang Y, Marton LJ, Woster PM. The design and development of polyamine-based analogues with epigenetic targets. *Royal Society of Chemistry Drug Discovery Series No. 17.* Thomas Graham House: Cambridge; 2012;238–56.
- Culhane JC, Cole PA. LSD1 and the chemistry of histone demethylation. *Curr Opin Chem Biol.* 2007;11:561–8.
- Fomeris F, Binda C, Battaglioli E, Mattevi A. LSD1: oxidative chemistry for multifaceted functions in chromatin regulation. *Trends Biochem Sci.* 2008;33:181–9.

36. Terranova-Barberio M, Thomas S, Ali N, Pawlowska N, Park J, Krings G, et al. HDAC inhibition potentiates immunotherapy in triple negative breast cancer. *Oncotarget*. 2017;8:114156–72.
37. Cao C, Vasilatos SN, Bhargava R, Fine JL, Oesterreich S, Davidson NE, et al. Functional interaction of histone deacetylase 5 (HDAC5) and lysine-specific demethylase 1 (LSD1) promotes breast cancer progression. *Oncogene*. 2017;36:133–45.
38. Janzer A, Stamm K, Becker A, Zimmer A, Buettner R, Kirfel J. The H3K4me3 histone demethylase Fbxl10 is a regulator of chemokine expression, cellular morphology, and the metabolome of fibroblasts. *J Biol Chem*. 2012;287:30984–92.
39. Li Q, Shi L, Gui B, Yu W, Wang J, Zhang D, et al. Binding of the JmjC demethylase JARID1B to LSD1/NuRD suppresses angiogenesis and metastasis in breast cancer cells by repressing chemokine CCL14. *Cancer Res*. 2011;71:6899–908.
40. Topalian SL, Hodi FS, Brahmer JR, Gettinger SN, Smith DC, McDermott DF, et al. Safety, activity, and immune correlates of anti-PD-1 antibody in cancer. *N Engl J Med*. 2012;366:2443–54.
41. Nishino M, Ramaiya NH, Hatabu H, Hodi FS. Monitoring immune-checkpoint blockade: response evaluation and biomarker development. *Nat Rev Clin Oncol*. 2017;14:655–668.
42. Garon EB, Rizvi NA, Hui R, Leigh N, Balmanoukian AS, Eder JP, et al. Pembrolizumab for the treatment of non-small-cell lung cancer. *N Engl J Med*. 2015;372:2018–28.
43. Herbst RS, Soria JC, Kowanetz M, Fine GD, Hamid O, Gordon MS, et al. Predictive correlates of response to the anti-PD-L1 antibody MPDL3280A in cancer patients. *Nature*. 2014;515:563–7.
44. Powles T, Eder JP, Fine GD, Braiteh FS, Loriot Y, Cruz C, et al. MPDL3280A (anti-PD-L1) treatment leads to clinical activity in metastatic bladder cancer. *Nature*. 2014;515:558–62.
45. Ali HR, Glont SE, Blows FM, Provenzano E, Dawson SJ, Liu B, et al. PD-L1 protein expression in breast cancer is rare, enriched in basal-like tumours and associated with infiltrating lymphocytes. *Ann Oncol*. 2015;26:1488–93.
46. Wimberly H, Brown JR, Schalper K, Haack H, Silver MR, Nixon C, et al. PD-L1 expression correlates with tumor-infiltrating lymphocytes and response to neoadjuvant chemotherapy in breast cancer. *Cancer Immunol Res*. 2015;3:326–32.
47. Rooney MS, Shukla SA, Wu CJ, Getz G, Hacohen N. Molecular and genetic properties of tumors associated with local immune cytolytic activity. *Cell*. 2015;160:48–61.
48. Ostrand-Rosenberg S, Horn LA, Haile ST. The programmed death-1 immune-suppressive pathway: barrier to antitumor immunity. *J Immunol*. 2014;193:3835–41.
49. Kim JM, Chen DS. Immune escape to PD-L1/PD-1 blockade: seven steps to success (or failure). *Ann Oncol*. 2016;27:1492–504.
50. Shayan G, Srivastava R, Li J, Schmitt N, Kane LP, Ferris RL. Adaptive resistance to anti-PD1 therapy by Tim-3 upregulation is mediated by the PI3K-Akt pathway in head and neck cancer. *Oncoimmunology*. 2017;6:e1261779.
51. Deken MA, Gadiot J, Jordanova ES, Lacroix R, van Gool M, Kroon P, et al. Targeting the MAPK and PI3K pathways in combination with PD1 blockade in melanoma. *Oncoimmunology*. 2016;5:e1238557.
52. Cao C, Wu H, Vasilatos SN, Chandran U, Qin Y, Wan Y, et al. HDAC5-LSD1 axis regulates antineoplastic effect of natural HDAC inhibitor sulforaphane in human breast cancer cells. *Int J Cancer*. 2018;143:1388–1401.
53. Huang Y, Vasilatos SN, Boric L, Shaw PG, Davidson NE. Inhibitors of histone demethylation and histone deacetylation cooperate in regulating gene expression and inhibiting growth in human breast cancer cells. *Breast Cancer Res Treat*. 2012;131:777–89.
54. Vasilatos SN, Katz TA, Oesterreich S, Wan Y, Davidson NE, Huang Y. Crosstalk between lysine-specific demethylase 1 (LSD1) and histone deacetylases mediates antineoplastic efficacy of HDAC inhibitors in human breast cancer cells. *Carcinogenesis*. 2013;34:1196–207.
55. Huang Y, Keen JC, Pledgie A, Marton LJ, Zhu T, Sukumar S, et al. Polyamine analogues down-regulate estrogen receptor alpha expression in human breast cancer cells. *J Biol Chem*. 2006;281:19055–63.
56. Huang Y, Stewart TM, Wu Y, Baylin SB, Marton LJ, Perkins B, et al. Novel oligoamine analogues inhibit lysine-specific demethylase 1 and induce reexpression of epigenetically silenced genes. *Clin Cancer Res*. 2009;15:7217–28.



# Nitro-fatty acid inhibition of triple-negative breast cancer cell viability, migration, invasion, and tumor growth

Received for publication, August 30, 2017, and in revised form, November 5, 2017. Published, Papers in Press, November 20, 2017, DOI 10.1074/jbc.M117.814368

Chen-Shan Chen Woodcock<sup>‡1</sup>, Yi Huang<sup>‡§1</sup>, Steven R. Woodcock<sup>‡</sup>, Sonia R. Salvatore<sup>‡</sup>, Bhupinder Singh<sup>‡</sup>, Franca Golin-Bisello<sup>‡</sup>, Nancy E. Davidson<sup>¶</sup>, Carola A. Neumann<sup>‡§</sup>, Bruce A. Freeman<sup>‡2</sup>, and Stacy G. Wendell<sup>‡3</sup>

From the <sup>‡</sup>Department of Pharmacology and Chemical Biology, University of Pittsburgh, Pittsburgh, Pennsylvania 15260, the

<sup>§</sup>Women's Cancer Research Center of the UPMC Hillman Cancer Center, Pittsburgh, Pennsylvania 15232, and the <sup>¶</sup>Fred Hutchinson Cancer Research Center and Department of Medicine, University of Washington, Seattle, Washington 98109

Edited by Alex Tokor

Triple-negative breast cancer (TNBC) comprises ~20% of all breast cancers and is the most aggressive mammary cancer subtype. Devoid of the estrogen and progesterone receptors, along with the receptor tyrosine kinase ERB2 (HER2), that define most mammary cancers, there are no targeted therapies for patients with TNBC. This, combined with a high metastatic rate and a lower 5-year survival rate than for other breast cancer phenotypes, means there is significant unmet need for new therapeutic strategies. Herein, the anti-neoplastic effects of the electrophilic fatty acid nitroalkene derivative, 10-nitro-octadec-9-enoic acid (nitro-oleic acid, NO<sub>2</sub>-OA), were investigated in multiple pre-clinical models of TNBC. NO<sub>2</sub>-OA reduced TNBC cell growth and viability *in vitro*, attenuated TNF $\alpha$ -induced TNBC cell migration and invasion, and inhibited the tumor growth of MDA-MB-231 TNBC cell xenografts in the mammary fat pads of female nude mice. The up-regulation of these aggressive tumor cell growth, migration, and invasion phenotypes is mediated in part by the constitutive activation of pro-inflammatory nuclear factor  $\kappa$ B (NF- $\kappa$ B) signaling in TNBC. NO<sub>2</sub>-OA inhibited TNF $\alpha$ -induced NF- $\kappa$ B transcriptional activity in human TNBC cells and suppressed downstream NF- $\kappa$ B target gene expression, including the metastasis-related proteins intercellular adhesion molecule-1 and urokinase-type plasminogen activator. The mechanisms accounting for NF- $\kappa$ B signaling inhibition by NO<sub>2</sub>-OA in TNBC cells were multifaceted, as NO<sub>2</sub>-OA (a) inhibited the inhibitor of NF- $\kappa$ B subunit kinase  $\beta$  phosphorylation and downstream inhibitor of NF- $\kappa$ B degradation, (b) alkylated the NF- $\kappa$ B RelA protein to prevent DNA binding, and (c) promoted RelA polyubiquitination and proteasomal degradation. Comparisons with non-tumorigenic human breast epithelial MCF-10A and MCF7 cells revealed that NO<sub>2</sub>-OA more selectively inhibited TNBC function. This was attributed

to more facile mechanisms for maintaining redox homeostasis in normal breast epithelium, including a more favorable thiol/disulfide balance, greater extents of multidrug resistance protein-1 (MRP1) expression, and greater MRP1-mediated efflux of NO<sub>2</sub>-OA-glutathione conjugates. These observations reveal that electrophilic fatty acid nitroalkenes react with more alkylation-sensitive targets in TNBC cells to inhibit growth and viability.

Triple-negative breast cancer (TNBC)<sup>4</sup> is characterized by an absence of estrogen receptor (ER), progesterone receptor, and human epidermal growth factor receptor-2 expression (2, 3). TNBC accounts for up to 20% of breast cancer incidence and is the subtype with the worst prognosis (4). The majority of TNBC tumors are "basal-like", with 5-year survival rates lower than for all other breast cancer phenotypes (~77% versus ~93%, respectively) (3). TNBC patients are also at greater risk for relapse during the first 5 years post-chemotherapy. The recurrent tumors are more aggressive and invasive (5, 6), resulting in a life expectancy of 3–22 months after reappearance (7, 8). Consequently, there is an urgent unmet need for new therapeutic strategies for TNBC, beyond the limited options of standard chemotherapy, ionizing radiation, and surgery.

Activation of nuclear factor- $\kappa$ B (NF- $\kappa$ B) is strongly linked with TNBC development and progression (9–11), with NF- $\kappa$ B signaling constitutively activated in ER-negative breast cancer cell lines and primary tumors (10–13). The inhibition of NF- $\kappa$ B activation, induced by overexpression of the non-degradable inhibitor of NF- $\kappa$ B (I $\kappa$ B $\alpha$ ) superrepressor (Ser-32/36 mutations of I $\kappa$ B $\alpha$ ), significantly inhibits the growth of several TNBC cell lines (13). The pro-inflammatory cytokine TNF $\alpha$  also contributes significantly to this complex inflammatory microenvironment that promotes tumor progression. TNF $\alpha$

This study was supported by United States Army Breast Cancer Research Breakthrough Awards W81XWH-14-1-0237 (to Y. H.) and W81XWH-14-1-0238 (to N. E. D.) and National Institutes of Health Grants R01-HL058115, R01-HL64937, P30-DK072506, and P01-HL103455 (to B. A. F.), R21AI122071-01A1 (to S. G. W.), and 5P30-CA047904 (to N. E. D.). B. A. F., S. G. W., S. R. W., and C. C. W. acknowledge interest in Complexa, Inc. No potential conflicts of interest were disclosed by other authors. The content is solely the responsibility of the authors and does not necessarily represent the official views of the National Institutes of Health.

This article contains supporting Methods and Figs. S1–S10.

<sup>1</sup> Both authors contributed equally to this work.

<sup>2</sup> To whom correspondence may be addressed. E-mail: freerad@pitt.edu.

<sup>3</sup> To whom correspondence may be addressed. E-mail: gstacy@pitt.edu.

<sup>4</sup> The abbreviations used are: TNBC, triple-negative breast cancer; ER, estrogen receptor; NO<sub>2</sub>-FA, electrophilic fatty acid nitroalkene derivatives; PTM, post-translational modification; IKK $\beta$ , inhibitor of NF- $\kappa$ B subunit kinase  $\beta$ ; ICAM-1, intercellular adhesion molecule 1; uPA, urokinase-type plasminogen activator; OA, oleic acid; NO<sub>2</sub>-OA, 10-nitro-octadec-9-enoic acid; NO<sub>2</sub>-SA, nitro-stearate; CDDO, 2-cyano-3,12-dioxooleana-1,9-dien-28-oic acid; FBS, fetal bovine serum; DMEM, Dulbecco's modified Eagle's medium; TNF, tumor necrosis factor; NF- $\kappa$ B, nuclear factor- $\kappa$ B; Bt, biotinylated; RLU, relative light units; NEM, N-ethylmaleimide; MRM, multiple-reaction monitoring; DP, declustering potential; CE, collision energy; qPCR, quantitative PCR.

activates tumor metastasis and invasion through NF- $\kappa$ B-mediated up-regulation of extracellular matrix degradation enzymes and adhesion molecule expression (14). Notably, a meta-analysis revealed that TNBC patients with elevated TNF $\alpha$  expression have an increased risk of tumor metastasis to distant organs (15). Thus, NF- $\kappa$ B activation and the downstream signaling actions of its pro-inflammatory mediators play a critical role in TNBC malignancy. This motivates the development of novel NF- $\kappa$ B inhibition strategies as a chemotherapeutic approach for countering metastatic TNBC.

Electrophilic fatty acid nitroalkene derivatives (NO<sub>2</sub>-FA) are endogenously formed by the acidic conditions of digestion and the complex redox milieu that is up-regulated during inflammation. These environments facilitate the reaction of the nitric oxide (NO) and nitrite (NO<sub>2</sub><sup>-</sup>)-derived nitrating species nitrogen dioxide (NO<sub>2</sub>) (16) with biological targets, such as unsaturated fatty acids. Basal plasma and urinary NO<sub>2</sub>-FA concentrations in healthy humans range from 2 to 20 nM, with additional pools of NO<sub>2</sub>-FA present as (a) Michael addition products with the abundant biological nucleophiles present in tissues and fluids and (b) esterified species in complex neutral and polar lipids (17, 18). Tissue NO<sub>2</sub>-FA levels are affected by both dietary lipid and nitrogen oxide concentrations and during metabolic stress can rise to concentrations as high as 1  $\mu$ M (19, 20).

The unique electrophilic character of fatty acid nitroalkene substituents promotes kinetically rapid and reversible Michael addition with nucleophilic Cys and, to a lesser extent, His residues of proteins (21, 22). This reversible protein adduction by fatty acid nitroalkenes decreases the potential for toxicity stemming from the accumulation of Schiff's base and Michael addition products characteristic of other lipid electrophiles, such as  $\alpha,\beta$ -unsaturated oxo (or keto) and cyclopentanone derivatives (21, 23, 24). Through transient post-translational modification (PTM) reactions with hyperreactive protein thiols, NO<sub>2</sub>-FA modulate signaling pathways involved in cell proliferation and inflammatory responses. This occurs as a result of the alkylation of functionally significant Cys residues in transcriptional regulatory proteins, including the Kelch-like ECH-associated protein-1 (Keap1) regulator of nuclear factor (erythroid-derived-2)-like 2 (Nrf2) signaling, the nuclear lipid receptor peroxisome proliferator-activated receptor  $\gamma$  (PPAR $\gamma$ ), and NF- $\kappa$ B (25–27). Of relevance to the present study, NO<sub>2</sub>-FA inhibit NF- $\kappa$ B-mediated signaling in diverse cell and murine models of metabolic and inflammatory stress to cardiovascular, pulmonary, and renal systems (27–29).

NO<sub>2</sub>-FA specifically alkylate Cys-38 of the RelA subunit of NF- $\kappa$ B, a functionally significant, lipid electrophile-reactive thiol located in the DNA-binding domain of RelA. Redox-dependent PTMs of RelA Cys-38 inhibit DNA binding and downstream pro-inflammatory mediator gene expression (27). Current data indicate that other electrophilic species, such as the isothiocyanate derivative sulforaphane, mediate therapeutic actions in preclinical models of breast cancer (30, 31), thus motivating the present studies. Moreover, the pleiotropic signaling actions of NO<sub>2</sub>-FA include the activation of angiogenesis via up-regulation of HIF-1 $\alpha$  signaling during hypoxia (32). Because these effects may potentially modulate cancer cell and tumor properties, it was important to test the impact of an

electrophilic NO<sub>2</sub>-FA in both *in vitro* and *in vivo* models of an aggressive cancer phenotype, TNBC.

This study reports the inhibition of TNBC (MDA-MB-231 and MDA-MB468) cell proliferation, invasion, and metastasis by a synthetic homolog of an endogenous electrophilic NO<sub>2</sub>-FA found in species ranging from plants to humans (10-nitro-octadec-9-enoic acid, termed nitro-oleic acid and NO<sub>2</sub>-OA). NO<sub>2</sub>-OA displayed lower cytotoxic and anti-proliferative effects on non-tumorigenic breast ductal epithelium (MCF-10A and MCF7) *versus* triple-negative human breast ductal epithelial cells, due to the more stable mechanisms for maintaining redox homeostasis in MCF-10A and MCF7 cells. NO<sub>2</sub>-OA also attenuated TNF $\alpha$ -induced TNBC cell migration and invasion via inhibition of NF- $\kappa$ B signaling. Two newly discovered mechanisms also accounted for NO<sub>2</sub>-OA inhibition of TNBC NF- $\kappa$ B transcriptional activity. First, NO<sub>2</sub>-OA alkylated the inhibitor of NF- $\kappa$ B subunit kinase  $\beta$  (IKK $\beta$ ), leading to inhibition of its kinase activity and downstream I $\kappa$ B $\alpha$  phosphorylation. Second, NO<sub>2</sub>-OA alkylated NF- $\kappa$ B RelA protein, a reaction that not only inhibited DNA binding, but also promoted proteasomal RelA degradation. As a consequence, NO<sub>2</sub>-OA inhibited the expression of two NF- $\kappa$ B-regulated, TNF $\alpha$ -induced genes that are central to tumor metastasis, intercellular adhesion molecule-1 (ICAM-1) and urokinase-type plasminogen activator (uPA). Finally, in a nude mouse xenograft model, NO<sub>2</sub>-OA reduced the growth of established MDA-MB-231 tumors. In aggregate, these findings reveal that electrophilic NO<sub>2</sub>-FA can mediate chemotherapeutic actions in treating TNBC and possibly other inflammation-related cancers.

## Results

### NO<sub>2</sub>-OA inhibits TNBC cell growth and viability

The endogenously occurring lipid electrophile NO<sub>2</sub>-OA and its non-electrophilic control fatty acids (NO<sub>2</sub>-SA and OA) were evaluated for their impact on normal and cancerous breast ductal epithelial cell growth and signaling responses (Fig. 1A). To examine whether NO<sub>2</sub>-OA preferentially inhibited TNBC cell growth, Hoechst 33258 was used for counting non-tumorigenic breast epithelial cells (MCF-10A), an ER<sup>+</sup> breast cancer cell line (MCF7), and two TNBC cell lines (MDA-MB-231 and MDA-MB-468). Each cell line was treated with a range of NO<sub>2</sub>-OA concentrations (0–15  $\mu$ M) for 48 h. NO<sub>2</sub>-OA significantly inhibited the growth of both TNBC cell lines but not ER<sup>+</sup> or MCF-10A cells (Fig. 1, B, C, and D). The IC<sub>50</sub> for NO<sub>2</sub>-OA was significantly greater for non-cancerous MCF-10A cells (7.7  $\pm$  1.93  $\mu$ M) and MCF7 (11.61  $\pm$  3.59  $\mu$ M), as opposed to TNBC MDA-MB-231 (2.7  $\pm$  0.11  $\mu$ M) and MDA-MB-468 (1.6  $\pm$  0.11  $\mu$ M) cells (Fig. 1E). In addition to preferential TNBC cell growth inhibition, 3-(4,5-dimethylthiazol-2-yl)-2,5-diphenyltetrazolium bromide (MTT) detection of intact cell electron transfer mechanisms revealed that NO<sub>2</sub>-OA also significantly reduced the viability of both MDA-MB-231 and MDA-MB-468 cells, but not MCF7 or MCF-10A cells (Fig. S1, A–C). No cytotoxicity was detectable in any cell line for up to 24 h at the 5  $\mu$ M NO<sub>2</sub>-OA concentrations typically used for subsequent cell signaling and functional studies that had durations ranging from 1 to 8 h. Non-electrophilic NO<sub>2</sub>-SA, structurally

## NO<sub>2</sub>-OA inhibits breast cancer cell function

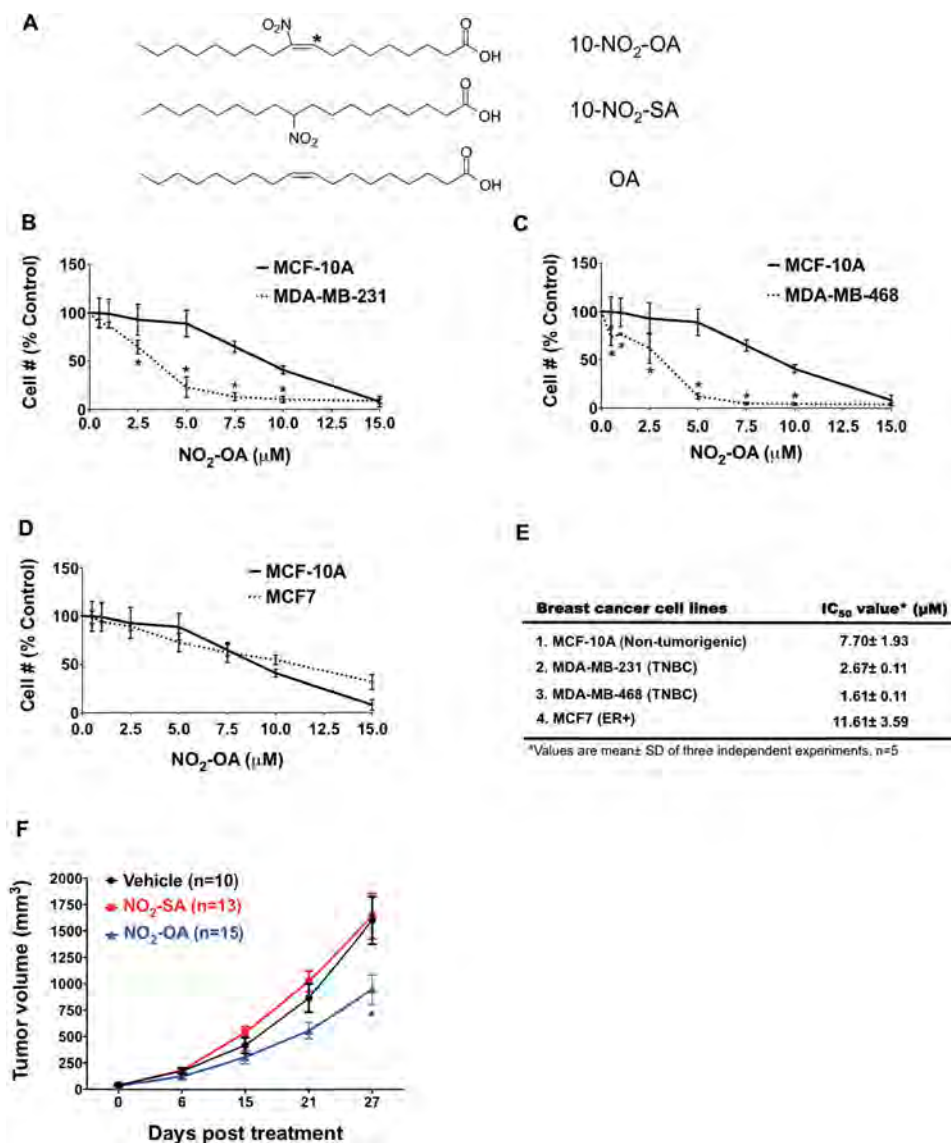


**Figure 1. NO<sub>2</sub>-OA inhibits TNBC cell growth *in vitro* and *in vivo*.** A, chemical structures of NO<sub>2</sub>-OA and the non-electrophilic NO<sub>2</sub>-SA and OA. \*, electrophilic carbon (35). The effect of NO<sub>2</sub>-OA on the growth of MDA-MB-231 (B), MDA-MB-468 (C), and MCF7 (D) was compared with the effect on MCF-10A cells. Data are shown as a percentage of untreated control cells (mean ± S.D. (error bars)). \*, *p* < 0.05 indicates significant difference between two cell types within each treatment. Three independent experiments were performed (*n* = 5 each). E, IC<sub>50</sub> values of NO<sub>2</sub>-OA in each breast cancer cell line. F, effect of NO<sub>2</sub>-OA (7.5 mg/kg daily) on MDA-MB-231 xenograft tumor growth (mean ± S.E. (error bars)). \*, *p* < 0.05 versus vehicle group within treatment time. Significance was determined by two-way analysis of variance followed by Tukey's post hoc test.

related to NO<sub>2</sub>-OA (Fig. 1A), did not affect TNBC cell growth (Fig. S2), affirming that NO<sub>2</sub>-OA-mediated TNBC cell growth inhibition is attributable to the electrophilic nitroalkene moiety.

### NO<sub>2</sub>-OA reduces MDA-MB-231 xenograft tumor growth

Given that TNBC cell growth and viability are inhibited by NO<sub>2</sub>-OA, the efficacy of NO<sub>2</sub>-OA on tumor growth was examined in a murine xenograft model of TNBC. MDA-MB-231 cells were injected into the fourth inguinal mammary fat pad of 6-week-old female athymic nude mice. Oral gavage with NO<sub>2</sub>-OA (7.5 mg/kg/day), NO<sub>2</sub>-SA (7.5 mg/kg/day), or sesame oil (vehicle control) was initiated and continued for 4 weeks after the average tumor sizes reached between 50 and 100 mm<sup>3</sup>. There was significantly reduced tumor growth in the mice treated with NO<sub>2</sub>-OA versus vehicle controls and NO<sub>2</sub>-SA-

treated mice at 27 days post-treatment (Fig. 1F). During the course of treatment, there was no weight loss in NO<sub>2</sub>-OA-treated or control mice (Fig. S3). These results indicate that NO<sub>2</sub>-OA mediates *in vivo* growth suppression of MDA-MB-231 cells with no overt toxic effects.

### NO<sub>2</sub>-OA induces cell cycle arrest and apoptotic cell death in TNBC cells

To determine whether the decreased cell numbers were due to NO<sub>2</sub>-OA-induced cell cycle alterations, FACS analysis was performed. NO<sub>2</sub>-OA significantly increased the percentage of cells at G<sub>2</sub>/M phase and decreased the percentage of cells in G<sub>0</sub>/G<sub>1</sub> upon 24-h treatment in MDA-MB-231 and MDA-MB-468 cells (Fig. 2, A and B). Notably, all cell cycle phase populations (G<sub>0</sub>/G<sub>1</sub>, S, and G<sub>2</sub>/M) of MCF-10A cells were not affected by NO<sub>2</sub>-OA (Fig. 2C). The cell cycle inhibition by NO<sub>2</sub>-OA was



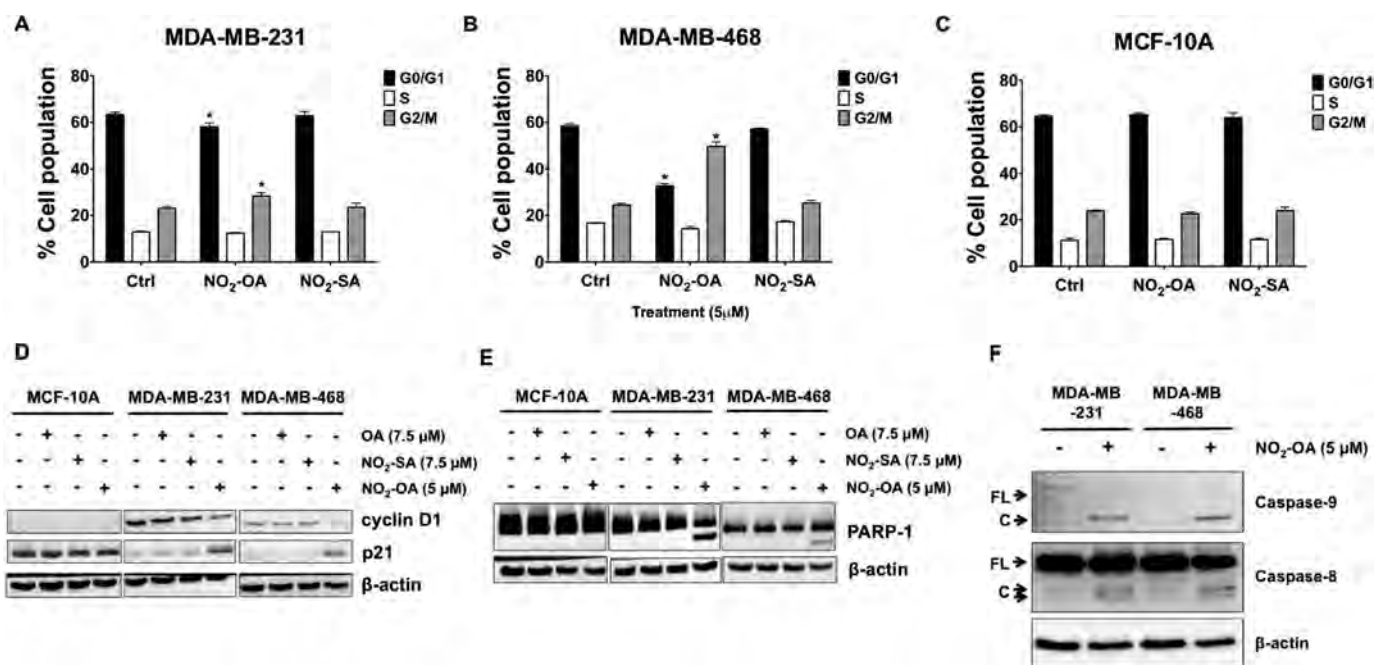


**Figure 2. NO<sub>2</sub>-OA promotes cell cycle arrest and apoptosis in TNBC cells.** Percentages of the cell population in each phase of the cell cycle (G<sub>0</sub>/G<sub>1</sub>, S, and G<sub>2</sub>/M) are shown for MDA-MB-231 (A), MDA-MB-468 (B), and MCF-10A cells (C) treated with NO<sub>2</sub>-OA (5 μM) for 24 h. Cells were harvested and analyzed by fluorescence-activated cell sorting. Significance was determined by one-way analysis of variance followed by Tukey post hoc test. Data are mean ± S.D. (error bars) (n = 3). \*, p < 0.05 versus control. D, immunoblot analysis of cyclin D1 and p21 in MCF-10A, MDA-MB-231, and MDA-MB-468 cells that were treated with OA (7.5 μM), NO<sub>2</sub>-SA (7.5 μM), or NO<sub>2</sub>-OA (5 μM) for 24 h. E, immunoblot analysis of PARP-1 cleavage in MCF-10A, MDA-MB-231, and MDA-MB-468 cells treated with OA (7.5 μM), NO<sub>2</sub>-SA (7.5 μM), or NO<sub>2</sub>-OA (5 μM) for 24 h. F, immunoblot analysis of caspase-8 and caspase-9 cleavage in MDA-MB-231 and MDA-MB-468 cells treated with or without NO<sub>2</sub>-OA (5 μM) for 24 h. β-actin was used as loading control. Data in D–F are representative of three independent experiments.

accompanied by an increase in p21 and a decrease in cyclin D1 protein expression in both MDA-MB-231 and MDA-MB-468 cells, but not MCF-10A cells (Fig. 2D). Consistent with the lack of an effect on cell growth and viability (Fig. S2), NO<sub>2</sub>-SA did not affect cell cycle populations or the expression of cell cycle-regulatory proteins in MCF-10A, MDA-MB-231, and MDA-MB-468 cells (Fig. 2D). The gene expression of cyclin D1 and p21 was also determined by quantitative RT-PCR. NO<sub>2</sub>-OA down-regulated cyclin D1 and up-regulated p21 gene expression after 24 h treatment of MDA-MB-231 and MDA-MB-468 cells, but not MCF-10A cells (Fig. S4). These results indicate that NO<sub>2</sub>-OA selectively induced cell cycle arrest in TNBC cells.

Increased sub-G<sub>1</sub> cell populations were apparent in both MDA-MB-231 and MDA-MB-468 cells 24 h after NO<sub>2</sub>-OA treatment (Fig. S5). To determine whether the effect of NO<sub>2</sub>-OA on sub-G<sub>1</sub> cells in TNBC cells was apoptosis-mediated, cleavage of poly(ADP-ribose) polymerase-1 (PARP-1) was examined by Western blotting. Treatment with NO<sub>2</sub>-OA for 24 h promoted caspase-3-mediated cleavage of PARP-1 (Fig. 2E) in MDA-MB-231 and MDA-MB-468 cells, but not in MCF-10A cells, indicating that NO<sub>2</sub>-OA preferentially induced TNBC apoptosis through caspase-3 activation. Also, it is possible that the increase in p21 blocks cell cycle entry into the S phase, resulting in the increase in sub-G<sub>1</sub> cells. To further investigate apoptotic signaling responses to NO<sub>2</sub>-OA in TNBC cells, the activation of initiator caspases (caspase-8 for the extrinsic pathway and caspase-9 for the intrinsic pathway) was analyzed using antibodies that detect both the pro-caspase and activated (cleaved) forms of these initiator caspases.

NO<sub>2</sub>-OA treatment increased cleavage of caspase-8 and caspase-9 in both MDA-MB-231 and MDA-MB-468 cells, suggesting that NO<sub>2</sub>-OA induced apoptosis through both intrinsic (mitochondria-dependent) and extrinsic (death receptor-dependent) apoptotic signaling mechanisms in TNBC cells (Fig. 2F). In aggregate, these results confirm that NO<sub>2</sub>-OA selectively modulates cell cycle arrest and apoptosis in TNBC cells versus MCF-10A cells.

#### Extracellular NO<sub>2</sub>-OA–glutathione adduct efflux is linked with multidrug resistance protein-1 (MRP1) expression

In the intracellular compartment, GSH and its reactive Cys moiety is more abundant than protein thiols; thus, GSH and other low-molecular weight thiols are the primary targets for oxidation and alkylation by free radicals, oxidants, and electrophiles (33). In the case of NO<sub>2</sub>-OA, which readily diffuses and gains access to the intracellular compartment and subcellular organelle protein targets (26, 34), GSH conjugates (NO<sub>2</sub>-OA-SG) are formed that can be actively transported from cells by the GSH-conjugate efflux pump MRP1 (1). This phenomenon was further investigated by measuring concentrations of extracellular NO<sub>2</sub>-OA-SG in the media of MCF-10A, MDA-MB-231, and MDA-MB-468 cells after a 1-h treatment with 5 μM NO<sub>2</sub>-OA. There were significantly lower levels of NO<sub>2</sub>-OA-SG being exported into the media of both MDA-MB-231 and MDA-MB-468 cells, as opposed to that released by MCF-10A cells (Fig. 3A). This 4–5-fold difference in extracellular NO<sub>2</sub>-OA-SG levels produced by MCF-10A and TNBC cells prompted comparison of the relative extents of expression of MRP1 protein and the GSH and GSSG content of TNBC and

## NO<sub>2</sub>-OA inhibits breast cancer cell function

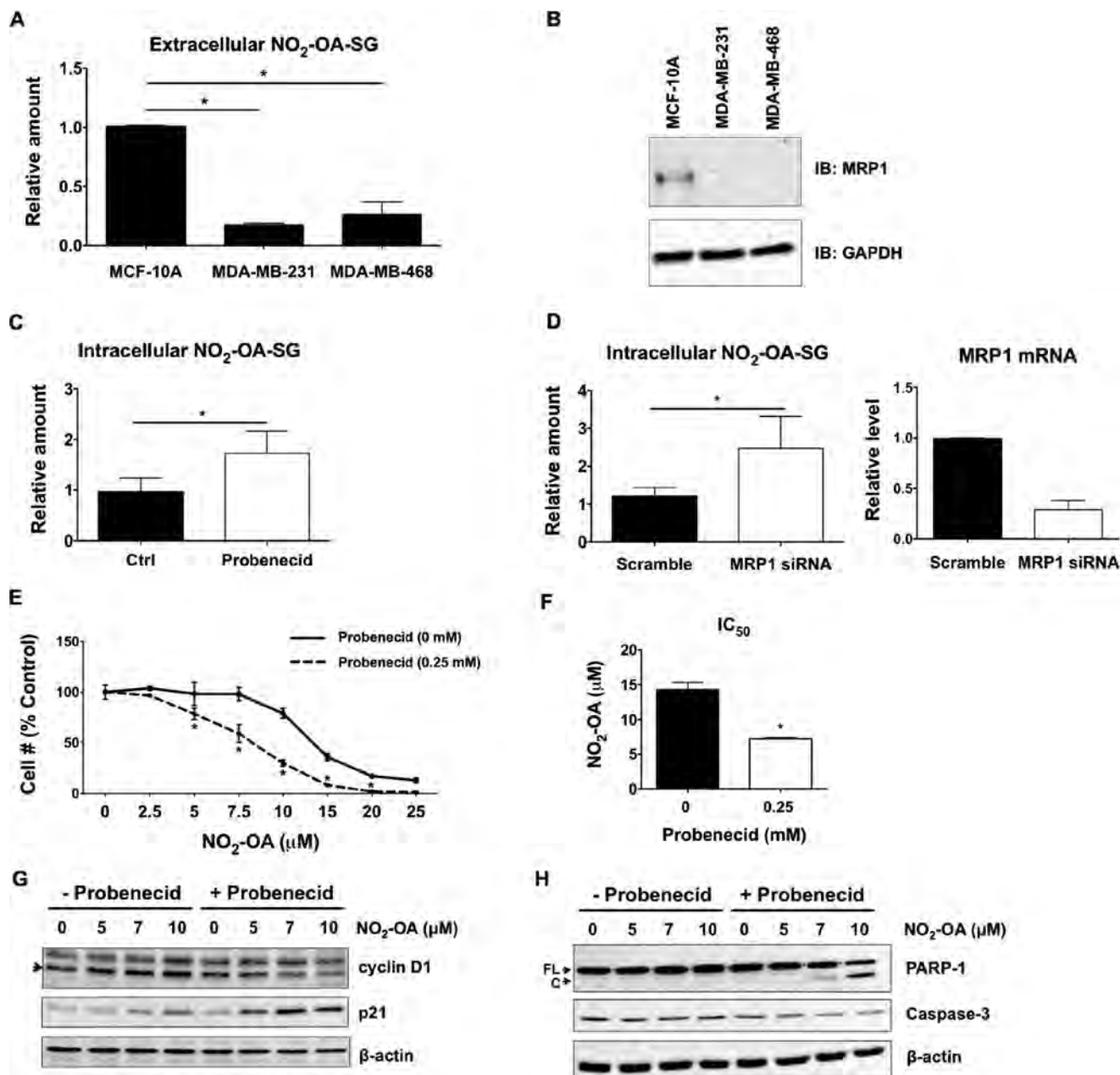


**Figure 3. MRP1 influences NO<sub>2</sub>-OA trafficking and signaling in TNBC cells.** A, the export of NO<sub>2</sub>-OA-SG by MCF-10A, MDA-MB-231, and MDA-MB-468 cells was measured by LC-MS/MS analysis. The relative extent of NO<sub>2</sub>-OA-SG export is reported as a ratio of NO<sub>2</sub>-OA-SG to an externally added <sup>15</sup>NO<sub>2</sub>-d<sub>4</sub>-OA-SG standard. \*, *p* < 0.05 versus MCF-10A, *n* = 4 (Mann-Whitney *U* test). B, representative immunoblot of endogenous MRP1 protein expression in MCF-10A, MDA-MB-231, and MDA-MB-468 cells. Suppression of MRP1 activity (C) and MRP1 expression (D) increased intracellular NO<sub>2</sub>-OA-SG adduct concentrations in MCF-10A cells. The relative amount represents the relative abundance of NO<sub>2</sub>-OA-SG to <sup>15</sup>NO<sub>2</sub>-d<sub>4</sub>-OA-SG standard, normalized to protein concentrations from each NO<sub>2</sub>-OA-treated sample divided by the abundance of control (*Ctrl*) or scrambled sample. \*, *p* < 0.05 versus control (*n* = 6) or scrambled (*n* = 9) was determined by Mann-Whitney *U* test. The siRNA knockdown efficiency of MRP1 was evaluated by real-time qPCR (*n* = 4). E, the effect of probenecid on NO<sub>2</sub>-OA growth inhibition of MCF-10A cells. Cells were pretreated with or without probenecid (0.25 mM) for 1 h and then combined with 0–25 μM NO<sub>2</sub>-OA for 48 h. A FluoroReporter dsDNA stain assay was performed to measure cell numbers. Data are shown as percentage of untreated control cells (*n* = 3); \*, *p* < 0.05 (0 mM versus 0.25 mM probenecid between treatments, two-way analysis of variance followed by Tukey post test). F, the average IC<sub>50</sub> values of NO<sub>2</sub>-OA in MCF-10A cells treated with or without probenecid. \*, *p* < 0.05, *n* = 3 (unpaired Student's *t* test). G, immunoblot analysis of cyclin D1 and p21 in MCF-10A cells treated with NO<sub>2</sub>-OA (5 μM) in the presence or absence of probenecid (1 mM used for this 24-h incubation). H, immunoblot analysis of caspase-3 and PARP-1 cleavage in MCF-10A cells treated with NO<sub>2</sub>-OA (5 μM) in the presence or absence of probenecid (1 mM) for 24 h. The full-length (FL) and cleaved (C) forms of PARP-1 and pro-caspase-3 protein level are shown. All data are mean ± S.D. (error bars). All immunoblots are representative of three independent experiments.

non-cancerous cell lines. Western blot analysis detected MRP1 protein expression in MCF-10A cells, but MRP1 was undetectable in both TNBC cell lines (Fig. 3B). MRP4 mRNA was detected at low levels in all three cell types, but protein expression was not evident by Western blotting (not shown).

### MRP1 influences NO<sub>2</sub>-OA bioactivity in MCF-10A cells

Two strategies, use of the organic anion transport inhibitor probenecid, often used as an MRP inhibitor, and siRNA knockdown of MRP1, facilitated investigation of the role of MRP1 in

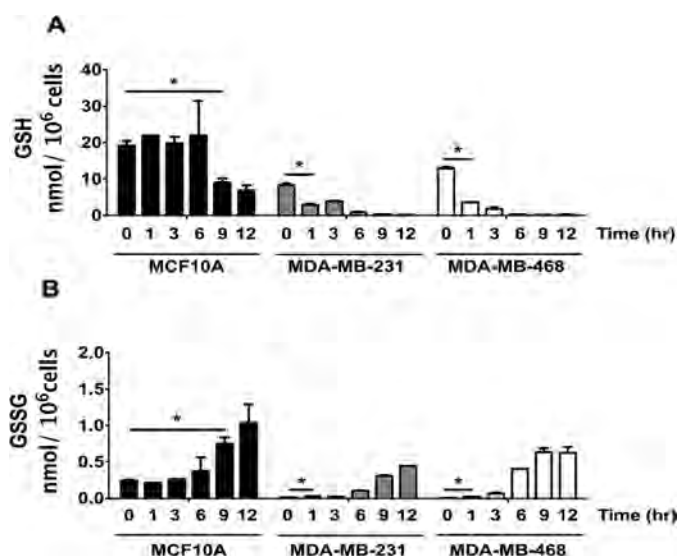


**Figure 4. NO<sub>2</sub>-OA depletes GSH levels and enhances GSSG formation in TNBC cells.** The response of cellular GSH (A) and GSSG (B) to NO<sub>2</sub>-OA in MCF-10A (black bars), MDA-MB-231 (gray bars), and MDA-MB-468 (white bars) cells is shown. Cells were treated with NO<sub>2</sub>-OA (5  $\mu$ M) for the indicated times (h). GSH and GSSG were extracted from cells ( $3 \times 10^6$  cells/ml) and quantitated by LC-MS/MS. \*,  $p < 0.05$  versus 0 h via unpaired two-tailed Student's *t* test. Data are presented as mean  $\pm$  S.D. (error bars) ( $n = 5$ ).

cellular responses to NO<sub>2</sub>-OA. Both probenecid and MRP1 siRNA knockdown (about 70% knockdown efficiency) enhanced intracellular levels of NO<sub>2</sub>-OA-SG adducts in MCF-10A cells (Fig. 3, C and D). Notably, probenecid also significantly enhanced MCF-10A cell growth inhibition by NO<sub>2</sub>-OA (Fig. 3E). The IC<sub>50</sub> of NO<sub>2</sub>-OA (7.23  $\pm$  0.15  $\mu$ M) was decreased 2-fold in MCF-10A cells pretreated with probenecid, compared with only NO<sub>2</sub>-OA treatment (14.23  $\pm$  1.05  $\mu$ M; Fig. 3F). Moreover, probenecid increased the extent of NO<sub>2</sub>-OA-induced cell cycle arrest of MCF-10A cells, as reflected by increased p21 levels and a concomitant decrease in cyclin D1 expression (Fig. 3G). Probenecid also enhanced NO<sub>2</sub>-OA-induced apoptosis in MCF-10A cells in the context of increased caspase-3 activation and PARP-1 cleavage (Fig. 3H). These observations are consistent with both the intracellular concentrations and the cell growth/cell survival signaling actions of NO<sub>2</sub>-OA being influenced by the extents of NO<sub>2</sub>-OA reaction with GSH and subsequent MRP1 export of NO<sub>2</sub>-OA-SG.

#### GSH and GSSG responses to NO<sub>2</sub>-OA in MCF-10A cells versus TNBC cells

LC-MS quantitation of GSH and GSSG from 0 to 12 h after treatment with 5  $\mu$ M NO<sub>2</sub>-OA revealed that basal GSH levels in MCF-10A cells (19.3  $\pm$  1.9 nmol/10<sup>6</sup> cells) were >2-fold that of MDA-MB-231 (8.3  $\pm$  0.8 nmol/10<sup>6</sup> cells) and ~1.5-fold greater than MDA-MB-468 cells (12.9  $\pm$  0.5 nmol/10<sup>6</sup> cells) (Fig. 4A). GSSG levels (Fig. 4B) at time 0 were greater in MCF-10A cells, resulting in an initial GSH/GSSG ratio of 82  $\pm$  16 compared with 653  $\pm$  68 for MDA-MB-231 cells and 2003  $\pm$  163 in MDA-MB-468 cells. MCF-10A cells maintained the GSH/GSSG ratio over the first 6 h after NO<sub>2</sub>-OA treatment, whereas the GSH/GSSG ratio rapidly decreased in MDA-MB-231 and MDA-MB-468 cells due to decreased GSH concentrations. In aggregate, the data in Figs. 3 and 4 indicate that there will be a more

extensive reaction expected between NO<sub>2</sub>-OA and cellular protein targets in TNBC cells because of the more favorable pharmacokinetics (greater intracellular concentration and longer  $t_{0.5}$ ) lent by the lower GSH concentrations and the suppression of NO<sub>2</sub>-OA-SG export by the MRP1-deficient TNBC cell phenotype. In MCF-10A cells, NO<sub>2</sub>-OA will be more readily glutathionylated and exported, thus limiting reactions with signaling pathway proteins.

#### NO<sub>2</sub>-OA inhibits TNF $\alpha$ -induced TNBC cell migration and invasion

Inflammatory stimuli, such as TNF $\alpha$ , induce responses in the tumor microenvironment that promote TNBC tumor metastasis and invasion (14). Because electrophilic NO<sub>2</sub>-FAs mediate anti-inflammatory signaling actions (27, 28), the impact of NO<sub>2</sub>-OA on TNF $\alpha$ -induced TNBC cell migration was evaluated. Boyden chamber migration analyses indicated that TNF $\alpha$  augmented migration of both MDA-MB-231 and MDA-MB-468 cells (Fig. 5A, images 3 and 8), compared with basal conditions (Fig. 5A, images 2 and 7). NO<sub>2</sub>-OA significantly inhibited both MDA-MB-231 and MDA-MB-468 cell migration induced by TNF $\alpha$  (Fig. 5, A (images 4 and 9), B, and C). NO<sub>2</sub>-OA modestly inhibited the basal, non-stimulated migration of MDA-MB-231 and MDA-MB-468 cells (Fig. 5, B and C). Next, cells were placed in Transwell permeable supports coated with Matrigel for invasion assays to assess the potential effect of NO<sub>2</sub>-OA on the invasive phenotype of TNBC cells. TNF $\alpha$ -induced invasion was significantly inhibited by NO<sub>2</sub>-OA treatment of MDA-MB-468 cells, whereas the non-electrophilic control fatty acid (NO<sub>2</sub>-SA) displayed no significant effect on tumor cell invasion (Fig. 5D). The inhibitory actions of NO<sub>2</sub>-OA on MDA-MB-468 invasion were compared with cell responses to the NF- $\kappa$ B inhibitor JSH-23, which inhibits nuclear translocation of the RelA subunit (36). Similar to JSH-23, NO<sub>2</sub>-OA inhibited TNF $\alpha$ -induced invasion in MDA-MB-468 cells (Fig. 5D).

#### NO<sub>2</sub>-OA inhibits TNF $\alpha$ -induced NF- $\kappa$ B transcriptional activity in TNBC cells

The inhibition of MDA-MB-468 cell invasion by JSH-23 (Fig. 5D) suggests that NO<sub>2</sub>-OA may also inhibit TNF $\alpha$ -induced breast cancer cell mobility due to a capacity to inhibit NF- $\kappa$ B signaling. To test this concept, the effect of NO<sub>2</sub>-OA on TNF $\alpha$ -activated NF- $\kappa$ B transcriptional activity in TNBC cells was examined. MDA-MB-231 and MDA-MB-468 cells were transiently transfected with an NF- $\kappa$ B luciferase reporter plasmid and treated with 5  $\mu$ M NO<sub>2</sub>-OA for 2 h, followed by activation with 20 ng/ml TNF $\alpha$  for 4 h. In addition to NO<sub>2</sub>-OA, the non-electrophilic lipid controls NO<sub>2</sub>-SA (5  $\mu$ M) and OA (5  $\mu$ M) were also examined. NO<sub>2</sub>-OA significantly inhibited NF- $\kappa$ B-dependent transcription of luciferase in both TNBC cell lines, compared with TNF $\alpha$  alone, whereas NO<sub>2</sub>-SA and OA had no effect. Moreover, the extent of inhibition of NF- $\kappa$ B-dependent luciferase expression by NO<sub>2</sub>-OA was similar to that induced by the NF- $\kappa$ B inhibitor JSH-23 (20  $\mu$ M; Fig. 6, A and B). These data indicate that the electrophilic reactivity of NO<sub>2</sub>-OA accounts for the inhibition of TNF $\alpha$ -induced NF- $\kappa$ B transcriptional activity in TNBC cells.

## NO<sub>2</sub>-OA inhibits breast cancer cell function

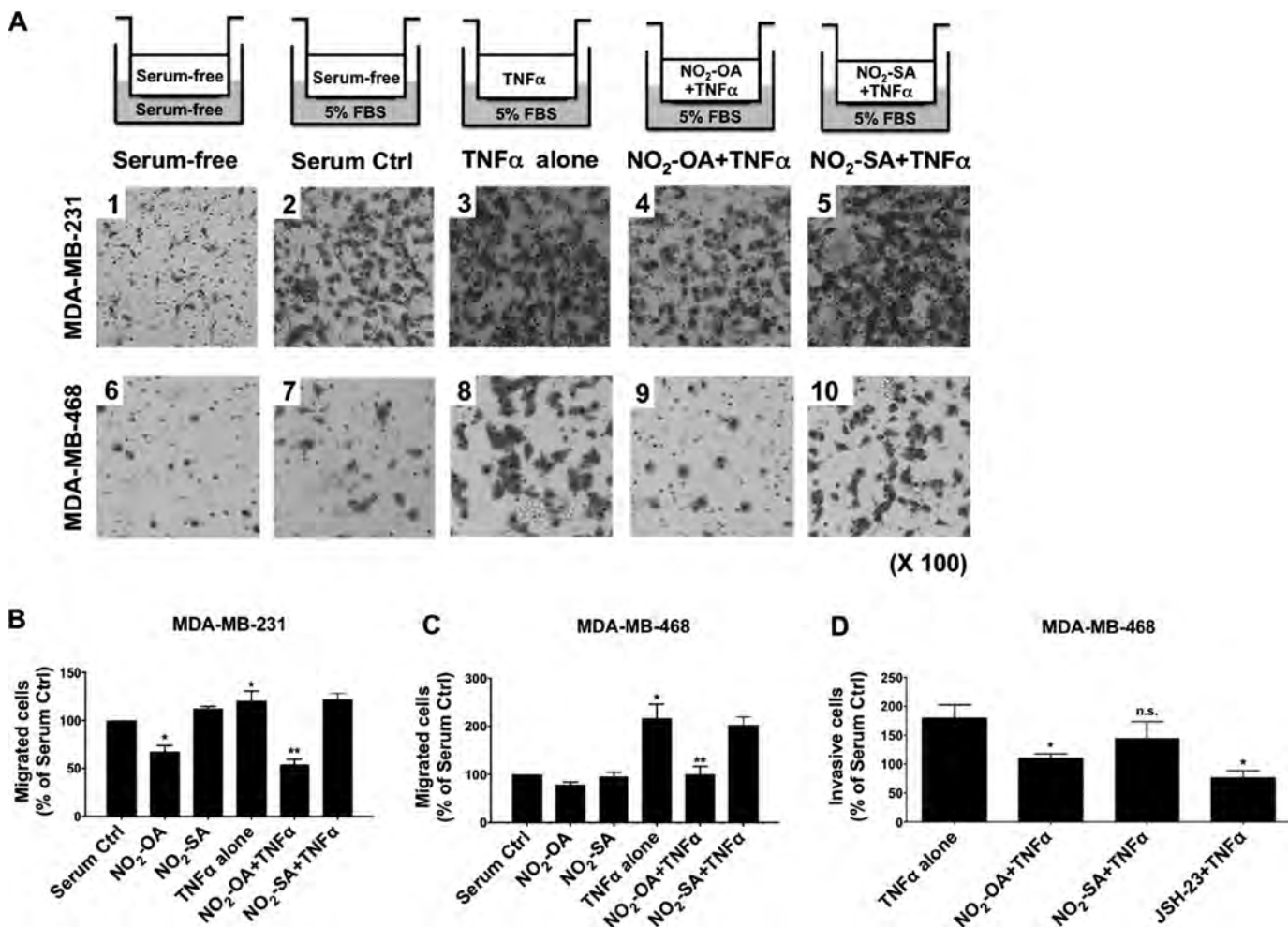


**Figure 5.** NO<sub>2</sub>-OA inhibits TNF $\alpha$ -induced TNBC cell migration and invasion. **A**, experimental schemes and representative images of crystal violet-stained migrating MDA-MB-231 or MDA-MB-468 cells. Cells ( $1 \times 10^5$ ) were placed in the upper chamber with serum-free medium under the indicated treatment conditions. Migrating cells were photographed using a light microscope at  $\times 100$ . **B** and **C**, quantitation of migrated cells from Fig. 4A was performed by solubilization of crystal violet and spectrophotometric analysis at  $A_{573}$  nm. The percentage of migrating cells in each treatment group was compared with numbers of migrating cells in the absence of TNF $\alpha$  stimulation (Serum Ctrl). \*,  $p < 0.05$  versus in the absence of TNF $\alpha$  stimulation; \*\*,  $p < 0.05$  versus TNF $\alpha$  alone. **D**, to test the impact of NO<sub>2</sub>-OA on TNBC cell invasion, MDA-MB-468 cells were incubated in serum-free medium containing 20 ng/ml TNF $\alpha$  combined with NO<sub>2</sub>-OA (5  $\mu$ M), NO<sub>2</sub>-SA (5  $\mu$ M), or JSH-23 (10  $\mu$ M), and then invasion was determined by the extents of cell migration through the Matrigel matrix toward a 5% FBS chemoattractant for 24 h. The percentage of invading cells in each treatment was relative to the number of migrating cells in the absence of TNF $\alpha$  stimulation. \*,  $p < 0.05$  versus TNF $\alpha$  alone n.s., not significant. Significance was determined by one-way analysis of variance followed by Tukey post hoc test. All data are mean  $\pm$  S.D. (error bars).

### NO<sub>2</sub>-OA inhibits NF- $\kappa$ B-regulated gene expression linked with TNBC tumor metastasis

Inhibition of NF- $\kappa$ B transcriptional activity by NO<sub>2</sub>-OA suggested that the expression of metastasis-related downstream target genes may be decreased. To investigate this, key NF- $\kappa$ B target genes were evaluated via RT<sup>2</sup> profiler PCR array analysis of MDA-MB-468 cells treated with NO<sub>2</sub>-OA (5  $\mu$ M) for 24 h. The expression levels of NF- $\kappa$ B target genes that were regulated by NO<sub>2</sub>-OA were compared with untreated MDA-MB-468 cells as a control. Data revealed that treatment with NO<sub>2</sub>-OA decreased the mRNA expression of multiple NF- $\kappa$ B target genes, including ICAM-1 and uPA, two critical mediators of tumor progression and metastasis (Fig. 6C). TNF $\alpha$  induces the expression of both ICAM-1 and uPA in MDA-MB-231 cells (37, 38). To more directly examine whether NO<sub>2</sub>-OA suppressed TNF $\alpha$ -induced expression of ICAM-1 and uPA in TNBC cells, MDA-MB-231 or MDA-MB-468 cells were

treated with 5  $\mu$ M NO<sub>2</sub>-OA and 20 ng/ml TNF $\alpha$ . Simultaneous treatment with either NO<sub>2</sub>-OA or RelA siRNA led to suppression of TNF $\alpha$ -induced expression of ICAM-1 and uPA genes in TNBC cells (Fig. 6, D, E, G, and H). The impact of NO<sub>2</sub>-OA and RelA siRNA on RelA-dependent target gene expression was further evaluated by real-time qPCR (Fig. 6, F and I). RelA mRNA levels were suppressed by RelA siRNA treatment, but not NO<sub>2</sub>-OA. Both NO<sub>2</sub>-OA and RelA siRNA inhibited gene expression of TNF $\alpha$ -induced ICAM-1 and uPA gene expression via NF- $\kappa$ B-dependent mechanisms. To determine whether NO<sub>2</sub>-OA suppressed TNF $\alpha$ -induced pro-metastatic ICAM-1 and uPA gene expression during cell migration, transcript levels of ICAM-1 and uPA genes were evaluated in MDA-MB-468 cells being studied in Boyden chamber migration assays (Fig. 5C). Under these conditions, NO<sub>2</sub>-OA significantly inhibited TNF $\alpha$ -induced expression of ICAM-1 and uPA in migrating tumor cells (Fig. S6, A and B), again indicating that

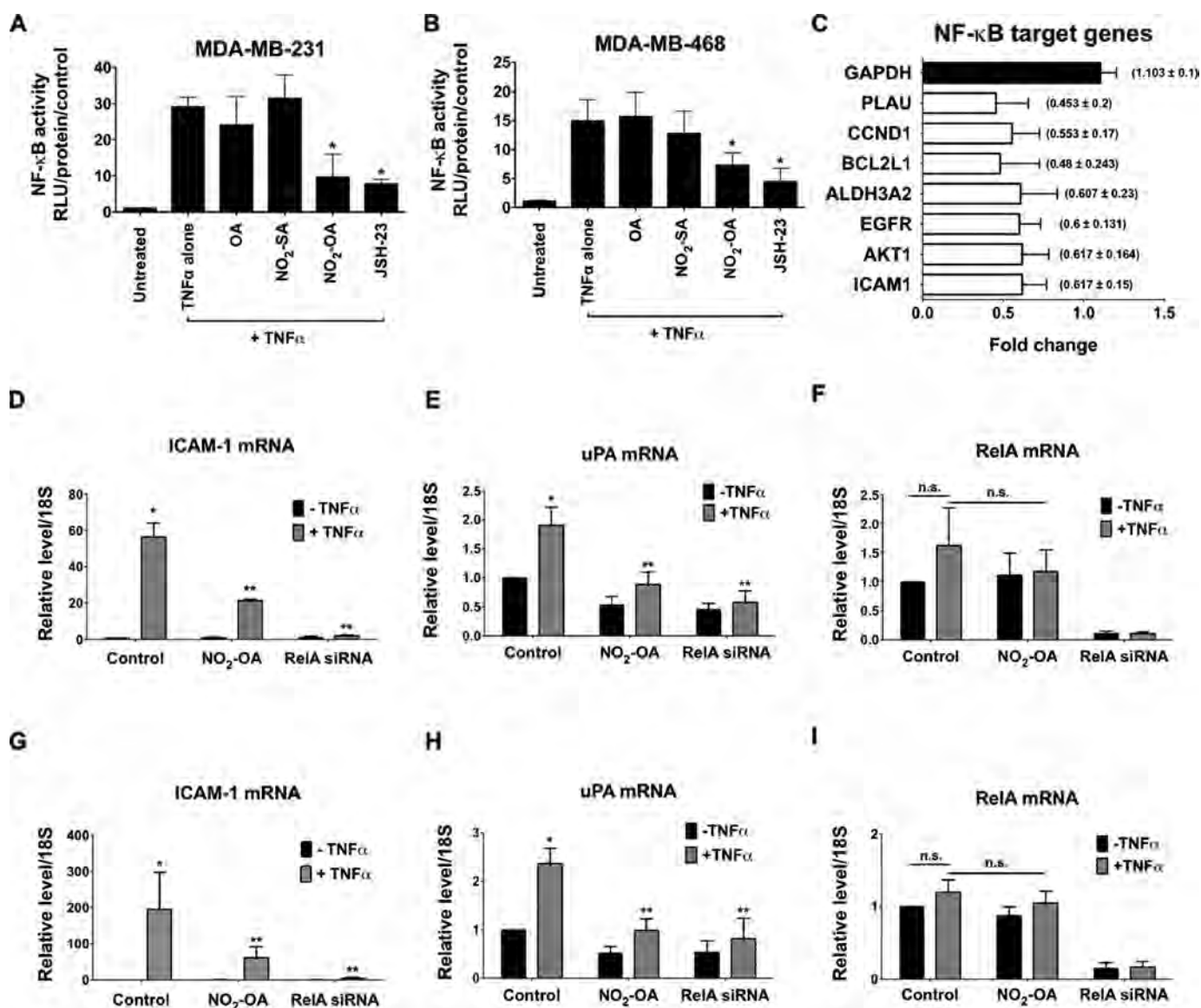


**Figure 6. NO<sub>2</sub>-OA inhibits TNF $\alpha$ -induced NF- $\kappa$ B transcriptional activity in TNBC cells.** The effect of NO<sub>2</sub>-OA on TNF $\alpha$ -induced activation of NF- $\kappa$ B-dependent reporter gene transcription was measured in NF- $\kappa$ B-luciferase reporter-transfected MDA-MB-231 (A) or MDA-MB-468 (B) cells. \*,  $p < 0.05$  versus TNF $\alpha$  alone ( $n = 3$ ). Significance was determined by Kruskal-Wallis test followed by Dunn's post test with Bonferroni corrections for multiple comparisons. C, determination of NF- $\kappa$ B target genes down-regulated by NO<sub>2</sub>-OA in MDA-MB-468 cells using a human NF- $\kappa$ B target PCR array. Histograms represent the fraction of mRNA expression in NO<sub>2</sub>-OA-treated versus untreated cells. GAPDH was used as an internal control (black bar). Shown is the effect of NO<sub>2</sub>-OA on expression of ICAM-1 (D), uPA (E), or RelA (F) genes in TNF $\alpha$ -induced MDA-MB-231 cells. Similarly, the effect of NO<sub>2</sub>-OA on expression of ICAM-1 (G), uPA (H), or RelA (I) genes in TNF $\alpha$ -induced MDA-MB-468 cells is shown. The -fold increase relative to untreated controls is presented. \*,  $p < 0.05$  versus untreated control; \*\*,  $p < 0.05$  versus TNF $\alpha$  alone. n.s., not significant. Significance was determined by one-way analysis of variance followed by Tukey post test. All data are presented as mean  $\pm$  S.D. (error bars) ( $n = 5$ ).

NO<sub>2</sub>-OA inhibited expression of NF- $\kappa$ B-regulated genes involved in metastasis.

#### NO<sub>2</sub>-OA suppresses TNF $\alpha$ -induced IKK $\beta$ /I $\kappa$ B $\alpha$ signaling in TNBC

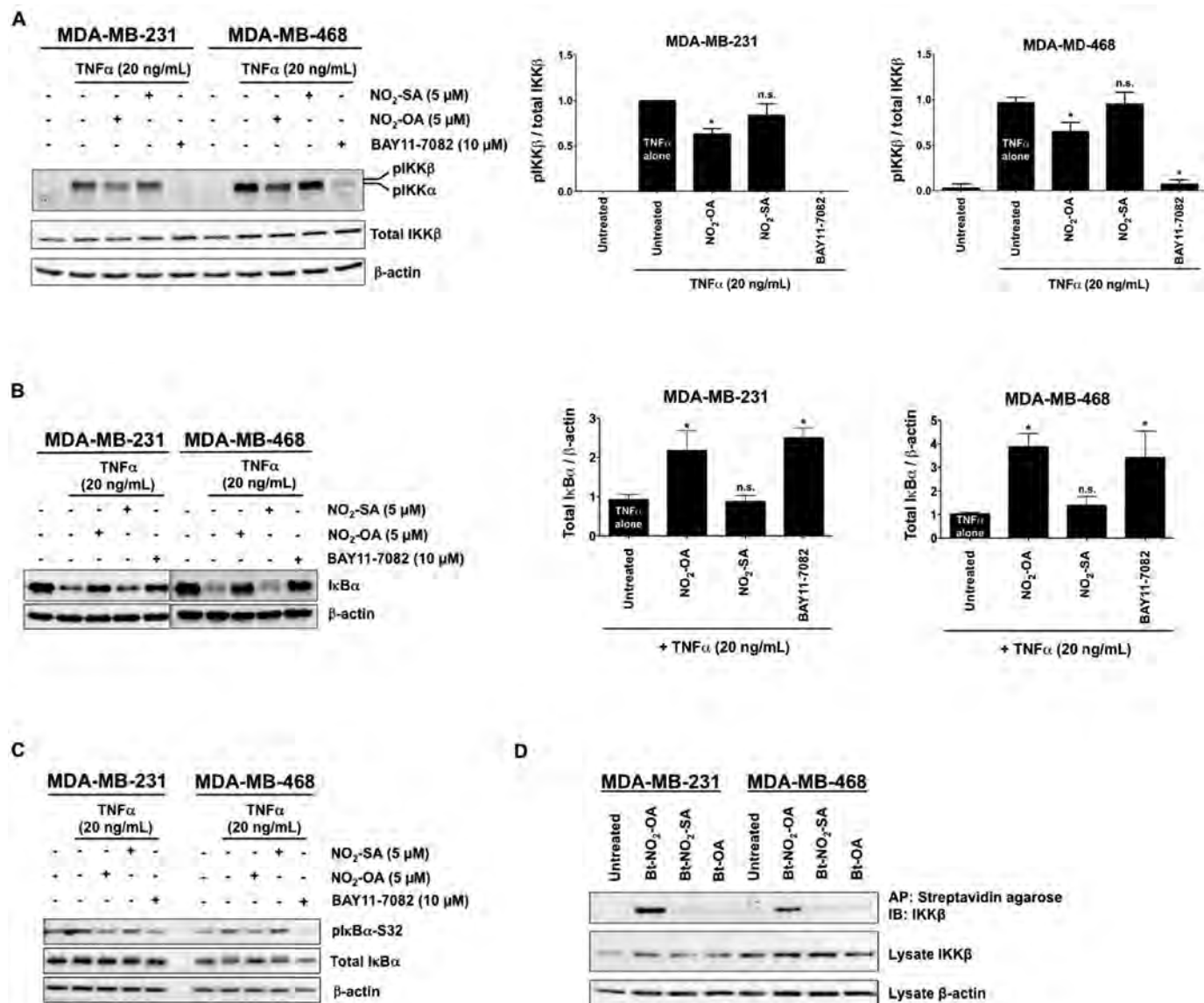
To better define mechanisms accounting for NO<sub>2</sub>-OA inhibition of TNF $\alpha$ -activated NF- $\kappa$ B signaling, MDA-MB-231 or MDA-MB-468 cells were pretreated with NO<sub>2</sub>-OA (5  $\mu$ M) or the IKK inhibitor BAY11-7082 (10  $\mu$ M) for 2 h before TNF $\alpha$  stimulation (20 ng/ml, 5 min). TNF $\alpha$ -induced IKK $\beta$  phosphorylation was diminished by both NO<sub>2</sub>-OA and BAY11-7082 (Fig. 7A). Both NO<sub>2</sub>-OA and BAY11-7082 also inhibited the degradation of I $\kappa$ B $\alpha$  following TNF $\alpha$  stimulation (20 ng/ml, 10 min;

Fig. 7B). Moreover, decreased I $\kappa$ B $\alpha$  phosphorylation occurred in cells pretreated with NO<sub>2</sub>-OA or BAY11-7082 and the proteasome inhibitor MG-132 (10  $\mu$ M; Fig. 7C). This indicates that NO<sub>2</sub>-OA suppresses TNF $\alpha$ -induced IKK $\beta$  phosphorylation and I $\kappa$ B $\alpha$  degradation, with these actions in turn inhibiting downstream NF- $\kappa$ B signaling in TNBC cells.

#### NO<sub>2</sub>-OA alkylates IKK $\beta$ and RelA proteins

Cys-179, located in the activation loop of IKK $\beta$ , is a target for oxidation and electrophile alkylation reactions (39, 40). Because NO<sub>2</sub>-OA suppresses TNF $\alpha$ -induced phosphorylation of IKK $\beta$  and I $\kappa$ B $\alpha$  in TNBC cells (Fig. 7, A and C), the potential for NO<sub>2</sub>-OA to alkylate IKK $\beta$  was investigated. Biotinylated

## NO<sub>2</sub>-OA inhibits breast cancer cell function



**Figure 7. NO<sub>2</sub>-OA inhibits TNF $\alpha$ -induced IKK $\beta$  phosphorylation and I $\kappa$ B $\alpha$  degradation and covalently adducts IKK $\beta$ .** MDA-MB-231 and MDA-MB-468 cells were used in all studies. *A*, representative immunoblot of IKK $\beta$  (Ser-180) phosphorylation, total IKK $\beta$  levels, and relative phosphorylated IKK $\beta$  levels. Then all phosphorylated IKK $\beta$  levels normalized to total IKK $\beta$  were quantified. *B*, representative immunoblot of I $\kappa$ B $\alpha$  protein levels is shown, and the relative total I $\kappa$ B $\alpha$  levels (normalized to total  $\beta$ -actin) are quantified in response to NO<sub>2</sub>-SA, NO<sub>2</sub>-OA, and the NF- $\kappa$ B inhibitor BAY11-7082. *C*, representative immunoblots of I $\kappa$ B $\alpha$  (Ser-32) phosphorylation and total I $\kappa$ B $\alpha$  are shown in response to NO<sub>2</sub>-SA, NO<sub>2</sub>-OA, and the NF- $\kappa$ B inhibitor BAY11-7082. *D*, NO<sub>2</sub>-OA alkylates TNBC IKK $\beta$  protein. Biotinylated NO<sub>2</sub>-OA, NO<sub>2</sub>-SA, and OA and adducted proteins were affinity-purified by streptavidin-agarose beads from cell lysates. Pulled-down IKK $\beta$  protein was then detected by immunoblotting. IKK $\beta$  and control  $\beta$ -actin immunoblots from the same input lysates used for affinity purification are shown below the panel. \*,  $p < 0.05$  versus TNF $\alpha$  alone. *n.s.*, not significant. Significance was determined by one-way analysis of variance followed by Tukey post test.

lipids (Bt-NO<sub>2</sub>-OA, Bt-NO<sub>2</sub>-SA, and Bt-OA) were synthesized (Fig. S7) to facilitate affinity capture-mediated measurement of NO<sub>2</sub>-OA and control fatty acid adduction of IKK $\beta$ . MDA-MB-231 or MDA-MB-468 cells were treated with 5  $\mu$ M Bt-NO<sub>2</sub>-OA, Bt-NO<sub>2</sub>-SA, or Bt-OA for 2 h, and then all alkylated proteins were pulled down from whole-cell lysates using streptavidin-conjugated beads. Western blotting revealed that IKK $\beta$  was pulled down by Bt-NO<sub>2</sub>-OA, but not by non-electrophilic control fatty acids (Fig. 7D). Similarly, Bt-NO<sub>2</sub>-OA (but not control fatty acids) promoted the pull-down NF- $\kappa$ B RelA (Fig. 8A).

NO<sub>2</sub>-OA inhibits LPS-induced NF- $\kappa$ B transcriptional activity, in part a consequence of the alkylation of RelA Cys-38 and inhibition of RelA DNA binding (27). LC-MS/MS proteomic analysis showed that RelA Cys-105 was also alkylated by

NO<sub>2</sub>-OA (Fig. S8), with the functional significance of the NO<sub>2</sub>-OA alkylation of RelA Cys-105 undefined. In aggregate, Bt-NO<sub>2</sub>-OA promotes the pulldown of IKK $\beta$  and RelA, and direct proteomic analysis revealed the NO<sub>2</sub>-OA alkylation of RelA. These observations underscore that NO<sub>2</sub>-OA mediates PTMs that inhibit multiple facets of pro-inflammatory NF- $\kappa$ B signaling.

### NO<sub>2</sub>-OA stimulates RelA protein proteasomal degradation

Proteolytic degradation of NF- $\kappa$ B contributes to the termination of its signaling. Thiol-alkylating and nitrosating agents induce the degradation of NF- $\kappa$ B subunit p50 via the PTM of Cys-62 in both HT29 and HCT116 tumor cell lines (41). Because NO<sub>2</sub>-OA covalently adducts RelA in both MDA-MB-

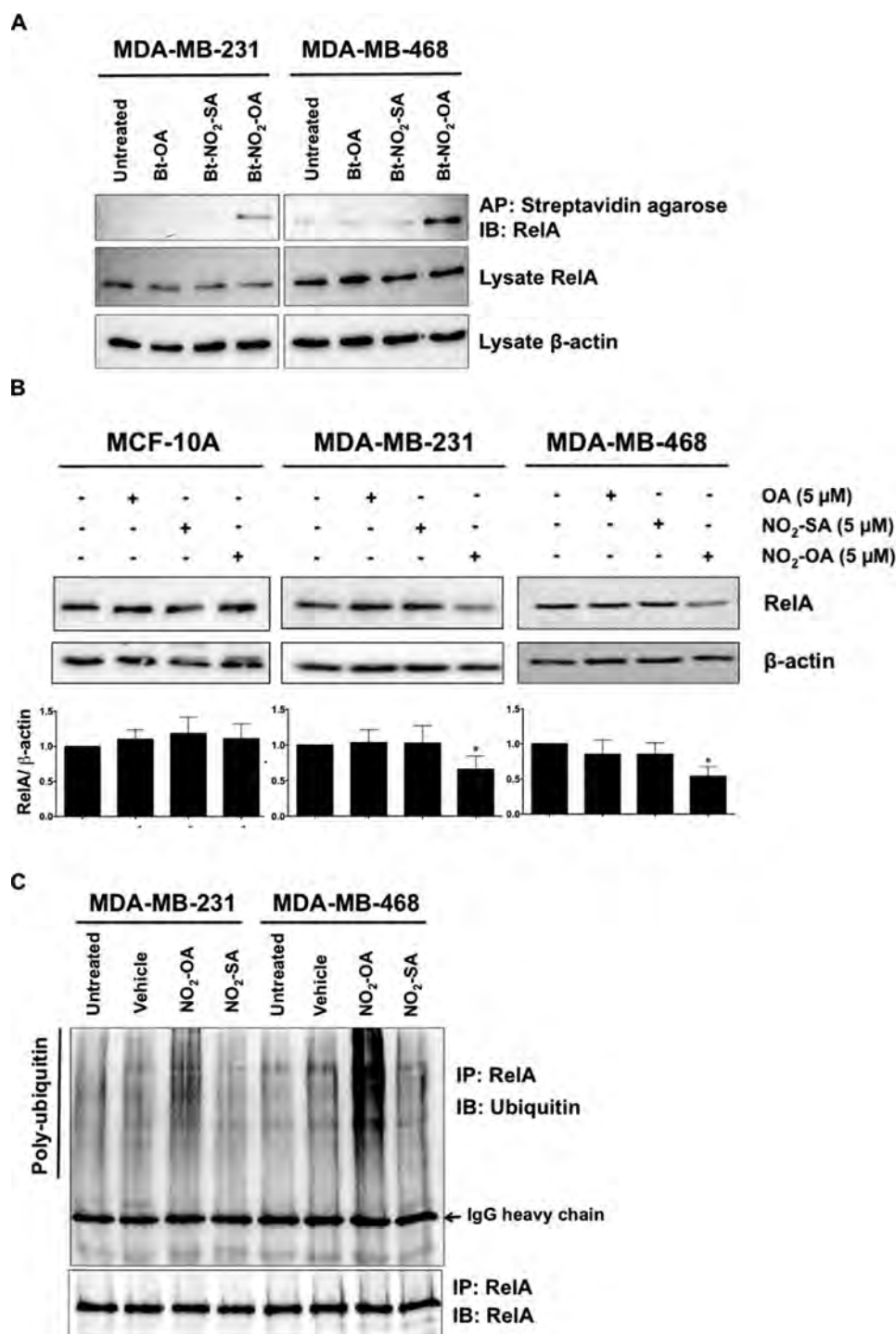


**Figure 8. NO<sub>2</sub>-OA alkylates and destabilizes NF- $\kappa$ B RelA protein in TNBC cells.** *A*, MDA-MB-231 or MDA-MB-468 cells were treated with 5  $\mu$ M Bt-NO<sub>2</sub>-OA, Bt-NO<sub>2</sub>-SA, or Bt-OA for 2 h. After cell lysis, biotinylated NO<sub>2</sub>-FAs with adducts were affinity-purified (AP) using streptavidin-agarose beads. Pulled-down RelA protein was then detected by immunoblotting (IB). RelA and control  $\beta$ -actin immunoblots from the same input lysates used for affinity purification are shown below the panel. *B*, endogenous RelA protein levels were detected by immunoblotting probed with anti-RelA antibody using  $\beta$ -actin as a loading control. The relative total RelA levels (normalized by total  $\beta$ -actin) compared with untreated controls were quantified. \*,  $p < 0.05$  versus untreated control. Significance was determined by one-way analysis of variance followed by Tukey post test. *C*, MDA-MB-231 or MDA-MB-468 cells were treated with vehicle (methanol), NO<sub>2</sub>-OA (5  $\mu$ M), or NO<sub>2</sub>-SA (5  $\mu$ M) for 6 h, and then cell lysates were harvested and immunoprecipitated (IP) by anti-RelA antibody followed by immunoblotting. Pull-down level of immunoprecipitated RelA proteins is shown below the panel.

231 and MDA-MB-468 cells (Fig. 8A), the impact of NO<sub>2</sub>-OA PTMs on RelA protein stability was investigated. To validate this putative mechanism, we first examined whether endogenous RelA protein expression responded to NO<sub>2</sub>-OA. MDA-MB-231, MDA-MB-468, and MCF-10A cells were treated with

5  $\mu$ M NO<sub>2</sub>-OA or control lipids (NO<sub>2</sub>-SA and OA) for 24 h. NO<sub>2</sub>-OA decreased the abundance of RelA in TNBC cells, whereas NO<sub>2</sub>-SA and OA had no effect (Fig. 8B). In contrast, RelA protein levels in MCF-10A cells were not altered by NO<sub>2</sub>-OA (Fig. 8B). In all three cell lines, RelA mRNA levels were

## NO<sub>2</sub>-OA inhibits breast cancer cell function

not altered by NO<sub>2</sub>-OA (Fig. S9). These data indicate that NO<sub>2</sub>-OA impacts RelA protein stability via alkylation of RelA in TNBC cells. RelA is regulated by ubiquitin- and proteasome-dependent degradation signals that govern NF- $\kappa$ B activation (42–44). To determine whether RelA modification by NO<sub>2</sub>-OA induced ubiquitination of endogenous RelA in TNBC cells, MDA-MB-231 or MDA-MB-468 cells were treated with 5  $\mu$ M NO<sub>2</sub>-OA or NO<sub>2</sub>-SA for 5 h. RelA protein was immunoprecipitated, and its polyubiquitination was detected by anti-ubiquitin. NO<sub>2</sub>-OA, but not NO<sub>2</sub>-SA, promoted polyubiquitination of RelA in both TNBC cell lines (Fig. 8C). This indicates that NO<sub>2</sub>-OA interacts with RelA and destabilizes RelA protein by promoting ubiquitination and proteasomal degradation in TNBC cells.

### Discussion

Compared with other breast cancer phenotypes, TNBC is an aggressive subtype with a poor prognosis (3). Patients are 4 times more likely to show visceral metastases to the lung, liver, and brain within 5 years after diagnosis (45). Because TNBC does not respond to endocrine therapy or other more targeted chemotherapeutic agents, DNA damage-inducing strategies, such as ionizing radiation, cisplatin, and doxorubicin, remain mainstay treatments. Adverse systemic responses to DNA-directed chemotherapeutic agents, including cardiac and renal toxicity, limit chemotherapy options because of cytotoxic effects on non-cancerous cells (46–48). Herein, NO<sub>2</sub>-OA inhibited cultured TNBC cell viability, motility, and tumor cell proliferation-related signaling reactions to an extent where *in vivo* tumor growth in MDA-MB-231 xenografted mice was attenuated by oral administration of NO<sub>2</sub>-OA. This initial observation motivates more detailed dose-timing, dose-response, and structure-function studies of nitroalkene-based drug candidates, with respect to effects on tumor growth and metastasis of multiple breast cancer phenotypes, both *in vitro* and in preclinical animal models.

At lower concentrations, there was selective cytotoxicity of NO<sub>2</sub>-OA toward TNBC cells, compared with non-tumorigenic MCF-10A breast ductal epithelial cells. One significant explanation for this selectivity of action stemmed from the analysis of both basal GSH levels and the formation and fate of NO<sub>2</sub>-OA-SG adducts in control and TNBC cells. Because of the abundance and reactivity of the GSH thiolate, GSH is a primary intracellular reaction target of endogenously generated and exogenously administered oxidants and electrophilic species (49). The rate of MRP1-mediated efflux of GSH-adducted electrophiles from cells is important, as it contributes to defining the net intracellular concentration, half-life, alternative reactions with target proteins, and thus the net cellular and tissue responses to lipid electrophiles (1, 50, 51). MRP1 was highly expressed in MCF-10A cells compared with TNBC cells, motivating the LC-MS/MS determination of extracellular NO<sub>2</sub>-OA-SG levels in the media of NO<sub>2</sub>-OA-treated MCF-10A *versus* MDA-MB-231 and MDA-MB-468 cells. Consistent with the relative extents of MRP1 expression, MCF-10A cells formed and exported 4–5-fold greater amounts of NO<sub>2</sub>-OA-SG adducts into the extracellular compartment compared with TNBC cells (Fig. 3A). This more extensive export of NO<sub>2</sub>-

OA-SG by MCF-10A cells, relative to MDA-MB-231 and MDA-MB-468 cells, was also notable because basal GSH concentrations and the GSH/GSSG ratio of MCF-10A cells were more stable after treatment with NO<sub>2</sub>-OA. In contrast, the GSH concentrations and GSH/GSSG ratio in MDA-MB-231 and MDA-MB-468 cells quickly decreased after treatment with NO<sub>2</sub>-OA (Fig. 4). These results indicate that MRP1 export of NO<sub>2</sub>-OA-SG and the more sufficient antioxidant capacity of the MCF10A cell line, as opposed to TNBC cells (52), plays a role in defining the vulnerability of TNBC cells to NO<sub>2</sub>-OA signaling actions. Another electrophile, 2-cyano-3,12-dioxoleana-1,9-dien-28-oic acid (CDDO), displays antitumor activity by inducing apoptosis in a variety of cancers. CDDO rapidly decreases mitochondrial GSH and induces increased generation of reactive species in pancreatic cancer cells (53, 54). In contrast, NO<sub>2</sub>-OA did not significantly impact cellular rates of H<sub>2</sub>O<sub>2</sub> production after both short-term and extended (6-h) treatment of TNBC cells, indicating that NO<sub>2</sub>-OA inhibition of TNBC cell growth and viability are not due to induction of oxidative stress (Fig. S10).

When the MRP1 transport activity of MCF-10A cells was inhibited by the organic acid probenecid (55), a more TNBC-like phenotype was conferred in the context of sensitivity to NO<sub>2</sub>-OA. For example, the impact of NO<sub>2</sub>-OA on cell growth arrest and killing (Fig. 3, C and D), cell cycle arrest (cyclin D1, p21), and apoptosis-regulating mediators (PARP-1, caspase-3) all supported the concept that NO<sub>2</sub>-OA signaling actions are enhanced in MRP1-depleted cells because of more favorable pharmacokinetics in the intracellular compartment. This affirms that the cellular concentrations of GSH, the reaction of GSH with NO<sub>2</sub>-OA, and the subsequent MRP1 export of NO<sub>2</sub>-OA-SG all influence downstream responses to NO<sub>2</sub>-OA. It is possible that other mechanisms, yet to be described, are also responsible for this differentiation of breast epithelial cell responses.

Anti-proliferative actions of NO<sub>2</sub>-OA on macrophages, vascular smooth muscle cells, and fibroblasts are observed in models of chronic vascular and pulmonary disease (56–61), but the impact of fatty acid nitroalkenes on cancer cell proliferation had not been considered. This motivated experimental consideration, because there are a limited number of reports suggesting that the up-regulation of Nrf2 signaling may result in intrinsic or acquired chemoresistance (62). In contrast, we observed the *in vitro* and *in vivo* inhibition of TNBC growth by NO<sub>2</sub>-OA (Fig. 1, B–E). This growth inhibition of TNBC cells was the result of alterations in signaling responses that were specific to TNBC cells and not non-transformed MCF-10A cells. Increased p21 and decreased cyclin D1 expression (Fig. 2D) were observed, along with an increase in the sub-G<sub>1</sub> population of TNBC cells (Fig. 2, A–C). Two distinct pathways of apoptotic signaling were engaged by NO<sub>2</sub>-OA in TNBC cells, initiated by both mitochondria-regulated (caspase-9 activation) and death receptor-regulated (caspase-8 activation; Fig. 2F) mechanisms. In aggregate, these data reveal that NO<sub>2</sub>-OA displays pleiotropic anti-cancer properties via the inhibition of cell proliferation and induction of apoptosis in TNBC. At this point, more detailed mechanisms of NO<sub>2</sub>-OA-induced apoptotic cell death remain to be defined; however, the electrophilic thiocyanate



sulforaphane also decreases Bcl-2 expression, activates cytochrome *c* release from the mitochondria, and increases FasL expression in TNBC cells (30). These actions imply that electrophilic fatty acid nitroalkene derivatives might mediate similar actions in the regulation of apoptosis.

The inhibition of NF- $\kappa$ B signaling by NO<sub>2</sub>-OA also limits TNBC cell migration and invasion. Pro-inflammatory cytokines, such as TNF $\alpha$ , enhance the metastatic potential of TNBC, with the up-regulation of TNF $\alpha$  expression and activity in TNBC patients strongly linked with tumor metastasis phenotype (63). TNF $\alpha$  stimulates the expression of the epithelial-mesenchymal transition and chemokine genes via the activation of AP-1 and NF- $\kappa$ B signaling in TNBC cells (14). Herein, NO<sub>2</sub>-OA significantly inhibited TNF $\alpha$ -induced TNBC cell migration and invasion (Fig. 5). Decreased expression of the pro-metastasis genes uPA and ICAM-1, via a decrease in NF- $\kappa$ B transcriptional activity, was also induced by NO<sub>2</sub>-OA (Fig. 6 (D and E) and Fig. S6 (A and B)). Consistent with this, electrophilic 15-deoxy- $\Delta^{12,14}$ -prostaglandin J<sub>2</sub>, dithiolethione, and dimethyl fumarate also inhibit breast cancer cell migration (38, 64, 65). NO<sub>2</sub>-OA also limited the migration of MDA-MB-231 cells in the absence of TNF $\alpha$  induction (Fig. 5B). It is likely that NO<sub>2</sub>-OA inhibits cell mobility upon reaction with molecular targets in addition to NF- $\kappa$ B, because the electrophilic cyclopentenone 15-deoxy- $\Delta^{12,14}$ -prostaglandin J<sub>2</sub> also interferes with mammary cancer cell migration via inhibition of F-actin reorganization and focal adhesion disassembly (64). Additional studies are in progress to identify other metastasis-related protein targets and signaling pathways that could be impacted by NO<sub>2</sub>-OA-mediated alkylation reactions.

The proteolytic degradation of NF- $\kappa$ B subunits contribute to the termination of NF- $\kappa$ B activation. RelA protein is regulated by ubiquitin- and proteasome-dependent degradation signals that terminate NF- $\kappa$ B activation (42–44, 66). Thiol-alkylating and S-nitrosating agents also promote the degradation of the NF- $\kappa$ B subunit p50 via post-translational modification of Cys-62 in HT29 and HCT116 tumor cell lines (41). Thus, the NO<sub>2</sub>-OA alkylation of NF- $\kappa$ B RelA induces functional responses similar to other alkylating agents (41). Notably, the alkylation of RelA by NO<sub>2</sub>-OA induced an increase in RelA ubiquitination in TNBC cells, an effect not observed for non-electrophilic NO<sub>2</sub>-SA (Fig. 7D). PPAR $\gamma$  acts as an E3 ubiquitin ligase, inducing RelA protein ubiquitination and degradation via physically interacting with RelA protein. The PPAR $\gamma$  ligands troglitazone and pioglitazone increase PPAR $\gamma$  E3 ligase activity by promoting its interaction with RelA protein, in turn, decreasing RelA half-life (67). Because NO<sub>2</sub>-OA is a partial agonist of PPAR $\gamma$  (26), one can speculate that NO<sub>2</sub>-OA also activates PPAR $\gamma$  E3 ligase activity, thus further destabilizing RelA protein in TNBC.

The inhibition of NF- $\kappa$ B signaling represents a viable anticancer strategy, especially because the aberrant activation of NF- $\kappa$ B is closely linked with the development of diverse human cancers (68, 69). The immunomodulatory electrophile dimethyl fumarate, approved by the Food and Drug Administration as an oral drug for treating multiple sclerosis, also inhibits NF- $\kappa$ B activity in breast cancer cells and inhibits TNBC cell proliferation (65). The present results, in which NO<sub>2</sub>-OA inhib-

ited multiple TNBC cell functions (proliferation, survival, mobility, and invasion), imply that electrophilic lipid nitroalkene species may display promising utility as pleiotropic chemotherapeutic agents.

In summary, we report that the lipid electrophile NO<sub>2</sub>-OA impacts NF- $\kappa$ B signaling in TNBC at multiple levels, including the suppression of IKK $\beta$  phosphorylation, inhibition of I $\kappa$ B $\alpha$  degradation, and enhanced ubiquitination and proteasomal degradation of RelA. These actions in turn contribute to the inhibition of TNBC cell migration and invasion *in vitro*. TNBC cells are in part more sensitive to NO<sub>2</sub>-OA due to lower GSH concentrations and suppression of NO<sub>2</sub>-OA export as the NO<sub>2</sub>-OA-SG adduct, a consequence of lower MRP1 expression. This GSH insufficiency-induced redox vulnerability of TNBC cells (70) in turn promotes more extensive protein thiol alkylation and oxidation reactions and instigates chemotherapeutic signaling responses at lower electrophile concentrations. The concentrations of endogenous free NO<sub>2</sub>-FAs, which are not protein-adducted or esterified to complex lipids, in healthy human plasma and urine are typically 1–5 nM (16, 18, 19). The oral administration of NO<sub>2</sub>-OA increased murine tumor NO<sub>2</sub>-OA levels to an extent sufficient to induce pharmacological responses, as evidenced by inhibition of MDA-MB-231 xenograft tumor growth. These results motivate more detailed future investigation of dose-response relationships and the impact of other lipid electrophiles on tumor growth and metastasis. At present, NO<sub>2</sub>-OA has cleared preclinical toxicology and pharmacokinetics testing in human Phase 1 safety trials of both oral and IV formulations (IV IND 122583; oral IND 124524) and is entering Phase 2 trials for treating chronic renal and pulmonary diseases. This present preclinical study provides the biochemical foundations for evaluating whether electrophilic NO<sub>2</sub>-FAs represent a useful new therapeutic candidate for treating breast cancer patients and possibly providing selectivity for treating TNBC, a cancer that currently lacks effective treatment options.

## Experimental procedures

### Cell culture and reagents

Cell lines were purchased from ATCC. MDA-MB-231 and MCF7 cells were cultured in Dulbecco's modified Eagle's medium, and MDA-MD-468 cells were cultured in improved minimum essential medium (Gibco), each supplemented with 5% fetal bovine serum (Hyclone, Logan, UT). MCF-10A cells were cultured in growth medium consisting of Dulbecco's modified Eagle's medium/F-12 (1:1) in 5% horse serum (Hyclone), and supplemented with 0.5  $\mu$ g/ml hydrocortisone, 0.1  $\mu$ g/ml cholera toxin, 20 ng/ml EGF, and 10  $\mu$ g/ml insulin (Sigma-Aldrich). Cells were incubated at 37 °C in a 5% CO<sub>2</sub> atmosphere. siRNAs directed against human RelA (L-003533-00-0005), human MRP1/ABCC1 siRNA (L-007308-00-0005), and non-targeting control siRNA (D-001810-10-05) were purchased from Dharmacon RNAi Technologies. Lipofectamine 2000 or 3000 (Life Technologies) was used for cell transfection. The MRP1 inhibitor Probenecid (4-[(dipropylamino)sulfonyl]benzoic acid) was purchased from Enzo Life Sciences and dissolved in 1 M sodium hydroxide. The NF- $\kappa$ B inhibitor JSH-23

## ***NO<sub>2</sub>-OA inhibits breast cancer cell function***

(4-methyl-*N*<sup>1</sup>-(3-phenyl-propyl)-benzene-1,2-diamine) and proteasome inhibitor MG-132 (benzyloxycarbonyl-L-Leu-D-Leu-L-Leu-al) were purchased from Sigma-Aldrich. The IKK $\beta$  inhibitor BAY11-7082 (3-[(4-methylphenyl)sulfonyl]-(2*E*)-propenenitrile) was purchased from Calbiochem, and TNF $\alpha$  was from BD Biosciences.

### ***Cell treatment for IKK $\beta$ phosphorylation, I $\kappa$ B $\alpha$ phosphorylation, and I $\kappa$ B $\alpha$ degradation***

All studies used two TNBC cell lines, MDA-MB-231 and MDA-MB-468. To determine the effect of NO<sub>2</sub>-OA on IKK $\beta$  phosphorylation induced by TNF $\alpha$  in TNBC cells, cells were pretreated with NO<sub>2</sub>-OA (5  $\mu$ M), NO<sub>2</sub>-SA (5  $\mu$ M), or BAY11-7082 (10  $\mu$ M) in serum-free medium (DMEM containing 0.1% fatty acid-free BSA) for 2 h before TNF $\alpha$  (20 ng/ml) stimulation for 5 min. For I $\kappa$ B $\alpha$  degradation, cells were treated as described above and stimulated for 10 min with 20 ng/ml TNF $\alpha$ . I $\kappa$ B $\alpha$  phosphorylation was measured in cells pretreated with MG-132 (10  $\mu$ M) in combination with NO<sub>2</sub>-OA (5  $\mu$ M), NO<sub>2</sub>-SA (5  $\mu$ M), or BAY11-7082 (10  $\mu$ M) in serum-free medium for 2 h before TNF $\alpha$  (20 ng/ml) stimulation for 10 min.

### ***NO<sub>2</sub>-FA synthesis and use***

OA was purchased from Nu-Chek Prep (Elysian, MN). Nitrostearic acid (NO<sub>2</sub>-SA; 10-nitro-octadecanoic acid) was obtained by the reduction of 10-nitro-oleic acid. Specifically, NO<sub>2</sub>-OA was dissolved in tetrahydrofuran/methanol and cooled, and then sodium borohydride was added. The flask was stirred, and aliquots were monitored by UV analysis until there was full loss of the nitroalkene, and then the reactions were quenched with acetic acid. NO<sub>2</sub>-SA was purified by first adducting any remaining NO<sub>2</sub>-OA with added cysteine, and then NO<sub>2</sub>-SA was chromatographically fractionated on silica gel, using an ethyl acetate/hexane gradient. OA, NO<sub>2</sub>-OA, and NO<sub>2</sub>-SA were dissolved in absolute methanol and diluted in culture medium immediately before use in all experiments, at a maximum methanol concentration of 0.1% (v/v). Biotinylated NO<sub>2</sub>-FAs (Bt-NO<sub>2</sub>-OA, Bt-NO<sub>2</sub>-SA, and Bt-OA) were synthesized from corresponding free fatty acids and biotin-(polyethylene glycol)-amine (see Ref. 27 and supporting Methods).

### ***Cell growth assay***

Cells were plated at a cell density of 5000 cells/well in 96-well plates. After attachment overnight, the medium was replaced, and cells were treated with 0–15  $\mu$ M NO<sub>2</sub>-OA, NO<sub>2</sub>-SA, or 0.1% methanol (vehicle) for 48 h. In an MRP inhibition study, MCF-10A cells were pretreated with 0.25 mM probenecid for 1 h, followed by 0–25  $\mu$ M NO<sub>2</sub>-OA for 48 h. Cells were counted using the FluoReporter dsDNA quantitation kit (Molecular Probes) according to the manufacturer's instructions. Fluorescence was measured using a SpectraMax M2 plate reader (Molecular Devices). The half-maximal inhibitory concentration (IC<sub>50</sub>) of NO<sub>2</sub>-OA was determined by using CalcuSyn software from Biosoft. Three individual experiments were done ( $n = 5$ /each), and statistical comparison between two cell lines across doses was determined by two-way analysis of variance followed by Tukey post-test.

### ***FACS***

MCF-10A, MDA-MB-231, and MDA-MB-468 cells were plated at a cell density of  $2.5 \times 10^5$  cells in 6-well plates for 24 h before treatment with 0.1% methanol (vehicle), 5  $\mu$ M NO<sub>2</sub>-OA, NO<sub>2</sub>-SA, or OA for 24 h. Adherent and nonadherent cells were collected, centrifuged at 2000 rpm for 10 min, washed with ice-cold phosphate-buffered saline, fixed with cold 70% ethanol at 4 °C for 30 min, and stained with 50  $\mu$ g/ml propidium iodide (Sigma-Aldrich). FACS analysis was performed at the University of Pittsburgh Department of Immunology Unified Flow Core Facility. Three individual experiments were done, and statistical comparisons among phases (G<sub>0</sub>/G<sub>1</sub>, S, and G<sub>2</sub>/M) were determined by one-way analysis of variance followed by Tukey post-test.

### ***Cell migration analysis***

MDA-MB-231 and MDA-MB-468 cells were subjected to cell migration analysis in Boyden chambers. The bottom of a 12-well membrane filter (BD Biosciences) was coated with 10  $\mu$ g/ml fibronectin for 12 h before each experiment. Cells were pretreated with 5  $\mu$ M NO<sub>2</sub>-OA or NO<sub>2</sub>-SA for 1 h and then in the absence or presence of TNF $\alpha$  (20 ng/ml) for an additional 2 h in culture medium containing 1% FBS. Cells were trypsinized and washed with migration medium (DMEM containing 0.1% fatty acid-free BSA) to remove serum. Cells at a density of  $10^5$ /well were then placed in the upper chamber with migration medium containing the same pretreatment conditions. The cells were allowed to migrate toward the 5% FBS chemoattractant for 5 h. Non-migrated cells from the top surface were removed with cotton swabs. Migrated cells were fixed with 4% paraformaldehyde (Electron Microscopy Sciences) and then stained with 0.5% crystal violet (Sigma-Aldrich) for 15 min. Migrated cell density on the filters was observed by microscopy. The crystal violet on migrated cells was destained with 10% acetic acid, and the absorbance in individual filters was determined at  $A_{573 \text{ nm}}$ . Images are representative of three individual experiments, and statistical comparison among treatments was determined by one-way analysis of variance followed by Tukey post-test.

### ***Cell invasion assay***

MDA-MB-468 cells were pretreated with NO<sub>2</sub>-OA (5  $\mu$ M), NO<sub>2</sub>-SA (5  $\mu$ M), or NF- $\kappa$ B inhibitor JSH-23 (10  $\mu$ M) for 1 h and then in the absence or presence of TNF $\alpha$  (20 ng/ml) for an additional 2 h in culture medium containing 1% FBS. Cells were then suspended in migration medium and placed in the top well of invasion chambers (EMD Millipore). Chemoattractant (5% FBS) was placed in the lower chamber for 24 h at 37 °C to attract invasive cells. Cells were then harvested, and invasion rates were determined according to the manufacturer's protocol. Three individual experiments were done, and statistical comparison among treatments was determined by one-way analysis of variance followed by Tukey post-test.

### ***Luciferase analysis of NF- $\kappa$ B activity***

Luciferase chemiluminescence-based analysis of NF- $\kappa$ B transcriptional activity was performed as described previously

(27) with minor modifications. MDA-MB-231 and MDA-MB-468 cells (~70% confluence) in 12-well plates were transiently transfected with a NF- $\kappa$ B-luciferase reporter plasmid (Stratagene, La Jolla, CA) with Lipofectamine 3000. After transfection (24 h), cells were pretreated with NO<sub>2</sub>-OA (5  $\mu$ M), NO<sub>2</sub>-SA (5  $\mu$ M), OA (5  $\mu$ M), or JSH-23 (20  $\mu$ M) for 2 h, followed by 20 ng/ml TNF $\alpha$  for an additional 4 h. Each transfection was performed in triplicate. Luciferase activity was measured using the Dual-Luciferase assay kit (Promega). Relative light units (RLU) were measured using a 96-well plate luminometer, according to the manufacturer's instructions (Victor II, PerkinElmer Life Sciences). Protein concentration was determined using the BCA assay (Thermo Fisher Scientific). Data represent the ratio of treated samples to controls in the context of mean RLU/protein content  $\pm$  S.D. Three individual experiments were done, and statistical significance was determined by Kruskal–Wallis test followed by Dunn's post-test with Bonferroni corrections for multiple comparisons.

### NO<sub>2</sub>-FA protein alkylation reactions

To determine whether NO<sub>2</sub>-FAs bind to RelA (p65) or IKK $\beta$  in TNBC cells, MDA-MB-231 or MDA-MB-468 cells were treated with 5  $\mu$ M Bt-NO<sub>2</sub>-OA, Bt-NO<sub>2</sub>-SA, or Bt-OA in DMEM containing 5% FBS. After 2 h, cells were harvested in lysis buffer containing 1% Triton X, 10% glycerol, 150 mM NaCl, 10 mM HEPES, 1 mM EDTA, 1 mM EGTA and supplemented with a mixture of protease and phosphatase inhibitors (Roche Applied Science) (26). Total cell lysates (0.5–1 mg) were mixed and incubated with streptavidin-agarose beads (Sigma-Aldrich) at 4 °C overnight. Beads were washed three times using lysis buffer. After SDS-PAGE, immunoblotting was performed using anti-RelA mouse monoclonal antibody (Santa Cruz Biotechnology) or anti-IKK $\beta$  rabbit polyclonal antibody (Cell Signaling). Proteomics analysis for the alkylation of RelA by NO<sub>2</sub>-OA was also conducted using recombinant RelA protein and LC-MS/MS analysis. See [supporting Methods](#) for more detail.

### Immunoprecipitation and NO<sub>2</sub>-OA-induced RelA protein polyubiquitination

To determine the induction level of RelA protein polyubiquitination by NO<sub>2</sub>-FA, MDA-MB-231 and MDA-MB-468 cells were treated with 0.1% methanol (vehicle), NO<sub>2</sub>-OA (5  $\mu$ M), or NO<sub>2</sub>-SA (5  $\mu$ M) for 6 h, and then cell lysates were harvested in lysis buffer supplemented with a mixture of protease and phosphatase inhibitors. Lysates were clarified by centrifugation at 14,000  $\times$  g for 10 min. Protein lysates (1 mg) were incubated with anti-RelA antibody and Protein G/A-conjugated agarose beads (EMD Millipore, Bedford, MA) at 4 °C overnight. Immunoprecipitation fractions were obtained by centrifugation at 14,000  $\times$  g for 1 min at room temperature and washed with lysis buffer three times. The immunoprecipitated RelA was resolved by an 8% SDS-polyacrylamide gel and transferred to nitrocellulose membrane (Bio-Rad) for immunoblotting probed with an anti-ubiquitin antibody (Santa Cruz Biotechnology). The blot was then stripped and probed with an anti-RelA antibody to assess amounts of RelA protein pull-down.

### Western blotting

Western blotting was performed as described previously (26). 20–60  $\mu$ g of total lysates per lane were loaded on 7, 10, or 12% SDS-PAGE and transferred onto nitrocellulose or polyvinylidene difluoride membranes (Bio-Rad). The membranes were probed with primary antibodies against caspase-3, MRP1, PARP-1, ubiquitin, or RelA; cyclin D1, p21, caspase-9, MRP4, IKK $\beta$ , pIKK $\beta$ , I $\kappa$ B $\alpha$ , or pI $\kappa$ B $\alpha$  (Cell Signaling); and caspase-8 (R&D Systems). Samples were normalized to  $\beta$ -actin (Sigma-Aldrich) or GAPDH (Trevigen). Protein bands were visualized, and digitized images were quantified using ImageLab software (Bio-Rad). Immunoblots are representative of at least three individual experiments. Quantitative results are an average of at least three individual experiments, and statistical significance was determined by one-way analysis of variance followed by Tukey post-test.

### RNA extraction, quantitative PCR, and RT<sup>2</sup> profiler PCR array

To determine the effect of NO<sub>2</sub>-OA on expression of NF- $\kappa$ B target genes in TNF $\alpha$ -induced MDA-MB-231 and MDA-MB-468 cells, cells were pretreated with NO<sub>2</sub>-OA (5  $\mu$ M) for 2 h and then stimulated with TNF $\alpha$  (20 ng/ml) for 6 h. Total RNA samples of tissues or cells were extracted using TRIzol reagents according to the manufacturer's instructions (Invitrogen). Total RNA (1  $\mu$ g) was reverse transcribed using the iScript cDNA kit (Bio-Rad) according to the manufacturer's instructions. cDNA (25 ng) was used for each subsequent real-time qPCR. All real-time qPCR was performed on the StepOne PLUS PCR system (Thermo Fisher Scientific) using TaqMan gene expression assays. -Fold change was calculated using the  $\Delta\Delta C_t$  method with 18S ribosomal RNA or human  $\beta$ -actin RNA serving as the internal control. Three individual experiments were done, and statistical significance was determined by one-way analysis of variance followed by Tukey post-test. For the RT<sup>2</sup> profiler PCR array, MDA-MB-468 cells were treated or untreated with NO<sub>2</sub>-OA (5  $\mu$ M) for 24 h. The expression of 84 human NF- $\kappa$ B target genes was analyzed with a 96-well plate format as instructed in the manufacturer's handbook (Qiagen). PCR amplification was conducted by the StepOne PLUS PCR system, and -fold change of gene expression was calculated according to the manufacturer's instructions.

### Analysis of NO<sub>2</sub>-OA-SG and NO<sub>2</sub>-OA in cell medium

MCF-10A, MDA-MB-231, or MDA-MB-468 cells were cultured in 6-well plates (1  $\times$  10<sup>6</sup> cells/well) for 24 h. Before treatments, cell medium was replaced with DMEM containing 5% FBS. NO<sub>2</sub>-OA (5  $\mu$ M) was added to the medium, and cells were incubated at 37 °C for 60 min before the cell culture medium was collected. For MRP1 inhibition studies, MCF-10A cells were pretreated with 1 mM probenecid for 1 h and then co-treated with 5  $\mu$ M NO<sub>2</sub>-OA for an additional 1 h. For MRP1 siRNA knockdown studies, MCF-10A cells were transiently transfected with non-target siRNA (scrambled) or MRP1 siRNA for 48 h before treatment with 5  $\mu$ M NO<sub>2</sub>-OA for 1 h. Cells were washed with PBS and then gently scraped off of the plate in 1 ml of PBS. 100  $\mu$ l of cell suspensions was lysed by sonication and used for protein concentration measurements via a BCA protein assay. The remaining 0.9 ml of cell suspen-

## NO<sub>2</sub>-OA inhibits breast cancer cell function

sion was used to determine the amount of intracellular NO<sub>2</sub>-OA-SG. NO<sub>2</sub>-OA-SG and free NO<sub>2</sub>-OA were extracted using a modified Bligh-Dyer method with NO<sub>2</sub>-OA-SG partitioning into the polar phase and NO<sub>2</sub>-OA into the organic. The cell culture medium was spiked with <sup>15</sup>NO<sub>2</sub>-d<sub>4</sub>-OA (5 nM) as an internal standard for free NO<sub>2</sub>-OA before extraction. Samples were centrifuged at 2800 rpm at room temperature for 5 min. The bottom (organic) layer was transferred to a clean vial, dried, and reconstituted in methanol before MS analysis. The upper (aqueous) layer containing NO<sub>2</sub>-OA-SG was desalted and concentrated using 3 ml of C18 SPE columns (Thermo Fisher Scientific). Columns were preconditioned with 1 column volume of 100% methanol, followed by 2 column volumes of 5% methanol before sample addition. Samples were vortexed and equilibrated at 4 °C for 5 min before extraction. Samples were washed with 2 column volumes of 5% methanol, and the column was dried under vacuum for 30 min before elution with 3 ml of 100% methanol. Solvent was then evaporated under N<sub>2</sub>, and the samples were reconstituted in methanol for further analysis.

### GSH and GSSG extraction and analysis

MCF-10A, MDA-MB-231, and MDA-MB-468 cells were seeded in 24-well plates at a density of 3 × 10<sup>5</sup> cells/well. Cells were cultured overnight before treatment with 5 μM NO<sub>2</sub>-OA for the indicated times. At each time point, cell medium was aspirated and washed two times with sterile PBS. Cells were then incubated with PBS containing 25 mM *N*-ethylmaleimide (NEM) for 15 min at 37 °C. Derivatizing solution (50 μl of 15% MeOH, 40 mM HEPES, 50 mM NaCl, 1 mM EDTA, 2 μM [<sup>13</sup>C<sub>2</sub><sup>15</sup>N]GSH, 2 μM [<sup>13</sup>C<sub>4</sub><sup>15</sup>N<sub>2</sub>]GSSG, and 25 mM NEM) was added to each well and incubated for 15 min at room temperature. Next, 50 μl of 10% (w/v) sulfosalicylic acid solution was immediately added to each well to stabilize GSH and GSSG. Supernatant was collected by centrifugation at 15,000 rpm for 10 min at 4 °C. Samples were diluted 1:5 in 5% sulfosalicylic acid, and 20 μl was injected for HPLC-MS/MS analysis. Cell numbers at time 0 were quantitated by a Hoechst 33258 DNA stain assay and used to normalize GSH or GSSG levels expressed as nmol/cells (× 10<sup>6</sup>).

### LC-MS/MS

NO<sub>2</sub>-OA, NO<sub>2</sub>-OA-SG, GSH, and GSSG were analyzed by high-performance LC-MS/MS using a Shimadzu/CTC PAL HPLC coupled to a Sciex 5000 triple quadrupole mass spectrometer (Sciex, San Jose, CA). NO<sub>2</sub>-OA, NO<sub>2</sub>-OA-SG gradient solvent systems consisted of water + 0.1% acetic acid (solvent A) and acetonitrile + 0.1% acetic acid (solvent B). NO<sub>2</sub>-OA and its metabolites were resolved using a Luna C18 reversed phase column (2 mm × 100 mm, Phenomenex, Torrance, CA) at a flow rate of 0.65 ml/min. Samples were applied to the column at 30% B and eluted with a linear increase in solvent B (30–100% in 9.7 min). The column was washed at 100% B for 3 min before returning to initial conditions for equilibration (2 min). NO<sub>2</sub>-OA-SG conjugates were resolved using a Luna C18 reversed phase column (2 mm × 150 mm; Phenomenex) at a 0.25 ml/min flow rate. Samples were applied to the column at 20% B, held for 5 min, and eluted with a linear increase in solvent B

(20–98% solvent B in 20 min), followed by a wash step at 98% B for 4.5 min, and switched back to initial conditions for 4 min. MS analyses for NO<sub>2</sub>-FAs used electrospray ionization in the negative-ion mode with the collision gas set at 5 units, curtain gas at 40 units, ion source gas number 1 at 55 units and number 2 at 60 units, ion spray voltage at –4500 V, and temperature at 600 °C. The declustering potential was –80 eV, entrance potential –5, collision energy –35, and the collision exit potential –3. Multiple-reaction monitoring (MRM) was used for the analysis of lipids showing loss of a nitro group (*m/z* 46) upon collision-induced dissociation (MRM: 326.2/46 and 331/47 for NO<sub>2</sub>-OA and <sup>15</sup>NO<sub>2</sub>-d<sub>4</sub>-OA, respectively) in negative-ion mode. The following parameters for the mass spectrometers were used for NO<sub>2</sub>-OA-SG conjugates in positive-ion mode: gas number 1, 50 units; gas number 2, 55 units; ion spray voltage, 5000 V; source temperature, 550 °C; declustering potential, 70 eV; entrance potential, 5; collision energy, 17; and collision exit potential, 5. The following MRM transitions were used: 635.2/506.2 and 640.2/511.2 for NO<sub>2</sub>-OA-SG and <sup>15</sup>NO<sub>2</sub>-d<sub>4</sub>-OA-SG (Fig. S7), respectively.

The method for simultaneous determination of GSH and GSSG involved sample (20 μl) separation on a Phenomenex C18 (2.1 × 150 mm; 3.5-μm pore size) column. The solvent system employed aqueous 0.1% formic acid (A) and 0.1% formic acid in acetonitrile (B) with a net flow rate of 0.6 ml/min. A linear gradient of 2% B to 75% B from 0.1 to 6.2 min, followed by wash with 100% B for 2 min and re-equilibration with 2% B for 6 min, was employed for separation. Unlabeled and <sup>13</sup>C<sub>4</sub><sup>15</sup>N<sub>2</sub>-labeled GSSG eluted at 2 min, whereas unlabeled and <sup>13</sup>C<sub>2</sub><sup>15</sup>N-labeled GS-NEM eluted at ~2.7 min. The Sciex 5000 mass spectrometer settings were as follows: CAD, 4 units; curtain gas, 40 units; GS1, 45 units; GS2, 50 units; ion spray voltage, 5500 V; source temperature, 550 °C; EP, 5 V; and CXP, 10 V. Multiple-reaction monitoring was performed in positive-ion mode. Transitions for respective species were as follows: GSH (Q1 308.3 → Q3 179.1; declustering potential (DP) 60 V, collision energy (CE) 18.5 V). <sup>13</sup>C<sub>2</sub><sup>15</sup>N GSH (Q1 311.3 → Q3 182.1; DP 60 V, CE 18.5 V). GS-NEM (Q1 433.0 → Q3 304.2; DP 65 V, CE 38 V); [<sup>13</sup>C<sub>2</sub><sup>15</sup>N]GS-NEM (Q1 436.0 → Q3 307.2; DP 65 V, CE 38 V); GSSG (Q1 613.2 → Q3 355.2; DP 60 V, CE 24 V); [<sup>13</sup>C<sub>2</sub><sup>15</sup>N]GSSG (Q1 619.2 → Q3 361.2; DP 60 V, CE 24 V). Calibration curves were generated using known GSH and GSSG standards and isotopic internal standards and showed linearity over 5 orders of magnitude, and the limit of quantification (71) for both GS-NEM and GSSG was 1 nM. Sample [GSH] and [GSSG] were determined from analyte/internal standard area ratios, and intracellular GSH and GSSG were normalized to cell number (10<sup>6</sup>), with results expressed as nmol of GSH or GSSG per 10<sup>6</sup> cells.

### Statistical analysis

Data analyses were conducted using Prism version 6 software (GraphPad Software). Results are presented as mean ± S.D. tumor volumes except in Fig. 1E, where results are presented as mean ± S.E. Statistical analysis was performed using Student's *t* test, one-way or two-way analysis of variance as appropriate. Statistical significance was achieved with *p* < 0.05.

**Author contributions**—C.-S. C. W., B. A. F., N. E. D., C. N., S. G. W., and Y. H. conceived the project; C.-S. C. W., Y. H., S. R. W., S. R. S., B. S., F. G.-B., and S. G. W. performed experimental studies; and all authors contributed to the writing of the manuscript.

**Acknowledgments**—We thank Dr. Chunyu Cao for technical assistance with xenograft tumor studies and Drs. Steffi Oesterreich and Abdolreza Zarnegar (University of Pittsburgh) for helpful discussions and comments on the manuscript.

## References

- Alexander, R. L., Bates, D. J., Wright, M. W., King, S. B., and Morrow, C. S. (2006) Modulation of nitrated lipid signaling by multidrug resistance protein 1 (MRP1): glutathione conjugation and MRP1-mediated efflux inhibit nitrooleic acid-induced, PPAR $\gamma$ -dependent transcription activation. *Biochemistry* **45**, 7889–7896 [CrossRef Medline](#)
- Brenton, J. D., Carey, L. A., Ahmed, A. A., and Caldas, C. (2005) Molecular classification and molecular forecasting of breast cancer: ready for clinical application? *J. Clin. Oncol.* **23**, 7350–7360 [CrossRef Medline](#)
- Bauer, K. R., Brown, M., Cress, R. D., Parise, C. A., and Caggiano, V. (2007) Descriptive analysis of estrogen receptor (ER)-negative, progesterone receptor (PR)-negative, and HER2-negative invasive breast cancer, the so-called triple-negative phenotype. *Cancer* **109**, 1721–1728 [CrossRef Medline](#)
- Smith, C., Mitchinson, M. J., Aruoma, O. I., and Halliwell, B. (1992) Stimulation of lipid peroxidation and hydroxyl-radical generation by the contents of human atherosclerotic lesions. *Biochem. J.* **286**, 901–905 [CrossRef Medline](#)
- Dent, R., Trudeau, M., Pritchard, K. I., Hanna, W. M., Kahn, H. K., Sawka, C. A., Lickley, L. A., Rawlinson, E., Sun, P., and Narod, S. A. (2007) Triple-negative breast cancer: clinical features and patterns of recurrence. *Clin. Cancer Res.* **13**, 4429–4434 [CrossRef Medline](#)
- Kwan, M. L., Kushi, L. H., Weltzien, E., Maring, B., Kutner, S. E., Fulton, R. S., Lee, M. M., Ambrosone, C. B., and Caan, B. J. (2009) Epidemiology of breast cancer subtypes in two prospective cohort studies of breast cancer survivors. *Breast Cancer Res.* **11**, R31 [CrossRef Medline](#)
- Heitz, F., Harter, P., Lueck, H.-J., Fissler-Eckhoff, A., Lorenz-Salehi, F., Scheil-Bertram, S., Traut, A., and du Bois, A. (2009) Triple-negative and HER2-overexpressing breast cancers exhibit an elevated risk and an earlier occurrence of cerebral metastases. *Eur. J. Cancer* **45**, 2792–2798 [CrossRef Medline](#)
- Dawood, S., Broglio, K., Esteva, F. J., Yang, W., Kau, S.-W., Islam, R., Albarracin, C., Yu, T. K., Green, M., Hortobagyi, G. N., and Gonzalez-Angulo, A. M. (2009) Survival among women with triple receptor-negative breast cancer and brain metastases. *Ann. Oncol.* **20**, 621–627 [CrossRef Medline](#)
- Huber, M. A., Azoitei, N., Baumann, B., Grünert S., Sommer, A., Pehamberger, H., Kraut, N., Beug, H., and Wirth, T. (2004) NF- $\kappa$ B is essential for epithelial-mesenchymal transition and metastasis in a model of breast cancer progression. *J. Clin. Invest.* **114**, 569–581 [CrossRef Medline](#)
- Nakshatri, H., Bhat-Nakshatri, P., Martin, D. A., Goulet, R. J., Jr., and Sledge, G. W., Jr. (1997) Constitutive activation of NF- $\kappa$ B during progression of breast cancer to hormone-independent growth. *Mol. Cell Biol.* **17**, 3629–3639 [CrossRef Medline](#)
- Biswas, D. K., Shi, Q., Baily, S., Strickland, I., Ghosh, S., Pardee, A. B., and Iglehart, J. D. (2004) NF- $\kappa$ B activation in human breast cancer specimens and its role in cell proliferation and apoptosis. *Proc. Natl. Acad. Sci. U.S.A.* **101**, 10137–10142 [CrossRef Medline](#)
- Sovak, M. A., Bellas, R. E., Kim, D. W., Zanieski, G. J., Rogers, A. E., Traish, A. M., and Sonenshein, G. E. (1997) Aberrant nuclear factor- $\kappa$ B/Rel expression and the pathogenesis of breast cancer. *J. Clin. Invest.* **100**, 2952–2960 [CrossRef Medline](#)
- Yamaguchi, N., Ito, T., Azuma, S., Ito, E., Honma, R., Yanagisawa, Y., Nishikawa, A., Kawamura, M., Imai, J., Watanabe, S., Semba, K., and Inoue, J. (2009) Constitutive activation of nuclear factor- $\kappa$ B is preferentially involved in the proliferation of basal-like subtype breast cancer cell lines. *Cancer Science* **100**, 1668–1674 [CrossRef Medline](#)
- Qiao, Y., He, H., Jonsson, P., Sinha, I., Zhao, C., and Dahlman-Wright, K. (2016) AP-1 is a key regulator of proinflammatory cytokine TNF $\alpha$ -mediated triple-negative breast cancer progression. *J. Biol. Chem.* **291**, 5068–5079 [CrossRef Medline](#)
- Li, H.-H., Zhu, H., Liu, L.-S., Huang, Y., Guo, J., Li, J., Sun, X.-P., Chang, C.-X., Wang, Z.-H., and Zhai, K. (2015) Tumour necrosis factor- $\alpha$  gene polymorphism is associated with metastasis in patients with triple negative breast cancer. *Sci. Rep.* **5**, 10244 [CrossRef Medline](#)
- Bonacci, G., Baker, P. R. S., Salvatore, S. R., Shores, D., Khoo, N. K. H., Koenitzer, J. R., Vitturi, D. A., Woodcock, S. R., Golin-Bisello, F., Cole, M. P., Watkins, S., St Croix, C., Batthyany, C. I., Freeman, B. A., and Schopfer, F. J. (2012) Conjugated linoleic acid is a preferential substrate for fatty acid nitration. *J. Biol. Chem.* **287**, 44071–44082 [CrossRef Medline](#)
- Fazzari, M., Khoo, N. K., Woodcock, S. R., Jorkasky, D. K., Li, L., Schopfer, F. J., and Freeman, B. A. (2017) Nitro-fatty acid pharmacokinetics in the adipose tissue compartment. *J. Lipid Res.* **58**, 375–385 [Medline CrossRef](#)
- Salvatore, S. R., Vitturi, D. A., Baker, P. R., Bonacci, G., Koenitzer, J. R., Woodcock, S. R., Freeman, B. A., and Schopfer, F. J. (2013) Characterization and quantification of endogenous fatty acid nitroalkene metabolites in human urine. *J. Lipid Res.* **54**, 1998–2009 [CrossRef Medline](#)
- Delmastro-Greenwood, M., Hughan, K. S., Vitturi, D. A., Salvatore, S. R., Grimes, G., Potti, G., Shiva, S., Schopfer, F. J., Gladwin, M. T., Freeman, B. A., and Gelhaus Wendell, S. (2015) Nitrite and nitrate-dependent generation of anti-inflammatory fatty acid nitroalkenes. *Free Radic. Biol. Med.* **89**, 333–341 [CrossRef Medline](#)
- Hughan, K. S., Wendell, S. G., Delmastro-Greenwood, M., Helbling, N., Corey, C., Bellavia, L., Potti, G., Grimes, G., Goodpaster, B., Kim-Shapiro, D. B., Shiva, S., Freeman, B. A., and Gladwin, M. T. (2017) Conjugated linoleic acid modulates clinical responses to oral nitrite and nitrate. *Hypertension* **70**, 634–644 [CrossRef Medline](#)
- Schopfer, F. J., Cipollina, C., and Freeman, B. A. (2011) Formation and signaling actions of electrophilic lipids. *Chem. Rev.* **111**, 5997–6021 [CrossRef Medline](#)
- Baker, L. M. S., Baker, P. R. S., Golin-Bisello, F., Schopfer, F. J., Fink, M., Woodcock, S. R., Branchaud, B. P., Radi, R., and Freeman, B. A. (2007) Nitro-fatty acid reaction with glutathione and cysteine: kinetic analysis of thiol alkylation by a Michael addition reaction. *J. Biol. Chem.* **282**, 31085–31093 [CrossRef Medline](#)
- Codreanu, S. G., Ullery, J. C., Zhu, J., Tallman, K. A., Beavers, W. N., Porter, N. A., Marnett, L. J., Zhang, B., and Liebler, D. C. (2014) Alkylation damage by lipid electrophiles targets functional protein systems. *Mol. Cell Proteomics* **13**, 849–859 [CrossRef Medline](#)
- Levonen, A. L., Hill, B. G., Kansanen, E., Zhang, J., and Darley-Usmar, V. M. (2014) Redox regulation of antioxidants, autophagy, and the response to stress: implications for electrophile therapeutics. *Free Radic. Biol. Med.* **71**, 196–207 [CrossRef Medline](#)
- Kansanen, E., Bonacci, G., Schopfer, F. J., Kuosmanen, S. M., Tong, K. I., Leinonen, H., Woodcock, S. R., Yamamoto, M., Carlberg, C., Ylä-Herttuala, S., Freeman, B. A., and Levonen, A.-L. (2011) Electrophilic nitro-fatty acids activate NRF2 by a KEAP1 cysteine 151-independent mechanism. *J. Biol. Chem.* **286**, 14019–14027 [CrossRef Medline](#)
- Schopfer, F. J., Cole, M. P., Groeger, A. L., Chen, C.-S., Khoo, N. K. H., Woodcock, S. R., Golin-Bisello, F., Motanya, U. N., Li, Y., Zhang, J., Garcia-Barrio, M. T., Rudolph, T. K., Rudolph, V., Bonacci, G., Baker, P. R. S., et al. (2010) Covalent peroxisome proliferator-activated receptor  $\gamma$  adduction by nitro-fatty acids: selective ligand activity and anti-diabetic signaling actions. *J. Biol. Chem.* **285**, 12321–12333 [CrossRef Medline](#)
- Cui, T., Schopfer, F. J., Zhang, J., Chen, K., Ichikawa, T., Baker, P. R. S., Batthyany, C., Chacko, B. K., Feng, X., Patel, R. P., Agarwal, A., Freeman, B. A., and Chen, Y. E. (2006) Nitrated fatty acids: endogenous anti-inflammatory signaling mediators. *J. Biol. Chem.* **281**, 35686–35698 [CrossRef Medline](#)
- Villacorta, L., Chang, L., Salvatore, S. R., Ichikawa, T., Zhang, J., Petrovic-Djergovic, D., Jia, L., Carlsen, H., Schopfer, F. J., Freeman, B. A., and Chen, Y. E. (2013) Electrophilic nitro-fatty acids inhibit vascular inflammation

- by disrupting LPS-dependent TLR4 signalling in lipid rafts. *Cardiovasc. Res.* **98**, 116–124 [CrossRef Medline](#)
29. Snyder, N. W., Golin-Bisello, F., Gao, Y., Blair, I. A., Freeman, B. A., and Wendell, S. G. (2015) 15-Oxoicosatetraenoic acid is a 15-hydroxyprostaglandin dehydrogenase-derived electrophilic mediator of inflammatory signaling pathways. *Chem. Biol. Interact.* **234**, 144–153 [CrossRef Medline](#)
  30. Pledgie-Tracy, A., Sobolewski, M. D., and Davidson, N. E. (2007) Sulforaphane induces cell type-specific apoptosis in human breast cancer cell lines. *Mol. Cancer Ther.* **6**, 1013–1021 [CrossRef Medline](#)
  31. So, J. Y., Lin, J. J., Wahler, J., Liby, K. T., Sporn, M. B., and Suh, N. (2014) A synthetic triterpenoid CDDO-Im inhibits tumorsphere formation by regulating stem cell signaling pathways in triple-negative breast cancer. *PLoS One* **9**, e107616 [CrossRef Medline](#)
  32. Rudnicki, M., Faine, L. A., Dehne, N., Namgaladze, D., Ferderbar, S., Weinlich, R., Amarante-Mendes, G. P., Yan, C. Y., Krieger, J. E., Brüne, B., and Abdalla, D. S. (2011) Hypoxia inducible factor-dependent regulation of angiogenesis by nitro-fatty acids. *Arterioscler. Thromb. Vasc. Biol.* **31**, 1360–1367 [CrossRef Medline](#)
  33. Lin, D., Saleh, S., and Liebler, D. C. (2008) Reversibility of covalent electrophile-protein adducts and chemical toxicity. *Chem. Res. Toxicol.* **21**, 2361–2369 [CrossRef Medline](#)
  34. Koenitzer, J. R., Bonacci, G., Woodcock, S. R., Chen, C. S., Cantu-Medellin, N., Kelley, E. E., and Schopfer, F. J. (2016) Fatty acid nitroalkenes induce resistance to ischemic cardiac injury by modulating mitochondrial respiration at complex II. *Redox Biol.* **8**, 1–10 [CrossRef Medline](#)
  35. Moody, W. E., Ferro, C. J., Edwards, N. C., Chue, C. D., Lin, E. L., Taylor, R. J., Cockwell, P., Steeds, R. P., Townend, J. N., and CRIB-Donor Study Investigators (2016) Cardiovascular effects of unilateral nephrectomy in living kidney donors. *Hypertension* **67**, 368–377 [Medline](#)
  36. Shin, H.-M., Kim, M.-H., Kim, B. H., Jung, S.-H., Kim, Y. S., Park, H. J., Hong, J. T., Min, K. R., and Kim, Y. (2004) Inhibitory action of novel aromatic diamine compound on lipopolysaccharide-induced nuclear translocation of NF- $\kappa$ B without affecting I $\kappa$ B degradation. *FEBS Lett.* **571**, 50–54 [CrossRef Medline](#)
  37. Evani, S. J., Prabhu, R. G., Gnanaruban, V., Finol, E. A., and Ramasubramanian, A. K. (2013) Monocytes mediate metastatic breast tumor cell adhesion to endothelium under flow. *FASEB J.* **27**, 3017–3029 [CrossRef Medline](#)
  38. Switzer, C. H., Cheng, R. Y.-S., Ridnour, L. A., Murray, M. C., Tazzari, V., Sparatore, A., Del Soldato, P., Hines, H. B., Glynn, S. A., Ambs, S., and Wink, D. A. (2012) Dithiolethiones inhibit NF- $\kappa$ B activity via covalent modification in human estrogen receptor-negative breast cancer. *Cancer Res.* **72**, 2394–2404 [CrossRef Medline](#)
  39. Rossi, A., Kapahi, P., Natoli, G., Takahashi, T., Chen, Y., Karin, M., and Santoro, M. G. (2000) Anti-inflammatory cyclopentenone prostaglandins are direct inhibitors of I $\kappa$ B kinase. *Nature* **403**, 103–108 [CrossRef Medline](#)
  40. Ahmad, R., Raina, D., Meyer, C., Kharbanda, S., and Kufe, D. (2006) Triterpenoid CDDO-Me blocks the NF- $\kappa$ B pathway by direct inhibition of IKK $\beta$  on Cys-179. *J. Biol. Chem.* **281**, 35764–35769 [CrossRef Medline](#)
  41. Paranjpe, A., and Srivenugopal, K. S. (2013) Degradation of NF- $\kappa$ B, p53 and other regulatory redox-sensitive proteins by thiol-conjugating and -nitrosylating drugs in human tumor cells. *Carcinogenesis* **34**, 990–1000 [CrossRef Medline](#)
  42. Natoli, G., and Chiocca, S. (2008) Nuclear ubiquitin ligases, NF- $\kappa$ B degradation, and the control of inflammation. *Sci. Signal.* **1**, pe1 [Medline](#)
  43. Tanaka, T., Grusby, M. J., and Kaisho, T. (2007) PDLIM2-mediated termination of transcription factor NF- $\kappa$ B activation by intranuclear sequestration and degradation of the p65 subunit. *Nat. Immunol.* **8**, 584–591 [CrossRef Medline](#)
  44. Ryo, A., Suizu, F., Yoshida, Y., Perrem, K., Liou, Y.-C., Wulf, G., Rottapel, R., Yamaoka, S., and Lu, K. P. (2003) Regulation of NF- $\kappa$ B signaling by Pin1-dependent prolyl isomerization and ubiquitin-mediated proteolysis of p65/RelA. *Mol. Cell* **12**, 1413–1426 [CrossRef Medline](#)
  45. Dent, R., Hanna, W. M., Trudeau, M., Rawlinson, E., Sun, P., and Narod, S. A. (2009) Pattern of metastatic spread in triple-negative breast cancer. *Breast Cancer Res. Treat.* **115**, 423–428 [CrossRef Medline](#)
  46. Wang, W., Li, C., and Yang, T. (2015) Protection of nitro-fatty acid against kidney diseases. *Am. J. Physiol. Renal Physiol.* **310**, F697–F704 [CrossRef Medline](#)
  47. Wang, H., Jia, Z., Sun, J., Xu, L., Zhao, B., Yu, K., Yang, M., Yang, T., and Wang, R. (2015) Nitrooleic acid protects against cisplatin nephropathy: role of COX-2/mPGES-1/PGE2 cascade. *Mediators Inflamm.* **2015**, 293474 [CrossRef Medline](#)
  48. Liu, S., Jia, Z., Zhou, L., Liu, Y., Ling, H., Zhou, S. F., Zhang, A., Du, Y., Guan, G., and Yang, T. (2013) Nitro-oleic acid protects against adriamycin-induced nephropathy in mice. *Am. J. Physiol. Renal Physiol.* **305**, F1533–F1541 [CrossRef Medline](#)
  49. Batthyany, C., Schopfer, F. J., Baker, P. R., Duran, R., Baker, L. M., Huang, Y., Cervenansky, C., Branchaud, B. P., and Freeman, B. A. (2006) Reversible post-translational modification of proteins by nitrated fatty acids *in vivo*. *J. Biol. Chem.* **281**, 20450–20463 [CrossRef Medline](#)
  50. Sibhatu, M. B., Smitherman, P. K., Townsend, A. J., and Morrow, C. S. (2008) Expression of MRP1 and GSTP1-1 modulate the acute cellular response to treatment with the chemopreventive isothiocyanate, sulforaphane. *Carcinogenesis* **29**, 807–815 [CrossRef Medline](#)
  51. Song, N.-Y., Kim, D.-H., Kim, E.-H., Na, H.-K., Kim, N.-J., Suh, Y.-G., and Surh, Y.-J. (2011) Multidrug resistance-associated protein 1 mediates 15-deoxy- $\Delta$ 12,14-prostaglandin J<sub>2</sub>-induced expression of glutamate cysteine ligase expression via Nrf2 signaling in human breast cancer cells. *Chem. Res. Toxicol.* **24**, 1231–1241 [CrossRef Medline](#)
  52. Alli, E., Sharma, V. B., Sunderesakumar, P., and Ford, J. M. (2009) Defective repair of oxidative DNA damage in triple-negative breast cancer confers sensitivity to inhibition of poly(ADP-ribose) polymerase. *Cancer Res.* **69**, 3589–3596 [CrossRef Medline](#)
  53. Samudio, I., Konopleva, M., Hail, N., Shi, Y.-X., McQueen, T., Hsu, T., Evans, R., Honda, T., Gribble, G. W., Sporn, M., Gilbert, H. F., Safe, S., and Andreeff, M. (2005) 2-Cyano-3,12-dioxooleana-1,9-dien-28-imidazole (CDDO-Im) directly targets mitochondrial glutathione to induce apoptosis in pancreatic cancer. *J. Biol. Chem.* **280**, 36273–36282 [CrossRef Medline](#)
  54. Wang, Y.-Y., Zhe, H., and Zhao, R. (2014) Preclinical evidences toward the use of triterpenoid CDDO-Me for solid cancer prevention and treatment. *Mol. Cancer* **13**, 30 [CrossRef Medline](#)
  55. Hagos, F. T., Daood, M. J., Ocque, J. A., Nolin, T. D., Bayir, H., Poloyac, S. M., Kochanek, P. M., Clark, R. S., and Empey, P. E. (2017) Probenecid, an organic anion transporter 1 and 3 inhibitor, increases plasma and brain exposure of N-acetylcysteine. *Xenobiotica* **47**, 346–353 [Medline](#)
  56. Cole, M. P., Rudolph, T. K., Khoo, N. K. H., Motanya, U. N., Golin-Bisello, F., Wertz, J. W., Schopfer, F. J., Rudolph, V., Woodcock, S. R., Bolisetty, S., Ali, M. S., Zhang, J., Chen, Y. E., Agarwal, A., Freeman, B. A., and Bauer, P. M. (2009) Nitro-fatty acid inhibition of neointima formation after endothelial vessel injury. *Circulation Res.* **105**, 965–972 [CrossRef Medline](#)
  57. Klinke, A., Möller, A., Pekarova, M., Ravekes, T., Friedrichs, K., Berlin, M., Scheu, K. M., Kubala, L., Kolarova, H., Ambrozova, G., Schermuly, R. T., Woodcock, S. R., Freeman, B. A., Rosenkranz, S., Baldus, S., *et al.* (2014) Protective effects of 10-nitro-oleic acid in a hypoxia-induced murine model of pulmonary hypertension. *Am. J. Respir. Cell Mol. Biol.* **51**, 155–162 [CrossRef Medline](#)
  58. Kelley, E. E., Baust, J., Bonacci, G., Golin-Bisello, F., Devlin, J. E., St Croix, C. M., Watkins, S. C., Gor, S., Cantu-Medellin, N., Weidert, E. R., Frisbee, J. C., Gladwin, M. T., Champion, H. C., Freeman, B. A., and Khoo, N. K. (2014) Fatty acid nitroalkenes ameliorate glucose intolerance and pulmonary hypertension in high-fat diet-induced obesity. *Cardiovasc. Res.* **101**, 352–363 [CrossRef Medline](#)
  59. Ambrozova, G., Martiskova, H., Koudelka, A., Ravekes, T., Rudolph, T. K., Klinke, A., Rudolph, V., Freeman, B. A., Woodcock, S. R., Kubala, L., and Pekarova, M. (2016) Nitro-oleic acid modulates classical and regulatory activation of macrophages and their involvement in pro-fibrotic responses. *Free Radic. Biol. Med.* **90**, 252–260 [CrossRef Medline](#)
  60. Rudolph, T. K., Ravekes, T., Klinke, A., Friedrichs, K., Mollenhauer, M., Pekarova, M., Ambrozova, G., Martiskova, H., Kaur, J. J., Matthes, B., Schwoerer, A., Woodcock, S. R., Kubala, L., Freeman, B. A., Baldus, S., and Rudolph, V. (2016) Nitrated fatty acids suppress angiotensin II-mediated

- fibrotic remodelling and atrial fibrillation. *Cardiovasc. Res.* **109**, 174–184 [CrossRef Medline](#)
61. Verescakova, H., Ambrozova, G., Kubala, L., Perecko, T., Koudelka, A., Vasicek, O., Rudolph, T. K., Klinke, A., Woodcock, S. R., Freeman, B. A., and Pekarova, M. (2017) Nitro-oleic acid regulates growth factor-induced differentiation of bone marrow-derived macrophages. *Free Radic. Biol. Med.* **104**, 10–19 [CrossRef Medline](#)
  62. Jaramillo, M. C., and Zhang, D. D. (2013) The emerging role of the Nrf2-Keap1 signaling pathway in cancer. *Genes Dev.* **27**, 2179–2191 [CrossRef Medline](#)
  63. Kalimutho, M., Parsons, K., Mittal, D., López, J. A., Srihari, S., and Khanna, K. K. (2015) Targeted therapies for triple-negative breast cancer: Combating a stubborn disease. *Trends Pharmacol. Sci.* **36**, 822–846 [CrossRef Medline](#)
  64. Diers, A. R., Dranka, B. P., Ricart, K. C., Oh, J. Y., Johnson, M. S., Zhou, F., Pallero, M. A., Bodenshtein, T. M., Murphy-Ullrich, J. E., Welch, D. R., and Landar, A. (2010) Modulation of mammary cancer cell migration by 15-deoxy- $\Delta$ 12,14-prostaglandin J<sub>2</sub>: implications for anti-metastatic therapy. *Biochem. J.* **430**, 69–78 [CrossRef Medline](#)
  65. Kastrati, I., Siklos, M. I., Calderon-Gierszal, E. L., El-Shennawy, L., Georgieva, G., Thayer, E. N., Thatcher, G. R. J., and Frasor, J. (2016) Dimethyl fumarate inhibits the nuclear factor  $\kappa$ B pathway in breast cancer cells by covalent modification of p65. *J. Biol. Chem.* **291**, 3639–3647 [CrossRef Medline](#)
  66. Maine, G. N., Mao, X., Komarck, C. M., and Burstein, E. (2007) COMMD1 promotes the ubiquitination of NF- $\kappa$ B subunits through a cullin-containing ubiquitin ligase. *EMBO J.* **26**, 436–447 [CrossRef Medline](#)
  67. Hou, Y., Moreau, F., and Chadee, K. (2012) PPAR $\gamma$  is an E3 ligase that induces the degradation of NF- $\kappa$ B/p65. *Nat. Commun.* **3**, 1300 [CrossRef Medline](#)
  68. Rayet, B., and Gélinas, C. (1999) Aberrant *rel/nfkb* genes and activity in human cancer. *Oncogene* **18**, 6938–6947 [CrossRef Medline](#)
  69. Karin, M., Cao, Y., Greten, F. R., and Li, Z.-W. (2002) NF- $\kappa$ B in cancer: from innocent bystander to major culprit. *Nat. Rev. Cancer* **2**, 301–310 [CrossRef Medline](#)
  70. Lien, E. C., Lyssiotis, C. A., Juvekar, A., Hu, H., Asara, J. M., Cantley, L. C., and Tokor, A. (2016) Glutathione biosynthesis is a metabolic vulnerability in PI(3)K/Akt-driven breast cancer. *Nat. Cell Biol.* **18**, 572–578 [CrossRef Medline](#)
  71. Zalba, G., Fortuño, A., Orbe, J., San José, G., Moreno, M. U., Belzunce, M., Rodríguez, J. A., Beloqui, O., Páramo, J. A., and Díez, J. (2007) Phagocytic NADPH oxidase-dependent superoxide production stimulates matrix metalloproteinase-9: implications for human atherosclerosis. *Arterioscler. Thromb. Vasc. Biol.* **27**, 587–593 [CrossRef Medline](#)